Faculty of Engineering and Science

Department of Civil Engineering and Construction

Mix Design Optimisation and Durability Study of High Performance Concrete Containing Micro and Nano Palm Oil Fuel Ash

Wan Nur Firdaus Binti Wan Hassan

This thesis is presented for the Degree of

Doctor of Philosophy

of

Curtin University

June 2019

DECLARATION

To the best of my knowledge and belief this thesis contains no material previously published by any other person except where due acknowledgment has been made This thesis contains no material which has been accepted for the award of any other degree or diploma in any university.

Signature: …….

Date: ……..

ABSTRACT

Globally, Malaysia is the second largest producer in palm oil industry. By 2020, the palm oil solid biomass production is expected to increase up to 100 million dry tonnes and generally about 5 million tonnes of palm oil fuel ash (POFA) is produced from the solid biomass. The huge amount of agriculture by-products have attracted the cement industry to utilise these wastes as supplementary cementitious materials. Feasibility studies of POFA as supplementary cementitious material started since 1990. The fineness of POFA provides a significant effect on the strength and durability properties of concrete. Micro-sized POFA has remarkably reduced the workability and compressive strength at an early age. Recently, nano-sized POFA has been used to solve the issues by utilising it in a high volume of replacement. However, the dilution effect affected the strength properties at an early age and high volume of nano POFA requires sufficient weak product for hydration process to produce strengthening gel. Therefore, this study investigated the effect of combining micro and low volume of nano POFA as supplementary cementitious materials on the strength and durability properties of high performance concrete.

Several characterisation techniques were conducted to obtain the characteristics of micro and nano POFA as pozzolanic material in terms of surface morphology, particle size, chemical and mineralogical composition. The main objective of this study is to develop the mathematical models to predict the mechanical properties of concrete containing micro and nano POFA. Under response surface methodology (RSM), a central composite design (CCD) was applied to design the experiment and numerical optimisation was performed to determine the optimal range of micro and nano POFA as a binder in the design mix. To verify the optimum proposed binders, durability tests were conducted to determine the significant effect of the micro and nano POFA on the concrete resistance to water absorption, chloride penetration, acid attack and corrosion of steel reinforcement. From the characterisation analysis, the results showed that micro and nano POFA have low loss on ignition value, high strength activity index, high silica content, traces of crystalline phases and Si-O functional group. These characteristics are significant for the pozzolanic material to react with weak product to produce secondary strengthening gel. The mathematical models developed to predict the workability, compressive, splitting tensile and flexural strengths of concrete were found to be in good agreement with the experimental results. Based on experimental data, results of workability and early strengths of concrete containing 10% of micro and 1-3% of nano POFA were increased by 7.1% and 3-4%, respectively. Reduction in workability and lower strengths were observed in concrete containing 20-30% of micro POFA and any replacement of nano POFA. A similar pattern was found in splitting tensile and flexural strengths but in different

magnitude. Numerical optimisation revealed the optimal solutions that ranged the combination of micro and nano POFA in the design mix. 10% of micro POFA with 1.12-2.85 % of nano POFA showed the optimum responses. Graphical optimisation pointed the highest desirability value at the area of 10% of micro POFA and 1-3% of nano POFA.

In order to verify the proposed optimum binders, the durability tests in terms of concrete resistance to water absorption, chloride penetration, acid sulphuric attack and corrosion of steel reinforcement were conducted. The results indicated that the water absorption and chloride penetration were benefited significantly in concrete containing micro and nano POFA within 6 months of exposure. In terms of acid resistance, concrete containing micro and nano POFA exhibited lower mass loss and strength reduction in comparison with the plain concrete. The SEM, EDX and XRD analyses have confirmed the traces of gypsum deposited on the surface of the concrete that induces to concrete spalling and cracking. Finally, to assess the corrosion of steel reinforcement embedded in concrete containing micro and nano POFA, three techniques were used to determine the steel weight loss, the equivalent electrical circuit of the concrete interface, polarization resistance and corrosion rate. Mass loss of steel reinforcement embedded in concrete containing micro and nano POFA showed the lowest by lost about 3.8%-6.5% compared with plain concrete that lost about 13.95%. By using impressed voltage, the plain concrete required about 37 days to crack whilst concrete containing 10% of micro POFA and 1-3% of nano POFA took about 43-45 days to initiate the crack under 15V supply. By electrochemical impedance spectroscopy test, a model of R (QR (QR) (QR) (CR)) was proposed to represent the interface of concrete containing micro and nano POFA. From the analysis, the results indicated the highest value of polarization resistance exhibited by steel reinforcement bar embedded in concrete containing 10% of micro POFA and 3% of nano POFA. At the 1-year period of the wetting-drying cycle, the corrosion rate of concrete containing 10% of micro POFA and 1-3% of nano POFA were 0.0452, 0.0159 and 0.0148 mm/year, respectively. In comparison with plain concrete, the corrosion rate has been reduced by about 80% from concrete containing micro and nano POFA. Overall, the optimum range of micro and nano POFA as a binder in the design mix has improved the mechanical properties of concrete especially workability, early strengths of concrete. Moreover, the improvement of durability properties including the corrosion resistance showed the lower permeability of the hardened structure due to the pozzolanic reaction forming the extra strengthening gel and produce denser concrete.

ACKNOWLEDGEMENT

Firstly, a special gratitude goes out to all at the Curtin University Malaysia for providing the scholarship for my PhD research work. No research is possible without the university support who provided facilities at the lab and library, the centre of learning resources. I also would like to express sincere gratitude to my supervisors, Assoc. Prof. Dr. Mohamed A.Ismail, Prof. Dr. Mohammad Ismail, Prof. Ir. Dr. Mohd Warid Hussin and Assoc. Prof. Dr. Muhammad Ekhlasur for the continuous support in my research works, their patience, motivation and knowledge. Not to forget to Prof. Dr. Han-Seung Lee and team members for providing the facilities for my testing at Hanyang University, Korea. To Prof. Dr. Mohammad Ismail, thank you for giving me the opportunity to do corrosion study at your Corrosion Lab, Universiti Teknologi Malaysia. I am grateful to my colleagues Dr Muhd Norhasri, Dr Faisal Amri, Dr Nor Hasanah Shukor Lim, Dr Farhayu Ariffin, Mr Wi, Bro Tang Wei Le, who provided me an idea, opinion and solution during my hard time and enlightened me the first glance of research. I am also grateful to the following university staff: Mrs. Florence, Mrs Helda, Ms Sharinna and Mr Anthony for their unfailing support and assistance.

Last but not the least, I would like to thank my family especially to my husband, Muhammad Sharaffuddeen Suhaimi for allowing me to stay apart for 3 years and always supported me in every possible way to see the completion of this work. I am very much indebted to my parents, Mr. Wan Hassan, Mrs. Zawahir and siblings who encouraged and helped me at every stage of my personal and academic life and also supporting me spiritually throughout this whole journey and my life in general. Many thanks! I could not describe in words how grateful I am to have them in my life.

Above all, I owe it all to Allah swt for granting me the wisdom, health and strength to undertake this research task and enabling me to its completion.

LIST OF PUBLICATIONS

Book chapter:

i. Wan Hassan, W.N.F., Ismail, M.A., Lee, H.S., Warid, M.W. & Muthusamy, K (2018). In K. Muthusamy et al. (Ed.), *Sustainable Special Concrete*. University Malaysia Pahang.

Journal paper:

i. Wan Hassan, W.N.F., Ismail, M.A., Lee, H. S., Hussin, M.W. and Ismail, M. (2017) Utilization of nano agricultural waste to improve the workability and early strength of concrete. *International Journal of Sustainable Building Technology and Urban Development*, 8(4):316-331.

ii. Tang W.L., Lee, H.S., Vimonsatit,V., Htut, T., Singh, J.K., Wan Hassan, W.N.F, Ismail, M.A., Seikh, A.H, and Alharthi, N. (2019) Optimization of Micro and Nano Palm Oil Fuel Ash to Determine the Carbonation Resistance of the Concrete in Accelerated Condition. *Materials*, 12(1), 130.

iii. Wan Hassan, W.N.F., Ismail, M.A., Ismail, M.A., & Lee, H. S., Hussin, M.W. (2019) Fresh and Hardened Properties of the High performance Concrete Utilizing Micro and Nano POFA. *Malaysian Construction Research Journal*.

iv. Wan Hassan, W.N.F., Ismail, M.A., Lee, H. S., Hussin, M.W., Ismail, M. & Singh, J.K. (2019) Mixture Optimization of High Strength Blended Concrete using Central Composite Design. *Construction & Building Materials.*(Full manuscript prepared in July 2018, submitted in December 2018).

Conference proceedings:

i. Wan Hassan, W.N.F., Ismail, M.A., Lee, H. S., Hussin, M.W. & Ismail, M.A. (2016) Durability Performance of Binary Blended Concrete: An Overview**.** *International Conference on Sustainable Built Environment, SBE16 SEOUL 11-14***.**

ii. Wi, K.W., Lee, H.S., Hussin, M.W., Ismail, M.A., & Wan Hassan, W.N.F. (2016) Experimental Study on Hydration Properties of Nano POFA. *International Conference on Sustainable Built Environment SBE16 SEOUL, 11-14 Dec.*

iii. Wan Hassan, W.N.F., Ismail, M.A., Lee, H. S., Hussin, M.W. & Ismail, M.A. (2018) Short Term Investigation on Palm Oil Fuel Ash from Different Sources as Supplementary Cementitious *Material. 1st International Conference on Durability of Building and Infrastructures (DuraBI) 2018 January 10th - 12th, Miri, Malaysia.*

iv. Wan Hassan, W.N.F., Ismail, M.A., Lee, H. S., Hussin, M.W. & Ismail, M.A. (2017) Optimum Mix Design of High Performance Concrete with Utilization of Palm Oil Fuel Ash. *Proceedings of One Curtin International Postgraduate Conference (OCPC) 2017 Miri, Sarawak, Malaysia, December 10 – 12.*

v. Wan Hassan, W.N.F., Ismail, M.A., Lee, H. S., Hussin, M.W. & Ismail, M.A. (2019) Engineering Properties of High Strength Blended Concrete Enhanced with Nano POFA. *IOP Conference Series: Materials Science and Engineering*. (unpublished yet)

vi. Wan Hassan, W.N.F., Ismail, M.A., Lee, H. S., Hussin, M.W. & Ismail, M.A. (2017) Compressive Strength of the High Performance Concrete Utilizing Micro Size of Palm Oil Fuel Ash Colloqium. *5th Postgraduate Borneo Research Colloquium, 4th – 6th July, Sarawak, Malaysia.*

TABLE OF CONTENT

LIST OF FIGURES

LIST OF TABLES

Chapter 1

Introduction

1.1 Background of the Study

Cement has been marked as a potential threat to sustainable development. In fact, the cement industry is responsible for about 25% of global carbon dioxide (CO_2) emissions. The process of cement manufacturing will directly release approximately 0.9 to 1 ton of carbon dioxide (CO_2) depending on the carbon content of fossil fuels used (Ramezanianpour, 2014). In 2017, the global cement production reported that about 3.39 billion metric tons of cement was produced and the amount is expected to increase to 4.83 billion metric tons in 2030 (U.S. Geological Survey, 2018). For that reason, the world's annual cement demand releasing the equivalent amount of CO_2 to the atmosphere.

The cement industry has been urged to reduce their CO_2 emission over the past decades. Hence, a technology roadmap called *Cement Technology Roadmap 2009: Carbon emissions reductions up to 2050* was developed to identify potential ways for the industry to contribute towards cutting the global CO_2 emission by 2050 by half (International Energy Agency (IEA), 2009). To date, the most effective and realistic way to reduce direct emission of CO_2 is by replacing the clinker content with supplementary cementitious materials (SCM) in concrete mix (Ludwig & Zhang, 2015). SCM such as fly ash, granulated blast furnace slag, rice husk ash, etc. have been reported to reduce the cement production, and consequently, the CO_2 emission and the use of energy. However, more research is required on the standardization of the specifications and mix design procedure at global level to continue contributing towards sustainable development (Samad & Shah, 2017).

Malaysia as the second largest player in the palm oil industry in the world has the potential to reduce the impact on environment by utilising palm oil biomass as the SCM. Due to the humid tropical climate coupled with hot weather and average distributed annual rainfall, Malaysia has the advantage of getting optimal growth production of palm oil. Malaysia and Indonesia have been strategic locations in the development of palm oil. In 2015, there were about 5.64 million hectares of palm oil

plants and this industry has become one of the major contributors to Malaysia's economy. Due to this huge development, this industry is able to abundantly supply biomass energy in larger mass compared than any other types of biomass. By 2020, Malaysia forecasts that the supply of biomass will reach about 85-111 million tons of solid biomass and 70-110 million tons of liquid biomass (Malaysia Innovation Agency, 2013). The biomass wastes such as empty fruit bunches, mesocarp fibers, palm kernel shells, oil palm trunks, oil palm leaves, palm oil mill effluents and oil palm fronds are produced from processing of palm oil. These wastes have been utilized in a number of ways, by using them as soil fertilizer, for paper production, furniture, electronics, packaging and in the automobile industry (Sumathi, Chai, & Mohamed, 2008).

Approximately 5% of solid biomass was produced in the form of ash from the combustion process of dried mesocarp fibre and empty fruit bunches at 800 –1000 ° C to generate electricity at the mills. This type of ash has low potassium content and can be used as soil fertilizers, thus it is disposed near the mills, creating environmental pollution and potential health hazards (Tay, 1990; Tay & Show, 1995). Since then, the initiatives towards creating a waste free type of industry has led to unique discoveries that benefits the palm oil and construction industry. Laboratory investigations have proven that the ashes called palm oil fuel ash (POFA) was found to be a good SCM and plays an effective role in producing strong and durable concrete (Awal & Hussin, 1999; Tay, 1990).

A large and growing body of literatures have investigated the utilization of POFA as a SCM in producing high performance concrete in the last ten years (Awal & Nguong, 2010; Awal & Abubakar, 2011; Chindaprasirt et al., 2007; Hussin & Abdullah, 2009; Megat Johari, Zeyad, Muhamad Bunnori, & Ariffin, 2012). The fineness effect of POFA can vary the engineering properties of concrete due to the surface area of the particles and the rate of the hydration process, which then affects the production of calcium silicate hydrate (CSH) gels (Kroehong, Sinsiri, & Jaturapitakkul, 2011). It has been recognized that ground POFA can be used successfully as a SCM for producing normal and high-strength concrete (Safiuddin, Abdus Salam, & Jumaat, 2011). Some of the technical issues reported by previous researchers related to the micro sized of POFA such as high water demand, poor workability and low early strengths (Damtoft, Lukasik, Herfort, Sorrentino, & Gartner,

2008). They found that the reduction of the particles' size interferes in the cement's kinetic reaction and made the curing process faster due to intense electrostatic forces and the bigger superficial area. Therefore, the researchers extended their study to accelerate the binder hydration by utilizing nanoparticles in cement matrix due to the higher surface energy act (Lim et al., 2015; Rajak, Majid, & Ismail, 2015). However, most of the studies investigated the nano POFA in cement paste and mortar to satisfy the strength properties. In addition, the utilization of nano POFA in concrete has not been studied extensively on durability of concrete especially on corrosion resistance.

Apart from strength, durability is another other important element of hardened concrete. The durability of concrete can be assessed through the permeability of the concrete whereby permeability of concrete is influenced by the environment and aggressive movement of fluids into the concrete, hence, deteriorating the concrete. The aggressive environment surrounds the concrete structure, contributing to chemical intrusion into the concrete consequently leading to spalling of concrete covers and corrosion of steel reinforcements bars in the concrete. Developing an impermeable pore system in a concrete is the solution to this problem by utilizing supplementary cementitious material. Therefore, this study was conducted to determine the effect of combination of micro and nano POFA in improving the durability of concrete. Besides permeability, other causes that affect the durability properties of concrete including chemical resistance, water absorption, sorptivity, and corrosion resistance were also studied.

Developing an approach in proportioning concrete mix design is a technique that allows optimum mix design to achieve the desired performance of concrete. This is an efficient, time reducing and cost effective tool in predicting the concrete performance in comparison with conventional methods (Simon, Lagergen, & Wathne, 1999). This approach is also recommended by Mehta (2009) to maintain sustainability other than using SCM to reduce the cement dosage. Most researchers have tried to use a statistical tool to optimize the mix design of concrete. The Design of Experiment (DOE) approach in conjunction with Response Surface Methodology (RSM) are the optimisation tools to adjust the mixture parameters to achieve optimisation criteria (Montgomery, 2017). This approach plays an important role in the mix design approach especially for concrete that consists of large content of cement such as high

strength and ultra-high strength. To respond to the above need, it is worthwhile to determine the optimal amount of binder in the mix design concrete using RSM, and to develop mathematical models to predict the fresh and hardened properties of concrete.

In order to develop the models, it is essential to prepare the same set of materials to generalise the results and to determine the effect of micro and nano POFA in strength and durability performance of concrete. In this study, two sizes of POFA were used as the binders in producing high performance concrete. The fresh and hardened properties of the concrete were investigated and the optimisation analysis was implemented in order to get the optimized binder in the mix design of concrete to achieve the desired performances. The criteria to optimize the binders in the mix design of concrete were designed based on the requirement of the fresh and hardened properties of high performance concrete. To further satisfy the performance of concrete with respect to the optimum binder proposed, the durability properties of concrete were studied, which includes the resistance of the steel reinforcement in high performance concrete to corrosion, due to chloride attack, moisture absorption, chloride penetration and acid attack.

1.2 Problem Statement

The application of agricultural by-products and wastages to replace expensive conventional materials fully or partially is being considered as major techniques to solve the sustainability issue. In Malaysia, the abundancy of biomass produced from the palm oil industry is mostly dumped near the mills due to the insufficient nutrients to be used as fertilizer. This type of wastage brings no profit to the palm oil industry plus it causes environmental pollution and potential health hazards. Past researchers focused on conducting feasibility studies on POFA as supplementary cementitious materials and it has been found that POFA has significant effects on the strength and durability properties of concrete. However, there are a few technical issues related to the micro size of POFA such as workability, high water demand and low early strength. To solve the issues, researchers have proposed high volume of nano POFA up to 80 % to accelerate the cement hydration and satisfy the strength properties of concrete. Therefore, a combination of micro and nano-sized of POFA was proposed in this study to improve the mechanical and durability properties of high performance concrete by utilizing optimum dosage of micro sized of POFA with low volume of nano POFA.

Improvements have been done by utilizing high volume of nano POFA to act as nano fillers and enhance the production of secondary CSH gels via pozzolanic reactions (Lim et al., 2015; Megat Johari et al., 2012). However, the recent utilization of nano POFA as pozzolanic material in high performance concrete is still limited and most of studies done by the researchers focusing on the nano POFA in mortar and paste. In addition, exploration of the micro and nano size of POFA in improving the strength and durability properties of high performance concrete has not been widely studied especially the resistance to corrosion. Therefore, a comprehensive study of micro and nano POFA as supplementary cementitious material in high performance concrete is highly recommended in this area that would be beneficial towards understanding the strength and durability properties of high performance concrete. Enhancement of durability properties of concrete is also necessary for high performance concrete. Concrete spalling, cracks and corrosion of steel reinforcement will significantly affect the durability and increase the maintenance cost to repair the damage. Therefore, the enhancement of durability properties of concrete in terms of permeability, chemical attack, moisture absorption, sorptivity and corrosion resistance was investigated on the concrete containing micro and nano POFA.

Mathematical models to predict the mechanical properties of concrete containing nanomaterial is still potentially open for extensive investigation and this outcome can provide relationship between the supplementary cementitious material and concrete properties. By conventional methods, it requires time and cost to achieve the desired performance of concrete while aiming to get the optimum binders. The optimal amount of proposed binders in the mix design of high performance concrete is truly necessary because of the large content of cement required to produce high performance concrete. Therefore, a statistical experimental design procedure is found to be a valuable and effective tool in the optimizing of binders to meet the desired performances of high performance concrete. From the analysis, mathematical models or prediction equations will be developed in order to predict the mechanical properties of high performance concrete. The optimized binders in the mix design of concrete is expected to satisfy the mechanical and durability properties of concrete as well. Besides strength, durability is another important property for concrete especially high performance concrete. Concrete deterioration such as cracking, spalling and corrosion of steel reinforcement indicate the high permeability of concrete which allow

aggressive chemical intrude into the concrete. Therefore, the optimum binders in concrete mix design is proposed as the supplementary cementitious materials to fulfil the mechanical and also durability properties of concrete which include resistance to chloride penetration, moisture absorption, chemical attack and corrosion.

1.3 Research Questions

In this study, the research questions are listed below:

1) What is the microstructural characteristics of the proposed binders (micro and nano POFA)?

2) What is the optimal amount of binders (micro and nano POFA) and mathematical models to predict fresh and hardened properties of concrete containing micro and nano POFA based on Response Surface Methodology?

3) How does the high performance concrete containing micro and nano POFA satisfy or fulfil the durability performance of high performance concrete in terms of water absorption, chloride penetration and resistance to chemical attack?

4) How does the high performance concrete micro and nano POFA resist the corrosion of the steel reinforcement due to chloride attack based on two types of corrosion measurements (destructive and non-destructive test)?

1.4 Research Objectives

This study investigates the potential of micro and nano POFA as a binder/supplementary cementitious material in improving strength and durability of high performance concrete. The main aim of this study is to determine the optimal amount of micro and nano POFA in the mix design and develop mathematical models to predict the fresh and hardened properties of high performance concrete. The durability study takes place to satisfy the performance of high performance concrete with the optimum binders proposed. The following objectives are identified to satisfy this aim:

i) To characterize the micro and nano POFA as binders in producing high performance concrete.

ii) To develop mathematical models to predict fresh and hardened properties of concrete using Response Surface Methodology and determine the optimal composition of binders in concrete mix design.

iii) To study the durability properties and microstructural analysis of high performance concrete utilizing micro and nano POFA.

iv) To assess the effect of high performance concrete utilising micro and nano POFA on durability affected by corrosion due to chloride.

1.5 Research Significance

In the year 2020, approximately 5 million tons of POFA was produced from the solid biomass of the palm oil industry (Al-Mulali, Awang, Abdul Khalil, & Aljoumaily, 2015). Since open burning has been prohibited (Yusoff, 2006), the waste is disposed in landfills, causing environmental issues such as air pollution and problems associated with groundwater quality due to the leaching of different metals from the ash (Madurwar, Ralegaonkar, & Mandavgane, 2013). Therefore, method of using and consuming the waste in civil engineering applications is considered as one of the efforts to resolve the burning issue with regards to the disposal of the huge quantity of waste materials from the Malaysian palm oil industry. The POFA revolution has attracted much attention mainly because of its abundant accessibility. Other than the significance in the civil engineering application, there is an additional advantage parallel with the scope of study. The use of the agricultural waste to improve the concrete properties is considered to help the concrete industry towards supporting sustainable development. This is because by utilizing the POFA, the cement dosage will be reduced in the concrete mix hence reducing CO_2 emissions. Another issue that the environment faces due to the palm oil industry is air pollution, a potential health hazard and groundwater pollution, due to the abundancy of waste dumped at the mill. By consuming the agricultural waste, the palm oil industry has the potential to become a waste-free type of industry.

The study of utilization of micro POFA as supplementary cementitious material has highlighted a few issues such as high water demand, reduction of workability and low early strength of concrete. By refining the POFA to nano particles, the higher surface area of particles can promote the uniform dispersion in concrete

mix, while accelerating the hydration process. In this study, the utilization of nano POFA was purposely combined with the micro POFA in high performance concrete to improve the fresh and hardened properties of concrete. Low volumes of nano POFA has the potential to compensate for the drawbacks of the micro POFA in producing high performance blended concrete by filling up all the micro and nano pores, which were left unfilled in the traditional cement based concrete. As stated in introduction, the utilization of the micro and nano POFA in high performance concrete is very limited especially in durability study. Other durability study such as corrosion resistance is still not been investigated. Therefore, in this study, the effect of the combination of micro and nano POFA in producing high performance concrete on the mechanical and durability properties of concrete is assessed. Enhancement of durability properties of concrete is important for high performance concrete and to assess that, several important measures were conducted such as resistance of concrete to chemical attack, moisture absorption, sorptivity, chloride penetration and corrosion due to chloride-induced.

The study also focuses on developing the mathematical models to predict fresh and hardened properties of concrete containing micro and nano POFA. The mathematical and statistical analysis is used to determine the optimal composition of proposed binders in satisfying the good criteria of concrete properties. The design of experiment based on Response Surface Methodology (RSM) is applied to achieve the objective of the study. From this analysis, the modelling can predict concrete performance including fresh and hardened properties of concrete without repeating the test and reducing the trial batches as well. By satisfying the fresh and hardened properties of concrete containing micro and nano POFA, consequently, there is an improvement in the durability properties due to lower permeability of the concrete, resistance of concrete to chemical attacks and durability of the concrete with respect to corrosion. The optimal composition of micro and nano POFA in concrete mix design is the solution to develop an impermeable pore system in concrete to solve the durability issue including chloride penetration, moisture absorption, chemical attack and corrosion.

1.6 Thesis Outline

This thesis comprises of eight chapters that aligns with the objectives of the study. Chapter 1 presents the introduction of the study and research motivations that address the problem statement. In this chapter, the objectives of the study, research questions and research significance are highlighted.

In chapter 2, the past and current related research findings are discussed. The review of the literature covers the present usage state of the POFA in the concrete, the latest finding of nanotechnology in concrete, the mix design optimisation in producing blended concrete and the effects of POFA on strength and durability of the concrete.

Chapter 3 provides the details of the materials used to produce high performance blended concrete, mix design process, standard testing procedures, optimisation analysis process and microstructural test employed in conducting the research. The testing conducted in this study are based on the accepted standards.

Chapter 4 presents the physical properties, chemical composition and the microstructural characteristic of micro and nano POFA. This chapter focuses on the POFA characterization as the supplementary cementitious material before it is being used in the concrete mix.

Chapter 5 focuses on the mathematical and statistical analysis using Response Surface Methodology. From this chapter, the input variables and responses are chosen and the design of experiment (DOE) presents the experimental program using Response Surface Methodology (RSM). The experimental data is based on the lab work program and will be analysed with the predicted data based on the RSM. This chapter develops mathematical models to predict the fresh and hardened properties of concrete containing micro and nano POFA to determine the optimal composition of proposed binders in the mix design of high performance concrete.

Chapter 6 highlights the durability study of the high performance concrete after the optimum binders are determined. In this chapter, the durability tests involving namely; moisture absorption, rapid chloride penetration test (RCPT), and resistance to acid are provided. The samples of concrete after the longest period of immersion were further investigated by the microstructural test to justify the results obtained from

durability test. This chapter also provides the durability study of high performance concrete to resist corrosion due to chloride attack. The corrosion of the steel reinforcement embedded in concrete was determined by using two types of measurements. The rapid measurement was conducted according to the accelerated corrosion test by impressed voltage and the electrochemical techniques involved two methods; Electrochemical Impedance Spectroscopy (EIS) and Tafel plot.

The final chapter, chapter 7, discusses the conclusions of the study and recommendations for the future works are listed.

Chapter 2

Literature Review

2.1 Introduction

This chapter covers the literature review of this study, which discusses significant and relevant information based on past researches in this field. The first subsection covers the overview of the present use of cement in construction activities and its increasing demand that leads the industry to the the utilization of supplementary cementitious materials. The next sub section reviews the potential of waste materials from the palm oil mill as supplementary cementitious materials. The review continues with the historical development of palm oil fuel ash (POFA) and the significant effects of the different fineness of POFA in the concrete mix. The technical issues faced when utilizing micro POFA has been highlighted and how nano POFA is used to overcome those issues will be discussed. The need of optimisation in the mix design is required especially in producing concrete with a larger content of cement. Therefore, to reduce the cost involving time by using trial batches to get the desired performance of concrete, an efficient tool using statistical analysis using Response Surface Methodology (RSM) is discussed. In the last sub section, the review of the utilization of POFA in concrete is emphasized. The effect of POFA on fresh and hardened properties of concrete is reviewed and the discussion is extended with studies done on the durability of POFA concrete. The review emphasises on the resistance of the concrete utilizing POFA to address issues of chemical attacks and chloride penetration. On top of that, the review on the resistance of reinforced POFA concrete to corrosion is also included. In this chapter, the research gap of this study is highlighted, and the discussion of the literature provides a better understanding of what has been done and what needs to be done in this particular study.

2.2 Cement today

In the year 2017, the global cement production is reported to have produced 3.39 billion metric tons of cement and the amount is expected to rise to 4.83 billion metric tons in 2030 (U.S. Geological Survey, 2018). The process of cement manufacturing will emit approximately 0.9 to 1 ton of carbon dioxide (CO_2) from 1

ton of cement depending on the carbon content of fossil fuels used (Ramezanianpour, 2014). Consequently, the construction and cement industry are the biggest contributors to global warming, thus raising issues on environmental sustainability due to the release of the high amounts of CO_2 to the atmosphere. By region, Asian countries are leading contributors, with China being the top leading country in cement production, manufacturing approximately 2.4 billion tons per year. This counts towards 56.5% of the world's production of cement. The increasing pattern of the cement demand cannot continue indefinitely. Hence, in the paper published by Aitcin (2000) entitled "Cements of yesterday and today, concrete of tomorrow", the binder of tomorrow from a sustainable perspective is one that has alternative/potential binders that are more environmentally friendly and can help the industry to support the aim of achieving sustainable development. Cement is still the main ingredient in producing concrete, but entering the modern era, it is no longer the most important material because concrete is blended with other materials to form blended cement. This type of cement of tomorrow will support some of the goals in sustainable development and today's cement industry should embrace this new alternative. Therefore, the cement and concrete industries have no choice but to transform the industry into green industries and try produce the durable green concrete of tomorrow (Aitcin, 2000).

The chemical composition of cement consists of various types of oxide components. The main components of cement are silica, SiO_2, lime, CaO, iron, Fe_2O_3 alumina, Al_2O_3. The other components are minor oxide, namely, potassium and sodium. The limited reaction of alkali-aggregates reaction is controlled by minor components of cement. All of these cement components will interact with each other to form compounds resulting as major constituent of cement (Neville, 2011). The strength, fracture and stability of concrete depends on the hydration products and the reaction between cement and water. The combination of cement and water forms hydrated phase, which is the 'glue' material called calcium hydrate silicate (CSH) gel and the excess of weak product namely, calcium hydroxide. The CSH is an important phase in concrete, hence is responsible for the mechanical properties of concrete. The amount of each component will vary depending on the reaction path (Chen, Thomas, Taylor, & Jennings, 2004).

2.3 Supplementary Cementitious Materials (SCM)

The process of the cement manufacturing consists of burning of fossil fuels, coal, petroleum, coke and fuel oils in the oven at a temperature of 1450 º C (Anand, Vrat, & Dahiya, 2006). This kind of production generates 7-8% of CO_2 gas emission from the factories hence, increasing greenhouse gases and posing as a potential threat to the environment (Alsubari, Shafigh, & Jumaat, 2016; Bouzoubaâ & Lachemi, 2001). The cement demand is expected to increase by 200% by the year 2050 (Taylor, Tam, & Gielen, 2006). In terms of energy consumption, the amount of 1ton cement produced requires approximately 1700 MJ/clinker and 1.5 tons of raw materials (Rashad, Bai, Basheer, Milestone, & Collier, 2013; Taylor, 2017). The cement industry alone consumes 5% of total energy (Sakulich, Miller, & Barsoum, 2010). The issue of the abundancy of the solid biomass waste from industrial and agricultural products has caused researchers to try and solve the environmental issue stemming from the cement industry (Amin, Alam, & Gul, 2015; Karim, Hashim, & Abdul Razak, 2016; Mo, Ling, Alengaram, Yap, & Yuen, 2017).

Due to rapid urbanization, industrial growth and construction booms, countries all over the world are facing difficulties in handling and managing the solid biomass waste (Kabir, Al-Shayeb, & Khan, 2016). There are three types of solid waste sources, and these can be categorized as industrial, municipal and agricultural waste. Due to drawbacks of unsustainable raw materials to the environment, solid waste plays an important role in the construction industry as supplementary cementitious materials (SCM) (Mehta & Siddique, 2016). For instance, the effects of using the supplementary cementitious materials can be seen from the fact that approximately 1% replacement of cement with fly ash results in an estimated 0.7% reduction in energy consumption per unit of concrete (Aïtcin, 2000). Apart from that, the SCM such as palm oil fuel ash, metakaolin, rice husk ash, slag and fly ash is able to improve certain mechanical properties of concrete such as the low early age of compressive strength (Dash, Patro, & Rath, 2016).

Studies on the utilization of SCM has helped to minimize the permeability in concrete mixes by altering the pore structure and hence, increasing the resistance of concrete due to the chemical attacks. In fact, replacement of cement with SCM not only enhances the strength and durability of concrete, but also helps in sustainable

development and reduces the concrete production cost. However, the percentage of replacement is very important to get the desired performance of concrete. The excessive amount of SCM replacement can lower the compressive strength of concrete. Other than that, the major hurdles to bring SCM to the global industry are the low quality of the local waste materials in certain regions, technical issues including complexity in the mix design and transforming the design to a mature system towards clean concrete (Jin & Chen, 2013; Wesseling & Van der Vooren, 2017). The novel formulation of cement and concrete mix design are necessary, alongside the technical guidelines for the production and usage (Imbabi, Carrigan, & McKenna, 2012).

The chemical reaction when SCM is added causes calcium hydroxide $Ca(OH)_2$ to be depleted and transformed into secondary calcium silicate hydrate, CSH gel, resulting in the reduction of larger pores into finer pores. Hydrated cement paste consists of 70% of CSH gel, 20% $Ca(OH)_2$, 7% sulpho-aluminate, and 3% of secondary phases. The cavities will appear in the cement matrix if there is the existence of weak products produced from hydration process. The weak product is soluble in water and has low strength. Therefore, supplementary cementitious material has the potential to become a good pozzolanic material and gives positive effects to concrete (Memon, Radin, Zain, & Trottier, 2002; Papadakis, Antiohos, & Tsimas, 2002).

2.3.1 Palm Oil Fuel Ash (POFA) and its present state in concrete

The core of the Malaysia economy comes from the palm oil plantations, due to huge plantation areas and the country being among the top producers of the world's palm oil. Malaysia is now the second world's biggest in the import and export of palm oil industry. The palm oil plantation area in Malaysia has increased from 54,000 in 1960 to 5.39 million hectares in 2014 which accounts for around 39% of the global production and 44% of world's exports (Awalludin, Sulaiman, Hashim, & Nadhari, 2015). The palm oil industry is now facing a problem due to the excess of huge quantities of liquid and solid biomass wastes such as empty fruit bunches mesocarp fibre, palm kernel shell, oil palm trunks, oil palm leaves, palm oil mill effluent and oil palm fronds that are produced from the palm oil processing. Malaysia has forecasted that the supply of solid biomass waste will reach about 85-111 million tons and 70-110 million tons of liquid biomass waste by the year 2020 (Malaysia Innovation

Agency, 2013). These wastes have been utilized in a number of ways such as being used as soil fertilizers, paper production, furniture, electronics, packaging and in the automobile industry (Sumathi, Chai, & Mohamed, 2008). A single palm fruit bunch produces about 23% of empty fruit bunches, 21% of palm oil, 14-15% of mesocarp fibres, 6-7% of kernels and 6-7% of shells (Dalimin, 1995). Approximately 5% from these solid biomass wastes are produced in the form of ash from the combustion process of dried mesocarp fibres and empty fruit bunches at 800–1000 ° C to generate the electricity at mills. Approximately 10 million tons of POFA is produced per year and the amount will continue to increase with time (Safiuddin, Abdus Salam, & Jumaat, 2011). This type of ash, namely palm oil fuel ash (POFA) has a low potassium content to be used as soil fertilizer thus, it was dumped near the mill creating environmental pollution and potential threat to human life (Tay, 1990; Tay & Show, 1995). There is an urgent need for the industry to find a new way to reduce this waste material in landfills. Studies have proven that the POFA can be utilized as supplementary cementitious material (SCM) and played an effective role in producing strong and durable concrete (Awal & Hussin, 1999, 2011; Awal & Abubakar, 2011; Chandara, Mohd Azizli, Ahmad, Saiyid Hashim, & Sakai, 2012; Jaturapitakkul, Tangpagasit, Songmue, & Kiattikomol, 2011; Kroehong, Sinsiri, & Jaturapitakkul, 2011; 2017). POFA can be classified as highly pozzolanic supplementary cementing material in accordance with ASTM C618 due to the cumulative mass of oxide components. The term pozzolan, as defined by the American Society for Testing of Materials (ASTM) is ”a material containing silica or silica alumina which possesses few or no cementitious properties but will chemically react with calcium hydroxide at normal temperatures to produce compounds possessing cementitious properties”. Pozzolanic materials are able to reduce the weak product in concrete and enhance calcium silicate hydrate (CSH) as well. The weak product gets used up from the reaction between silica oxide content in the pozzolanic materials with calcium hydroxide, $Ca(OH)_2$ from the hydration process to produce more calcium silicate hydrate (C-S-H) gel which helps to enhance the strength of concrete (Bamaga, Ismail, Majid, Ismail, & Hussin, 2013).

Research on POFA was started by Tay (1990) where the author studied the potential of POFA in enhancement of compressive strength at 3, 7, 14 and 28 days. The replacement of cement with POFA ranging between 10 to 50% showed the

decrease of the compressive strength in POFA concrete. Tay (1990) discovered that the type of POFA used in his study can be categorized as a weakly pozzolanic material. In 1995, Tay & Show (1995) furthered the previous study with an engineering feasibility study of POFA in concrete. By using the same replacement of POFA, the study found similar results to that of previous research where the lower compressive strength exhibited by POFA concrete was at 10-50% of POFA replacement compared to that of plain concrete. The study suggested that POFA could be a potential supplementary cementitious material in small percentage replacements, (10%) due to high range of loss on ignition value of POFA.

In another study, the unground POFA with 20% replacement has shown a good match to that of plain concrete in compressive strength and durability properties (Sumadi & Hussin, 1995). Different replacement percentage was used in a study by Awal & Hussin (1997) where 40% of POFA replacement showed the greatest improvement in compressive strength of concrete containing POFA and positive result in alkali silica reactions. Since then, many experiments were done to utilize POFA as supplementary cementitious material to produce normal, high strength, high performance, self-compacting and aerated concretes. 20% of ground POFA was used to replace the cement to produce high strength concrete and it showed the highest strength (Sata, Jaturapitakkul, & Kiattikomol, 2004).

In the year 2011, an observation was made to determine the behaviour of concrete containing POFA to time-temperature test. POFA reduced the heat release from the hydration process and delayed the time of the peak temperature (Awal & Hussin, 2011). Other than normal and high strength concrete, POFA has also been used to produce self-compacting concrete. In the study of the effects of POFA on fresh properties of self-compacting concrete, 10-15% of POFA can be used to improve the resistance to segregation and provide adequate filling and passing ability of concrete (Safiuddin et al., 2011). Another finding worth to be mentioned is that the high volume replacement of POFA can lead to a decrease in the compressive strength of concrete. In a study by Awal & Abubakar (2011), they discovered the range of replacement 50-70% of POFA was found to lower the early strength and later strength of compressive and tensile strengths than that of plain concrete. However, this study is only valid for the 45 µm size of POFA.

The study of pozzolanic reactivity of the ground and treated POFA has been conducted to determine the effects of massive concrete in preventing the volume change and micro-cracks that has resulted from the thermal stress. Both types of POFA are good and have potential in preventing the issue related to thermal stress. However, due to the removal of unburned carbon, the treated POFA was found to have greater pozzolanic reactivity than the ground POFA. The study showed that the major issue of the unburned residue left in the POFA can lead to low pozzolanic reactivity of the POFA (Chandara et al., 2012). Another study that had also used treated POFA was conducted by Zeyad, Johari, Bunnori, Ariffin, & Altwair (2012) to enhance the strength of high strength concrete. The study showed that at high replacement of treated POFA of up to 60%, the concrete achieved strength at a later age and had exhibited lower strength at early age.

In 2016, a study of the effect on the engineering and fluid transport properties of high strength concrete utilizing treated and untreated POFA was conducted. The fineness, unburned composition and the amount of the pozzolanic minerals is an important criteria to attain better performance of high strength concrete in terms of the transport properties and strength as well. The findings revealed that the 20% of ground POFA provides bad effects on the permeability performance of high strength concrete and up to 60% of ultrafine treated POFA can promote better performance in terms of strength and transport properties (Zeyad, Megat Johari, Tayeh, & Yusuf, 2016).

Zeyad, Megat Johari, Tayeh & Yusuf (2017) discovered that the heat treatment of POFA at a temperature of 500 º C and the fineness are factors that improve the pozzolanic reactivity, but this also depends on the pozzolanic minerals in POFA. The study also found that the phase of the volatility of carbon occurred at the temperature of 300 º C whereas the conversion state could happen at 650 º C. These factors are important to improve fresh and hardened properties of high strength concrete at substitution level ranging between 20 to 60% and thus could have a potential to be utilized in marine and corrosive environments. In 2018, (Alsubari, Shafigh, Ibrahim, & Jumaat, 2018) supported this finding by studying the microstructural characteristics of paste containing treated POFA.

The heat treatment and the grinding process have been proven to enhance the physical and chemical composition of concrete. Study also showed how the analysis

of the thermogravimmetry analysis (TGA) displayed the remaining weak product formed by the treated POFA during the hardening whereas the field emission scanning electron microscopy (FESEM) showed how the CSH gel looks in the form of floc-like and fibrous-like in the paste containing treated POFA. The latest development of POFA in concrete is to utilize POFA with other abundant waste from the carpet industries, for example, carpet fibres. The combined effect of these two wastes decreased the workability and the compressive strength of concrete. However, a notable development was observed in the enhancement of tensile strength of concrete containing these two wastes (Mohammadhosseini, Tahir, Mohd Sam, Abdul Shukor Lim, & Samadi, 2018).

2.3.2 Significance of fineness of POFA

Activation techniques are very important to enhance the pozzolanic reactivity of supplementary cementitious materials and help to achieve greater strength of concrete either at an early or later age (Shi & Day, 2000). There are many types of activation techniques that can theoretically be found in the literature such as mechanical, chemical, water-controlled, supplementary cementitious materials-controlled and curing/temperature activation (Liew, Sojobi, & Zhang, 2017). The mechanical activation technique should be explored in relation to the fineness of POFA because it involves the reduction of the particles size of supplementary cementitious material using mechanical milling/grinding in order to increase the specific surface area and particles fineness (Sajedi & Razak, 2011). The method was proven effective due to the larger surface area, which would accelerate the hydration reaction. However, the sufficient activation time requires trial and error of different milling stages in order to determine the optimum activation time that provides the best mechanical performance (Liew et al., 2017).

The enhancement of the pozzolanic reactivity has opened the door for researchers to study the effects of POFA fineness on concrete properties. In the study conducted by Sata et al. (2004), the raw POFA with coarser particle size had weakened the microstructural characteristics of concrete and the ground POFA with median particle size about 10 μm improved the pozzolanic reactivity and the filling ability function of high performance concrete. In 2007, POFA size of 11 μm was used to study the effects of minimizing the superplasticizer dosage in producing the high strength

concrete. The utilization of ultrafine POFA is effective compared to silica fume in minimizing the dosage of superplasticizer (Sata, Jaturapitakkul, & Kiattikomol, 2007). In the study of durability properties of concrete, 20% replacement of POFA with 7.4 µm size is able to provide a higher resistance in marine environment and improved compressive strength of concrete at the later age of 90 days (Rukzon & Chindaprasirt, 2008).

Other than that, in a study conducted by Tangchirapat & Jaturapitakkul (2010) they found that the small size of POFA (10 µm) reduced water permeability, and enhanced the durability of high strength concrete. However, the ground POFA was significantly increased the compressive strength of concrete at later age and showed reduction pozzolanic reaction at the early age (Jaturapitakkul et al., 2011). Further investigations have revealed that ultrafine POFA with median size of 2 µm has good potential as a pozzolanic material due to greater enhancement of compressive strength of concrete. The high fineness of POFA has led to higher replacement of POFA that can be used up to 30% of the cement weight (Kroehong et al., 2011). By using the same size POFA, Zeyad et al. (2012) revealed that the workability of high strength concrete as well as the compressive strength increased at later age. In recent years, the high volume of POFA was used as a supplementary cementitious material in concrete. However, the study concluded only that 10% of POFA with size of 45 µm can improve the compressive strength of normal concrete at 90 days and 20% of 10 µm POFA can be used in producing self-compacting concrete (Islam, Mo, Alengaram, & Jumaat, 2016; Ranjbar, Behnia, Alsubari, Birgani, & Jumaat, 2016).

2.4 Nanotechnology in Concrete

The study on the contributions of nanotechnology in concrete have been conducted since the early millennium, due to the increased need in the concrete industry that demands for superior properties for concrete. Nanotechnology has been applied in concrete industry due to the physical properties of the nanomaterials in generating denser binding in cement matrix (Ghafari, Costa, & Júlio, 2015). The term nano concrete is the utilization of nanoparticles in concrete, where the size is less than 500 nm (Aitcin, 2000). Nanoparticles act as a superb filler and binding medium in the cement matrix, which produces denser concrete. Due to the combined effects of fillers and the reaction in the hydration process, the nanomaterials in concrete are able to

enhance the strength and durability of concrete (Birgisson, Mukhopadhyay, Geary, Khan, & Sobolev, 2012; Nik & Bahari, 2012).

In high performance concrete mix, high strength and better durability properties are two important characteristics to be observed. Conventionally, the silica fume is normally utilized to develop high performance concrete. Due to the high cost of silica fume and difficulty of getting stock, better alternatives for silica fume had been developed by utilizing the nanomaterials, which mimics the action of silica fume (Yu, Spiesz, & Brouwers, 2014). The examples of nanomaterials that has been used in concrete are nano titanium oxide, alumina, silica, carbon nano tube and polycarboxylates (Adak, Sarkar, & Mandal, 2014; Massa et al., 2014; Morsy, Alsayed, & Aqel, 2011; Navarro-Blasco et al., 2014). Other than improving the strength and durability of concrete, nanomaterials can also accelerate the initial hydration process and reduce the porosity of concrete (Mondal, Shah, Marks, & Gaitero, 2010). The positive implementation of nanotechnology in concrete has been discussed in various research, and one of them is by utilizing nano silica in concrete (Yu, Spiesz & Brouwers, 2014).

The findings have found that the nano silica is able to improve the packing effect in the concrete matrix, while reducing its porosity. In another study, using the same nano particles, researchers found that the workability, compressive strength and the resistance to water penetration were also improved (Singh, Karade, Bhattacharyya, Yousuf, & Ahalawat, 2013). The nanoparticles are also proven to contribute towards high strength at early age and improve the durability properties at low dosage consumption (Du, Du, & Liu, 2014). The exposure of the nanomaterials in concrete industry has raised concerns in terms of health effects due to capability of the ultrafine particles (Srikanth & Asmatulu, 2013). Hence, there are several protective measures suggested by researchers and social agencies. The protective measures include the use of the ventilated enclosures equipped with high efficient particulate air filters, a proper procedure for cleanup processes, medical screening and the use of personal protective equipment when dealing with the particles (European Comission, 2013; Nasterlack, Zober, & Oberlinner, 2008; OSHA, 2013).

2.4.1 Production of nanomaterials

Since nanomaterial has become a highly effective material in enhancing the strength and durability of concrete, the idea to produce the nanomaterial become an area of great interest for the researchers. Various methods have been developed to produce the nanomaterials. In the early development of nanoscience, was a challenging task to synthesis the nanomaterials due to high cost and the complexity of the process. Two methods were used by the previous researchers to produce nanomaterials such as bottom up and top down approaches. The top down approach is mainly to reduce the particle size from a larger size to nano size while the original properties are maintained. The bottom up approach, also called molecular nanotechnology or manufacturing, is the process of assembling or self- assembling of the engineered materials from atom or molecular component. Figure 2.1 shows how the two approaches produce nano-structured materials. The selection of the two approaches is based on suitability, cost and expertise of dealing with nanomaterial properties (Sanchez & Sobolev, 2010).

The nano-sized cementitious component can be produced using the top down approach (high-energy milling). This method has been widely used among all top down approaches. High energy milling has also been used to boost the early strength of concrete and to improve the supplementary cementitious material efficiency (Awal & Shehu, 2013). In the context of this study, nanomaterials from agricultural waste such as nano palm oil fuel ash was produced using the top down approach to enhance the workability and early strength of concrete (Lim et al., 2015). The approach is preferred due to the availability of the high-energy ball mill and easy modified, and there is no chemical or electronic devices required. For the grinding, the ball mass to powder ratio of 5 to 10 is preferred and typically used (Yadav, Manohar Yadav, & Pratap Singh, 2012).

However, the researchers are concerned with the drawbacks of using the top down approach where the final product of nanoparticles is not consistent. Hence, some modifications of milling technique is required to improve the quality, such as the type of grinding media, speed of grinding, number of grinding media and the type of jar being used (Abdoli, Farnoush, Asgharzadeh, & Sadrnezhaad, 2011; Saleh, Ibrahim, & Salman, 2015; Yadav et al., 2012). Other than that, milling also can contribute to the contamination of the particles. This issue occurs if the steel milling chamber and balls

are used. Low energy milling has less contamination effect; in fact, the impact is often negligible. Besides that, short milling time and self-coating of the balls with milled material are suggested to reduce the contamination (Suryanarayana, Ivanov, & Boldyrev, 2008).

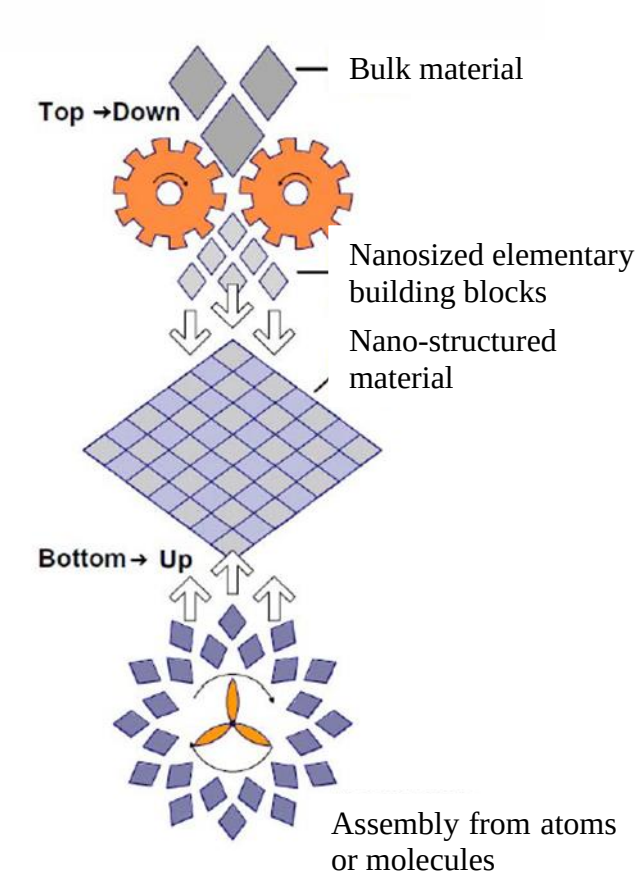

Figure 2.1: Two approaches in nanotechnology (Sanchez & Sobolev, 2010)

2.4.2 Utilization of nano POFA in concrete

Several studies have been conducted to produce POFA up to nano scale as supplementary cementitous material. Due to the potential of nanoparticles in improving the strength and durability of concrete, nano POFA has been utilized to produce high strength concrete. A study conducted by Johari, Zeyad, Muhamad Bunnori, & Ariffin (2012) proved the potential of ultrafine POFA in improving the workability of concrete. However, the study also revealed that the high strength concrete containing 60% of ultrafine POFA had a reduced compressive strength at early age (1, 3, and 7 days) but experienced enhanced strength at 28 days up to 95

MPa. Except for the early strength, the concrete with the ultrafine POFA had improved the transport properties such as rapid chloride permeability, water permeability, porosity, gas permeability and initial surface absorption.

In a study by Rajak, Majid, & Ismail (2015) they revealed that there is significant improvement in microstructure of cement paste containing micro and nano POFA fillers. The strength of cement at an early age mainly depends on the tricalcium silicate produced. However, the appearance of nano POFA was found to be very reactive due to the higher surface area and energy, thus acting as nano filler to accelerate cement hydration. In addition, the increase of fibrous-like of calcium-silicate-hydrate gel showed a dense and highly compact structure in the cement matrix. Other than that, the microstructure analysis showed a reduction of weak product in the cement paste because it was used in the pozzolanic reaction to produce secondary calcium-silicate-hydrate gel. Therefore, the study concluded that nano POFA has the potential to produce a dense and closely packed microstructure in the cement paste compared to the Portland cement and micro POFA due to the good filling effect and enhancement of pozzolanic reaction (Rajak et al., 2015).

Meanwhile, Lim et al. (2015) conducted another study on utilization of nano POFA. The findings revealed that by utilizing a high volume of nano POFA of up to 80%, the compressive strength of the mortar improved at a later age. The study also found that the utilization of nano POFA could reduce the heat of hydration. A similar study was conducted by Abutaha, Abdul Razak, & Kanadasan (2016) to find out the effect of utilizing high volume nano POFA in cement mortar. Both studies concluded that the incorporation of high volume of nano POFA could improve the strength of concrete with the qualities of being more sustainable. However, more studies are required on the area of durability of high performance concrete utilizing nano POFA to know more about the potential of nano POFA in concrete research area.

2.5 Mix Design and Optimisation Analysis

Previous practices of concrete mix rely upon historical data or guidelines (Simon, 2003). These approaches need trial batches where the results are analysed by adjustment of the concrete mix proportions and final concrete acceptance. However, both approaches do not provide concrete mix design optimisation and holistic design.

Therefore, the statistical approach is proposed as a tool to determine the optimum mix design. Statistical approach or design of experiments or statistical factorial are the tools to obtain the optimum concrete mix design. Conventional methods requires selecting one starting mix proportion and adjusting the mix by through a trial and error method to achieve optimal solution. For each concrete mix, the trial batches cover a chosen range of proportions based on the established statistical procedures. Then, trial batches are implemented, test specimens are cast and tested and the outcomes are analysed. The analysis includes an empirical data fitting for each performance criteria. Each response can be represented by one reliable predictive model or an equation. In addition, this method also allows for the optimisation of any property, subject to constraints of other properties (Muthukumar & Mohan, 2004; Simon, 2003; Sonebi & Bassuoni, 2013; Soudki, El-Salakawy, & Elkum, 2001; Xiaoyong & Wendi, 2011).

The mix design optimisation allows the ability to reduce the number of adjustments of mix proportions (typically, only one variable can be adjusted). Thus, the proportions can be prioritized to only the most preferred choices based on the designers' preferences. This process saves time and makes the concrete mix more cost effective, and thus can be utilized by the concrete industry without having to produce repeat the trial batches to get the most optimal choices (Simon, 2003). One good example of statistical experimental design procedure that has been commonly used in the industrial engineering world is response surface methodology (RSM). The RSM method was used to evaluate the relationship among the key concrete constituents on concrete performance criteria to optimize the mix design. The method is a technique that includes developing, improving, and optimizing the process and mix. The application of the RSM in concrete mix design is still limited in use in many projects. Therefore, the United States Federal Highway Administration (FHWA) has proposed an extensive study on the application of statistical method in concrete mix design (including RSM). The findings revealed that RSM is a valuable and effective tool to be used in concrete mix design. Other studies that have used RSM has also proven the effectiveness of the RSM in evaluating the effect of conventional concrete proportions on compressive strength (Cihan, Güner, & Yüzer, 2013). In other studies, RSM was proven useful and beneficial in the development of concrete mix design containing pozzolanic materials and non-conventional concrete. The following studies applied RSM in the concrete mix design and this design was proven effective in producing

self-consolidating concrete (Alqadi, Mustapha, Naganathan, & Al-Kadi, 2012); pervious concrete (Sonebi & Bassuoni, 2013); foamed concrete (Nambiar & Ramamurthy, 2006); concrete containing paper mill residue (Mohammed, Fang, Anwar Hossain, & Lachemi, 2012); concrete containing recycled-aggregates (Lovato, Possan, Molin, Masuero, & Ribeiro, 2012) and concrete containing fly ash (Kockal & Ozturan, 2011).

2.5.1 Mix proportion of high performance concrete

A mix proportion of high performance concrete involves a low water cement ratio and porosity. The design becomes more complicated because it involves additional materials such as superplasticizer and supplementary cementitious materials (fly ash, silica fume, etc.). A concrete is categorized as high strength if the compressive strength is more than 40 MPa and the addition of superplasticizer makes the desired concrete strength possible to achieve 60-120 MPa. Conventionally, an engineer needs to practise designing a concrete mix based on the experience (Islam, A-Mattarneh, Zain & Basri, 2002). Mehta & Aitcin (1990) defined high performance concrete as concrete that exhibits high strength, high workability and high durability. Neville & Aitcin (1998) explained that the term high performance concrete could only be used if the concrete has high compressive strength. Now, the term high performance concrete is more than just high strength. In 2005, the American Institute Committee (ACI) has revised the definition of high strength concrete to be concrete mixtures with a specified design strength of 55 MPa or more. For high performance concrete, ACI defines high strength concrete as "*a concrete meeting special combinations of performance and uniformity requirements that cannot always be achieved routinely using conventional constituents and normal mixing, placing, and curing practice*" (ACI Committee 363, 2005).

Recently, in another study, researchers claimed that the basic theory for high performance and ultra-high performance concrete is the same, where the reduction in the porosity and water-binder ratio and the range of compressive strength for high performance concrete is between 40-100 MPa (Shi et al., 2015; Yu et al., 2014). The common guidelines used for high strength mix design are based on De Larrard and the American Concrete Institute 363R (ACI). The method uses a mathematical approach in designing, without employing too much figures and tables as in the method of

British Standard (de Larrard & Sedran, 1994; de Larrard & Sedran, 2002). The mixing procedure is very important to select the best good mix proportion for concrete. The wrong mixing step will end up with small particles such as silica fume to form pellet balls and this makes the concrete mix dry when the small powder of additives and water get entrapped in the mixture (Sohail et al., 2018).

Additives such as carbon fibers or supplementary cementitiuos materials are important items in high performance concrete mixes to achieve high strength. To break the pellets, a longer mixing time is required. Therefore, the superplasticizer needs to be added after mixing the dry ingredients for certain amount of time. The role of the superplasticizer in the mix is to enhance the workability of concrete. In the concrete mixing process, the preferred method is to get the dry ingredients into a homogenous mixture before adding water or superplasticizer (liquid form). If the superplasticizer is in powder form, it should be added with the dry ingredients at the early stages. The reason behind this is to reduce the water demand by letting the small particles fill the pores between larger particles at the early stage. This way, there is water content available for the hydration process and this enhances workability (Sohail et al., 2018).

A review of the literature on the mix design of high performance concrete revealed that the methods of proportioning studied targets on achieving high strength while also satisfying the durability criteria. De Larrard (1990) developed a method to improve the workability while designing a mix of high strength concrete. The study revealed that the dosage of admixture and packing structure of aggregates influenced the water-binder ratio on workability. Empirical relation was also established to predict the effects of silica fume on the fresh properties of concrete. In a different study, de Larrard & Sedran (1994) developed a design mix of ultra-stable high performance concrete for a bridge deck by using the concept of particle packing dense aggregates. The concrete has a low binder content, low drying shrinkage, low autogenous and lower heat of hydration. However, the findings of the study show that the concrete had a longer setting time due to the high carbon content of the fly ash and high dosage of high range water reducer (de Larrard & Sedran, 1994).

Other recommendations for proportioning of high performance concrete is from Mehta & Aitcin (1990). The authors claimed that the two important criterion in proportioning of high performance concrete are impermeability and dimensional

stability. The high permeable concrete is due to the formation of bleed channels at the interfacial transition zone especially between coarse aggregates and cement paste. They suggested improving the permeability by reducing the maximum aggregate size and using the lowest water-binder ratio while other requirements are complied. While, Aitcin (1998) also developed a mix design for high performance concrete, based on ACI committee 211 due to the wide acceptability in the industry and the mix design combined empirical and mathematical calculations according the method of absolute volume (Aitcin, 1998).

Other studies that have developed a mix proportions for high performance concrete are summarized in the Table 2.1. Several state-of-the-art mixture proportions of high performance concrete are based on what have been developed since late 1990. The bar graph shown in the figure is arranged based on the low to high value of the compressive strength of concrete. The information on waste-binder (w/b), compressive strength (f_c') and slump are stated at the bottom of x-axis. The box above the bar graph for each mix states the percentage of fiber content (if applicable). The mix proportions in the table is given in unit of kg/m^3. In the table below, Knickerbocker (2005) conducted a study to produce a high performance concrete that exhibits high compressive strength by using water-binder ratio of 0.25. The study obtained a compressive strength of about 71.5 MPa due to the replacement of cement with fly ash of about 50%. In another study, Miller (2001) revealed that the compressive strength of high performance concrete can achieve up to 86 MPa with a low water binder ratio of 0.30. Additives like silica fume and small amounts of coarse aggregates are the reasons that contribute to the higher strength. Other studies on mix proportions for high performance concrete are also conducted by El-Dieb (2009), de Larrard & Sedran, (2002), Le Roy, Le Maou, & Torrenti (2017), Megat Johari, Brooks, Kabir, & Rivard, (2011), Ozbay, Gesoglu, & Guneyisi (2011).

Table 2.1: Mix proportion of high performance concrete

References (w/b, f'_c in MPa/ slump in mm)	C	FA	CA	SF	GGBS	F	W	HRWR
Miller (2001) (0.32, 62, 127-178)	446	845	993.3	32.6	-	-	153.1	7.4
(de Larrard & Sedran, 2002) (0.43, 78.1, 160)	408	608	912	39	-	-	190	5.6
(Knickerbocker, 2005) (0.5, 71.5, 203)	443	578	1139	-	-	448	222.8	0.4
(El-Dieb, 2009) (0.24, 85, >600)	900	1293.6	-	135	-	-	252	-
(Megat Johari et al., 2011) (0.28, 58 , 200)	180	675	1125	-	270	-	126	14
(Ozbay et al., 2011) (0.28, 99, 150)	550	863	740	-	-	-	151.3	21
(Le Roy et al., 2017) (0.28, 98 , NA)	412	861	1037	41	-	127	13.7	-
*C: cement, FA: Fine aggregates, CA: coarse aggregates, SF: silica fume, GGBS: ground granulated blast slag, F: fly ash, W: water, HRWR: high range water reducer (unit: kg/m^3)								

2.5.2 Design of Experiment (DOE)

Design of experiments (DOE) was first proposed by Ronald A. Fisher as a methodology to solve his work when dealing with agricultural application. Since then, many researchers have used statistical methods to develop various DOE techniques (Fisher & Mackenzie, 1923). Using DOE based on RSM, concrete mix can be obtained with a narrow set of experiments without the need of including all possible combinations experimentally (Muthukumar, Mohan, & Rajendran, 2003). DOE is an approach based on statistic methods in order to determine the outcome with less effort while saving time, cost and resources (Myers, Montgomery, & Anderson-Cook, 2016). In a research done by Upasani & Banga (2004), the benefits of DOE has been highlighted, which include developing significant models with relevant variables and responses, reducing the number of trial batches, revealing the effect between the

variables and possessing the ability to determine the optimum mix design within the range of test data. Various designs were studied to implement the response surface methodology. A RSM is a set of DOE methodologies that assists the researcher to have a better understanding while simultaneously determining an optimal response.

A central composite design (CCD) and Box-Behnken design are two main types of designs based on RSM. The most common use of DOE in determining the functional interaction between the variable and response is CCD (Aldahdooh, Muhamad Bunnori, & Megat Johari, 2013b). CCD also has the capability to estimate quadratic or second-order models for each response without having to complete a three-level factorial experiment, hence reducing the number of trial batches (Berry, Kappes, & Kappes, 2015). This type of DOE is suitable in the case of sequential experimentation because the design includes information from a correctly planned factorial experiment. Unlike the other designs (Box-Behnken), CCD has more experimental design with five levels per variable and is less expensive while allowing researchers to obtain all the significant variables. CCD can include runs from a factorial experiment and all variables whether at maximum or minimum settings. In addition, factorial design like CCD is able to do mapping for a region of response surface, show the interaction between the variables and responses in order to determine the optimum variables with optimal responses and select the operating conditions to meet desired performances (Alqadi et al., 2012). On the condition that CCD has the features of perpendicularity and is rotatable, it can produce more reliable solutions to solve the response surface problems (Berry et al., 2015).

The CCD is based on two factors which are shown in the Figure 2.2. It can be divided into three categories of experimental points. The first category is the center point where the coded values is (0, 0). The second category includes the corner point, namely factorial points. The number of corner points will affect the number of variables set in experimental design by using formula 2k where, k is the number of variables. The variables in coded value can be written as (±1, ±1). The third category is the axial points. The points are located at the distance of $\alpha = 1$ or $\alpha = \sqrt{k}$ from the center point. Those points can be written as (±α, 0) and (0, ±α), the number of points related to the number of variables by using formula 2k. Axial points can be extended further than ±1 therefore, there is a chance to run the tests for higher order curvature

effects. Another advantage of axial points is the model precision of the fitting data is not affected by the direction but only by the distance from the center point due to the chosen value of α that makes the design rotatable (Kutner, 2005). The general equation for response function of k variables is written in Equation 2.1.

$$E(Y) = \beta_0 + \beta_1 X_1 + \cdots + \beta_k X_k + \beta_{11} X_1^2 + \cdots + \beta_{kk} X_k^2 + \beta_{12} X_1 X_2 + \cdots + \beta_{k-1,k} X_{k-1} X_k + e \qquad \text{Equation 2.1}$$

Where:

X_1, …. , X_k : the research variables

β_1, …, β_k: the regression linear main effect coefficients,

β_{11}, …, β_{kk}: the regression quadratic main effect coefficients,

β_{11}, β_{12}, β_{13}…, $\beta_{k-1,k}$: the regression interaction effect coefficients

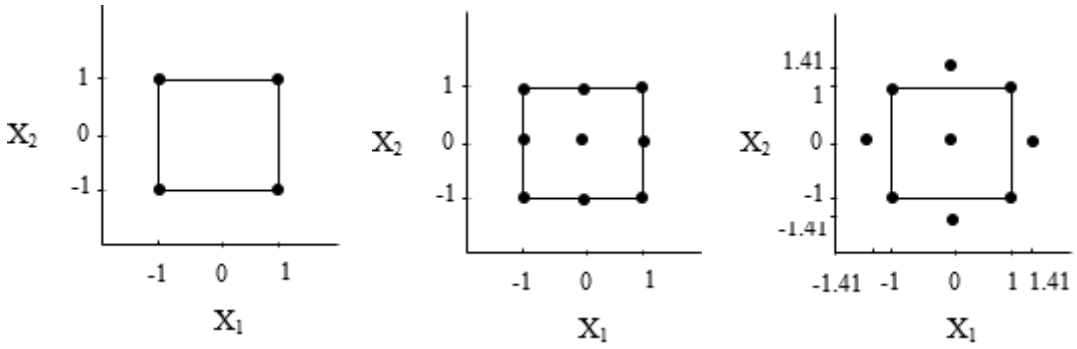

2^2 Central Central

Figure 2.2: CCD schematic examples for two variables (Kutner, 2005)

If the number of coefficient increases with the k value the the number of trial batches needed to obtain the interaction between the variables must also increase. The list of number of runs required for different number of variables is tabulated in Table 2.2.

Table 2.2: Run and variables required for CCD experiment

Number of variables	Factorial points	Axial points	Center points	Center point for rotatability	Total
2	2	4	3	1.4142	12
3	8	6	3	1.6818	18
4	16	8	3	2.0000	28
5	16	10	3	2.0000	30

The selection of appropriate types of model was obtained using an iterative model fitting process that includes the analysis of variance (ANOVA) and least square method (Simon, 2003). The polynomial model suggested is considered significant and represents the response surfaces. This approach is considered logical and straightforward in the development and validation of prediction models for factorial designs. From ANOVA, the sequential F-tests for each of the model are performed. The highest significance models will be chosen and evaluated based on probability. If the probability < 0.05, the model is considered significant. The probability decreases in value as the F-statistic increases. F-statistic evaluated from the data exceeds the theoretical value. The next step after the model is chosen is to perform the lack of fit test where the residual error is compared with the pure error obtained from replication.

The process of verification takes place that involves the summary statistic of each model. The calculation provides root mean square error, predicted R-squared, R^2, adjusted R^2, and prediction error sum of squares (PRESS). A good predictive model consists of low value of square root, mean square error, high value predicted R^2 and low value of PRESS. The root mean square error represents the standard deviation obtained from the experimental error. The R^2 is a measure of the amount of variation explained by the model and R^2 will be adjusted based on the number of parameters in the model. The predicted R^2 measures the amount of variation in the new data explained by the model. Prediction error sum of square (PRESS) is the total sum of the differences between the estimated and actual values of all design points. The PRESS value indicates if the efficiency of the model fits the data in the design and the value

evaluated from the estimation of each point using all the design points except the current estimation model (Simon, 2003).

2.5.3 Optimisation analysis using Response Surface Methodology (RSM)

The optimisation process takes place after the fitting of models is done. The optimisation process can be divided into two types; numerical or graphical. Optimisation allows simultaneously optimizing one or more goals. Numerical optimisation is more practical for the cases that involves a few responses that need to be optimised (Simon, 2003). The goals requires the user to define the optimisation criteria whether it is within the specific range, maximum or minimum or at specified target value. The goals can also be assigned by weightage; one to five, where one is the least important and five is the most important. Targeted performances and goals weights are combined in an overall desirability functions. Figure 2.3 presents examples of the common types of desirability functions.

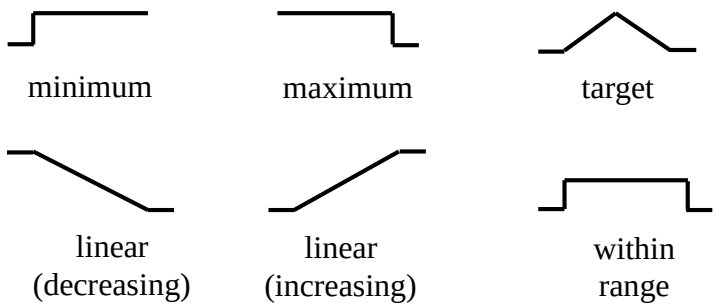

Figure 2.3: Types of desirability functions that commonly used (Simon, 2003)

The commercial software *Design Expert* can be used to determine simultaneous optimisation of multiple responses obtained from the factorial experimental plan. The software is designed to search for the greatest overall desirability functions. The individual desirability function for each goal criteria is denoted as d_i and all the goals are combined to obtain overall desirability function, D. To achieve that, one of the methods that is commonly used is geometrical mean of desirability functions as shown in Equation 2.2 (Derringer and Suich, 1980; Simon, 2003).

$$D = (d_1 \cdot d_2 \cdot \ldots \cdot d_n)^{1/n} \qquad \text{Equation 2.2}$$

Where,

$d_1 \ldots d_n$: the individual desirability functions for each response

n: number of goal criteria preferred for optimisation

D: overall desirability function

Recently, a few studies were conducted in the development of statistical models and optimisation analysis in proportioning of concrete mix. This method of proportioning has been used for many types of concrete such as high performance, self- compacting concrete, ultra-high performance concrete and porous concrete. Kockal & Ozturan (2011) applied the RSM using Design Expert Software in optimizing properties of fly ash aggregates for suitability in high strength lightweight concrete. The study was able to establish the interaction between the variables (binder type, binder content, temperature) and measured responses (water absorption, specific gravity). Methods of historical data technique was used to develop the models statistically and the models predicted closely agreed with the experimental data. Hence, the RSM was performed successfully in optimising the properties of fly ash aggregates and can be utilized for further study.

Zaitri, Bederina, Bouziani, Makhloufi, & Hadjoudja (2014) presented the mixture design modelling of high performance concrete utilizing local materials from Laghouat, Algeria as cement substitutions. The cement content and content of the cement substitutions were chosen as the variables to study the influence of those additions on the properties of high performance concrete. Statistical analysis was performed to develop models that exhibit the best results. The mixture design method was an effective approach to establish the effects of the cement substitutions and fresh and hardened properties of high performance concrete either through binary or ternary system. By using visual tools of optimisation, the graphical representations were found to be a simple tool in order to relate the variables and specific performance criteria.

Jimma & Rangaraju (2015) developed statistical models using RSM to establish the interaction between superplasticizers, viscosity modifying admixtures, and set-retarding admixtures with paste properties of pervious concrete. Concrete producers can use the mathematical models once the models are appropriately

established. The technique also reduces the number of trial batches needed to finalize the mix proportioning. The measured responses include film-forming ability, flowability and film-drying time. The mathematical equations and response surfaces for each response were established and the study included a few case studies discussing the data using the developed models. Hence, the study recommended this method to concrete producers to design good quality and pervious concrete mix.

Matos, Maia, Nunes, & Oliveira (2018) suggests the best model that provides the best combination of constituent materials in order to minimize shrinkage and heat of hydration of self-compacting high performance concrete (mortar phase). White Portland cement, metakaolin and limestone fillers were used as variables and design of experiments (DOE) was applied to establish the effects between the variables and fresh mortar properties. The study concluded that DOE is the best approach to develop models, and to understand and optimize the mortar phase of self-compacting high performance concrete for applications with multiple response requirements. Other than that, all the other variables were found have significant interaction with the mortar properties in finding an impermeable concrete.

2.6 Effect of POFA on fresh and hardened properties of concrete

Abundant amounts of POFA from the palm oil biomass results in environmental issues if not treated directly (Thomas, Kumar, & Arel, 2017). Academicians and researchers are encouraged to assist the cement and construction industry by highlighting the potential of the POFA in concrete and cement production. The studies on utilization of POFA as supplementary cementitious material in producing many types of concrete are presented in this sub chapter. The effect of POFA on fresh and hardened properties of concrete are also discussed. The below discussion also highlights the advantages and disadvantages of utilizing POFA in concrete.

2.6.1 Effect of POFA on workability

Fresh properties such as workability is an important parameter to ensure the quality of concrete in terms of strength. If the concrete is able to obtain 100%

compaction, then maximum strength can be achieved. Workable concrete can be explained as the ease of fresh concrete to be mixed, handled, compacted and molded. A number of studies were done to determine the fresh properties of concrete with utilization of POFA as the supplementary cementitious material. Tay (1990) found that the workability of concrete reduced with increased amounts of POFA in comparison with control concrete. Concrete with high volume (50%) of POFA replacement achieved 120 mm of slump height, which was lower than that of control concrete. The size of POFA used in the study was 150 μm. In producing high strength concrete, Tay & Show (1995) added superplasticizers to achieve the slump height that ranged between 175 mm and 225 mm in producing high strength concrete. However, the results of high strength concrete with POFA also showed reduction in workability with increasing POFA replacement, compared with the control concrete. The study revealed that no segregation occurred during preparation of concrete and the compacting factor was in good category, which ranged between 0.93 and 0.97.

In 2007, Sata et al. (2007) revealed that the surface feature of POFA contributed to the reduction of workability. The porous structure of POFA caused more water absorption hence, reducing the water content required for lubrication. Therefore, the concrete with POFA needed higher amounts of superplasticizer to maintain the slump height reading compared to the control concrete. Increasing the amount of POFA percentage demanded higher amounts of superplasticizer. To achieve 200 mm of slump height, 8.5 kg/m^3 was needed for concrete with POFA while lower dosage was required for the control mix to achieve the targeted slump. In another study, the unground and ground POFA were studied to find out the effects on the workability of concrete. Due to the factors of higher surface area, angularity, irregularity and porous structure, ground POFA required more water than that of unground POFA to achieve certain slump heights (Chindaprasirt et al., 2007). In this study, the rice husk ash was also used as a supplementary cementitious material to achieve the slump height between 60 to 90 mm. Like POFA, rice husk ash also demands more dosage of superplasticizers to achieve the targeted slump due to the shape and surface features of both particles.

Due to the physical properties of POFA that affects the workability of concrete, one study investigated the utilization of low volume of POFA as supplementary cementitious materials in concrete. The concrete mix with 15% of POFA replacement showed the same pattern as previous studies where the lower compacting factors and

lower slump height readings were obtained in comparison with the control mix. In another study, Hussin, Ismail, Budiea, & Muthusamy (2009) refined the size of POFA to 10 and 45 μm with the cement replacement percentage of 20% in determining the workability of concrete. The authors concluded that the reduction in the workability was due to the higher surface area of POFA. Awal & Abubakar (2011) proved that workability improved at satisfactory level with an additional 2% of superplasticizer by cement weight. The high volume of POFA (50%, 60% and 70%) without superplasticizer had a lower slump with increasing POFA amounts and the slump reading was observed to be moderate by adding the superplasticizer (Awal & Abubakar, 2011).

In 2012, Megat Johari, Zeyad, Muhamad Bunnori, & Ariffin (2012) used ultrafine POFA with median particles about 2 μm as pozzolanic material with cement replacing levels of 20%, 40% and 60% for the production of high strength concrete. The ultrafine POFA reduced the water demand of the concrete and improved workability as the amount of POFA increases. The authors explained that the reasons were due to the strong binder paste volume since POFA has a lower specific gravity. Besides, the ultrafine POFA reacted as a coating and filled the gap between the aggregates, thus providing better lubricant. By utilizing the ultrafine POFA, the study found that low amounts of superplasticizers are needed in the design mix of concrete (Megat Johari et al., 2012; Zeyad et al., 2016). Noorvand, Ali, Demirboga, Noorvand, & Farzadnia (2013) also utilized finer particles to achieve the desired workability. Unground POFA was combined with nanosilica in concrete to reduce water demands and improve workability. The nanosilica in concrete containing unground POFA was able to reduce the dosage of superplasticizers in order to improve workability.

Utilization of ultrafine particles was observed in improving the workability of concrete. Hence, recent study conducted by Aldahdooh, Muhamad Bunnori, & Megat Johari (2013a) concluded that by utilising ultrafine POFA particles that has lower unburned carbon content and lower loss of ignition (LOI) value, the workability of concrete increased. The authors observed that the replacement of cement with ultrafine POFA indicated the reduction in the binder paste content due to lower specific gravity of ultrafine POFA than that of Portland cement. In addition, the high value of LOI indicates the porous structure of POFA (cellulose) resulting in the increase of the water

content in the fresh mix concrete. Other methods to improve workability is by using Na_2O in ultrafine POFA and ground blast furnace slag. Yusuf et al. (2014) found the positive results of the impact of H_2O/Na_2O molar ratios on the workability of concrete. However, there was negative impact on the compressive strength of the concrete (Yusuf, Megat Johari, Ahmad, & Maslehuddin, 2015).

Another study was conducted to combine POFA as supplementary cementitious material with the oil palm shell treated as coarse aggregates. Muthusamy, Zamri, Zubir, Kusbiantoro, & Ahmad (2015) studied the benefits of other biomass waste from palm oil production on the concrete properties. The authors observed that the range of POFA between 20-30% achieved the desired workability and compressive strength (Muthusamy et al., 2015). In other type of concretes like lightweight concrete aggregates, as the POFA increases, the workability decreases. Islam et al. (2016) reported that the pattern of reduction in workability can be seen if the POFA replacement level is more than 30%. If the replacement level is less than 20%, the slump will not be affected in producing lightweight aggregate concretes (Islam et al., 2016). Salami, Johari, Ahmad, & Maslehuddin (2016) suggested adding water in the fresh mix of concrete containing POFA to improve workability. The slump height was observed as zero in concrete containing POFA in the study conducted by Bashar et al. (2016). The authors concluded that the high volume of POFA replacement level and the porous structure of POFA were the two factors that contributed to high quantity of water absorption by POFA, resulting in the reduction in workability.

Recent studies have added fiber in concrete containing POFA to improve the workability of concrete. Studies conducted by Awal & Mohammadhosseini (2016) revealed positive impacts in improving workability by utilizing 20% of POFA as cement replacement and incorporating waste carpet fiber (0.25% to 1%). The increase of 25 mm in slump height was recorded in concrete mix containing POFA with additional 1% of fiber. Due to lack of studies in the area, the study recommended the combination of POFA with other plastic materials like fiber to improve the fresh properties of concrete. In other studies, Islam et al. (2016) concluded that the concrete containing fibers resulted in a reduction in workability due to the large surface area hence, absorbing more water in fresh concrete mix.

2.6.2 Effect of POFA on Concrete strengths (compressive, splitting tensile, flexural)

Compressive strength is the most important property of hardened concrete. Other hardened properties like tensile strength, abrasion resistance, pull-off strength, modulus elasticity etc. are dependent on compressive strength. There are many factors affecting compressive strength of concrete such as mix design, type of material used, curing condition etc. In this study, the review of literature discussed the effect of utilisation of POFA as a supplementary cementitious material on compressive strength of concrete. The investigation started by Tay (1990) and Tay & Show (1995) studied unground POFA in concrete with 10-50% replacement and concrete with water-binder ratio of 0.6 and mix ratio (1:2:4). The study recorded that the compressive strength of concrete decreased as the POFA amount increased. The descending pattern of compressive strength development can be seen from early to later ages. Therefore, in the study the authors suggested to replace cement with POFA of about 10% to avoid significant effects at long-term age (1 year).

Hussin and Awal (1996, 1997) have attempted to improve the compressive strength of concrete by utilizing a value of 40% of ground POFA. The study reported that 40% of ground POFA as supplementary cementitious material in concrete gained 30% of compressive strength of concrete without any adverse effects in comparison with the control concrete. In a study by Sata et al. (2004), the high strength concrete containing 20% POFA showed the highest compressive strength at the age of 28 days. The study compared the compressive strength of POFA concrete with the control concrete and concrete containing 5% of condensed silica fume. In parallel with their study, a research done by Tonnayopas et al. (2006), showed reduction in the compressive strength of concrete at the early age, however at the later age, the strength exhibited was higher than that of control concrete. The study concluded that the optimum value of POFA replacement content was 20%.

In aerated concrete, Abdullah, Hussin, Zakaria, Muhamad, & Hamid, (2006) revealed that their finding had a similar pattern in normal and high strength concretes as the amount of POFA replacement increased. However, the authors recommended that POFA can be utilized within the range of between 10-35% in aerated concrete to obtain satisfactory results in compressive strength. The surface feature of POFA was

found to be significant in enhancing the compressive strength of concrete. Studies conducted by Jaturapitakkul, Kiattikomol, Tangchirapat, & Saeting (2007) and Tangchirapat, Saeting, Jaturapitakkul, Kiattikomol, & Siripanichgorn (2007) found that the reduction in the compressive strength was due to the porous particles of unground POFA that increased the water demand in concrete. The high porosity of unground POFA resulted in the increase of water absorption hence, lowering the compressive strength of concrete.

A study by Chindaprasirt et al. (2007) stated that POFA has to satisfy standards provided by ASTM C618 before it was used in concrete as supplementary cementitious material. The criteria such as the chemical components, especially the major oxide components and loss on ignition (LOI) value were found to be very important in enhancing the compressive strength of concrete. The study confirmed the potential of POFA as a supplementary cementitious material, and the fineness of POFA used was 8 µm. The study concluded that 20% of POFA exhibited higher compressive strength of concrete while 40% had lower strength. However, at later age of 90 days, at all replacement levels of POFA, POFA concrete enhanced slightly in compressive strength of concrete. Tangchirapat et al. (2007) extended the study by increasing the fineness until size of 7.4 µm. The findings showed concrete containing 20% of fine POFA exhibited higher compressive strength at the age of 90 days. The study concluded that original size of POFA or larger size of POFA had lowered the compressive strength of concrete compared to traditional concrete, however, higher compressive strength at the age of 90 days observed in concrete containing finer POFA.

The enhancement of compressive strength at an early age can be found in a study conducted by Sata et al. (2007). The concrete containing 10% of ground POFA exhibited higher compressive strength than that of control concrete. The authors explained the satisfactory micro filling ability and pozzolanic activity of the ground POFA that leads to earlier maturity of concrete to produce strengthening gel hence, increasing its compressive strength (Isaia, Gastaldini, & Moraes, 2003). Safiuddin, (2008) added that both filler effect and pozzolanic activity of POFA also depends on the water binder ratio of concrete. Efficiency of POFA as pozzolanic material will increase in both mechanisms that incorporates water binder ratio. Tangchirapat,

Jaturapitakkul, & Chindaprasirt (2009) and Hussin et al. (2009) found similar patterns as previous studies and reasoned that the positive impact of POFA concrete is due to high content of silica oxide present in POFA and the high fineness of POFA particles. Both factors helped the pozzolanic reaction to produce more calcium silicate hydrate hence, providing greater enhancement in the compressive strength of concrete.

A study of the combination two supplementary cementitious materials was conducted by Rukzon & Chindaprasir (2008) where the study used a blend of fly ash and POFA with a ratio of (1:3) in producing concrete. At the later age, concrete containing both pozzolanic materials exhibited higher compressive strength by 102-106% compared with the control concrete at replacement level of about 10-20%. However, slow pozzolanic reaction was observed at an early age. In 2010, raw POFA and 45 μm POFA were utilized in concrete to determine the effects on the compressive strength. Under the same replacement level and water binder ratio, concrete containing 45 μm POFA was observed to get double the compressive strength of the concrete containing the raw POFA. The study concluded that the higher surface area of pozzolanic material affected the pozzolanic reaction, and also the compressive strength of concrete (Awal & Nguong, 2010). Using the same size of POFA, Sata, Jaturapitakkul, & Rattanashotinunt (2010) concluded that the optimum replacement level of POFA was 10% due to higher compressive strength of observed concrete than that of the control concrete.

The reason that contributes to the early strength of compressive concrete is due to the void filling ability and at a later age, the enhancement of compressive strength was attributed to the silica oxide in the POFA that reacted with the calcium hydroxide in formation of secondary calcium silicate hydrate gel. The pozzolanic reaction improves the binding paste between the binder and aggregates which then enhances the compressive strength of concrete (Sata et al., 2010). Jaturapitakkul et al. (2011) added that the high fineness of POFA also helped to increase the pozzolanic reaction due to the how well the arrangement of the fine particles fit within the binder matrix. However, the study claimed that the pozzolanic reaction of POFA was still low at the early age but it has increased with time.

In the next study, the utilization of ultrafine and nano materials were utilized to enhance the compressive strength of concrete. Johari et al. (2012b) found that by

having ultrafine POFA in high strength concrete, the compressive strength yielded higher values at a later age. The compressive strength reduced at an early age. The ultrafine POFA used in the study was 2-µm in size with low loss on ignition (LOI) value of 2.53%. Noorvand et al. (2013) conducted a study involving nano materials in concrete. The study used unground POFA and nano silica to improve the mechanical properties of concrete. The findings concluded that the nano materials in concrete containing unground POFA had caused overall enhancement in the compressive strength of concrete. The authors reasoned that the finding was due to the attribute of the ultrafine particles that are concentrated near the paste and aggregates matrix interface hence, improving the internal bonding and particle packing density (Stroeven & Stroeven, 1999).

Another study that also used nano material was conducted by Lim et al. (2015). The nano POFA with the size of 1-100 nm was utilized in producing cement mortar. The replacement 80% of nano POFA in cement mortar exhibited higher strength at the early and later ages compared with the control mortar. The utilization of nano POFA as the binder and filler in cement matrix relies on the forces of Van der Waals that results in higher strength (Stroeven & Stroeven, 2001). In addition, the potential of nanoparticles that has high surface energy could modify the "wall effect" hence, forming an intact matrix around the aggregates (Ollivier, Maso, & Bourdetted, 1995).

Tensile strength is one of the hardened properties of concrete. The test of splitting tensile is a test to measure the tensile strength of concrete. Beside compressive strength, tensile strength is also amongst the most important properties of concrete. It is essential for the concrete design to be subjected to transverse and shear effects to reduce cracking problems, enhance the shear strength and minimize the failure in tension in parts of the concrete structure (Singh & Siddique, 2012). The splitting tensile strength is normally about 9-10% of the compressive strength. From the literature, a few studies were conducted to obtain data on the significant effects of concrete containing POFA on the splitting tensile strength. High strength concrete containing 20-30% of POFA had shown slightly higher values compared to the control concrete at the age of 90 days. Sata et al. (2007) observed that the highest splitting tensile strength was found in the concrete that contained 20% of POFA, as the higher fineness of POFA enhanced the filling effect and increased the rate of pozzolanic

reaction. The study also found that the pattern of the tensile strength was similar to the compressive strength pattern.

In another study, Eldagal (2008) found negative effects of the POFA utilization in concrete on tensile strength. The POFA concrete exhibited lower tensile strength than that of the control concrete. Hence, the author recommended that further investigation is needed in order to examine the significant effects of POFA on the tensile strength of concrete. Awal & Nguong (2010) also discovered the same patterns where the tensile strength of concrete containing up to 50% of POFA was found to be lower compared to the control concrete. However, at the low volume replacement percentage (10-20%) of POFA, the tensile strength of concrete exhibited was higher than that of the control concrete at the age of 90 days. The reason for the increment of tensile strength was due to the small size of POFA (10 μm) used in the study. The high fineness of POFA can be attributed to the pozzolanic reaction with cement to produce strengthening gel hence, increasing the splitting tensile strength. Awal & Abubakar (2011) meanwhile discovered that the tensile strength of concrete containing POFA was lower at the early ages but exhibited strength higher at the later ages.

Jaturapitakkul et al. (2011) found that the splitting tensile strength of high strength concrete containing ground POFA had improved using POFA. The replacement between10-30% of POFA with the water-binder ratio of 0.28 were recorded to enhance the splitting tensile strength of concrete containing POFA. In other types of concrete, utilization of POFA in foamed concrete also improved the splitting tensile strength than that of control concrete at the age of 90 days. Lim, Tan, Lim, & Lee, (2013) stated that the increase can be explained by the formation of secondary calcium silicate gel from the pozzolanic reaction, which makes the bonding stronger. Similar findings were found by Altwair, Johari, & Hashim (2012) who discovered that there were improvements of about 9% in the splitting tensile strength of concrete containing POFA in comparison with the control concrete at the same water binder ratio of 0.4.

A study of flexural strength of concrete containing supplementary cementitious material was found very limited in the literature (Al-Mulali, Awang, Abdul Khalil, & Aljoumaily, 2015; Safiuddin et al., 2011). By definition, flexural strength is a measure to resist failure in the bending of an unreinforced concrete. The modulus of rupture or

flexural strength of concrete is approximately 10-20% of the compressive strength and is generally determined by three four point loading or center point loading (Dash et al., 2016). In 2008, a study by Eldagal (2008) observed that the high strength concrete containing 10 and 45 μm of POFA with the replacement of 20-30% had lower flexural strength than that of the control concrete. The results found that at the replacement level of 30%, the flexural strength reading was close to the value recorded in the control concrete. Hence, more research is needed to obtain data about the flexural capacity of concrete containing POFA.

Altwair, Johari, & Hashim (2012) obtained data on the flexural strength of engineered cementitious composites (ECCs) utilizing ground POFA. To measure the flexural performance of ECC mixes, the four-point bending test was conducted. The parameters that varies in ECC were water-binder ratio and POFA amount. The results showed that the flexural strength decreased as the water-binder ratio increased, and at the ratio of 0.38, the flexural strength of concrete containing POFA showed higher values than that of the control ECC mix at all ages. For the case of lightweight foamed concrete, Lim et al. (2013) observed that at a later age (90 days), the foamed concrete containing 10% of POFA showed greater improvements in terms of flexural strength compared to the control concrete. The author justified that the increment was due to density of concrete microstructure due to production of secondary strengthening gel produced from the pozzolanic reaction of the silica in the POFA.

Bashar et al. (2016) conducted a study to determine the flexural tensile of the hybrid concrete containing high volume POFA, and palm oil shell as coarse aggregates with the addition of steel fibers. The improvement in the flexural tensile strength recorded increments of about 7-18% compared with the control concrete. The higher surface area of particles in the hybrid concrete enabled a stronger bond with the binding matrix and provided higher resistance to cracks. Other studies using carpet fibers and POFA in concrete was also observed to improve the flexural tensile strength. The study by Awal & Mohammadhosseini (2016) explained that the carpet fibers acts as crack arresters and resisted the crack face from separating during stretching, hence providing higher energy absorption capacity. In contrast, Ranjbar et al., (2016) showed in their study that flexural strength of self-compacting concrete containing POFA had reduced in comparison with control concrete. The decrease of the flexural

performances can be explained by the high content of porous structure of POFA in the concrete which caused the stress concentration and weakened the binding between aggregates and paste.

2.6.3 Effect of POFA on Water absorption

Functional properties of concrete such as water absorption is one of the sources of damage in concrete structure. Fluids movement through concrete not only flows through the pore system but also by diffusion and absorption. A concrete with high water absorption value is susceptible, and this effects the durability of the reinforcement embedded in the concrete (Ithuralde, 1992). Several studies have been conducted to investigate the effects of POFA in concrete on water absorption properties. The first study was conducted by Tay (1990) using unground POFA with 150 μm size in concrete to determine the effects on water absorption. The water absorption of concrete containing 50% of POFA was recorded to be higher than that of control concrete. Hence, the author concluded that water absorption increased with the increasing amount of unground POFA. In 1995, Tay and Show also revealed the same pattern was replicated similar to those in the previous study. The authors explained that the reason behind the higher water absorption was due to higher content of unground POFA that has porous structure. Thus, the author ended the study with a recommendation to reduce the water absorption by using ground POFA due to its satisfactory micro filling ability and higher rate of pozzolanic reaction (Tay & Show, 1995).

By using the same procedure according ASTM C642-13, Chindaprasirt et al. (2007) revealed in their study that 10% replacement of POFA in high strength concrete exhibited lower water absorption coefficients compared with the control mix. The finer particles used in the study modified the pore in the concrete matrix thus reducing the porosity of concrete. In the study of other types of concrete, Hadi and Hanizam (2015) reported that the foam concrete containing POFA exhibited lower water absorption and lower sorptivity than that of the control concrete if the POFA replacement is less than 25%. A higher content of POFA disrupts the pore structure of foam concrete causing the concrete paste to be more porous. In a study by Lim et al. (2015), the authors revealed that by utilizing a high volume of POFA with nano size, the mortar

used had lower water absorptions due to less porosity in the binder paste than that of the control mortar.

Recent studies by Zeyad et al. (2016) presented a study where they utilised high volume replacement (20% – 40%) of ultrafine POFA in high strength concrete that exhibited lower rate of water absorption than that of the control mix. At early and later ages, POFA concrete was observed to be lower in water absorption compared with the control concrete. The trend that was observed was that the higher content of ultrafine POFA, the lower rate of water absorption of concrete, hence resulting in greater reduction in porosity. However, there was negative impact on the water absorption and porosity because the POFA used contained a high amount of unburned carbon. The authors concluded that the pore filling effect has played an important role in pore refinement and total volume of pores (Chandara et al., 2010; Cordeiro, Filho, & Fairbairn, 2009). In addition, the study implied that the use of ultrafine POFA contributed to the tortuosity of the microstructures due to the high fineness of particles and its low value of loss on ignition (LOI).

In contrast, Liu, Alengaram, Santhanam, Zamin, & Mo(2016) in a study conducted to improve the water absorption, found that the addition of foam in concrete containing POFA increased the water absorption beacuse the foam created more pores in the concrete matrix. The negative effects of the water absorption also leads to the reduction of compressive strength of concrete. Islam et al. (2016) also showed the same pattern in the study of concrete containing 10-70 % of POFA. The test conducted at 28 and 90 days showed that the water absorption rose as the amount of POFA increased due to the delay of hydration causing the concrete to absorb more water. The study conducted by Lau, Teo, & Mannan (2017) proved that other factors which contributed to reduction of water absorption is high temperature of sintering in lightweight concrete containing POFA and lime treated sewage sludge. Recent studies done included a study combining POFA with other wastes like waste polypropylene (PP) in producing concrete. The study by Mohammadhosseini, Yatim, Sam, & Awal (2017) demonstrated that the combination of both waste in concrete reduced water absorption and penetration of chloride.

2.7 Effect of POFA on Concrete Durability

According to ACI Committee 201 (2008), the durability of concrete lies in its resistance to deteriorating factors which may come through from unknown factors in the concrete itself, or which exists in the exposed environment. A concrete is considered durable if it possesses minimum porosity, is resistant to alkali-silica reaction, has better corrosion protection ability, reduces heat of hydration and improves resistance to aggressive chemical attacks (Hossain, Karim, Hasan, Hossain, & Zain, 2016).

2.7.1Resistance to Chloride penetration

The rapid chloride penetration test is a method to determine the performance of concrete to resist the chloride ions penetration. The major issue related to chloride penetration is corrosion in reinforced concrete structure. The ingress of chloride ions into concrete will increase due to seawater wetting and air drying exposure (Hong & Hooton, 1999; Taylor, 2017; Thomas, 1996). Rukzon & Chindaprasirt, (2008) conducted a study of chloride ion ingress into concrete. Their findings showed improvements of POFA mortar to resist chloride penetration due to pozzolanic reaction causing the lower porosity in concrete. Hussin et al. (2009) also found similar findings in high strength concrete containing POFA compared to the control concrete. The higher fineness of POFA that accelerated the pozzolanic reaction has made the concrete denser and exhibited lower chloride penetration depth. In another study, the improvement of POFA concrete in resisting chloride ions penetration was due to the improvement of the bonding interface between the paste and aggregates. Hence, it was determined that the POFA concrete was denser and impermeable (Bamaga, Ismail, Lee & Budiea, 2010).

In high strength and high workability concrete containing POFA, Chindaprasirt, Chotetanorm, & Rukzon (2011) found that the concrete containing 20-30% of POFA showed a higher reduction of total charge pass than that of control concrete. The findings revealed that as POFA increases, the chloride penetration decreases. This study recommended 20% of POFA be used in high workability concrete to reduce the dosage of superplasticizer due to the high cost. At the early age of concrete, Johari et al. (2012b) revealed that concrete containing high volumes

(60%) of ultrafine POFA increased the total charge passed. The authors claimed that due to high replacement of POFA, concrete will have low cement content and experience dilution effect that will delay the pozzolanic reaction at the early stage. In addition, the pozzolanic reaction requires sufficient weak product from the hydration process to react with POFA. Therefore, the study found that the longer curing period, the better the ability to reduce the total charge passed for concrete containing POFA. This can be seen at the age of one year, the POFA concrete had almost negligible total passed charges compared with the control concrete. The study concluded that the ultrafine POFA in high strength concrete was able to improve the durability properties in terms of chloride penetration.

Recent studies conducted by Zeyad et al. (2016) showed the high total charge passed at the early age in the control concrete and concrete containing ground POFA. The less dense microstructural attribute of both concretes caused the concrete to be susceptible to chloride penetration. The study observed that ground POFA was has high compositions of unburned carbon. Thus, the study concluded that an adequate curing period was important to avoid the delay of pozzolanic reaction and too much of unburned carbon could cause adverse effects on resistance of concrete in seawater environment. Similar findings were observed by Kroehong, Damrongwiriyanupap, Sinsiri, & Jaturapitakkul (2016) in that the utilisation of POFA in cement paste was found to reduce the chloride penetration depth and had lower coefficient of chloride diffusion than that of control cement paste. The reason behind this was due to the higher fineness POFA used in the cement paste thus decreasing the chloride penetration and chloride diffusion coefficient.

In the production of POFA, POFA can be obtained from kernel shells and empty fruit bunches. A study conducted by Mujah (2016) investigated the two types of POFA in mortar and its resistance towards chloride ingress. The results showed that the POFA mortar yielded a lower charge pass compared to the control mortar. The total charge passed showed a decreasing pattern as the amount of both POFA types increased. The best quality POFA can be seen in mortar containing POFA from empty fruit bunches with the highest reduction of total charge passed. The amount of C_3A in POFA was found to be very important in the study as it leads to the chloride chemical binding effects. The study highlighted that the decrease of free chlorides is due to the

formation of calcium chloro-aluminates and calcium chloro ferrites from the reaction between the C_3A and C_4AF (Mujah, 2016).

2.7.2 Resistance to chemicals attack

The presence of sulphuric acid can be found in waste from chemical based industry, ground water, or in acid rain, etc. The structures built that surround those environments are exposed to aggressive environments where degradation can take place. This type of durability issue affects the performance of the concrete structures. It increases the maintenance cost and affects the life cycle performance of the structure. In comparison with sulphate attack, the attack from sulphuric acid is more risky due to the dissolution effect by hydrogen ions when acid reacts with the calcium hydroxide which will weaken the concrete paste structure (Bassuoni & Nehdi, 2007).

Awal & Hussin (1999) found that by immersing POFA concrete in 5% hydrochloric acid solution, the mass loss was recorded to be lower than that of the control concrete after 1800 hours. The visual inspection showed that the surface condition of POFA concrete was better due to the densified microstructure from the pozzolanic behaviour of POFA and low lime content of POFA. Due to the low lime content of POFA, the amount of weak product, calcium hydroxide was less thus strengthening gel was produced. This resulted in a dense concrete with low porosity that led to a lesser attack of acid in the internal part of concrete. However, the study did not differentiate between the effects of unground and ground POFA or the optimum content of POFA. The authors concluded that due to limited research carried out, further research was required to investigate the effects of POFA on durability properties especially with regards to resistance to acid attack.

Low amounts of calcium oxide in POFA plays an important role in determining if concrete has better resistance against acid attack. Živica (1999) proved the role of calcium oxide in the production of calcium hydroxide, which was vulnerable to acid attacks that cause concrete deterioration. In geopolymer concrete, Ariffin, Bhutta, Hussin, Tahir, & Aziah (2013) investigated the resistance of concrete containing POFA and pulverized fuel ash (PFA) against 2% sulphuric acid for 18 months. The study observed that geopolymer concrete had less severe deterioration than that of control concrete as the time increased. After the period of exposure, in terms of mass

loss, the geopolymer concrete yielded only 8% as compared with control that had 20% of the mass loss. Severe deterioration can be seen in control concrete from the loss of compressive strength up to 80% than that of geopolymer concrete where the loss was recorded at only 35%.

A recent study by Alsubari et al. (2016) found that POFA concrete had more resistance against acid attack than that of control concrete. The penetration of acid into the internal part of POFA concrete was reduced because of the better surface condition and minimum empty voids observed on the concrete. The low amount of calcium oxide about 6% caused a low amount of weak product as well, which led to denser concrete. The weak product in hydration process is highly susceptible to chemical attacks and causes concrete deterioration. The latest study by Mohammadhosseini et al. (2018) showed that concrete containing 20% of POFA and carpet fibers exhibited a reasonable level of resistance against acid attack where the lowest mass loss and loss in compressive strength can be observed in concrete containing 20% POFA and 1.25% of carpet fibers.

Other factors that cause concrete deterioration is when the concrete is exposed to marine environment. The external sulphate attack is a serious problem affecting concrete durability due to the ability of sulphate ions to react with hydrated phase, thus causing the expansion, and cracking of concrete. The reaction forms free calcium hydroxide in cement, which leads to the formation of calcium sulphate and calcium sulphoaluminates that can increase the volume up to 227% of the original aluminates. The consequences of the reaction leads to the existence of ettringite and/or thaumasite, gypsum and results in disastrous effects such as loss of strength, spalling, cracking and other types of damage to concrete (Thomas et al., 2017). Several studies have been conducted to investigate the effects of POFA in concrete and its resistance to sulphate attack, and will be discussed below

Jaturapitakkul et al. (2007) studied the resistance of concrete containing POFA with varying sizes. The concrete was immersed in 5% magnesium sulphate for 24 months. The findings revealed that the concrete containing higher fineness of POFA exhibited less expansion. The higher fineness of POFA not only reduced the weak product but also acted as a filler to reduce the voids between aggregates and paste hence, leading to a denser concrete. Similar findings were found by Tangchirapat et

al. (2009) where they discovered that the expansion of the POFA concrete containing fine POFA decreased together with the loss in compressive strength. Therefore, the study concluded that 20% of fine POFA would give no adverse effects to concrete exposed to 5% magnesium sulphate solution.

Hussin et al. (2009) conducted a study on the resistance of concrete containing two different sizes of POFA in mortar bars to sulphate attack. The sulphate attack was simulated by immersing the concrete in 10% of sodium sulphate for 3 months. The findings show that the mortar which has higher fineness of up to 10 μm POFA yielded lower loss in compressive strength and expansion compared to the control mortar and mortar with 45 μm. The higher fineness increased the reactivity of the fine POFA to accelerate the pozzolanic reaction causing the densification of the matrix in the mortar and causing more resistance to sulphate attack. In another study by Tangchirapat et al. (2009), concrete containing POFA was immersed in 10% magnesium sulphate up to 180 days. The reduction in expansion and loss in compressive strength can be observed in concrete containing 10-30% of POFA compared with the control concrete. Tangchirapat, Khamklai, & Jaturapitakkul (2012) extended the study by increasing the amount of POFA and immersion period. The study found lesser expansion of concrete containing 20%, 35% and 50% POFA than that of control concrete after 9 months of exposure.

The authors reasoned the lower expansion of concrete containing POFA in immersion of sulphate was due to the amount of weak product and C_3A that decreased when the cement was replaced, hence, reducing the formation of gypsum and ettringite recrystallization. In addition, the authors explained that high fineness was also a significant parameter that may be responsible for the acceleration of pozzolanic reaction and reduction of pore structure (Tangchirapat et al., 2012). While Bamaga, Ismail, Majid, Ismail, & Hussin (2013) mentioned that the sulphate exposure was closely related to the sulphate ions and main oxide components in POFA. As the aluminum oxide and iron oxide component in POFA increases, the POFA concrete exhibits higher expansion in sulphate exposure.

A recent study by Yusuf (2015) combined the ultrafine POFA with slag in concrete and studied the effects of those concrete on resistance to sulphate attack. The study used a solution of 5% sodium sulphate and 5% magnesium sulphate for an

immersion period of 6 months. The difference between those solutions can be observed from high loss in compressive strength and mass loss in specimens that were immersed in sodium sulphate compared to magnesium sulphate. In the magnesium sulphate solution, white depositions of calcium sulphate could be seen on the surface of concrete specimens due to cation exchange while no deposit was observed in the sodium sulphate solution. In the latest study by Mohammadhosseini et al. (2018) they showed that in aggressive environments, the concrete containing low volume of carpet fibers and 20% of POFA exhibited lower expansion and loss in compressive strength than the control concrete. The control concrete specimens had higher expansion due to the high calcium oxide content.

2.7.3 Resistance to Water Sorptivity

In a durability study, sorptivity is a kind of moisture transport property and thus it is an important property to concrete durability. The sorptivity test is used to determine how water or other injurious agents penetrate the concrete. In addition, the test allows researchers to measure the quality of near surface concrete, which is one important index of concrete durability that is related to corrosion reinforcement (Dias, 2000). The coefficient of sorptivity is important to predict the service life of concrete and to improve the structural performance (Martys & Ferraris, 1997). Studieson sorptivity in concrete is very limited in the literature. Recent studies have shown improvements in sorptivity with increased amounts of POFA at certain water binder ratio. Islam et al. (2016) demonstrated that the sorptivity of the POFA concrete was exhibited lower at 90 days compared with those in 28 days. This occurrence showed that at prolong curing; the hydration process continues and reduces the pores connectivity. The findings also showed as the amount of POFA increased, the sorptivity value also increased due to the greater porosity that contributed to concrete sorptivity. This study corresponded well with the findings by Chindaprasirt et al. (2011) and Mo et al. (2016).

Other studies on concrete sorptivity conducted by Mohammadhosseini et al., (2017) showed similar findings where the lower sorptivity of concrete containing POFA and carpet fiber was exhibited at age of 90 days. The lower pozzolanic reaction of POFA can be observed at the early age of curing. The authors stated that the low value in sorptivity is related to greater porosity due to the POFA and fiber contents

added in the concrete hence increasing the voids and capillary pore. However, a denser microstructure of concrete was developed after a prolonged period.

In other combination of waste and POFA, Mohammadhosseini et al. (2018) showed that concrete containing waste metalized plastic fibers and POFA reduced the sorptivity value than that of the control concrete at the age of 90 days. The positive impactof the findings can be explained by high pozzolanic reaction of POFA; as the time increased the moist curing condition of POFA-based concrete yielded lower sorptivity value. In the latest study conducted by Lau, Teo, & Mannan (2018) they showed significant findings in terms of sorptivity from the concrete containing Posslite lightweight aggregates in comparison with the normal weight aggregates concrete. Posslite lightweight aggregates are made from lime-treated sewage sludge and POFA.The result showed that POFA-based concrete was comparable to the normal weight aggregate concrete (Lau et al., 2018).

2.7.4 Resistance to Corrosion of Steel Reinforcement

The corrosion of reinforced concrete structures has been a main factor that contributes to premature deterioration especially for structures exposed to a marine environment. There are important factors that causes corrosion to occur, mainly due to penetration of chloride and carbon dioxide on the steel's surface (Abdullah, Salamatinia, Mootabadi, & Bhatia, 2009). The chloride ingress is increased by the exposure cycle of air drying and seawater wetting (Hong & Hooton, 1999). The corrosion initiation leads to formation of the corrosion products such as iron oxides and hydroxides. Those products are normally deposited around the steel in the concrete causing the concrete to expand, spall and cause cracks in the concrete cover. The issue becomes crucial and is a major part of financial spending on infrastructure because it involves a high cost of repair (Song & Saraswathy, 2007). Therefore, it is very important to decrease the permeability of the concrete against corrosion to slow the penetration rate of oxygen, moisture and chloride to reach steel reinforcement.

One way to improve the durability of concrete is by decreasing the permeability is to utilize supplementary cementitious materials. The use of supplementary cementitious materials such as POFA, fly ash, silica fume, metakaolin, and ground granulated blast-furnace slag has been used in concrete to increase the time required

for corrosion initiation (Mangat & Molloy, 1992). The studies of utilisation of pozzolanic materials in concrete has remarkably improved the resistance of the reinforced concrete to corrosion. To monitor the corrosion performance of reinforced concrete structures, suitable methods and measures are required. Nowadays, corrosion measurements are able to provide complete information of changing conditions of structure in time (Elsener, Buchler, Stalder, & Bohni, 1999; Montemor, Simoes, & Ferreira, 2003; Saremi & Mahallati, 2002). There are several methods that involve electrochemical, destructive and non-destructive techniques available to determine corrosion rates, such as concrete resistivity measurement, accelerated corrosion test using impressed voltage, linear polarization resistance, electrochemical impedance spectroscopy (EIS) and Tafel plot extrapolation (Montemor et al., 2003).

The studies on the effects of POFA concrete on corrosion resistance to steel reinforcement are very limited. Rukzon & Chindaprasirt (2008) studied the resistance to corrosion of steel reinforcement in mortar with embedded steel. The corrosion evaluation was obtained from the open circuit potential (OCP) which gives general guidelines based on half-cell readings. The result showed that the utilisation of POFA in mortar can significantly improve the corrosion resistance. The embedded steel in mortar containing 20% POFA was recorded under the threshold limit of corrosion activity after 180 days' exposure. In another study by Lee, Song, Ann, & Ismail(2009), electrochemical techniques was used to determine the corrosion resistance exhibited by control and POFA concrete. The OCP reading of POFA concrete showed lower values than that of the control concrete which entails that there will be a lower probability of corrosion. The higher the polarization resistance exhibited by the steel in POFA concrete showed, the higher the corrosion resistance compared with the control concrete. Overall, the findings concluded that the POFA concrete showed superior corrosion resistance than that of control concrete. The same method and similar findings were also found by Yahaya, Muthusamy, & Sulaiman (2014). The study proved that POFA concrete indicated a better resistance against corrosion due to the enhancement of C-S-H gel that make the concrete denser.

Other studies were conducted by Chindaprasirt et al. (2011) that used accelerated corrosion test by applying impressed voltage to determine the corrosion resistance. The steel bars were embedded in high strength and high workability

concrete containing POFA. The specimens were subjected to impressed voltage of 12V. The reinforced concrete was immersed in 5% of sodium chloride, NaCl solution as shown in Figure 2.4 throughout the test. The result was monitored by recording the current output until the concrete start to crack. The time required for the concrete containing 30% of POFA was much longer than that of the control concrete. The results indicated that the existence of higher fineness POFA in concrete reduced the weak product and improved the corrosion resistance of concrete. In addition, the authors explained that the increase of the pozzolanic activity was also due to high silica content and high degree of reactivity of POFA. The study recommended that the optimum value of POFA replacement should be 20% to produce high strength and high workability of concrete. The 30% replacement required a high amount of superplasticizer which would increase the cost of mix production (Chindaprasirt et al., 2011).

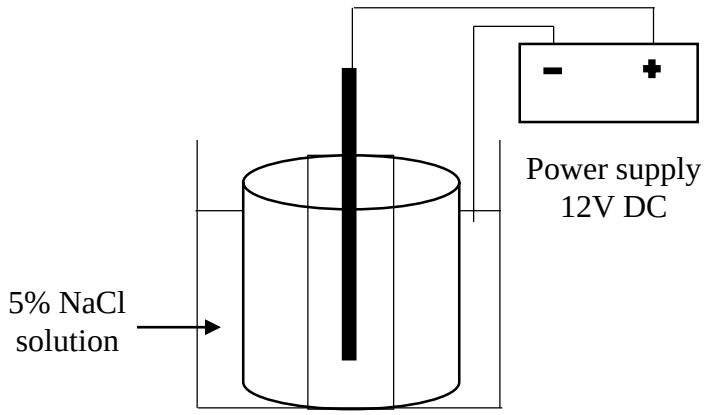

Figure 2.4: Accelerated corrosion test using impressed voltage (Chindaprasirt et al., 2011)

2.8 Summary of research gap

From this chapter, the review provides a few important issues to note, which leads to the aim of study. The increasing demand of cement is a cause of concern that leads to the utilization of supplementary cementitious materials in cement industry. Entering a modern era has caused cement to no longer be an important material because the cement of today is blended with other materials called blended cements. Since Malaysia is one of the world's top players in the palm oil industry, the solid biomass wastes from there has been used as supplementary cementitious materials. The review of the literature on the POFA showed that POFA concrete can provide

better strength for concrete at the later age. The micro size of POFA has the potential to achieve the strength properties of concrete. Then, high volume of nano POFA up to 80% was introduced to improve the workability and early strength of concrete. This will be an issue due to the challenging nature of producing nanomaterials and due to health concerns issued by OSHA. In addition, most of the researchers have been investigated the utilization of nano POFA in mortar and cement paste and it is worth noting that the study has not focusing on the durability properties of concrete. From the literature, there is no significant work has been done in the study of utilization of nano POFA on the durability study in terms of corrosion of steel reinforcement embedded in high performance concrete. Therefore, to fill the gap, the combination of micro and nano POFA are the main components examined in this study where the micro POFA and nano POFA will be used to examine significant effects on the mechanical and durability properties of high performance concrete.

The process of determining mix design parameters includes the dosage levels of binder that involves many trial runs of experiment conventionally. One good and commonly used technique in the industry-engineering world is Response Surface Methodology. From the review of the literature, there is lack of mathematical models to predict the mechanical properties of concrete containing supplementary cementitious materials. Thus, this study is also conducted to determine the optimum proportion of binders in the mix design of high performance concrete and develop mathematical models to establish the relationship between micro and nano POFA and measured responses (workability, compressive, splitting tensile and flexural strengths). To satisfy the optimum dosage of binders proposed from the optimisation analysis, the durability study will be assessed such as sorptivity, rapid chloride penetration test, chemical attack test and corrosion test.

Chapter 3

Materials and Methods

3.1 Introduction

In this chapter, the materials used to produce the high performance blended concrete are described. Several tests are explained in this chapter to determine the physical properties of the constituent materials. The use of palm oil fuel ash (POFA) in this study is discussed in different sizes starting from the raw followed by micro and then nano sizes. The production of POFA from the palm oil mill is presented in the flowchart and process of refining the waste particles is presented. There are two sizes of POFA used in this study, and in this chapter the steps to refine the particles are explained and the process of verification of the size are stated. The micro and nano POFA are characterized based on microstructural properties using x-ray fluorescence (XRF), x-ray diffraction (XRD) analysis, scanning electron microscopy (SEM) and fourier transform infrared (FTIR). In addition, the mixing procedure and curing method used for the concrete specimens are specified. The mix design of the high performance concrete was developed based on ACI Committee 211. The fresh properties of concrete were obtained by conducting slump test and the strength of concrete was evaluated based on compressive strength, splitting tensile strength and flexural strength tests. The experimental data and the variables used in the study were used in the development of the mathematical model using statistical approach. In order to determine the relation between the variables (micro and nano POFA) on the fresh and strength properties of concrete, the Central Composite Design under Response Surface Methodology was used. The software used to generate the models is the Design Expert Software. Based on the results of this software, the optimum mix design to predict the best responses can be developed. The durability study was done by conducting several durability tests including the corrosion resistance of steel reinforcement embedded in high performance blended concrete. All the test methods

were performed according to the relevant standards. The summary of the test program in this study is presented in the last sub chapter.

3.2 Preparations of Materials

The materials used in preparing the concrete specimens include Type I Portland cement, POFA in two sizes (micro and nano), local river sand and quarry dust as fine aggregates, crushed granite as coarse aggregates, superplasticizer and water.

3.2.1Cement

The cement used is Type I Portland Cement from the company Cahya Mata Sarawak Berhad. The specific gravity of cement is 3.15. The chemical properties are listed in Table 3.1 with the requirement of ASTM C150-12 (2012). The cement was kept in an air tight container inside Curtin's Civil Engineering lab, away from direct sunlight and moisture.

Table 3.1: Chemical properties of cement from Cahya Mata Sarawak

Test Item	Cement (%)	ASTM C150-12 (Cement type I)
SiO_2	20.0	-
Fe_2O_3	3.27	-
Al_2O_3	5.66	-
CaO	62.52	-
MgO	1.21	6 Max
SO_3	2.47	3 Max
LOI	2.86	3 Max
Na_2O	0.11	-
Free Lime	1.65	-
Insoluble Residue	0.3-0.5%	0.75

3.2.2 Aggregates

The coarse aggregates used in this study is crushed granite from a local source with maximum nominal size of 10 mm. The selection of aggregates with the optimum size was in accordance with Mehta & Monteiro (2014) and Maholtra & Mehta (1996). The grading of the aggregates conformed to ASTM C 33-16. The aggregates used were in a saturated surface dry condition during the mixing process. For fine aggregates,

local river sand was used. The grading of the river sand was not according to the limit stated in ASTM C33-16. Further discussion of the grading analysis will be discussed in the next chapter. The quarry dust was also used and combined with the river sand to form fine aggregates. All the materials used in this study were obtained from local suppliers.

3.2.2.1Tests on Aggregates

There are several tests conducted to determine the bulk density, specific gravity, water absorption, aggregates crushing value and sieve analysis to determine the physical properties of aggregates. These properties are important and will be used in the mix design process of concrete mix.

3.2.2.1.1Water absorption and specific gravity of aggregates

Specific gravity and absorption of coarse and fine aggregates were obtained according to ASTM C127-15 and ASTM C128-15 standards, respectively. The specific gravity or relative density of aggregates is based on the calculation of ratio weight of aggregates to the weight of equal volume in water. The normal range of specific gravity for the coarse aggregates is between 2.4 and 3.0. For the coarse aggregates, the aggregates were immersed in the water for 24 hours. The aggregates are then removed from the immersion and the water at the surface of aggregates was wiped off. The weight of coarse aggregates in saturated surface dry condition was recorded. Then, the weight of aggregates suspended in water was recorded. Finally, the aggregates was dried to constant weight in the oven at a temperature of 110 ºC and the weight of oven dried aggregates was recorded. The calculation of the specific gravity in saturated surface dry, apparent and water absorption of coarse aggregates can be calculated using

Equation *3.1*-Equation 3.3, respectively.

$$\text{Specific gravity} = \frac{W_2}{W_2 - W_1} \qquad \text{Equation 3.1}$$

$$\text{Apparent specific gravity} = \frac{W_3}{W_3 - W_1} \qquad \text{Equation 3.2}$$

$$\text{Absorption} = \frac{W_2 - W_3}{W_3} \times 100\% \qquad \text{Equation 3.3}$$

Where, W_1 is weight of aggregates suspended in water, W_2 is weight of saturated surface dry aggregates in air, W_3 is weight of oven dried aggregates.

For the fine aggregates, the method used was according to ASTM C128-15 standards. The procedure is the same as above, the fine aggregates was immersed in water for 24 hours. Then, to get the state of saturated surface dry for fine aggregates, a dryer was used. The saturated surface dry condition of fine aggregates can be checked using a cone method. The weight of fine aggregates in saturated surface dry condition was recorded. Next, about 500 g of saturated surface dry fine aggregates was inserted in the pycnometer and the water added until reaching the mark of pycnometer which is about 90% of its capacity. The total weight of pycnometer, fine aggregates and water was recorded. Then, the fine aggregates was taken out from the pycnometer and then was placed to dry in the oven at a temperature of 110 ºC until it reached a constant weight. The oven dried aggregates was recorded. The specific gravity of fine aggregates and water absorption was be calculated based on the *Equation 3.4* and *Equation 3.5*, respectively.

$$\text{Specific gravity} = \frac{W_1}{W_p + W_1 - W_{total}} \qquad \text{Equation 3.4}$$

$$\text{Apparent specific gravity} = \frac{W_2}{W_p + W_2 - W_{total}} \qquad \text{Equation 3.5}$$

Where, W_1 is weight of saturated surface dry aggregates in air, W_p is weight of pycnometer, W_{total} is weight of pycnometer, water and aggregates, W_2 is weight of oven dried aggregates.

3.2.2.1.2 Bulk density

The bulk density or the unit weight of dry-rodded aggregates is the weight needed to fill a container after it has been rodded to achieve the optimum packing. The

standard used to determine the bulk density was ASTM C29-17. This property is important as it will be crucial in the concrete mix design process. In this method, the saturated surface dry aggregates is placed in the known volume container. The placing involves 3 stages, the first time includes placing with the 25 times tamp using tamping rod. The placing and tamping is continued until the container was full, then the top part of the container was levelled using a rod. The weight measurement was recorded and the bulk density was then calculated.

3.2.2.1.3 Sieve analysis

The grading of aggregates can be obtained using the sieve analysis test. This analysis is to determine the particle size distribution of the coarse and fine aggregates. The test is based on ASTM C136-14 standards. The aggregates is dried first in an oven at a temperature of 100 º C until the constant mass is obtained. The amount of sample is weighed and placed in the sieves size set according to the standard. After the sieving process is completed, the mass of samples retained on each sieve is recorded. Calculations of the total percentage of retained and passing are obtained and grading distribution curve is plotted. The limits of grading for coarse and fine aggregates are shown in Table 3.2 and Table 3.3, respectively.

Table 3.2: Grading limits of coarse aggregates

Sieve size	Percentage passing (%)	ASTM C33- 16	
		Upper limit (%)	Lower limit (%)
19.0 mm	100	100	100
12.5 mm	90	100	90
9.50 mm	58	70	40
4.75 mm	2	15	0
2.36 mm	1	5	0
Pan	0	0	0

Table 3.3: Grading limits of fine aggregates

Sieve size	Percentage passing (%)	ASTM C33- 16	
		Upper limit (%)	Lower limit (%)
4.750	100	100	95
2.360	81	100	80
1.180	66	85	50
0.600	46	60	25
0.300	21	30	5
0.150	8	10	0
Pan	0	0	0

3.2.3 Superplasticizer

Superplasticizer was utilised to reduce the quantity of water used in concrete mix therefore increasing the workability of concrete. The superplasticizer that was used is Master Glenium Ace 8538 was obtained from Basf Petronas Chemicals. This type of superplasticizer contains polycarboxylate ether polymers and is free of chloride. It complies with the requirements of ASTM C494-16 standards. The application of this type of superplasticizer was supervised by Basf Chemical personnel and a few trial mixes were produced to obtain the performance of superplasticizer. The dosage of superplasticizer used was 0.2% out of cement weight.

3.2.4 Palm Oil Fuel Ash (POFA)

Palm oil fuel ash was collected from the Palm Oil Mill in Bekenu, Sarawak. POFA is the waste product from the palm oil mill. POFA is produced from the burning of mesocarp fibres and shells of the palm oil fruitlet at temperatures between 800-1000 ^{o}C to produce steam which can be used in turbines to supply electrical energy for the whole process in the mill. The ashes were obtained from the combustion chimney. The process of the POFA from Bekenu, Sarawak mill is presented in Figure 3.1. The press cake from the palm fruitlet goes through the process of burning in the furnace. The press cake consists of mesocarp fibres and the palm oil kernels as shown in Figure 3.2. Then, the ashes from the burning process goes through the conveyor before it reaches the boiler ash storage as shown in Figure 3.3. This type of ash is called palm oil fuel

ash (POFA). This type of agricultural waste is then disposed near the mill, causing environmental pollution and health hazards.

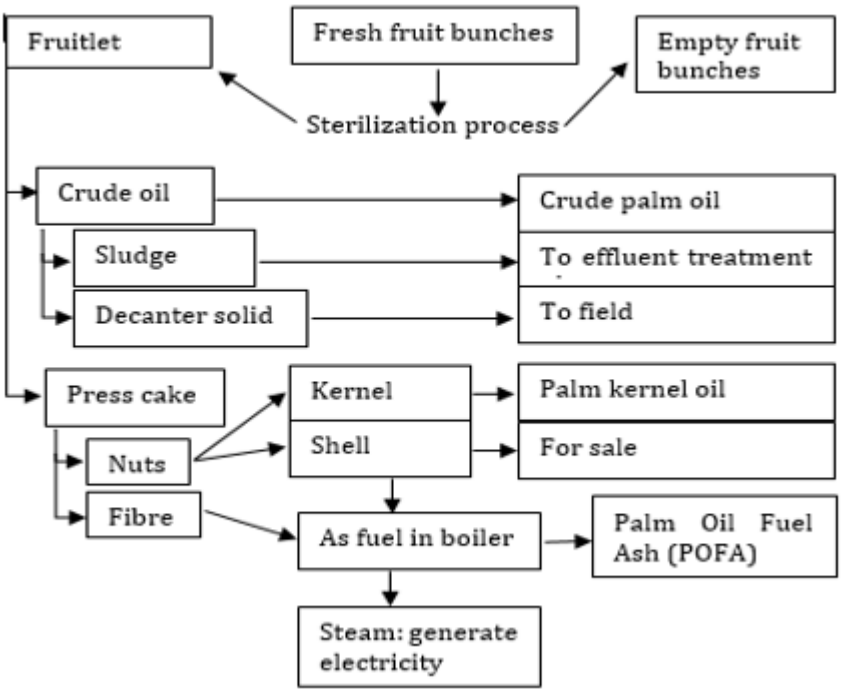

Figure 3.1: Flowchart process of palm oil fuel ash (POFA) at MJM Palm Oil Mill, Bekenu, Sarawak.

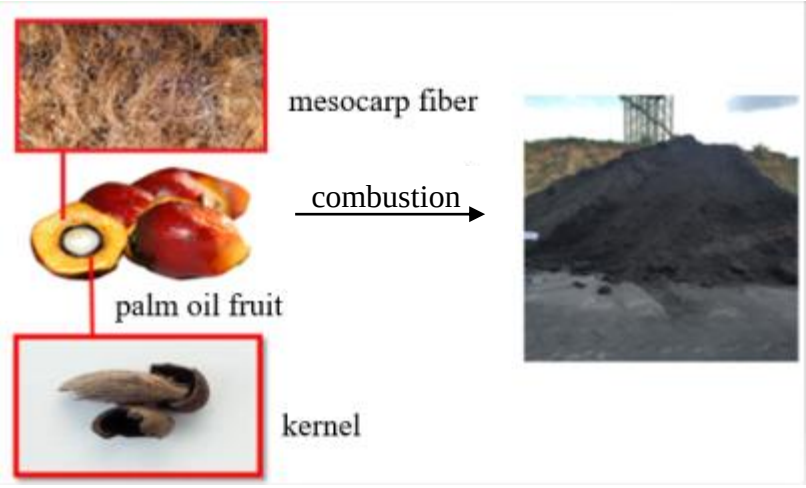

Figure 3.2: POFA went through combustion process of mesocarp fibre and palm oil kernel from the palm oil fruit

Figure 3.3: Storage for POFA after burning process

3.2.4.1 Micro POFA

Figure 3.4 shows how micro size of POFA was produced. POFA ash was dried for 24 hours at temperature of 100°C ± 5 °C to remove existing moisture content before the ash was sieved. Then, the POFA was sieved through 300 μm to remove any coarser particles and then sieved again through 150 μm sieve to remove 15–22% of the coarser particles as shown in Figure 3.4. The unwanted coarser particles consist of fibres, dry leaves and tiny pieces of palm oil shell. The sieved POFA then went through the grinding process to ensure 90% passes through 45-μm size.

The POFA passing through 150 μm sieve was then ground with the high energy ball mill machine (Model 3 VS, Capco Test Equipment Company, Suffolk, UK) to get micro size of 45 μm for 1 hour as shown in Figure 3.5. The pot volume of the ceramic jar is about 0.032 m^3 and the total weight of the stainless steel ball was 30 kg with various sized steel balls being used during the experiment. The diameter of the steel balls were 5 mm, 15 mm and 25 mm with the weight of each size being 9 kg, 9kg and 12 kg, respectively. Ideally, the pot of the ball mill machine should be approx. 50% by volume full of grinding media and 25% by volume of product to be ground. For each grinding, the amount of POFA loaded to the ball mill was about 1.8 kg based on the capacity of the pot volume and steel ball's weight. The size of 45 μm POFA particles was verified until 90% of POFA passing the 45 μm sieve according to ASTM C618-12 standards under physical requirements of pozzolan. The process of removing unburnt carbon took place after the second grinding where the temperature of the treatment was at 500 ºC for an hour using furnace as shown in Figure 3.6. After the heat treatment process, the micro POFA is then called treated micro POFA.

Figure 3.4: Raw POFA was sieved through 300 and 150 µm sieve.3.5

Figure 3.5: POFA was grinded using high energy ball mill machine to get micro POFA.

Figure 3.6: Removal of unburnt carbon using furnace.

3.2.4.2 Nano POFA

The production of nano POFA was proceed by reducing the size of treated micro POFA. The treated micro POFA was loaded into the jar first and the steel balls on the top of it. The process of second grinding took place immediately after the heat treatment was finished. At this stage, the micro POFA particles were still in hot and in a looser, permeable condition. The grinding took about 5 hours with the same ball to powder ratio. To determine the fineness of the nano POFA, six samples of nano POFA were collected at different cycles of grinding. The images of nano POFA were captured using the Transmission Electron Microscopy (TEM) and then, the imageJ analysis was performed. This software is a standard software for quantification of markers which was first developed at the National Institute of Health (Schneider, Rasband, & Eliceiri, 2012). Production of the nano POFA in this study was in accordance with top to down approach. There are two methods that were developed to form the nano particle. The first is first is the top down approach (Abdoli, Farnoush, Asgharzadeh, & Sadrnezhaad, 2011) and second is the bottom up approach (Jankowska & Zatorski, 2009). These two approaches were based on suitability, cost and expertise of nano behavior (Sanchez & Sobolev, 2010). In this study, the grinding of treated micro POFA to form nano POFA using high energy ball milling applied the top down approach. Basically, the top down approach occurs when larger structures are reduced to nanoscale size without changing the original properties, chemical composition and atomic level control (Crainic & Marques, 2002; ,Shah, Konsta-Gdoutos, Metaxa, & Mondal, 2009).

3.2.4.3Tests on POFA characterization

For the characterization of POFA as pozzolanic material, several microstructural tests were conducted such as XRF, SEM, TEM, XRD, and FTIR. These tests were conducted for the characterization of the POFA in terms of physical, chemical and mineralogical perspectives. A Few of the analysis required in the durability study to describe in details the microstructural structure of concrete samples after the attack by the chemicals for certain period. To determine the particle size of micro POFA, the wet analysis test was conducted according to ASTM C325-14 standards. For the nano POFA, the Transmission Electron Microscopy (TEM) machine was used and further analysis was done using image J software. The chemical composition of the micro and nano POFA was done using X-Ray fluorescence (XRF) analysis. The crystalline pattern was determined by X-Ray diffraction (XRD) and the shape and surface morphology was obtained using Scanning Electron Microscopy (SEM). There are few analyses that were performed to characterise the micro and nano POFA including FTIR and EDX analysis to support the macro structural of this study.

3.2.4.3.1Loss on Ignition (LOI)

The LOI value in POFA is important to determine the quality of the waste material before it can be used as supplementary cementitious material. The high LOI value of pozzolanic material requires a longer time of heat treatment process and high temperature is needed to reduce the LOI value. LOI value is proven to affect the strength and durability of concrete. This test was in accordance with ASTM D7348-13 standards. The procedure was conducted by measuring 1.0 ± 0.5 g of POFA using analytical balance. The POFA sample was placed in a crucible and heated in an oven at temperature 110 º C for an hour. Then, the sample was placed in a desiccator for 60 minutes to cool before the weight was recorded. The loss in weight at this stage was recorded as moisture loss. The next step was heating the samples in a furnace for 2 hours at a temperature of 950 º C. The fired sample was then cooled to room temperature in a desiccator and the weight recorded. The weight loss at this stage is known as the LOI value. The LOI maximum value for different class of pozzolanic material are given in Table 3.4.

3.2.4.3.2X-ray Fluorescence (XRF)

The chemical components in POFA are important at the early stages of study to classify the class of pozzolanic material according to ASTM C618-15 standards. In this study, the POFA was analysed for its chemical components using the Bruker S4 Pioneer model based on ASTM C114-15 standards. The samples were prepared (less than 90 μm) and weighed using a weighing balance before being pressed into pellets. The pellets were then analysed in the spectrometer. The main chemical components of pozzolan are silica, alumina, iron oxide, and sulfur trioxide, with varying amounts of volatiles substances, as measured by the loss on ignition (LOI). Table 3.4 shows the chemical requirements for different class of Pozzolan referring to the ASTM C618-15 standards.

Table 3.4: Chemical Requirements for Different Class of Pozzolan based on ASTM C618-15

	Class		
	N	F	C
Silicon oxide (SiO_2) plus aluminium oxide (Al_2O_3) plus iron oxide (Fe_2O_3), min, %	70.0	70.0	50.0
Sulfur trioxide (SO_3), max, %	4.0	5.0	5.0
Moisture content, max, %	3.0	3.0	3.0
Loss on ignition, max, %	10.0	6.0^	6.0

^ The use of Class F pozzolan containing up to 12% loss on ignition may be approved by the user if either acceptable performance records or laboratory test results are made available.

3.2.4.3.3 Wet sieve analysis

The physical characterization in terms of fineness was determined using wet sieve analysis. The analysis guidelines are given following the ASTM C325-14 standards. A sample of 100 g was prepared and it was subjected to wet sieve using water in the 45 μm sieve size. Then, the sieve was dried in an oven at 100 º C until dry. The residue left at the sieve was properly removed using a brush and the weight was recorded. For this test, the limit of fineness has been set according ASTM C618- 15 standards for different class of pozzolanic materials as shown in Table 3.5.

Table 3.5: Physical requirement for Different Class of Pozzolan ASTM C618-15

Physical test		Class	
	N	F	C
Fineness Retained on a 45 μm sieve (%)	34 max.	34 max.	34 max.

3.2.4.3.4Thermogravimetric analysis (TGA)

This analysis is conducted to determine the thermal temperature for the heat treatment of POFA. About 25 mg of POFA sample was used for the analysis under circulation of atmosphere using nitrogen gas with a gas flow of 50 ml/minute. The start temperature was 30 ºC and the end temperature was 1000 ºC with the heating rate of 20 ºC/minute. The TGA curve is produced to indicates the temperature range and the weight loss of the POFA. A weight loss within a specific temperature range indicates the composition of a particular chemical compound in POFA and the magnitude of weight loss identifies the amount of the chemical compound (Kosmatka, Kerkhoff, & Panarese, 2008).

3.2.4.3.5Scanning Electron Microscopy (SEM)

Under this analysis, raw, micro and nano POFA were analysed using scanning electron microscopy of Philips XL 30 from North Billerica, USA which operated at 15kV. The samples were attached on two side with adhesive black tape and kept in a vacuum state to get the images. Different magnification level for each image was used to spot the topography and morphology of the materials. The microscope was equipped with an energy x-ray spectroscopy (EDX) to determine the element composition of the specific spectrum of each images.

3.2.4.3.6 Transmission Electron Microscopy (TEM)

For nano POFA, the physical characterization was analysed using TEM, JEOL-1230 from Tokyo, Japan. The TEM images can be used to quantify particles size, size distribution and morphology. This analysis is a vital characterization tool for nano-sized materials. From the images, the average particle size and also size distribution can be obtained. The analysis was further done using image processing and by

measuring using Image J analysis, a free Java based software package provided by the National Institute of Health (NIH). For sample preparation, a thin layer of formvar needs to be placed first on copper grid, then the small drops of solution containing nano POFA was placed on top of the thin film as shown in Figure 3.7 and 3.8. The samples were allowed to dry and covered to avoid any impurities. The imaging process was started the next day by taking images at several spots on the copper grid. The image quality of the nanoparticles depends on the contrast of the sample and background view in TEM software.

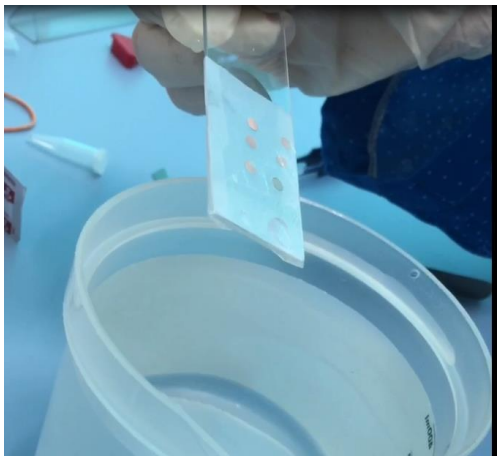

Figure 3.7: Placing the thin film of formvar onto copper grid

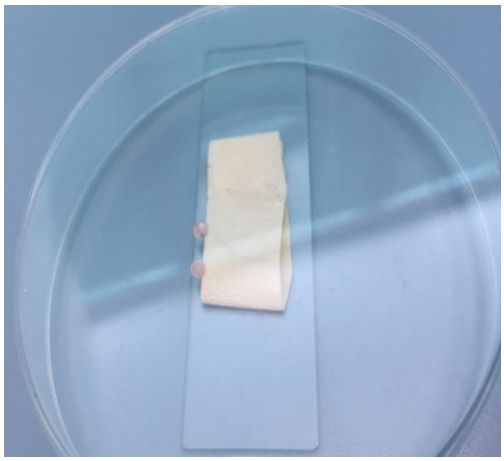

Figure 3.8:Small drop of solution containing nano POFA was placed on top of the thin film

3.2.4.3.7X-Ray Diffraction (XRD)

For mineralogical characterisation of micro and nano POFA, the XRD analysis was conducted using the D/Max 2500 XRD of Rigaku Corporation. This analysis is to identify the crystalline phase of the POFA and it will also be performed in the durability study to identify the phase transformation of concrete after it has been attacked by chemicals. The setting in the equipment were 2Θ angle range from 5 to 70 degree at a scan speed of 5 degrees per minute during measurement. The samples were prepared in powder form, and for the concrete samples, the high energy ball mill was used to prepare the sample for XRD analysis.

3.2.4.3.8Fourier Transforms Infrared Spectroscopy (FTIR)

The FTIR analysis is one of the quantitative and qualitative tools to determine the group of organic/inorganic materials and chemical bonding formed from the

cement hydration process. The equipment used to perform the analysis was Varian 660-IR of Varian Medical Systems with the scan range of 400 to 4000 cm-1. Other than characterisation, FTIR also was conducted in the durability study to identify the bonding formed in the concrete samples. The concrete samples were prepared in powder form (< 45 μm). Then, samples were ground with potassium bromide (KBr) and prepared into pellets before being placed in the FTIR machine.

3.3 Mix Design

The mix design of high performance concrete was designed based on ACI 211.4R-08 as presented in Table 3.6. The material proportion for each mix is described in Table 3.7. This reference mix was designed as the reference without the pozzolanic materials. Therefore, the water binder ratio was fixed at 0.30 and the other constituents materials were added to the mixture as well, except for the binder. In this study, the target compressive strength is between 50-80 MPa at the age of 28 days. The slump range is between 100-150 mm. The 7-days concrete strength is estimated to be about 75% of the 28-days strength (Kostmatka, Kerkhoff, & Panarese, 2002). The reliability of the early strength is very important for the estimation of 28-days strength especially for today's fast track construction and demoulding formwork. It is like a warning signal for the concrete producers at the batching plant to predict the results.

Table 3.6: Mix design of HPC based on ACI 211-4R (2008)

	Component	ACI 211-4r guidelines
1.	Target slump (after adding high range water reducer)	Table A1.5.2.1
2.	Maximum size of aggregates	Table A1.5.2.2
3.	Water content, w non-air entrapped of 2%	Table A1.5.2.3
4.	Water/cement ratio, w/c	Table A1.5.2.4
5.	Cement, c	Calculated from w/(w/c)
6.	Mass of coarse aggregates, W_{ca} = Bulk volume x Bulk density	Table A1.5.2.6
7.	Volume of water, V_w = (water/specific gravity *1000)	
	Volume of cement, V_c= (cement/specific gravity *1000)	
	Volume of coarse aggregates, V_{ca} = (W_{ca}/specific gravity *1000)	
	Volume of fine aggregates, V_f = 1-(V_w+V_c+V_{ca})	Absolute volume method
	Mass of fine aggregates, W_f = V_f x specific gravity x 1000	

Table 3.7: Mix proportion of high performance concrete

Component	Weight
Cement	588 kg/m^3
Coarse Aggregates	1093 kg/m^3
Fine Aggregates	536 kg/m^3
Water with superplasticizer	183 kg/m^3

3.3.1 Experiment design using response surface methodology (RSM)

Response surface methodology is a technique based on mathematical and statistical data in determining the interactions between the variables and responses (Myers, Montgomery, & Anderson-Cook, 2016). Identification of the variables, responses and the process is called design of experiment (Soares, Mohamed, Venturini, & Lemaire, 2002). By using RSM, the common method used to determine the functional relationship between the input variables and responses is known as central composite design (CCD) (Aldahdooh, Muhamad Bunnori, & Megat Johari, 2013). The CCD approach was used to provide a set of running experimental program. The results of the experimental program were used to develop a model that consists of regression

equations used to relate the input variables and the responses. Unlike Box Behnken approach, CCD is a method that is capable of predicting second- order model without completing the three-level factorial design. Therefore, the set of running experimental program was reduced. Design Expert Software version 9.0.6.2 was employed for the design, mathematical modelling, statistical analysis and optimisation process. In the design, the micro POFA was coded as A and nano POFA was coded as B, both were chosen as the potential variables and were studied at three different levels. The high levels of the factors were coded as +1 and the low levels as -1. The variables and levels are shown in Table 3.8.

Table 3.8: Variables and variables levels adopted for RSM

Variables	**Code**	**Variable levels of code**		
		Low : -1	Intermediate: 0	High: 1
Micro POFA, MP (%)	A	10	20	30
Nano POFA, NP (%)	B	1	2	3

The total number of experiments based on the variables selected were 13, obtained as ($2k + 2k + 5 = 13$) where k, the number of variables is 2. Thirteen different combinations were presented in the design with five replications of the mean case. The replication considered at the mid-level to study and improve the precision of the experiment. From the CCD experimental design, the experimental programs are presented in Table 3.9. After this step, the experiments were carried out based on the run order. An average of at least 140 recorded measurements were obtained from the variables and responses.

Table 3.9: Mix proportion based on the design of experiment

Run	Uncoded variables		Mixture proportion (kg/m^3)				
	MP (%)	NP (%)	Cement	Coarse aggregates	Fine aggregates	Water	SP (%)
0	0	0	588	1093	536	183	0.20
1	10	1	523	1093	536	183	0.20
2	10	2	517	1093	536	183	0.20
3	10	3	512	1093	536	183	0.20
4	20	1	465	1093	536	183	0.20
5	20	2	459	1093	536	183	0.20
6	20	2	459	1093	536	183	0.20
7	20	2	459	1093	536	183	0.20
8	20	2	459	1093	536	183	0.20
9	20	2	459	1093	536	183	0.20
10	20	3	453	1093	536	183	0.20
11	30	1	406	1093	536	183	0.20
12	30	2	400	1093	536	183	0.20
13	30	3	394	1093	536	183	0.20

* MP: micro POFA, NP: nano POFA, SP: Superplasticiser.

The responses to study the interactions with the variables were fresh properties namely slump, and hardened properties namely compressive strength, splitting tensile strength and flexural strength at 7, 28 and 90 days. The interactions between the variables (micro POFA and nano POFA) and responses (workability, compressive strength, splitting tensile strength, flexural strength) were determined from the analysis of variance (ANOVA). In order to quantify the quality of the quadratic prediction models, to evaluate the model terms, and to check the model term's statistical significance, the coefficient of determination R^2, the probability (P-value) with 95% confidence level, and (t-test) at 5% significance level were determined, respectively. Moreover, the ramp function graph was used to identify the optimum region. After the regression model between the variables and responses was established, the input variables were varied simultaneously and independently to determine the optimum mixture design. The optimum solution tends to satisfy the optimisation criteria for each response as much as possible without excessively compromising any of the requirements (Myers et al., 2016). General steps to use the response surface methodology was summarized in the flowchart as presented in Figure 3.9.

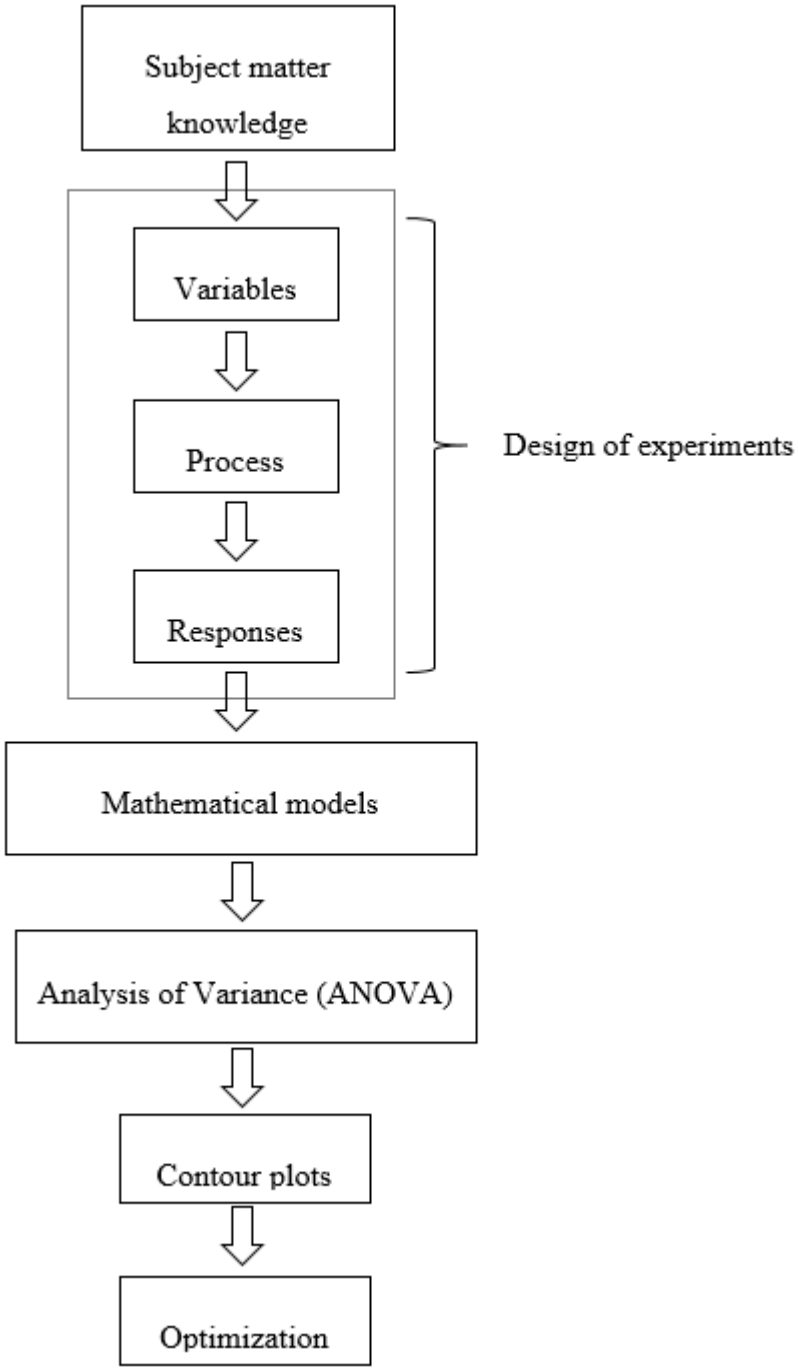

Figure 3.9: Steps using RSM

3.4 Mixing, placing and curing process

The mixing of concrete was done for each experimental run based on the order designed in CCD. The concrete mixing was performed using a horizontal pan mixer with capacity of 0.05 m^3 as shown in Figure 3.10. The procedure of mixing was kept consistent to minimize the error during the process, while ensuring uniformity. The

aggregates used in saturated surface was in a dry condition. For the coarse aggregates, the specific amount needed per cast was weighed and immersed for at least 24 hours, and before the mixing started, the aggregates were wiped off using a towel to remove surface moisture. For the fine aggregates, a cone test was performed to make sure the fine aggregates are in a saturated surface, in a dry condition. The condition of aggregates is important to avoid the aggregates from absorbing the water that is supposedly used completely for the hydration process. The process of mixing was started by placing the aggregates in the mixing drum followed by the combined cement, micro and nano POFA. Without stopping the mixer, water with the superplasticizer were added to the dry mix. The mixing was continued until the fresh concrete achieved consistency. The slump test was conducted right after the mixing process. Then, the concrete mix was placed and layered properly in the mould before it was vibrated on a vibration table as shown in Figure 3.11. The concrete specimens were demoulded after 24 hours and were immersed in water for curing process as shown in Figure 3.12

Figure 3.10: Mixing concrete using horizontal pan mixer

Figure 3.11: Placing concrete mix in moulds

Figure 3.12: Water curing of concrete specimens

3.5 Tests on engineering properties

3.5.1Slump test

After the mixing of concrete process, the fresh properties of concrete was obtained. Three layers of equal volume were filled and each layer was tamped using a rod of 600 mm long and 16 mm in diameter. The cone was vertically removed. The distance between the top of the slump and original height was marked as the slump height as shown in Figure 3.13.

Figure 3.13: Slump height measurement

3.5.2 Compressive strength

The compression test was conducted according to the ASTM C109-16 standards. A total of 126 cube specimens of 100 x 100 x 100 mm were prepared according to the designated experimental program. All the concrete specimens were placed in a curing room at 95% humidity and were fully cured in water. Before the testing, the specimens were removed from the curing tank and the surface moisture was allowed to dry. The testing was performed by placing the cubes in the center testing platform and the uniform load was applied by the compression machine as shown in Figure 3.14. The maximum capacity of the machine is 2000 kN. The compressive strength is calculated based on the average of three maximum failure loads and the cross-sectional area of cube specimens. The testing was performed at three different curing periods (7, 28 and 90 days).

Figure 3.14: Testing of compression strength

3.5.3 Splitting /Indirect Tensile Strength

The splitting tensile strength test is one of the indirect tests to determine the tensile strength of concrete. The test is conducted by applying the tension force in the form of splitting (Neville, 2011). The test procedure was according to the ASTM C496-11 (2011) standards as shown in schematic diagram in

Figure 3.15. A total of 126 cylinder specimens of 100 mm diameter and 200 mm height were prepared according to the experimental program. All the specimens were placed in a curing room at 95% humidity and was fully cured in water. For the test set-up, a plywood strip was placed along the top and bottom of cylinder concrete and the load was applied along the length of the cylinder concrete until failure or split as shown in Figure 3.16. The maximum load of failure was recorded and the tensile strength was evaluated using Equation 3.6. The testing was performed at three different curing periods (7, 28 and 90 days).

$$f_{sts} = \frac{2P}{\pi LD} \qquad \text{Equation 3.6}$$

Where, f_{sts} is splitting tensile strength (N/mm^2), P is maximum failure load (N), L is length of the specimen (mm) and D is diameter of the specimen (mm).

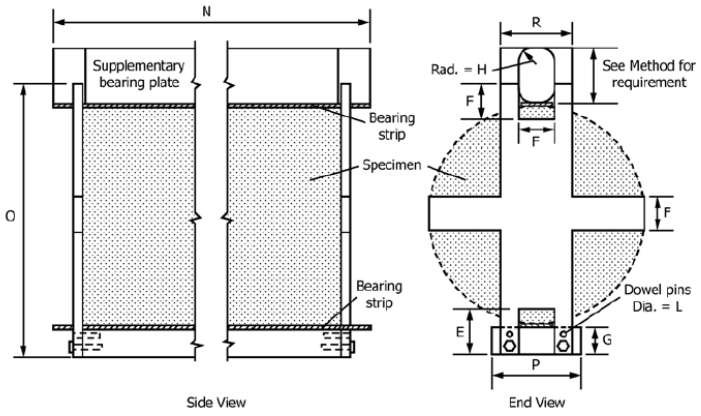

Figure 3.15: Schematic of splitting tensile strength test procedure ASTM C496-11

Figure 3.16: Testing of splitting tensile strength

3.5.4 Flexural Strength

The flexural strength test was conducted according to ASTM C78-16 (2016) standards. A schematic diagram of this test was referred to, based on the standard as shown in Figure 3.17. A total of 126 prisms specimens of 100 mm x 100 mm x 500 mm were prepared and tested at 7, 28 and 90 days. The beam was set up using two point loading arrangement as stated in the standard test method shown in Figure 3.18. When the test was running, the crack development was observed. The maximum failure load was recorded and the flexural strength was calculated using Equation 3.7.

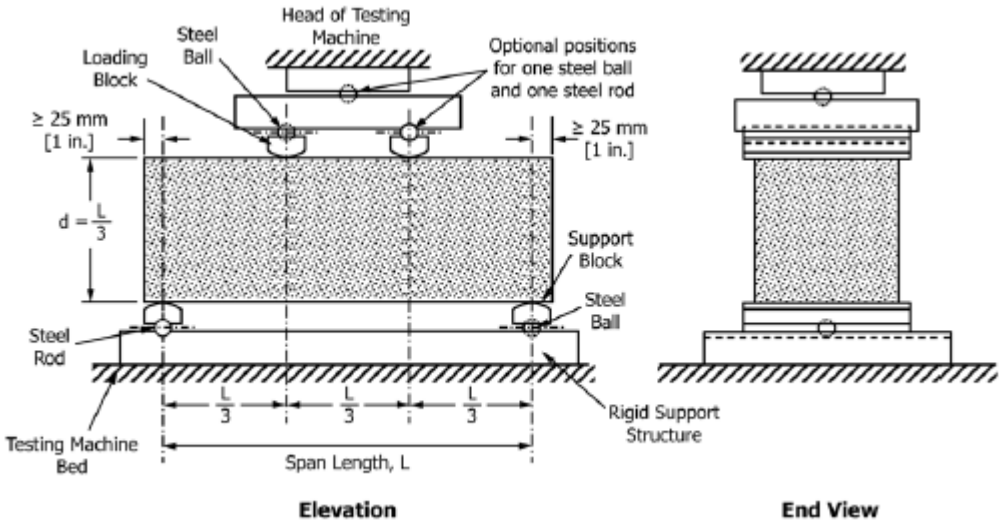

Figure 3.17: Schematic of flexural strength test procedure ASTM C78-16

Figure 3.18: Testing of flexural strength

$$f_{fs} = \frac{3P(L - L_{ls})}{2BD^2}$$

Equation 3.7

Where, f_{fs} is flexural strength (N/mm^2), P is maximum failure load (N), L is total length (mm), L_{ls} is length between the loadings, this case is for the loading span is neither 1/3 nor 1/2 of the support span (mm), B is width (mm) and D is thickness (mm).

3.5.5 Water absorption

This test was conducted according to ASTM C642-13 (2013) standards. The test was conducted to assess the quality of hardened concrete at certain age in terms of density, durability and imperviousness. Minimal void volume in the concrete indicates a good quality concrete. In terms of durability, the pore volume can be obtained in the hardened concrete to avoid the penetration and attack by chemicals such as chloride, acid, sulphate etc. In this test, there is no specification for the test specimen, it may be pieces of cylinder, cores or beams except the volume of each is not less than 35 cm3 or 800 g weight. In this study, the disc samples were cut from cylindrical specimens where the size of each sample was 100 mm in diameter and 50 mm thickness. The specimens were dried in an oven for 24 hours at temperature of 110 C ±5 ºC and the weight for each specimens was recorded after the samples cooled down. Then the specimens were immersed in water for 2 days and the weight of the samples were recorded in saturated surface dry condition. The specimens were placed in a container covered with tap water, and the boiling process was done for 5 hours. After cooling down the specimens, the weight of the specimens was recorded. The specimens were then suspended in water using a wire basket and the weight of specimens suspended in water were recorded. This test was conducted to concrete at the age of 28, 56, 90 and 180 days. The evaluation of water absorption, bulk and apparent density and void volume are given in Equation 3.8 to Equation 3.11, respectively.

$$\text{Water absorption (\%)} = \frac{B-A}{A} \times 100\% \qquad \text{Equation 3.8}$$

$$\text{Bulk density, } g_1 = \left(\frac{A}{C-D}\right) \times \rho_{water} \qquad \text{Equation 3.9}$$

$$\text{Apparent density, } g_2 = \left(\frac{A}{A-D}\right) \times \rho_{water} \qquad \text{Equation 3.10}$$

Volume of permeable pore space (voids) (%)

$$= \frac{g_2 - g_1}{g_2} \times 100\% \qquad \text{Equation 3.11}$$

Where, A is mass of oven-dried (g), B= mass of after the immersion (g), C= mass of after the immersion and boiling (g), D= apparent mass in water after immersion and boiling (g) and ρ_{water}= density of water (g/cm^3).

3.5.6 Sorptivity test

This test was done in accordance with ASTM C1585-13 (2013) standards. This type of moisture absorption is not correlated with permeability. The rate of water absorption or sorptivity was conducted using the disc concrete samples with 50 mm thickness and 100 mm in diameter. Samples were prepared by cutting the cylinder concrete specimen into 4 discs and the middle part of two discs were taken for this test. The disk specimens were placed in an oven at 50 ºC for 3 days until constant weight is achieved. Then, the disc samples were kept in a sealed container to achieve uniform moisture distribution. Next, the specimens were placed in a distilled water container as shown in Figure 3.19.The weight gain measurements were taken from the 0 second to the first of 6 hours to determine the initial absorptions. The process was continued until the end of the 8 days. During the measurement, the excessive surface water was wiped off. This test only allows a one-dimensional diffusion where only one surface was in free contact with water while the top and bottom of the disk specimens are sealed with an impermeable coating. The test was conducted within the range of 28, 56, 90 and 180 days. The sorptivity, I is the change in mass divided by the product of the cross-sectional area of the test specimen and the density of water. The initial rate of water absorption value (mm/s$^{1/2}$) is calculated as a slope of the linear part of the sorptivity, I versus square root of time.

Figure 3.19: Disc specimens in distilled water

3.5.7 Rapid Chloride Penetration Test (RCPT)

The rapid chloride penetration test was conducted according to ASTM C1202-18 (2018) standards. This test examines the permeability of concrete where low permeability plays an important role to protect the concrete from the penetration of harmful substances like chloride ions. The test specimens used in this test were 50 mm thickness and 100 in diameter for each disc. The samples were cut from the 100 x 200 mm cylindrical specimen. The equipment to conduct the test is shown in Figure 3.20. The curve surface of the disc was covered with the epoxy coating. Then, the disc samples were placed in a sealed container and connected to the vacuum pump for 3 hours. Under the running of the vacuum pump, a certain amount of distilled water was poured into the container until it completely immersed the samples. The pump was still running for an additional one hour after the water addition. Then, the pump was switched off and the specimens were left and immersed in the water for 18 hours. The saturated samples were clamped in between the two cells and connected to a data logger with voltage supply of 60 V direct current. For the positive cell, 0.3 M of sodium hydroxide (NaOH) was filled into the cell and 3% of sodium chloride (NaCl) was filled into the negative cell as shown in Figure 3.20. The current reading was recorded at 30 minutes intervals for about 6 hours. The interpretation of the results can be obtained by calculating the total charge that passed through the concrete samples. The charge passed indicates the chloride permeability of concrete and can be obtained by using Equation 3.12. Classification of concrete in terms of chloride permeability based on the charge passed is shown in Table 3.10

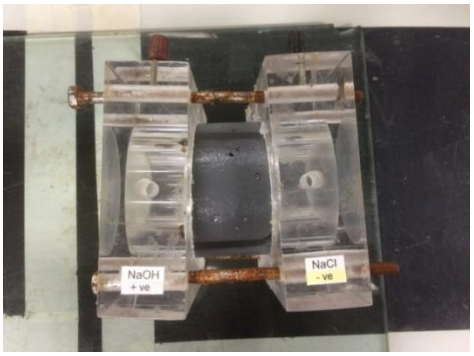

Figure 3.20: Setup equipment for RCPT test Setup of the test cell with the disc sample

$$Q_p = 900(I_0 + 2I_{30} + 2I_{60} + \cdots + 2I_{330} + I_{360}) \quad \text{Equation 3.12}$$

Where, Q_p is the charge passed (Coulombs), I_0 is the initial current reading after the voltage is applied (amperes) and I_t is the current at t minutes after the voltage is applied (amperes).

Table 3.10: Chloride Permeability Based on Charge Passed (ASTM C1202-18)

Charge passed (Coulombs)	Chloride permeability
<1000	Very Low
1000-2000	Low
2000-4000	Moderate
>4000	High

3.5.8 Chemical Resistance Test

The chemical resistance test was conducted according to ASTM C267-12 standards. This standard was used as the basic procedure to determine the resistance of concrete to the exposure of harmful chemicals such as sulphuric acid. The cube specimens with a dimension of 100 x 100 x 100 mm were used for these tests. The specimens were subjected to 5% of sulphuric acid solution. The immersion period was about 28, 56, 90 and 180 days. During the period of immersion, the pH value of the solution was monitored using the pH meter to maintain the pH value. The test was

evaluated based on the residual compressive strength of the concrete, change in the mass and dimension, and the surface condition after the chemical exposure. While taking the measurements, the concrete specimens were cleaned up using water and scrubbed gently using a wire brush. The surface moisture was wiped off and the mass of the specimens was recorded. The relative compressive strength of concrete was calculated using the following equation in Equation 3.13.

$$\text{Residual compressive strength (\%)} = \frac{f_t - f_{28days}}{f_{28days}} \times 100\% \qquad \text{Equation 3.13}$$

Where, f_t is compressive strength at t days of immersion and f_{28days} is compressive strength at 28 days.

3.5.9 Corrosion Measurements

There are two types of techniques employed to simulate the corrosion process and to evaluate the corrosion resistance of concrete. First, a rapid test used in the study was an accelerated corrosion test using impressed voltage. Second, an electrochemical technique of corrosion measurements were also employed in this study by using electrochemical impedance spectroscopy (EIS) and linear polarization resistance. The EIS can only provide the corrosion resistance, therefore linear polarization resistance was incorporated with Tafel plot technique was employed to determine the corrosion rate. For the corrosion test, the test specimen used was a cylindrical concrete specimen (100 mm diameter and 200 mm height) with 20 mm diameter of reinforcement bar embedded at the center of the concrete cylinder. Before inserting the bar in concrete, the bar was cleaned up to remove the dust particles and the impermeable coating was applied at the top part of the bar. The initial weight of the reinforcement bar was recorded. The coating was applied to avoid the corrosion of the protruded part of the bar. The test specimens for corrosion test is shown in Figure 3.21.

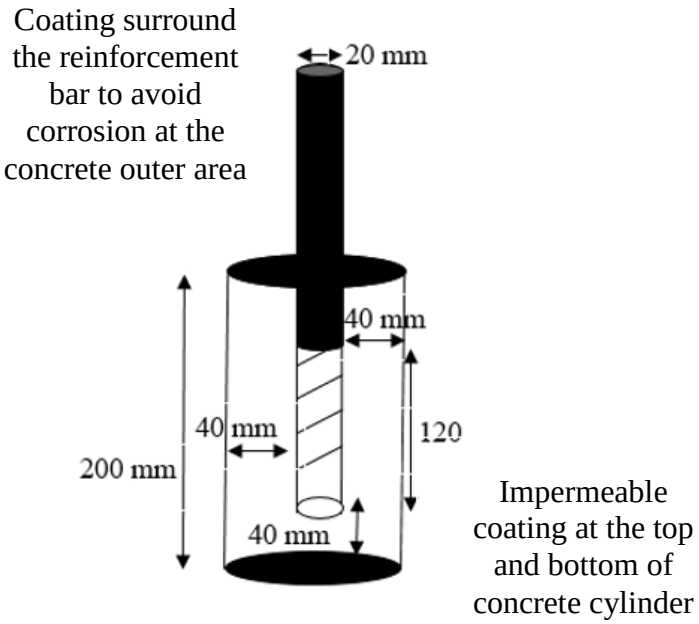

Figure 3.21: Schematic diagram of test specimen

3.5.9.1 Accelerated Corrosion Test (ACT) using impressed current method

This technique has been used in corrosion study due to its ability to control the rate of corrosion and because this is considered a valid method to study the corrosion (Caré & Raharinaivo, 2007). In addition, this accelerated technique of corrosion is able to determine the permeability of the concrete indirectly and thus determine its corrosion resistance (Ha et al., 2007). The test specimens had to undergo a wetting and drying process for cycle of 7 days. The period of the cycle was obtained from the sorptivity test. In the wetting process, the specimens were soaked in a 3.5% sodium chloride, NaCl solution to accelerate the process of corrosion. During the 7 days of wet cycle, the specimens were immersed in the chloride solution with the water level above the exposed area of reinforcement bar. The bar that acts as the anode was connected to a 12V DC power supply. To complete the connection, a positive terminal of power supply was connected to the bar (working electrode) and the negative terminal was connected to the stainless steel that acts as the cathode (counter electrode). A fixed DC was impressed between the electrodes and the current fluctuation was monitored and recorded for each specimen every one hour using DTS-303 data logger. The setup test is shown in Figure 3.22 and the schematic diagram is shown in Figure 3.23. The test continued running until cracks appeared on the surface

of concrete. The weight of the reinforcement bar after the crack appeared was recorded and the corresponding anodic current was observed.

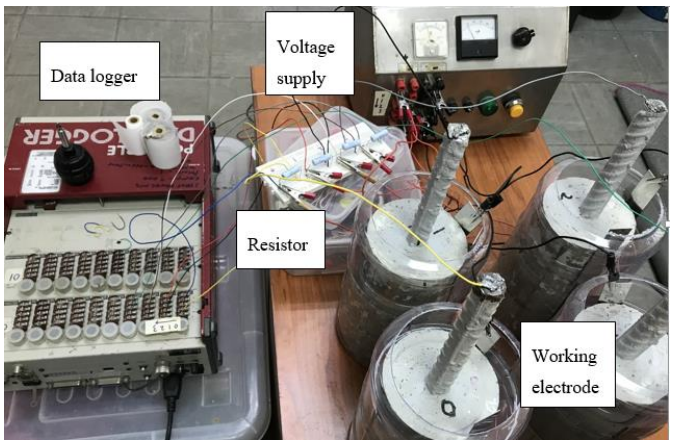

Figure 3.22: Setup test for ACT

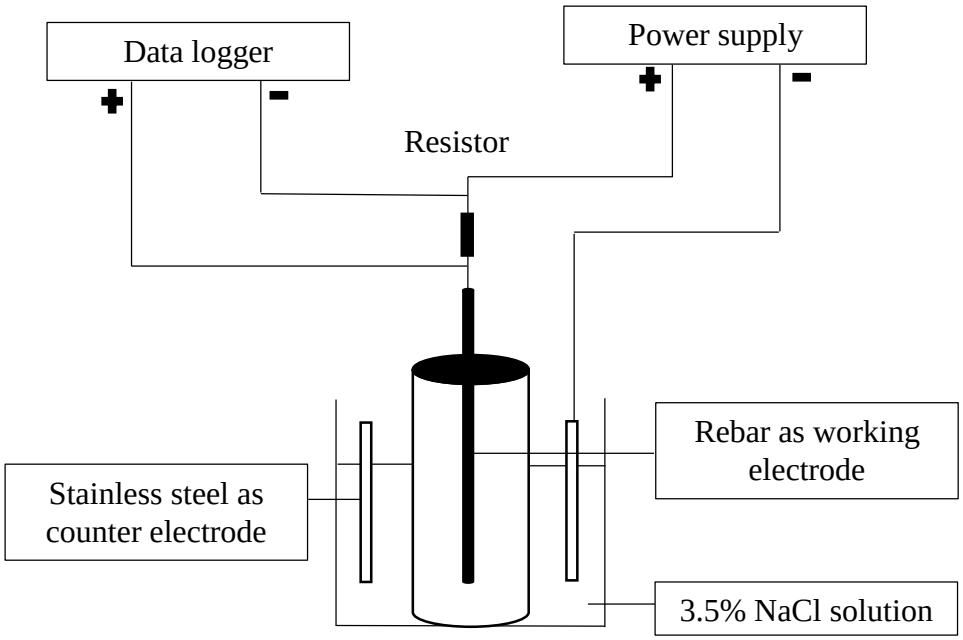

Figure 3.23: Schematic diagram for ACT

The actual weight loss was obtained according to ASTM G1-17 standards as shown in Equation 3.14.

$$M_{act} = \frac{W_i - W_f}{\pi DL}$$ Equation 3.14

Where, M_{act} is the actual mass loss (g/cm^2), W_i is the initial weight of bar (g), W_f is the weight after corrosion occurred (g), D is diameter of the bar (cm) and L is the length of bar (cm).

3.5.9.2 Electrochemical Impedance Spectroscopy (EIS)

This electrochemical test was conducted using VersaSTAT 3 Potentiostat/Galvanostat (Princeton Applied Research) with a built-in software called ZSimpWin as shown in Figure 3.25 (labeled as potentiostat). The cylindrical specimen with bar embedded were demoulded after 24 hours of cast and were immersed in water for 28 days. Then, the concrete specimens were immersed in a 3.5% of sodium chloride solution as shown in Figure 3.24. Three electrodes were needed for the test where a reinforcement bar was employed as a working electrode, stainless steel bar worked as a counter electrode and a saturated calomel electrode (SCE) as the reference electrode. These electrodes were set up to be in same distance to each other and a distance of 12 mm was fixed throughout the test. The test setup is given in Figure 3.25 and the schematic diagram for the test shown in Figure 3.26. A wide range of frequency was set, between 100 kHz and 10 mHz to get coverage of the Nyquist and Bode diagrams. Suitable equivalent circuit was used to analyze the impedance data and to fit the Nyquist plot. The circuit was modeled to correlate the chemical kinetics with the electrical behaviour. Once the circuit modeled, the solution resistance (R_s), charge transfer resistance (R_{ct}), Helmholts double layer capacitance (*Cdl*) and diffusion double layer capacitance can be obtained. The EIS measurement was recorded during 7 days of wetting and drying cycles within a period of 91 days, 182 days, and 365 days.

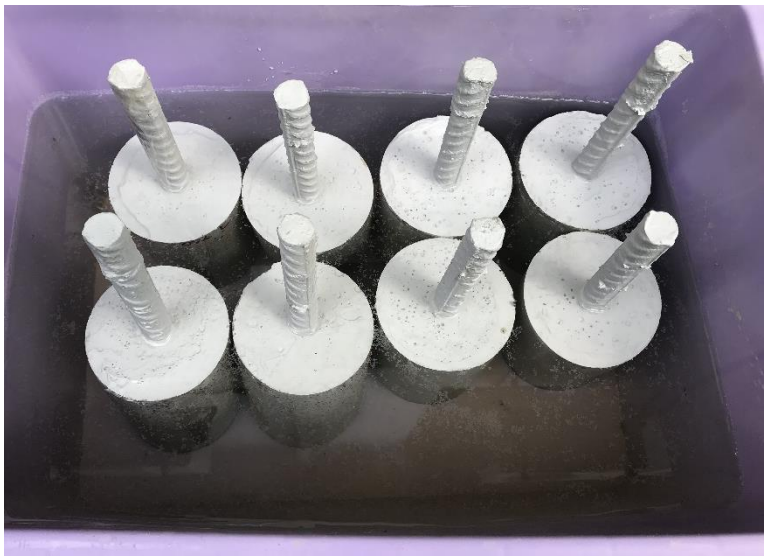

Figure 3.24: Specimens at wetting stage in 3.5% NaCl solution

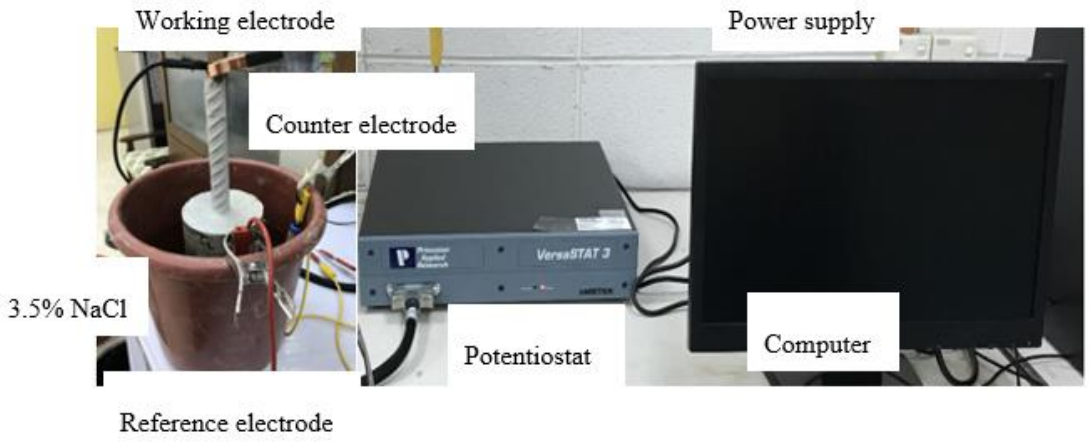

Figure 3.25: Test setup for electrochemical techniques of corrosion measurement (EIS, LPR, TP)

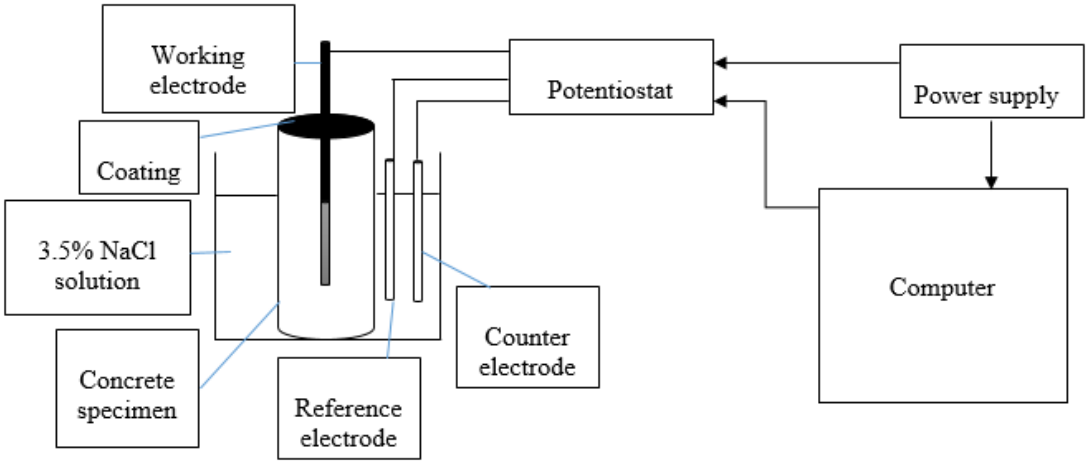

Figure 3.26: Schematic diagram for electrochemical tests

3.5.9.3 Tafel plot

Tafel plot methods was conducted to determine the corrosion rate of reinforcement bar in concrete. The three electrodes were needed for these methods as in EIS corrosion measurement and the setup as well. The details of the reinforcement bars were inserted in the software including the expose area (69.12 cm^2), equivalent weight (27.92) and density of the reinforcement bar (7.85 g/ml). The polarization resistance, R_p indicates the resistance to oxidation after voltage is applied. The value of Tafel constant can be evaluated from the running of the potentiostat using Tafel plot technique. The potential scan, E_{corr} of $\pm$ 250 mV was applied at scan rate of 0.2 mV/sec. For this plot, there were 2501 points to complete one Tafel plot for each specimen. The value of Tafel constant obtained from the plot was used in the Stern-Geary equation to calculate the corrosion rate of reinforcement bars in concrete. Both techniques were evaluated at 13th (91 days), 26th (182 days) and 52nd (365 days).

The polarization resistance is related to the corrosion current, i_{corr} through Stern-Geary relationship as in Equation 3.15.

$$i_{corr} = \frac{B}{R_p} \qquad \text{Equation 3.15}$$

Where, B is the constant of Stern-Geary and can be determine using the Equation 3.16.

$$B = \frac{\beta_a \beta_c}{2.3(\beta_a + \beta_c)}$$ Equation 3.16

Where, β_a is anodic Tafel constant and β_c is cathodic Tafel constant (mV/decade).

3.6 Summary of test program

According to the aim and objectives of the study and the materials and methods listed in the previous sub chapters, the summary of the test program is given in Table 3.11. The concrete mixing and specimens cast based on the test program stage as tabulated in the table below.

Table 3.11: Summary of test program for the study

Stage	Objective	Tests	Remark
1	Production of treated micro and nano POFA and its characteristics.	Physical: LOI, sieve analysis, SEM, TEM Thermal analysis: TGA Chemical: XRF test Microstructural/mineralogy : XRD and FTIR analysis	Refer to Chapter 4 Micro POFA: 200 kg Nano POFA: 50 kg
2	Optimum mix design of concrete containing micro and nano POFA according to the targeted performance criteria. (14 mixes including control mix)	Slump, compressive (C), splitting tensile (ST) and flexural strength (FS) test. Testing at: 7, 28, 90 days After all the tests finished, optimisation analysis using Design Expert Software was performed.	Refer to Chapter 5 C:126 cubes concrete specimens (100 x 100 x 100 mm) ST:126 cylindrical concrete specimens (100 diameter x 200 mm) FS:126 beam concrete specimens (100 x 100 x 500 mm)
3	Durability study concrete containing micro and nano POFA (4 mixes including control based on the optimum mix design obtained in previous objective).	Water absorption (WA), RCPT, acid resistance (AC) test. Testing at: 28, 56, 90 and 180 days. Microstructural tests of concrete samples after the attack of aggressive chemical. (SEM, EDX, XRD analysis)	Refer to Chapter 6 WA: 32 disc concrete specimens (100 diameter x 50 mm) RCPT: 32 disc concrete specimens (100 diameter x 50 mm) AC: 48 cubes concrete specimens (100 x 100 x 100 mm)
4	Assess the effect of corrosion on concrete containing micro and nano POFA. (4 mixes including control based on the optimum mix design obtained in previous objective).	Accelerated corrosion test (ACT) using impressed voltage. Testing running until the surface of concrete crack. Non-destructive test: Electrochemical measurement including EIS and Tafel plot (TP). Testing at 91,182 days and 365 days	Refer to Chapter 6 ACT: 8 cylindrical reinforced concrete specimens EIS, TP: 8 cylindrical reinforced concrete specimens. Same specimens used to monitor the corrosion process and record the data for the 3 measurements throughout the whole testing period.

Chapter 4

Materials Characterization

4.1 Introduction

In this chapter, the primary objective is to determine the materials characterization in terms of physical, chemical, microstructure and mineralogical compositions. These characteristics are very important for the utilization of micro and nano POFA as supplementary cementitious materials. Furthermore, the information is important to understand their effect on the engineering properties of concrete. Other raw materials used in concrete were also investigated to satisfy their use as stipulated in the standards. Physical characterization includes the Loss on Ignition (LOI), strength activity index, Scanning Electron Microscopy (SEM), Transmission Electron Microscopy (TEM), and Thermal analysis using thermogravimetric analysis. Chemical characterization includes analysis of X-Ray Fluorescence (XRF) and Energy-Dispersive X-ray (EDX). Mineralogy characterization includes analysis of X-Ray Diffraction (XRD) and Fourier Transform Infrared Spectroscopy (FTIR). At the end of this chapter, the properties of materials used in the study are revealed with some modification to cope with the concrete related standards.

4.2 Physical Properties of Aggregates

The coarse aggregates used in this study is crushed granite from a local source (Miri, Sarawak) with the aggregates crushing value of 22.5%. The maximum size of coarse aggregates was chosen to be 12.5 mm in order to produce workable high performance concrete without segregation problems (Neville & Aitcin, 1998). The fineness modulus, specific gravity and water absorption of the coarse aggregates used in the mix design calculation were 7.0, 2.69 and 0.5%, respectively according to the tests conducted. The details of the specific gravity in other condition are given in Table 4.1.

Table 4.1: Specific gravity and water absorption of the fine and coarse aggregates

Sample Type	Specific gravity			Water absorption (%)
	Air dry	Saturated surface dry	Apparent	
Crushed granite	2.71	2.69	2.75	1.24
River sand	2.64	2.62	2.64	2.47
Quarry dust	2.66	2.62	2.69	1.50

The grading distribution graph for coarse aggregates is given in Figure 4.1. From this sieve analysis, the curve fell within the limits as shown in Figure 4.1 and the fineness modulus obtained was 2.67. The river sand used as fine aggregates in this study was also obtained from a local source. The grading distribution of the sand was not matching the standards' limits. After conducting the sieve analysis, the curve did not fall within the standards range according to ASTM C33-16 standards. The fineness modulus was 0.99 indicating high fineness of sand. The results of the sieve analysis of the original sand is shown in Figure 4.2 where the curve line shows a fall out of the standards limits. Therefore, in this study the combination of river sand and quarry dust with a weight ratio of 1:1 was used as fine aggregates. The combination grading curve is proven to be good grading because the curve falls within the standard limit. To ensure the size of the fine aggregates within the range, quarry dust was sieved and the final size used was those passing 4.75 mm sieve. The specific gravity for the river sand and quarry dust were the same, which is 2.62, and the water absorption was 2.47 and 1.50, respectively.

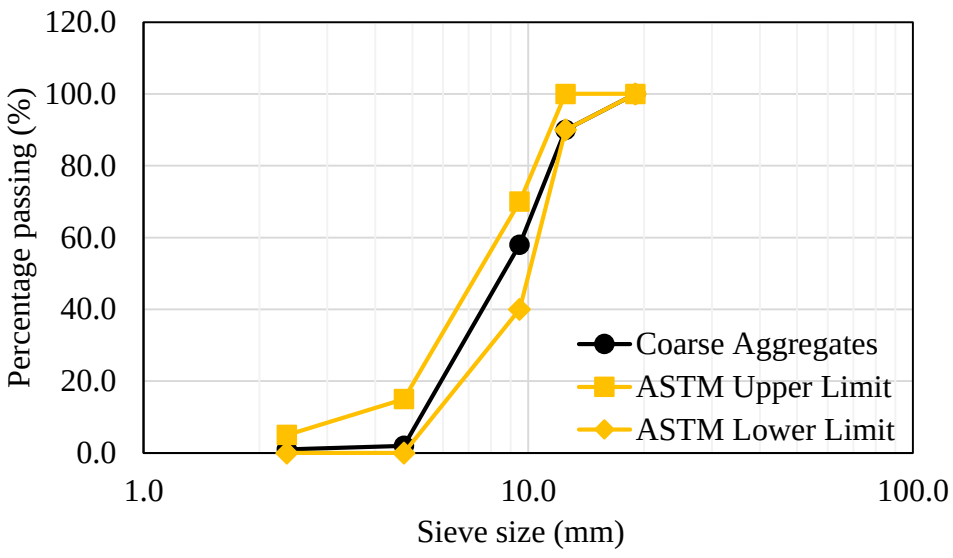

Figure 4.1: Sieve analysis of coarse aggregates

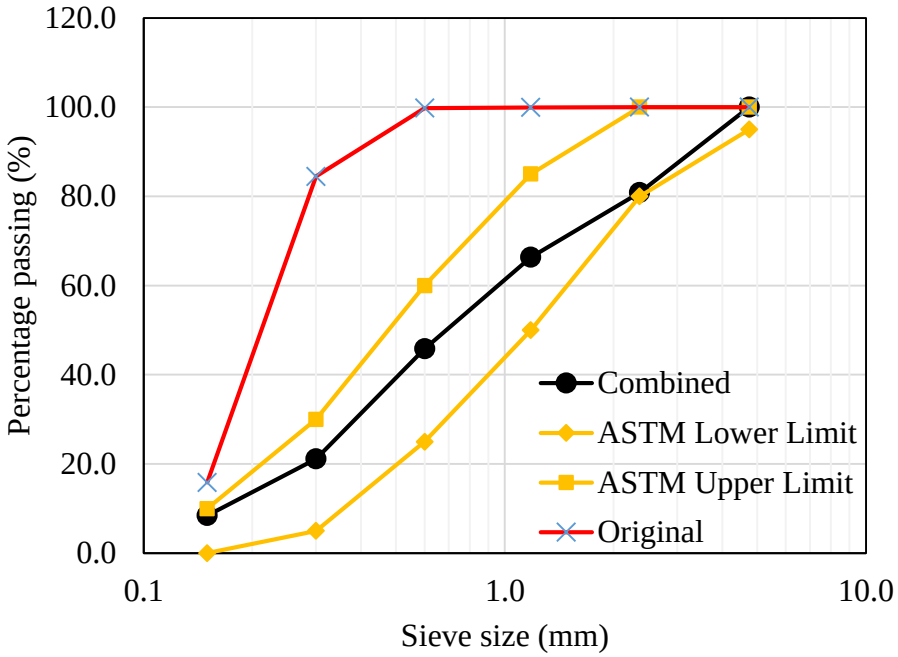

Figure 4.2: Sieve analysis of original sand and combined fine aggregates

The bulk density of aggregates or unit weight of dry rodded unit weight is one the important properties in the concrete mix design. The high bulk density is necessary to allow the space for the cement paste as the binding medium. Normally, the bulk density of the fine aggregates is larger than that of the coarse aggregates. The method in determining the bulk density was conducted based on ASTM C29-17 and the results are tabulated in Table 4.2.

Table 4.2: Bulk density of the fine and coarse aggregates

Sample Type	Loose	Compacted
	Bulk density (kg/m^3)	Bulk density (kg/m^3)
Crushed granite	1481	1600
River sand	1400	1658
Quarry dust	1381	1622

4.3 Physical properties of POFA

The raw palm oil fuel ash (POFA) was collected from Bekenu, Sarawak. It was obtained from the combustion of mesocarp fibers and shells from the palm oil fruitlet at temperature 800-1000 ºC. The raw POFA was obtained from the combustion chimney. Raw POFA taken from the mill was not fully burnt because the burning

process was done in huge amounts and due to that, there were still unburnt residues left (Chandara et al. , 2010). At the preliminary stage, the LOI test was done for the raw POFA to check the unburned carbon in the sample. The LOI values for the raw, micro and nano POFA were 10%, 4.67 and 1.80%, respectively as presented in Table 4.3. The test of LOI was in accordance with ASTM D7348-13. Through the heat treatment of POFA, LOI value was reduced to below than 6% as the limit stated in ASTM C618-15. The colour of raw POFA before the heat treatment was darkish compared with the micro POFA that had undergone the heat treatment. Figure 4.3 shows the relation between the colours of POFA with the unburnt carbon. The whitish colour can be found in the absence of unburnt carbon (Abdullah, Hussin, Zakaria & Muhamad, 2006).

Table 4.3: Colour and LOI results for POFA

POFA size	LOI%	ASTM C618-15 LOI Requirement (%)	Colour
Raw	10.0	max 6%	Darkish
Micro POFA (45 µm)	4.67		Greyish
Nano POFA (1-100 nm)	1.80		

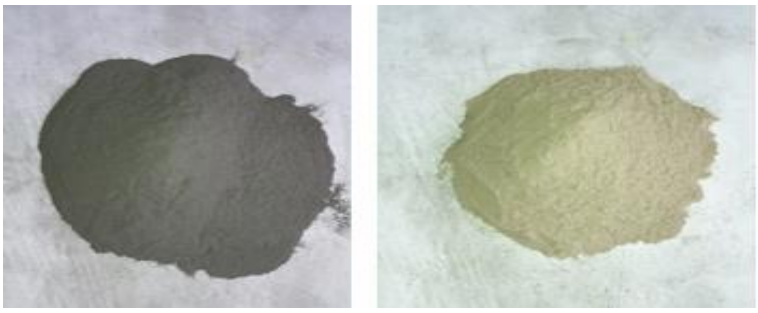

Figure 4.3: Darkish raw POFA before (left) and greyish POFA after heat treatment (right)

Other physical properties of micro and nano POFA are shown in the Table 4.4. The fineness of micro POFA was expressed with regards to the particle mass passing through the sieve no. 325 or 45-µm sieve size. According to ASTM C618-15, the permissible limit for the particle passing the 45-µm sieve is ≥ 34%. The micro POFA and nano POFA were 90 and 100 %, respectively passing the 45-µm sieve and the percentage increased after the second stage of grinding to produce nano POFA. In

terms of the strength activity index, the combination of micro and nano POFA as supplementary cementitious material in concrete exhibits 97% where it is above the permissible limit stated in ASTM C618-15. The micro POFA exhibits lower values than the specified minimum limit with a value of 70%. Nano POFA possesses a good strength activity index as can be seen in Table 4.4. The strength activity index above the permissible limit indicates good reactivity or pozzolanic reaction of the supplementary cementitious material (Safiuddin, Abdus Salam, & Jumaat, 2011).

Table 4.4: Physical properties of micro and nano POFA

Properties	Micro POFA	Nano POFA	Combined	ASTM C618-15 Requirement (%)
Passing sieve 45 µm (% mass)	90	100	-	≥ 34
7-days strength activity index (%)	70	74	97	≥ 75

4.4 Thermal analysis of POFA

As discussed in the previous chapter, the unburned carbon left in the raw POFA was 10% where 6% is the maximum limit allowed by ASTM C618-15. Therefore, the heat treatment process is necessary to remove the unburned carbon in the POFA that can affect the compressive strength of concrete (Chandara et al., 2010). The unburned carbon residue in the supplementary cementitious material absorbs the water content and superplasticizer, consequently affecting the workability of concrete and compressive strength as well. This issue requires a greater amount of superplasticizer in order to maintain the fluidity of the concrete mix. To improve the quality of POFA, POFA has to undergo the heat treatment process to remove the carbon content. The temperature of this thermal process can be obtained through thermogravimetric analysis (TGA).

Figure 4.4 shows the three stages of weight loss of POFA. The first weight loss was noticed at approximately 3.16 % at the temperature of 38.47 to 433.62 ºC that indicates the process of moisture evaporation and degradation of cellulose (lower molecular weight) in POFA. The major weight loss was recorded at temperatures

between 433.62 to 803.65 ºC with 8.28 % of weight loss. The high amount of loss occurred is due to the minimal contribution of decarbonation process in POFA and degradation of the sugar based polymers in the POFA such as lignin and cellulose. The source of that carbon can be obtained from the shell and fruit bunch of palm oil. Since the POFA was produced from the combustion process of empty fruit bunches and palm oil fibre with random proportion, thus the waste produced sugar based polymer such as cellulose and hemicellulose with protein, lignin and inorganic components (Hesas, Arami-Niya, Daud & Sahu, 2013). Hence, the weight loss between the temperature ranges was quite high due to the composition of the organic carbons in the palm oil fruit. The last stage of weight loss was recorded at a temperature range of 803.65 to 1007.81 ºC. This minor loss of 0.88% indicates degradation of the process of high molecular weight of lignin (Awal & Hussin, 1997; Mo, Liu, Al-Tabbaa, Deng & Lau, 2015; Tangpagasit, Cheerarot, Jaturapitakkul & Kiattikomol, 2005).

Based on the TGA analysis, the temperature of the heat treatment can be determined from the highest weight loss of POFA where it indicates that the carbon content was fully burned. Temperatures of 500 °C was found suitable for the heat treatment due to the major mass loss within the temperature range of 444.62 to 803.65 °C. Similar observations were found by other researchers where the temperature range of 500 to 650 °C was found suitable due to major carbon loss observed, and the significant increase in the compressive strength of concrete (Hill & Folliard, 2006; Nagi, 2007). The POFA was heat treated at 500 °C for one hour to remove the unburned carbon and this process also transforms the colour of POFA from darkish to greyish colour.

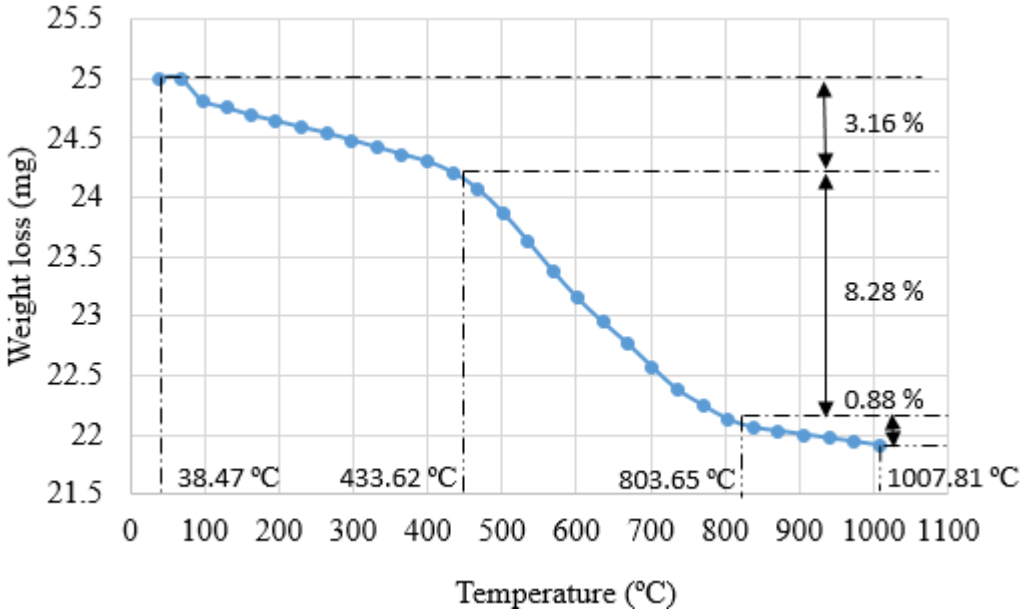

Figure 4.4: TGA analysis of POFA

4.5 Chemical Properties of POFA

At the preliminary stage, the chemical properties of raw POFA was obtained before it proceeded to the production of micro and nano POFA. Based on the previous study on POFA, it was observed that POFA has variations in the chemical components. The variations are dependent on many factors such as temperature during the combustion process, ratio of feeder in the boiler, geological factors and type of feeder burned in the boiler (Di Blasi, 2009). As stated in ASTM C618-15, pozzolanic material can be classified into two classes, Class C-fly ash has the total weight of oxide components ($SiO_2 + Al_2O_3 + Fe_2O_3$) below 70% by weight and Class F-fly ash consists of the main oxide components above 70% by weight. It is important to determine the variation of oxides component in the supplementary cementitious materials to assess the class of pozzolanic materials and its pozzolanicity. Researchers have highlighted that POFA with higher silica content was produced from the burning of the palm kernel while POFA produced from the burning of fruit brunches showed higher carbon content. More unburned carbon left in POFA can affect the strength development of concrete (Megat Johari, Zeyad, Muhamad Bunnori, & Ariffin, 2012; Zeyad, Johari, Bunnori, Ariffin, & Altwair, 2012). The good pozzolanic material that is probable to

produce good quality concrete consists of silicon oxide range between 43% to 71% (Hamada et al.,2018).

The chemical composition of raw POFA can be found in Table 4.5. Silica oxide content, SiO_2 is the major chemical composition of raw POFA, which is 59.3%. The total content of silica, aluminum and ferum oxide is 70%. SO_3 is 2.6%, which is within the limit of 4.0%. From this information, it shows that the raw POFA has the potential in enhancing pozzolanic reaction and contributing to the strength of concrete. Thus, from Table 4.5, POFA has a higher percentage of silica content compared with ordinary Portland cement (OPC). According to ASTM C618-15, POFA used in this study can be classified as Class F due to the sum of silica, aluminum and iron oxide is equal to 70%.

Table 4.5: Chemical composition of OPC and raw POFA

Chemical composition (%)	OPC	Raw POFA	Class F fly ash (ASTM C618-15)
SiO_2	20.0	59.3	Minimum 70 %
Fe_2O_3	3.27	6.4	
Al_2O_3	5.66	4.1	
K_2O	-	10.4	
CaO	62.52	8.9	
P_2O_5	-	3.7	
MgO	1.21	2.7	
Na_2O	-	0.2	
SO_3	2.47	2.6	Maximum 5%

The production of micro POFA continued with the sequence process of sieving, grinding and heat-treating. second stage of grinding takes place to produce nano POFA. These processes have transformed the micro and nano POFA to increase the pozzolanitic due to the increase of silica content. As shown in Table 4.6, the silica content in micro and nano POFA are 66.62% and 65.08%, respectively. The results of the chemical compositions of both materials show better properties than that of the raw POFA and OPC. From these results, it is clearly shown that the chemical composition was improved after the refining of POFA particles and heat treatment applied. The higher silica content in micro and nano POFA provides formation of additional calcium silicate hydrate (CSH) gel hence, enhancing the strength of concrete.

Table 4.6: Chemical Composition in micro and nano POFA

Material	SiO_2	Fe_2O_3	Al_2O_3	CaO	MgO	SO_3
Micro POFA	66.62	2.25	1.98	9.56	4.21	1.35
Nano POFA	65.08	2.56	2.53	10.29	4.86	0.88

4.6 Morphology properties of POFA

The morphology properties of raw, micro and nano POFA were obtained using Scanning Electron Microscopy (SEM). These morphological properties are able to provide geometrical part of cementitious materials. Generally, the raw POFA consists of larger and irregular shaped particles and porous structure (Tangchirapat & Jaturapitakkul, 2010). In this study, the raw POFA showed the same characteristics as in the previous study. Figure 4.5 shows the raw POFA surface morphology. It is observed that the sample consists of very porous structures and the shape of the raw POFA particles are irregular. This image was analysed using SEM as soon as the raw POFA produced at the palm oil mill.

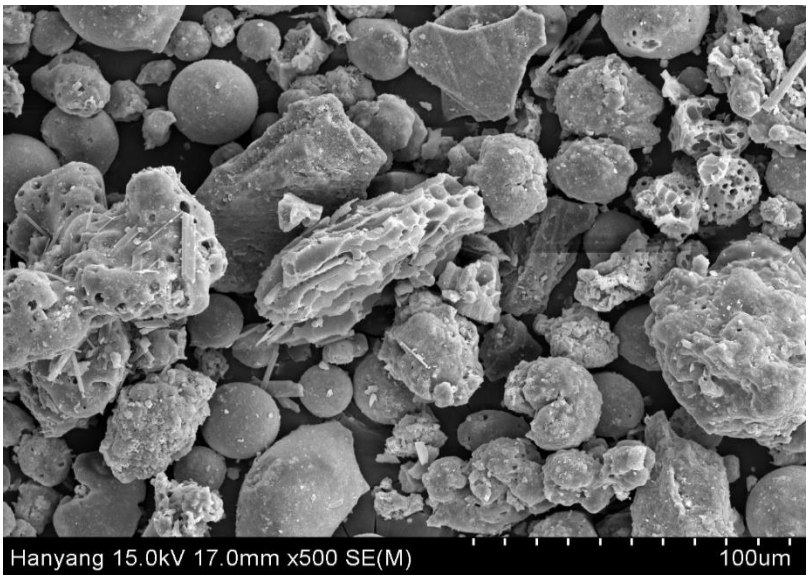

Figure 4.5: Surface morphology of raw POFA

Unlike the raw POFA, the micro POFA has different morphology properties due to the process of sieving and mechanical milling. The micro POFA showed less porous particles due to removal of coarser particles through the sieving and grinding

process. The SEM images of micro POFA shown in Figure 4.6 (a) and (b) consist of round and ball-shaped particles that vary in size. The spherical shape of the cementitious material can provide good workability concrete at low water cement ratio (Ranjbar, Mehrali, Alengaram, Simon, & Metselaar, 2014). In Figure 4.6 (b), the close-up SEM image shows the pore on the surface of micro POFA particles which appears less porous than raw POFA. The porous structure of the POFA can contribute to moisture absorption and reduce the workability of concrete (Noorvand et al., 2013). The results of elemental analysis of micro POFA are shown in Figure 4.7 and Table 4.7 by using energy-dispersive X-ray spectroscopy (EDX) analysis. The data was generated from the mapping method to identify the chemical compositions of the material. The spectrum point was identified from the SEM image as shown in Figure 4.6 (a) to determine the weight percentage of the major elements in the micro POFA at the particular spectrum.

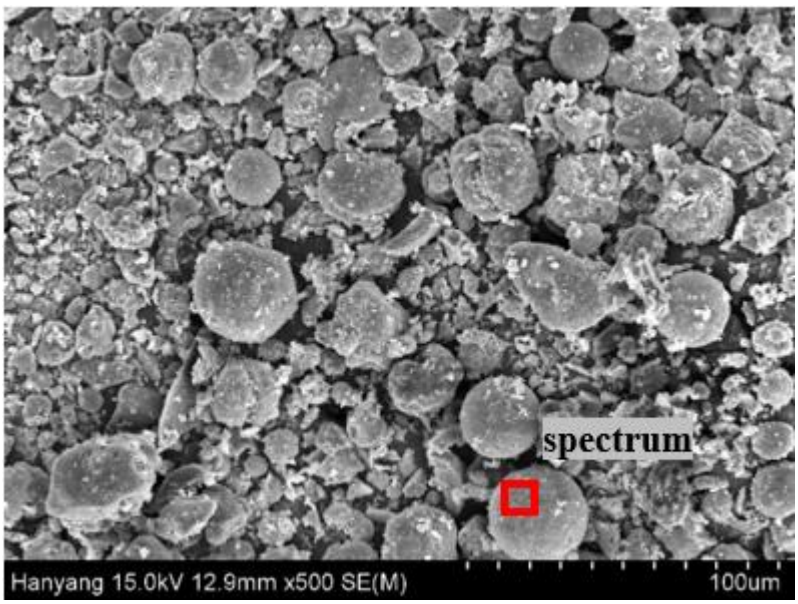

(a)

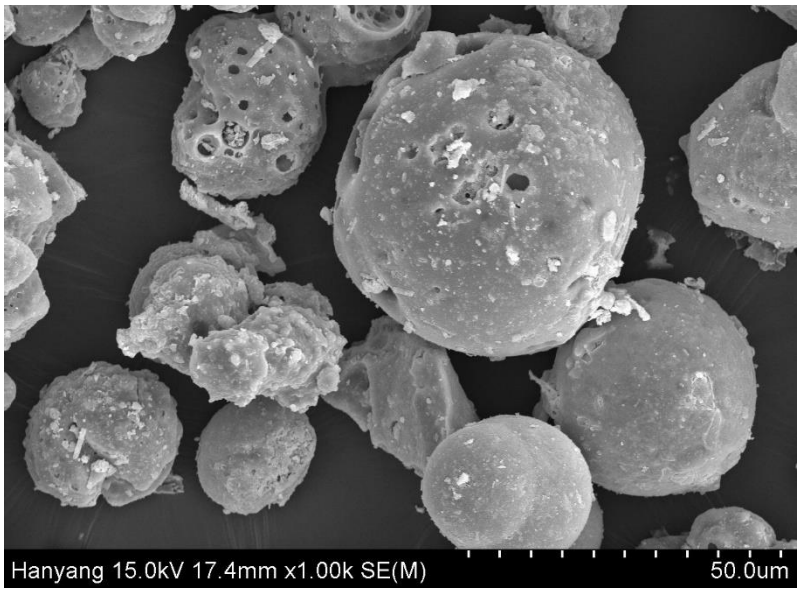

(b)

Figure 4.6: Surface morphology of micro POFA with different magnification

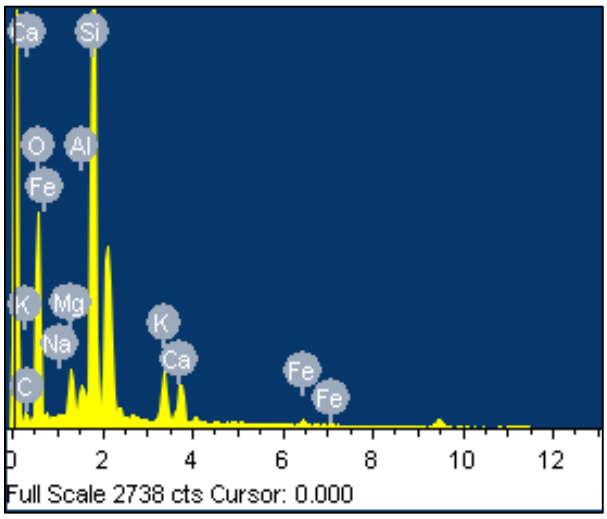

Figure 4.7: SEM-EDX analysis of micro POFA

Table 4.7: Element analysis of micro POFA

Element	Weight%
Si	15.10
C	-
O	36.74
Na	0.03
Mg	4.02
Al	2.34
K	5.78
Ca	6.62
Fe	2.68
Zr	24.80
W	1.88
Totals	100.00

The SEM images of nano POFA can be found in Figure 4.8 (a) and (b). The surface morphology of nano POFA could not be clearly seen but the shape can be observed, hence, leading to particle size analysis using transmission electron microscopy (TEM). Figure 4.8 (a) shows the SEM image of nano POFA in the same magnification scale of micro POFA (Figure 4.6(a)). Nano POFA has an irregular shape and is significantly thinner than the micro POFA. The single particle of nano POFA cannot be seen due to the second stage of grinding using mechanical milling. The particles have decreased to nano range and it tends to agglomerate due to strong Van der Waals forces between the particles (Safiuddin, Gonzalez, Cao, & Tighe, 2014). The second image in Figure 4.8 (b) at magnification scale of 70,000 shows the nano POFA particles agglomerated (in the round circle). The element microanalysis for the nano POFA was performed using EDX analysis. The results of the element analysis are shown in Figure 4.9 and Table 4.8 based on the spectrum identified. The silica content in nano POFA was found to be higher compared to the micro POFA. This could overcome the drawback of the micro POFA and lead to the enhancement of strength and durability of higher performance concrete. The higher amount of silica and higher fineness of nano POFA does help in the strength development of concrete and durability as well.

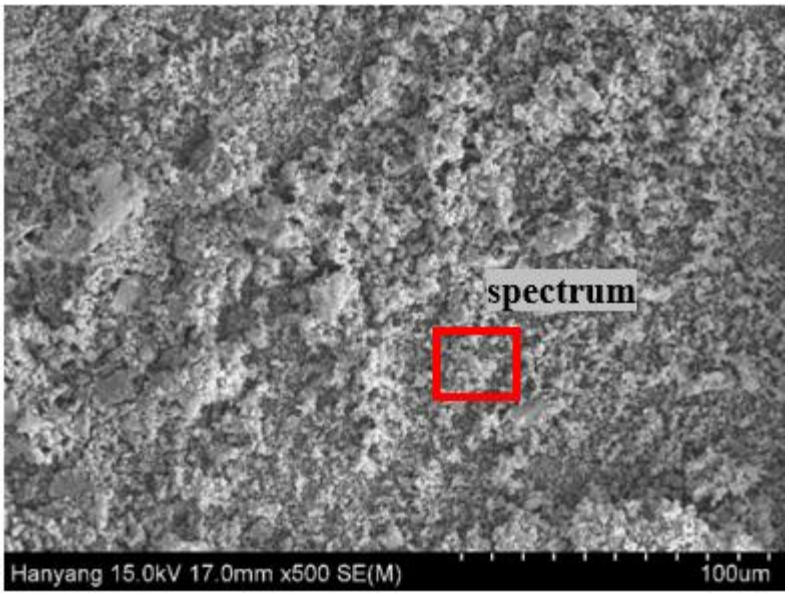

(a)

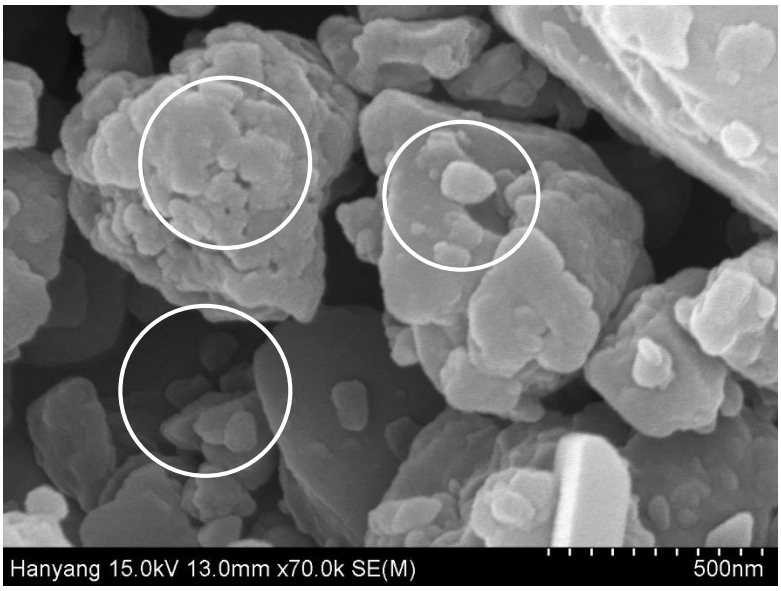

(b)

Figure 4.8: Surface morphology of nano POFA

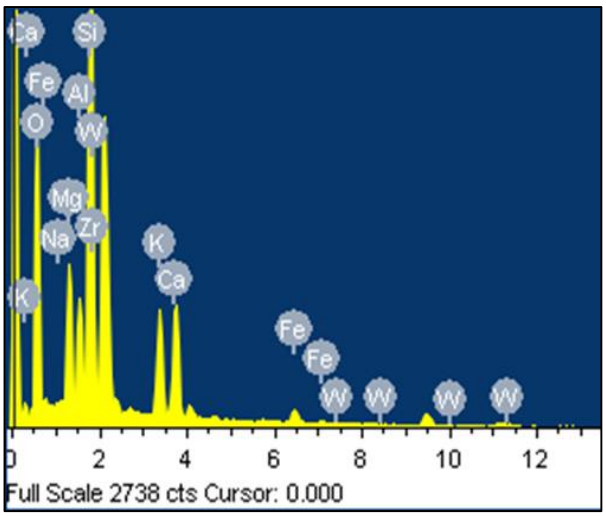

Figure 4.9: SEM-EDX analysis of nano POFA

Table 4.8: Element analysis of nano POFA

	Nano POFA	
Element	Weight%	Atomic%
Si	31.60	23.27
C	3.19	5.50
O	47.00	60.77
Na	0.18	0.16
Mg	3.00	2.55
Al	1.15	0.88
K	6.01	3.18
Ca	5.29	2.73
Fe	2.58	0.96
Zr	-	-
W	-	-
Totals	100.00	

Figure 4.10 shows the TEM micrograph of nano POFA particles that was captured from the analysis of transmission electron microscopy. Single particles of nano POFA are visible in the image and the spherical shape of the nano POFA can be clearly observed. The measurement of particle size was recorded during the TEM analysis. The particles size analysis was further performed to determine the size range for each of the image using Image J analysis. This software is a standard software for quantification of markers which was first developed at the National Institute of Health (Schneider, Rasband, & Eliceiri, 2012). About 240 nano POFA particles from six TEM micrographs were taken to proceed with the Image J analysis. Then, the tabulated data from the measured particles were carried out with statistical analysis. The results of the statistical distribution for the measured particles is shown in Figure 4.11. The average size of nano POFA particles is 40 nm with standard deviation of 13 nm. The maximum size of the measured particles is 90 nm and the minimum diameter is 20 nm. The range of diameter of nano POFA particles size falls within 20 nm to 90 nm. From the data, the particle size distribution of nano POFA can be obtained as shown in Figure 4.12. Approximately 90% of nano POFA particles were found to be smaller than 60 nm and the average size was observed to measure around 40 nm as illustrated in Figure 4.12.

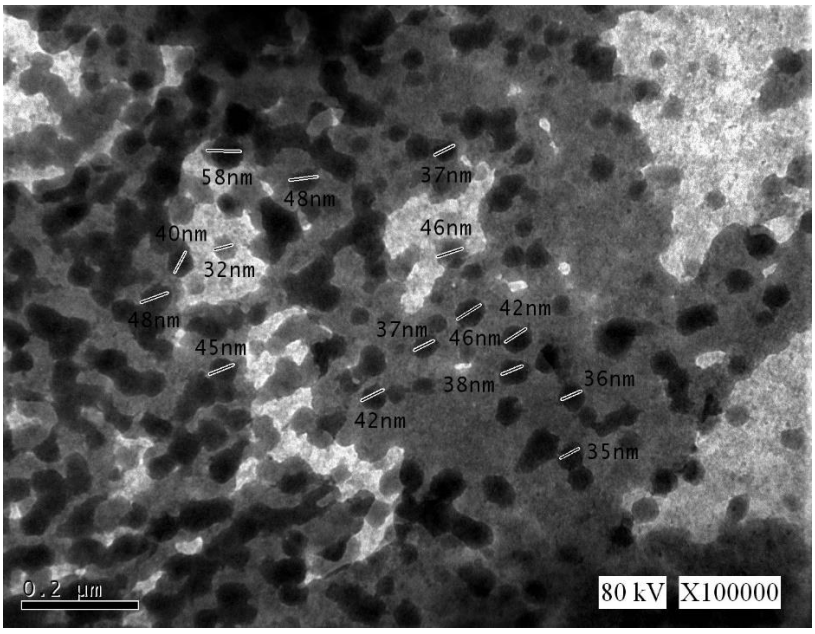

Figure 4.10: TEM micrographs of nano POFA particles

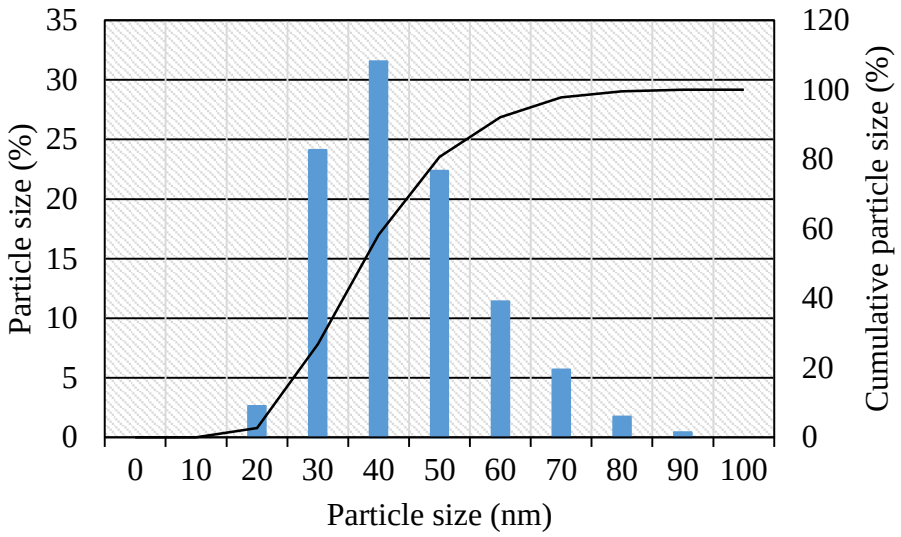

Figure 4.11: Particle size analysis of nano POFA using Zetasizer

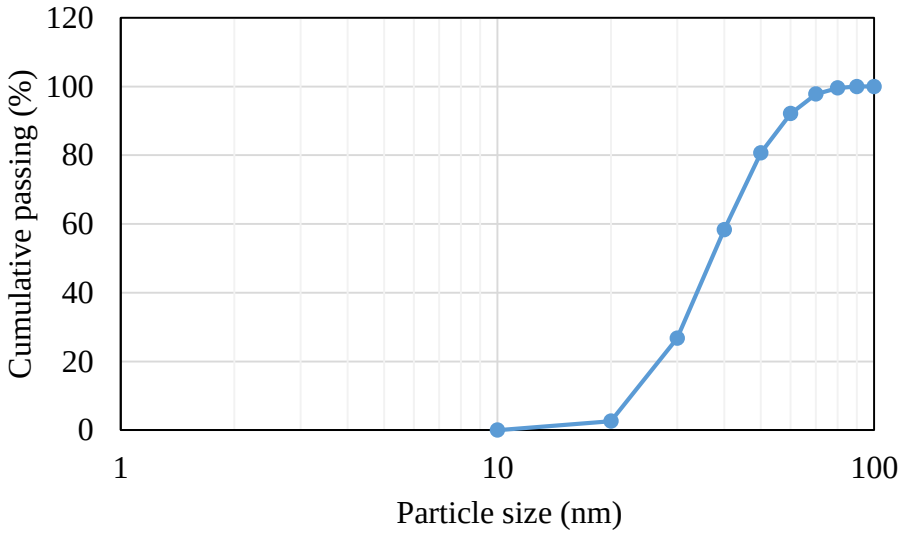

Figure 4.12: Particle size distribution of nano POFA

4.7 Mineralogy properties of POFA

Figure 4.13 and Figure *4.14* show the X-ray diffraction (XRD) analysis of micro and nano POFA. This analysis provides mineralogy properties of cementitious material where the crystalline nature of the material can be observed. The XRD

analysis detects the crystalline phase compositions which is significant in affecting the cement matrix, hence also impacting the strength of the concrete (Karim, Hashim, & Abdul Razak, 2016). Previous studies have shown that POFA consists of three mineralogical compositions where the main phase is quartz and the two minor phases are cristobalite and potassium aluminum phosphate, $K_3Al_2(PO_4)_3$ (Chandara et al., 2010). According to Chandara et al. (2010), the amorphous phase occurs at the 2-theta range 20º to 30º and at this point, the cementitious material exhibits high pozzolanic activity (Wang et al., 2014). However, the rate of pozzolonic activity relies on the surface area, chemical component of the cementitious material and composition of active phase. As for the overall pozzolanic reaction, the thermodynamic stability is an essential parameter (Karim et al., 2016). A peak of 26.5º (2-theta) was observed as the highest intensity for micro and nano POFA as shown in Figure 4.13 andFigure *4.14*. The high peaks in both graphs corresponding to quartz and the difference between the two cementitious materials was the intensity. The intensity of quartz for micro and nano POFA was 3400 and 3900 counts, respectively. The rest of the peaks belong to other minor phases presented in the graphs such as cristobalite and potassium aluminum phosphate, $K_3Al_2(PO_4)_3$.

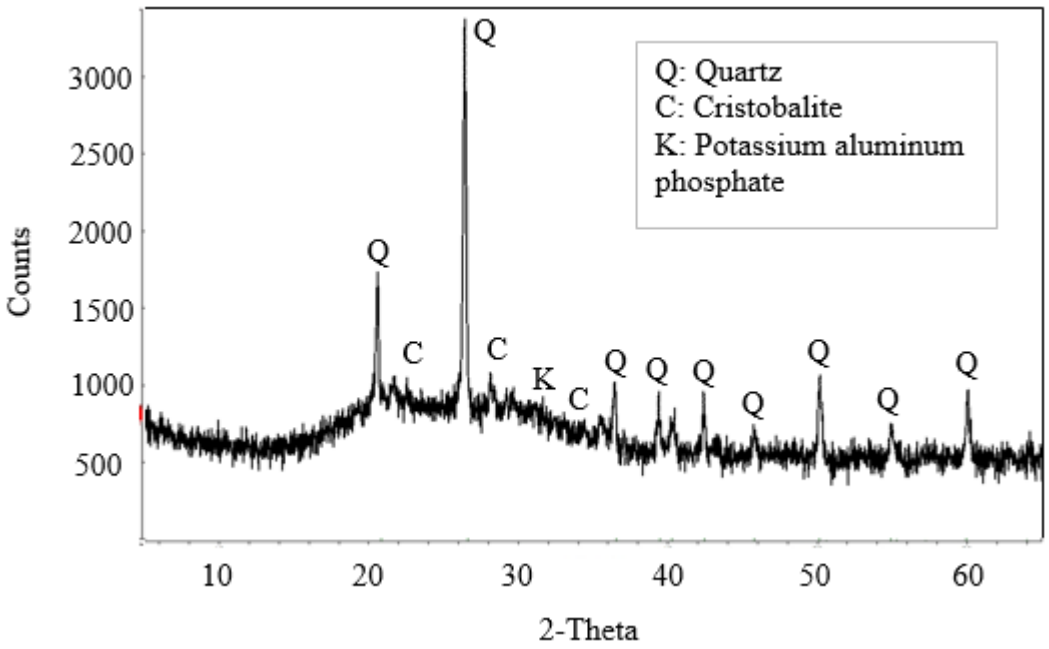

Figure 4.13: XRD pattern of micro POFA

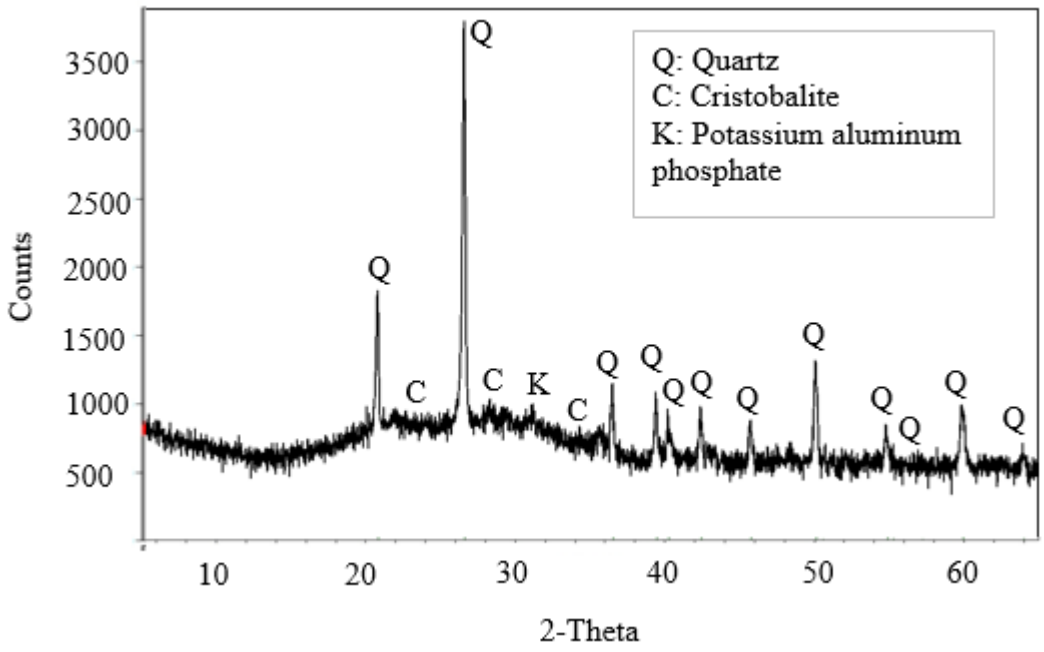

Figure 4.14: XRD pattern of nano POFA

Figure 4.15 and Figure 4.16 show the Fourier transform infrared spectroscopy (FTIR) spectrum graph for micro and nano POFA, respectively. The mineralogy properties in terms of crystalline phases, which was identified by XRD analysis, showed that quarts is the major phase in both cementitious materials. Besides, the XRF analysis also showed that silicon oxide, SiO_2 content as one of the major components present in the samples. Therefore, FTIR analysis was conducted to confirm the identified chemical properties of micro and nano POFA in terms of the chemical bonding. Since the silica content is the major component, the Si-O stretching band was found in micro and nano POFA at 1000 cm^{-1} and 1041 cm^{-1}, respectively. The spectrum of nano POFA was observed to have wider peak than that of micro POFA spectrum. The stretching band at 3000-3500 cm^{-1} and 1400-1700 cm^{-1} are attributed to the water component of O–H and H-O-H groups of water molecules respectively. All the stretching bands were labelled in both FTIR spectrum in Figure 4.15 andFigure *4.16*. The FTIR spectra for the nano POFA was found to have a wider peak compared to the micro POFA. These spectrum patterns for Si-O band were within the range as the most agricultural waste's spectrum. The Si-O band for an agricultural waste was in between 1000 to 1100 cm^{-1} while recording a wavenumber of 1650 cm^{-1} for the water bands (Karim et al., 2016). These patterns were in line with the previous studies that highlighted the wavenumber of certain chemical bonds such as Si-O stretching band

at 1040 cm^{-1}, O-H stretching band at 3465 cm^{-1} and H-O-H band at 1650 cm^{-1} (Lim et al., 2015).

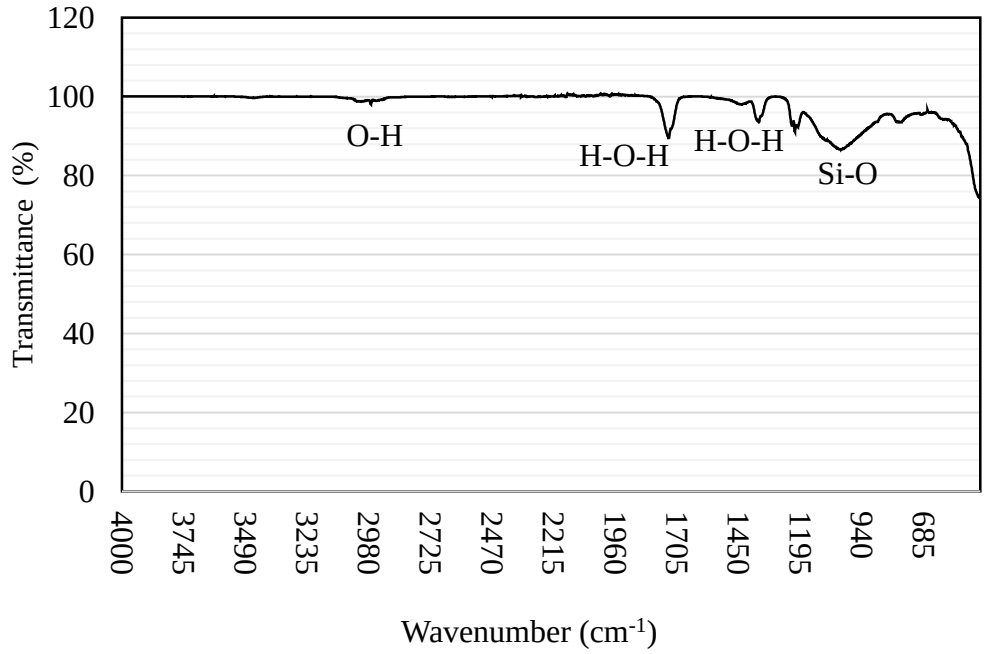

Figure 4.15: FTIR spectrum for micro POFA

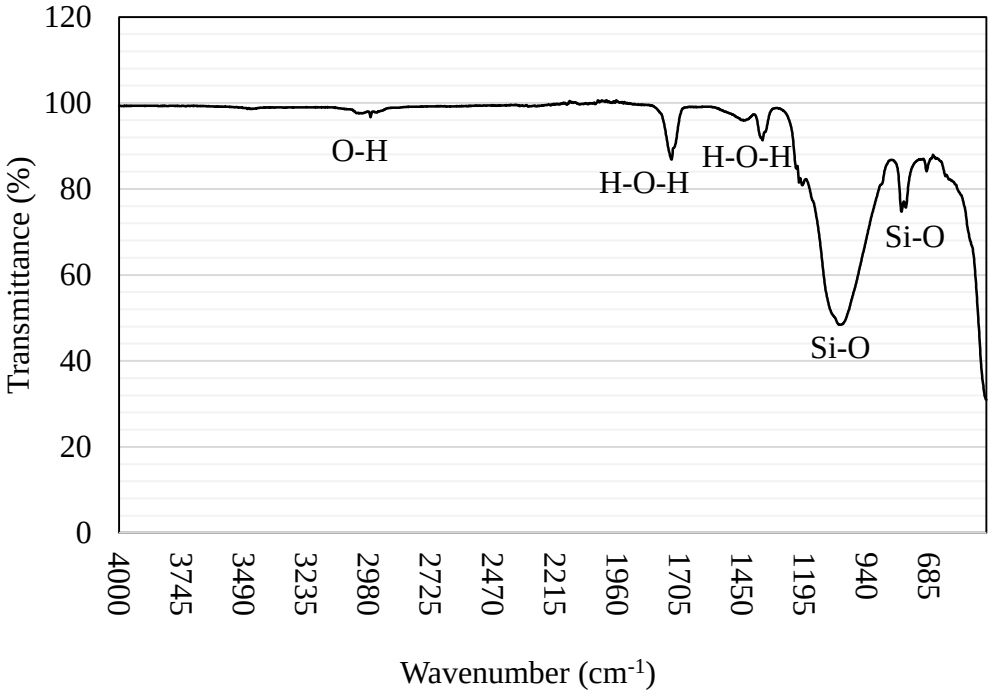

Figure 4.16: FTIR spectrum for nano POFA

4.8 Concluding Remarks

Based on the characterization of supplementary cementitious materials used in this study, the following conclusions can be drawn:

a) The physical properties of raw POFA showed the unburned residue left and the LOI value was above the ASTM C618-15 permissible limit. The heat treatment of POFA is necessary to fulfil the requirement as a pozzolanic material. Fineness of micro POFA was observed at 90%, passing the 45 µm sieve size while 100% passing for nano POFA. The strength activity index for the combination of micro and nano POFA exhibited 97% where above the permissible limit stated in ASTM C618-15. The strength activity index above the permissible limit indicates good reactivity or pozzolanic reaction of the supplementary cementitious material.
b) The TGA analysis of raw POFA showed a major weight loss of 8.28% in the temperature range between 444.62 to 803.65 °C. To fulfil the requirement of the LOI permissible limits in the ASTM C618-15, the temperature for the heat treatment was finalized at 500 ºC for 1 hour. The LOI of micro and nano POFA were reduced to 4.67% and 1.80% respectively, after the heat treatment and the colour of the POFA changed from darkish to greyish due to removal of unburned carbon during the heat treatment.
c) The chemical component of raw, micro and nano POFA showed that the total three main oxide components (SiO_2, Fe_2O_3, Al_2O_3) are all equal and above 70% which can be classified as Class F-fly ash. Higher silica content was observed in micro and nano POFA with 66.62% and 65.08%, respectively after the refining of POFA particles and heat treatment applied. These processes have transformed the micro and nano POFA to increase the pozzolanicity due to increased silica content.
d) Morphology properties through SEM observations revealed that the raw POFA is weak and consists of many impurities with larger, irregular and highly porous particles. By sieving and grinding the POFA to produce micro and nano POFA, the morphology properties of micro POFA can be seen as less porous than the raw POFA with round shape but which varies in size. The surface

morphology of nano POFA could not be clearly seen due to strong Van der Waals forces between the nanoparticles thus, leading to TEM analysis. Both elemental analysis of micro and nano POFA showed the major element is silica, which can contribute to formation of addition CSH gel.

e) TEM analysis has confirmed the single size of nano POFA and the particle size distribution graph was developed. The diameter range of nano POFA particles size falls within 20 nm to 90 nm. From the measured particles data, approximately 90% of nano POFA particles smaller than 60 nm. This meets the requirement that the nanoparticles must be within the size of 1 to 100 nm.

f) In the XRD analysis, the crystalline phase in the micro and nano POFA showed that quartz is the major phase in both of the materials at a peak of 26.5º (2-theta). The higher intensity of 3900 counts was recorded in nano POFA.

g) The FTIR spectrum confirmed the mineralogy properties found from XRD analysis. The FTIR spectrum data for micro and nano POFA showed the Si-O stretching band was found in micro and nano POFA at 1000 cm^{-1} and 1041 cm^{-1}, respectively. The wider stretching was observed from the nano POFA spectrum.

Chapter 5

Binder Optimisation Using Response Surface Methodology

5.1 Introduction

This chapter presents the design of experiments process in order to determine the optimum amount of binder (variables) proposed based on the goals of optimising the mechanical properties of concrete (responses). The overall aim of this chapter is to develop a set of the prediction models for workability, compressive strength, splitting tensile strength and flexural strength of high performance concrete at different ages. The design of experiment began with the identifications of variables and responses based on the analysis and the level selection for the variables to be applied in response surface methodology (RSM). By using RSM, the relation between the variables and responses can be determined. Under RSM, the Central Composite Design (CCD) approach was used to provide a set of running experimental program based on design of experiment (DOE). The experiments were conducted based on the designated matrix and in random order, to minimize the systematic error in the experiments. The mechanical properties for fresh and hardened properties of high performance concrete were carried out according to the standard procedure mentioned in a previous study. The design expert software version 9.0.6.2 was used to develop the mathematical models and the best model fit for the experimental data. The coefficient of each model was determined through regression analysis and the adequacy of the models developed was obtained using analysis of variance (ANOVA). For optimisation analysis, the desirability approach was used to optimise the multiple responses in this study. This approach searches for the most suitable combination of variable levels while at the same time satisfying the optimisation criteria proposed. If one of the combination is outside the desired criteria, the analysis will eliminate the proposed solution.

5.2 Design of Experiment (DOE) using Central Composite Design (CCD)

The central composite design (CCD) was used in the design of experiment (DOE) to determine the optimum binder in concrete mix. CCD is a suitable method to find a functional relationship between the variables and responses in one analysis and it limits the number of trial batches to run (Khodaii, Haghshenas, & Tehrani, 2012). In

addition, this method is capable of predicting second-order model without completing the three-level factorial design. Design Expert Software version 9.0.6.2 was employed for the design, mathematical modelling, statistical analysis and optimisation process. In the design, the micro POFA is coded as A and nano POFA is coded as B. Both were chosen as the potential variables and were studied at three different levels (-1, 0, 1). The variables and levels are shown in Table 5.1. The total number of experiments based on the variables selected were 13, obtained as ($2k + 2k + 5 = 13$) where the number of variables is two. Thirteen different combinations were presented in the design with five replicates of the mean case at central points. According to Myers, Montgomery, & Anderson-Cook (2016), 3 to 5 center runs are recommended to use as replicates to get a better estimation. The mid-level replication was considered to improve the precision of the experiment and determine the experimental error for the modelled responses. Then, a total number of experimental run was setup by CCD in random order as shown in Table 5.2. The testings were carried out based on the design and symbol M and N, denoted as micro and nano POFA, respectively. The following number after the alphabet M and N indicates the percentage replacement by weight of cement.

Table 5.1: Input variables and the coded levels adopted for CCD

Variables	**Code**	**Variable levels of code**		
		Low -1	Intermediate 0	High 1
Micro POFA (%)	A	10	20	30
Nano POFA (%)	B	1	2	3

Table 5.2: Experimental design run according to DOE in coded values

Run	Block	A	B	Symbol
1	1	-1	-1	M10N1
2	1	1	-1	M30N1
3	1	1	0	M30N2
4	1	0	0	M20N2
5	1	0	0	M20N2
6	1	0	0	M20N2
7	1	0	1	M20N3
8	1	0	-1	M20N1
9	1	0	0	M20N2
10	1	1	1	M30N3
11	1	-1	0	M10N2
12	1	-1	1	M10N3
13	1	0	0	M20N2

The reference mix proportion of high performance concrete without supplementary cementitious material was obtained based on ACI 211 as discussed in chapter 3. The parameters in the mix proportion except the proposed binders remain unchanged to determine the relationship of the proposed binders with the mechanical properties of high performance concrete. Therefore, the statistical models developed are valid for the mix with cement content of 586 kg/m^3, water-binder ratio of 0.3 by mass of OPC, superplasticizer dosage of 0.2% out of cementitious materials while the coarse and fine aggregates is at 1093 kg/m^3 and 536 kg/m^3, respectively. The trial batches of the reference mix was done in order to achieve the performance requirements of HPC. These include meeting the the target compressive strength of approximately 50-80 MPa at the age of 28 days, achieving the slump range between 100-150 mm and the ensuring that the 7-days strength is about 75% of the 28-days strength. These criteria are based on the ACI Committee 363 that states, "in producing high performance concrete, the targeted design strength is 55 MPa or more and possess high workability and high durability properties" (ACI Committee 363; Mehta & Aitcin, 1990).

5.3 Experimental Data

The experiments were conducted based on the chosen responses and the procedures are based on the ACI Committee standards. Four types of responses were tested and modeled using CCD to determine the relationship with the proposed binders. About 378 concrete specimens were prepared based on the CCD experimental design runs. Each of the hardened properties was tested at three different ages to indicate the strength development of high performance concrete containing micro and nano POFA. In order to predict the model for each response, the specimens prepared for compressive strength test were 126 cube specimens of 100 x 100x 100 mm, 126 cylinder specimens of 100 mm diameter and 200 mm height for splitting tensile strength test and 126 prism specimens of 100 mm x 100 mm x 500 mm for flexural strength test. The binder proportions and the responses obtained from the experimental study are presented in Table 5.3. Figure 5.1 presents the experimental data for fresh properties of high performance concrete containing micro and nano POFA. One of the fresh properties tested in this study was the slump test. As compared to the control mix, it can be seen that there is an enhancement of the fresh properties in concrete with 10% of micro POFA and 1-3% replacement of nano POFA. The highest slump height was recorded in M10N3 mix with 150 mm which is about 7% increment compared to the control mix. M10N2 also showed good workability where the value of slump height was 140 mm with Rincrements of about 3.6% than that of control mix. M10N1 mix was a bit out of the range of targeted slump as the value of slump was reduced to 100 mm. The significant increment of the slump height was attributed to the lower amount of the loss on ignition (LOI) which indicates a lower carbon content of the POFA (Megat Johari et al., 2012). Another reason highlighted by Alsubari, Shafigh, & Jumaat (2016) is that the fine particles of the treated POFA are absorbed by the oppositely charged surfaces of cement particles which prevents them from flocculation. This causes the cement particles to disperse effectively and will not trap large amounts of water. This result is in line with the study done by Aldahdooh, Muhamad Bunnori, & Megat Johari (2013) in which the study also used ultrafine POFA 2.06 μm as cement replacement to produce high performance concrete. Other mixes that consists of 20% and 30% of micro POFA with combination of 1-3% of nano POFA showed reduction in workability as shown in Figure 5.1. Studies by Chandara, Sakai, Azizli, Ahmad, & Hashim (2010) and Awal & Abubakar (2011) argue that the

reduction of workability occurs due to the increasing replacement of micro POFA. The authors claimed that the higher amount of micro POFA contributes to the increase of unburned carbon in concrete that absorbs more water content and superplasticizer. Based on the characterisation analysis of micro POFA, in this study it was found that the LOI value has been reduced as per the requirements in ASTM C618-19. However, the surface morphology showed the porous structure of micro POFA, which is related to higher moisture absorption during the concrete mixing process. The slump heights were recorded in the range of 30 to 65 mm where the values are out of the targeted range of slump. A review about nanoparticles by Reches (2018), he revealed that the high surface area and reactivity may affect the mechanical and durability properties of concrete. Generally, the nanoparticles give negative effects on the workability of concrete however, in some cases they have improved the workability of concrete (Aggarwal, Singh, & Aggarwal, 2015; Sanchez & Sobolev, 2010) . The findings of this research was similar to those of this study in terms of the workability of concrete.

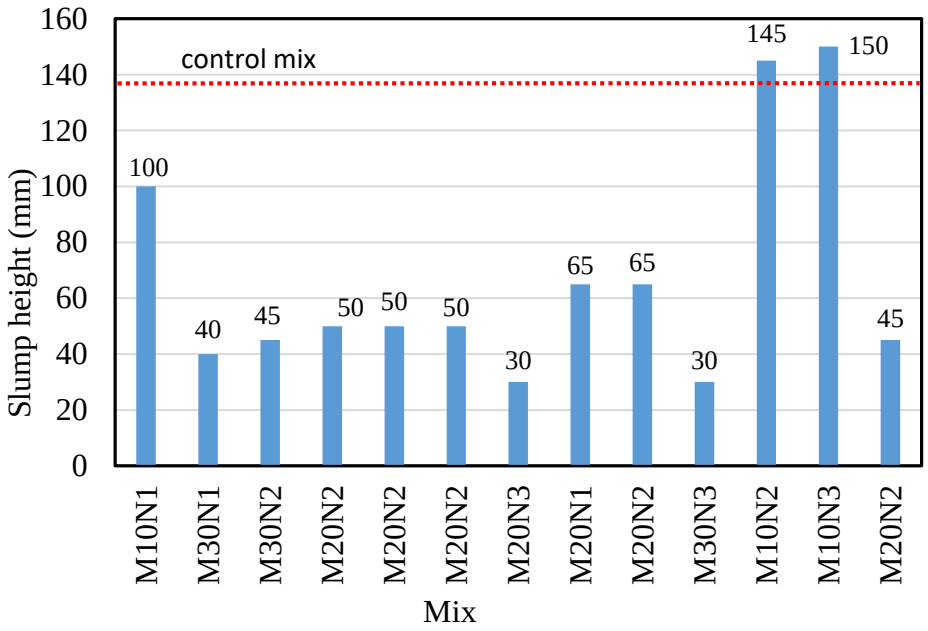

Figure 5.1: Slump height for each mix

For mechanical properties of high performance concrete, the experimental data/ responses used in the analysis were compressive strength, splitting tensile strength and flexural strength at the age of 7, 28 and 90 days. The ages represent the early and later strength development of concrete. Figure 5.2 shows the results for the compressive strength of each concrete mix containing 10-30% of micro POFA (M)

and 1-3% of nano POFA (N). The control mix containing 0% of micro and 0% of nano POFA was used as the reference mix to determine the significance of both proposed supplementary cementitious materials in enhancement of compressive strength. The mix M10N1 containing 10% of micro POFA and 1-2% of nano POFA exhibited higher compressive strength at an earlier age than that of the control mix. The increment of the compressive strength of about 3 – 4% showed the early maturity of the concrete due to the formation of secondary CSH gel at an early age. The improvement at the early age was attributed to the void filling in cement matrix caused by the nano POFA particles that reacts with the weak products during the hydration process to form additional calcium silicate hydrate. Therefore, this affects the density the concrete matrix at the early stages.

At a later age of 28 and 90 days, similar patterns of strength development can be seen. The increment of compressive strength recorded was approximately 2.2%, 0.5% and 3.5% yielded by mix M10N1, M10N2 and M10N3 respectively, compared to the control mix at the age of 28 days. More increment was recorded at the age of 90 days where M10N1, M10N2 and M10N3 exhibited increments of about 3.2%, 3.2% and 3.7%, respectively than that of the control mix. This finding shows that the increasing replacement of nano POFA at 1-3% is significant in enhancing the compressive strength of concrete containing micro POFA. This finding is in line with the findings of Saleh, Ibrahim, & Salman (2015). The reason behind this was explained by Bjornstrom, Martinelli, Matic, Borjesson, & Panas (2004) that nanoparticles in cement matrix acts as nucleation sites to further promote and accelerate the hydration process. The nano POFA that is dispersed in the concrete matrix proved that the higher surface energy (nucleation sites) is able to enhance the compressive strength at all ages.

However, an increasing amount of micro POFA with 1–3% of nano POFA was observed to decrease the compressive strength at all ages. This comparison was made with the control specimen containing 0% of micro and nano POFA. The decrease in the strength was due to the high amounts of micro POFA in the mix that contains porous particles which absorbs the water content needed for cement hydration (Jaturapitakkul, Kiattikomol, Tangchirapat, & Saeting, 2007; Tangchirapat, Khamklai, & Jaturapitakkul, 2012). However, other patterns can be seen from mix containing

10%, 20% and 30% of micro POFA with increasing amounts of nano POFA where the compressive strength was observed higher as the nano POFA increase.

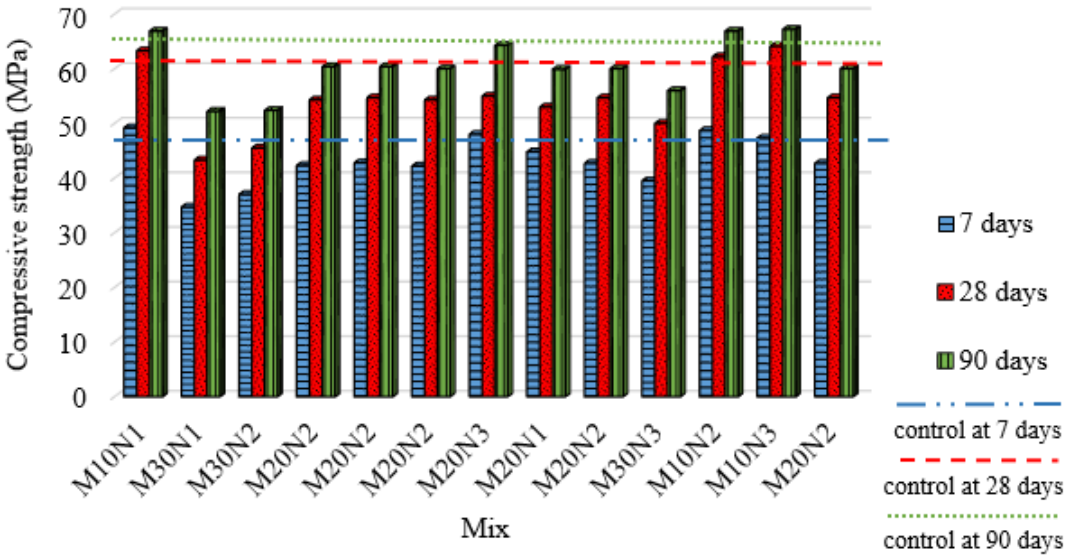

Figure 5.2: Compressive strength for each mix

For the splitting tensile strength test, the results in the Figure 5.3 showed the same pattern as the compressive strength. Mix M10N3 containing 10% of micro POFA and 3% of nano POFA exhibited higher values by approximately 10% than the control mix at the early age of 7 days. The combination of micro and nano POFA was observed to improve the splitting tensile strength where it was recorded that the mix showed increments of about 3%, 6.5% and 10 % yielded by M10N1, M10N2 and M10N3, respectively as compared with the control mix. The replacement of micro and nano POFA in the mix enhanced the strength due to pore refinement of the concrete matrix hence, increasing the pozzolanicity. It was also reflected that at the early age of 7 days, splitting tensile strength showed significant improvements due to the higher strength. The replacement of nano particles was observed to help the acceleration of the hydration process to produce the structural 'glue' for concrete. Similar finding was found for the mixes at the age of 90 days where the splitting tensile strength was recorded to be higher by 4%, 7% and 2% from mix M10N1, M10N2 and M10N3 as compared with the control mix. The positive contributions of nanomaterials on the strength properties have been discussed by other researchers as reviewed by Lim, Raman, Lai, Zain, & Hamid (2018). The researchers revealed that the nanoparticles from rice husk ash, POFA and ground granulated blast slag form a novel high

performance composite binder. Bjornstrom et al. (2004) also proved that the nanoparticles including nanosilica was able to provide rapid effect on the cement hydration. Singh, Karade, Bhattacharyya, Yousuf, & Ahalawat (2013) found that nanosilica improved the workability, compressive strength and resistance to water penetration and Du, Du, & Liu (2014) claimed that the nanoparticles contributes to the enhancement of the early strength of concrete and durability properties as well.

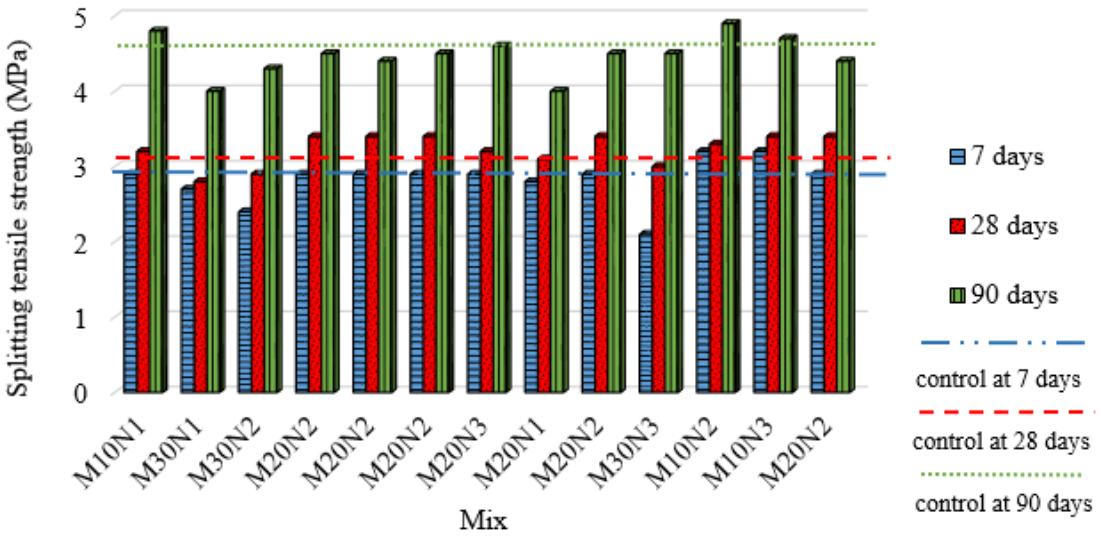

Figure 5.3: Splitting tensile strength for each mix

Figure 5.4 shows data of flexural strength for each concrete mix at different ages. The pattern of the flexural strength development are similar to compressive and splitting tensile strengths at all ages of concrete, but the increase in amount of micro POFA with nano POFA does not reflect positives result due to the porous particles of micro POFA which leads to the reduction of flexural strength (Mihashi et al. 2007). At the early age of 7 days, concrete mix M10N1 and M10N2 containing 10% of micro POFA and 1-2% of nano POFA yielded 4% and 3%, of increment respectively as compared to the control mix. The mix containing 10% of micro POFA and 2% of nano POFA gives the highest flexural strength. At the age of 28 days, M10N1, M10N2, and M10N3 exhibited higher flexural strength by 8%, 5%, and 1%, respectively as compared with the control mix. At the later age of 90 days, the same increment occurred in concrete mix M10N1, M10N2 and M10N3 where the flexural strength increased about 12%, 10% and 3%, respectively. The strength increment of the flexural strength could have been attributed to the less porous microstructure of micro POFA particles in the concrete mix because only 10% of micro POFA was replaced with

cement. In addition, the higher fineness of nano POFA could also enhance the reactivity of the bonding in the cement paste. This strength enhancement is attributed to the contributions of the nano POFA replacement as the filler to refine the concrete matrix microstructure. The filler effects on improving mechanical properties of concrete has also been proven by other researchers (Jaturapitakkul, Tangpagasit, Songmue, & Kiattikomol, 2011; Rajak, Majid, & Ismail, 2015). The physical properties of nanoparticles that has high surface area helps to increase the acceleration reaction of silica with calcium hydroxide which results in the formation of CSH gel. As the calcium hydroxide depletes, the strength of the concrete is enhanced. For other concrete mix containing higher amounts of micro POFA with nano POFA, the pattern of flexural strength decreases due to the porous structure of the micro POFA, as was discussed in the previous chapter. In other studies that focus on the diminished strength of mechanical properties of concrete, Kafi, Sadeghi-nik, Bahari, Sadeghi-nik, & Mirshafiei (2016) explained that non-homogenous microstructure decreases the strength of concrete where the weak areas in the cement matrix formed which leads to reduction of the overall strength of concrete.

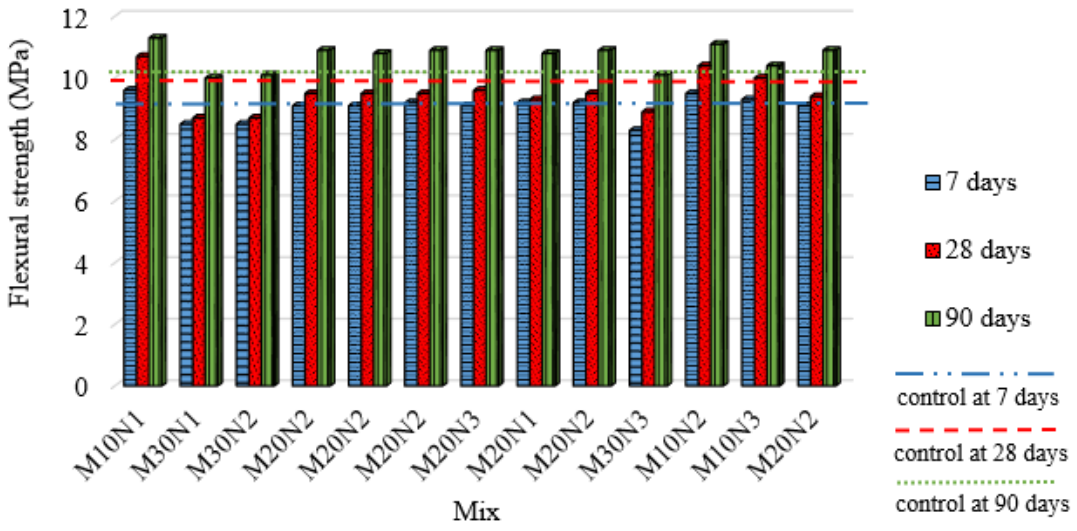

Figure 5.4: Flexural strength for each mix

Summary of results of strengths can be found in Table 5.3. The impact of the mechanical properties of high performance concrete containing micro and nano POFA as discussed in previous section can be explained by studying the microstructure using Scanning Electron Microscopy (SEM). Overall, M10N1, M10N2 and M10N3 yielded data on the enhancement of workability, compressive, splitting tensile and flexural strengths at all ages as compared with the control mix without present of micro and nano POFA. The SEM images demonstrates the main component of the hydration phase in the concrete. The improvement at the early age of the compressive, tensile and flexural strengths of concrete mix containing 10% of micro POFA and 1-3% of nano POFA were attributed to the early maturity of concrete due to rapid consuming of $Ca(OH)_2$ during the hydration process related to high surface area of nano POFA. This accelerates the hydration process, and the secondary CSH gel produced fills the void in the cement matrix causing an enhancement to the concrete strength compared to the control mix without the pozzolanic material. The occurrence of the hydration and CSH structures can be found in Figure 5.5b, Figure 5.5c and Figure 5.5d in mix M10N1, M10N2 and M10N3, respectively. Denser morphology can be seen in the figures due to the CSH gel produced in the form of hydrated needle shapes. The hexagonal platelets of Ca(OH)2 could not be seen much in those figures due to the presence of pozzolanic materials in the mix that used up the $Ca(OH)_2$ for the formation of secondary CSH gel. Figure 5.5a presents clearly the hexagonal platelets of $Ca(OH)_2$ in the control mix which creates more void in the concrete matrix. Clear formation of CSH gel spotted in Figure 5.5f, Figure 5.5g, and Figure 5.5h in the form of porous and densified hydrated look in mix M10N1, M10N2 and M10N3, respectively at 28 days. It is noticed that the $Ca(OH)_2$ is less in those images compared with control mix at 28 and 90 days shown in Figure 5.5e and Figure 5.5i. The hexagonal platelets of $Ca(OH)_2$ appears in high concentration rates due as there is no pozzolanic materials in the control mix. From these images, the reduction of the concrete strength on control mix can be related to the high formation of the $Ca(OH)_2$ compared to the mix with 10% of micro and 1-3 % of nano POFA. At 90 days, the SEM images also shows clear CSH structure in a form of needle shaped and fibrous bundles as shown in Figure 5.5i, Figure 5.5k, Figure 5.5l for mix M10N1, M10N2 and M10N3, respectively. The micro and nano POFA that acts as micro and nano filler not only fills the voids and accelerates the hydration process, but also acts as a nucleation center that creates denser concrete.

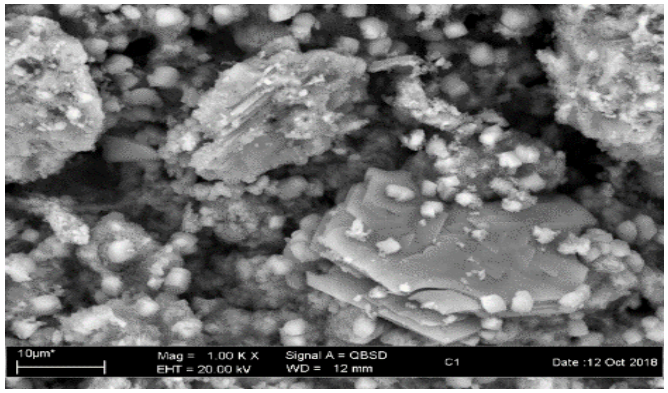

(a) Control mix at 7 days

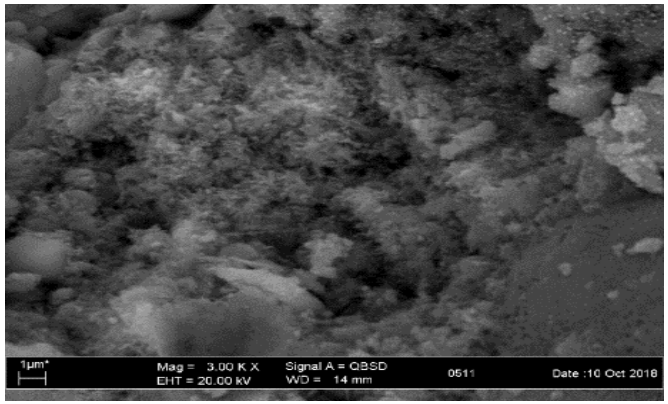

b) M10N1 at 7 days

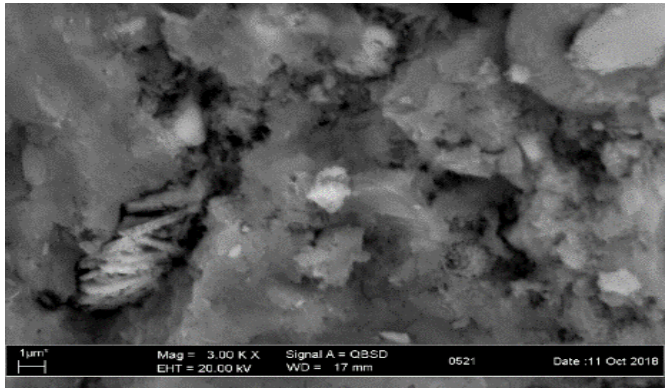

c) M10N2 at 7 days

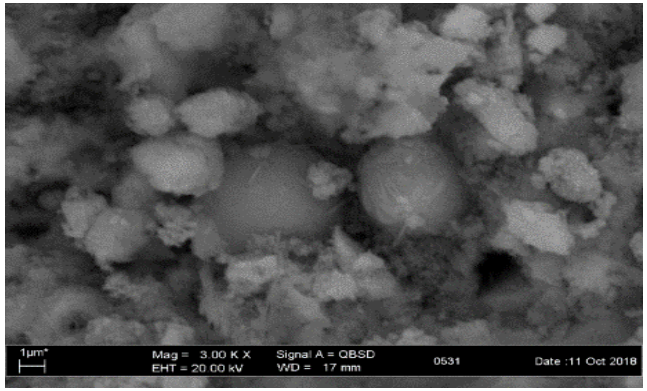

d) M10N3 at 7 days

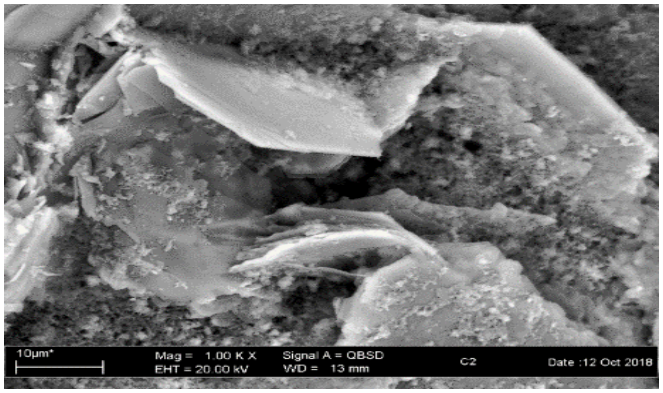

e) Control mix at 28 days

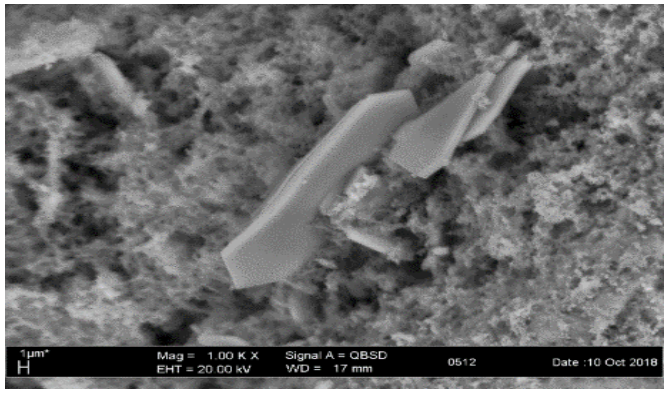

f) M10N1 mix at 28 days

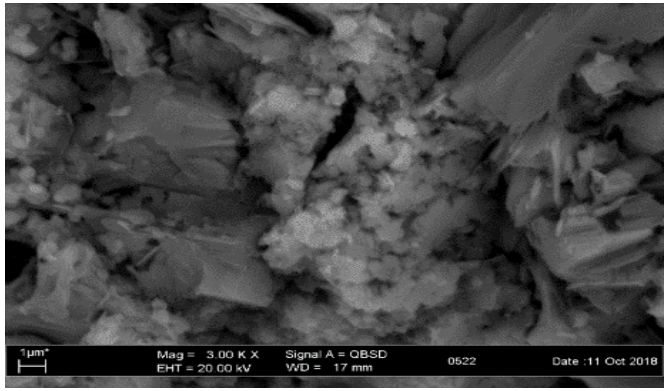

g) M10N2 mix at 28 days

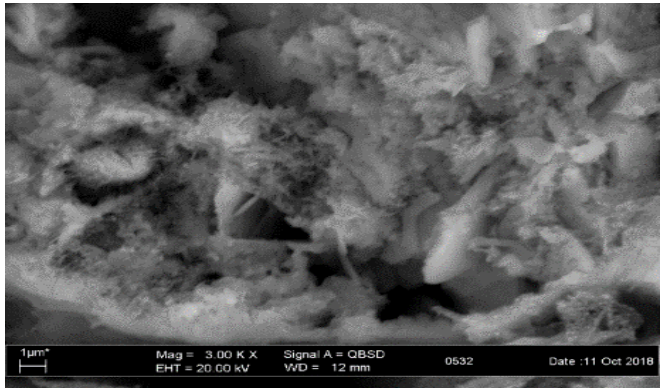

h) M10N3 mix at 28 days

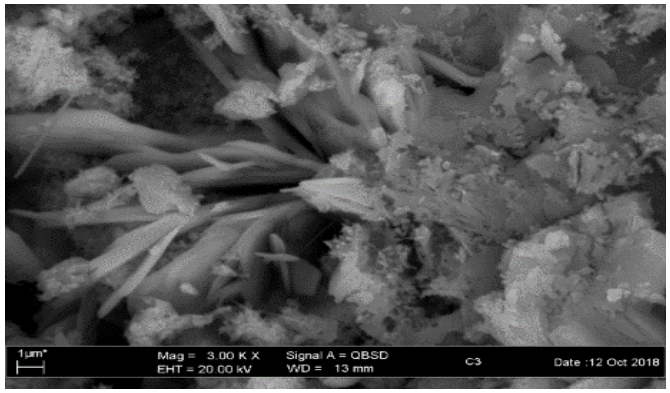

i) Control mix at 90 days

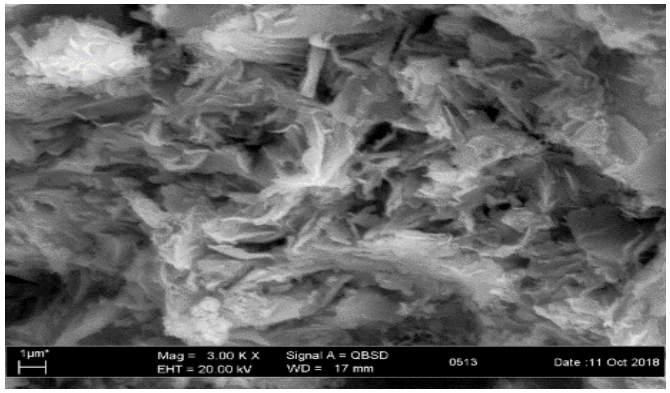

j) M10N1 mix at 90 days

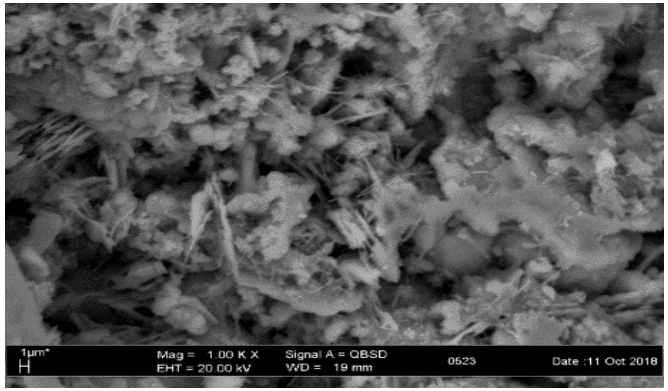

k) M10N2 mix at 90 days

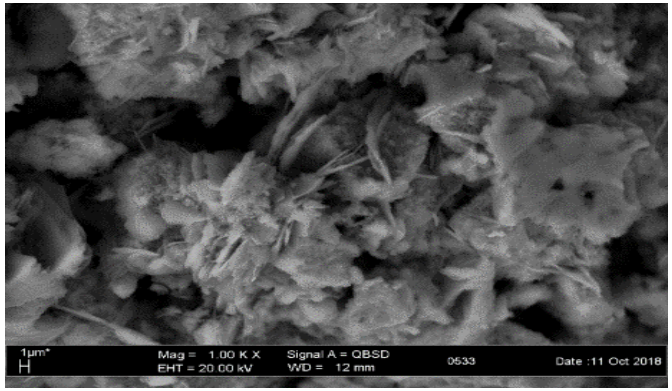

l) M10N3 mix at 90 days

Figure 5.5: SEM images for control, M10N1, M10N2 and M10N3 mix at 7, 28 and 90 days

Table 5.3: Binder proportions and responses obtained

Run	Variables		Binder proportion		Results/ Responses									
	A	B	Micro POFA (kg/m^3)	Nano POFA (kg/m^3)	Slump (mm)	Compressive strength (MPa)			Splitting tensile strength (MPa)			Flexural strength (MPa)		
					Y_w	Y_{c7}	Y_{c28}	Y_{c90}	Y_{t7}	Y_{t28}	Y_{t90}	Y_{f7}	Y_{f28}	Y_{f90}
1	-1	-1	58.6	5.86	100	49.2	63.3	66.9	2.9	3.2	4.8	9.6	10.7	11.3
2	1	-1	175.8	5.86	40	34.7	43.3	52.2	2.7	2.8	4	8.5	8.7	10
3	1	0	175.8	11.72	45	37	45.5	52.4	2.4	2.9	4.3	8.5	8.7	10.1
4	0	0	117.2	11.72	50	42.3	54.3	60.4	2.9	3.4	4.5	9.1	9.5	10.9
5	0	0	117.2	11.72	50	42.8	54.7	60.4	2.9	3.4	4.4	9.1	9.5	10.8
6	0	0	117.2	11.72	50	42.2	54.3	60	2.9	3.4	4.5	9.2	9.5	10.9
7	0	1	117.2	17.58	30	48	55	64.3	2.9	3.2	4.6	9.1	9.6	10.9
8	0	-1	117.2	5.86	65	44.8	53	59.9	2.8	3.1	4	9.2	9.3	10.8
9	0	0	117.2	11.72	65	42.7	54.7	60	2.9	3.4	4.5	9.2	9.5	10.9
10	1	1	175.8	17.58	30	39.5	50	56	2.1	3	4.5	8.3	8.9	10.1
11	-1	0	58.6	11.72	145	48.7	62.2	66.9	3.2	3.3	4.9	9.5	10.4	11.1
12	-1	1	58.6	17.58	150	47.3	64.1	67.2	3.2	3.4	4.7	9.3	10	10.4
13	0	0	117.2	11.72	45	42.7	54.7	60	2.9	3.4	4.4	9.1	9.4	10.9
Ref./control			0	0	140	47.3	61.9	64.8	2.9	3.1	4.6	9.2	9.9	10.1

5.4 Development of mathematical models

5.4.1 Prediction equations

According to the experimental data, the relationship between the micro and nano POFA with slump height (Y_1), compressive strength (Y_2), splitting tensile strength (Y_3) and flexural strength (Y_4) at three different age was analysed using the Response Surface Methodology (RSM). Each of the response was predicted using regression analysis that explains the relationship between variables and responses. Under the Central Composite Design (CCD), the mathematical prediction equations are provided in Equation 5.1to Equation 5.10 for each response. The prediction equations were made as a function of percentage of micro POFA replacement, x_1 and percentage of nano POFA replacement denoted as x_2. Next, the insignificant terms were omitted to modify the performance of the prediction equations (Aldahdooh et al., 2013). Each mathematical model was obtained according to the experimental data and this data has been used to describe the shape of surface for each response (Bayramov, Tasdemir, & Tasdemir, 2004). The prediction equations proposed for each response indicate good correlation between the experimental (actual) and predicted results. The below equations presented are the quadratic model that fits with the experimental data except for the 28 days compressive and flexural strength. The findings points to the importance of including the two-factor interaction model. Each of the model proposed will be further explained in the next section using analysis of variance (ANOVA), model summary statistics and lack of fit analysis.

Slump (mm),

$$Y_1 = 219.52 - 15.38x_1 + 30.83x_2 - 1.5x_1x_2 + 0.34x_1^2 \quad \text{Equation 5.1}$$

Compressive strength (MPa) at 7 days,

$$Y_2 = 60.19 - 0.25x_1 - 9.98x_2 + 0.17x_1x_2 - 0.0164x_1^2 + 1.91x_2^2 \quad \text{Equation 5.2}$$

Compressive strength (MPa) at 28 days, Equation 5.3

$$Y_2 = 74.21 - 1.14x_1 - 1.37x_2 + 0.1475x_1x_2$$

Compressive strength (MPa) at 90 days,

$$Y_2 = 76.23 - 0.45x_1 - 6.13x_2 + 0.0875x_1x_2 - 0.01x_1^2 + 1.45x_2^2$$ Equation 5.4

Splitting tensile strength (MPa) at 7 days,

$$Y_3 = 2.34 + 0.0508x_1 + 0.4180x_2 - 0.0195x_1x_2 - 0.0012x_1^2 - 0.0174x_2^2$$ Equation 5.5

Splitting tensile strength (MPa) at 28 days, Equation 5.6

$$Y_3 = 2.69 + 0.0359x_1 + 0.42x_2 - 0.0014x_1^2 - 0.0876x_2^2$$

Splitting tensile strength (MPa) at 90 days,

$$Y_3 = 5.21 - 0.116x_1 + 0.5387x_2 + 0.0115x_1x_2 + 0.0016x_1^2 - 0.1526x_2^2$$ Equation 5.7

Flexural strength (MPa) at 7 days,

$$Y_4 = 9.53 + 0.031x_1 - 0.065x_2 - 0.0003x_1x_2 - 0.0021x_1^2 - 0.01x_2^2$$ Equation 5.8

Flexural strength (MPa) at 28 days,

$$Y_4 = 12.07 - 0.1248x_1 - 0.485x_2 + 0.0223x_1x_2 - 0.0021x_1^2$$ Equation 5.9

Flexural strength (MPa) at 90 days,

$$Y_4 = 11.24 + 0.048x_1 - 0.2837x_2 + 0.0218x_1x_2 - 0.0034x_1^2 - 0.0674x_2^2 \quad \text{Equation 5.10}$$

5.4.2 Statistical Analysis of Responses

The prediction equations proposed from the regression analysis are based on statistical analysis to validate the parameters for all the responses. These results highlight the most influential variables which is then used as the basis for the mathematical model. The analysis of variance (ANOVA) for surface response models are summarised in Table 5.4 to Table 5.13. The analysis provides sum of squares, degree of freedom, mean, F value and p-value at the 0.05 significance level. The lack of fit test was used to evaluate the adequacy of the model by comparing the residual error to the pure error from replication and gives F values for all the models. F value helps in finding the significance of the analysis and must be lower to be significant. The model is not significant if the p-value is larger than 0.05 and the insignificant model with a p-value larger than 0.1 will be excluded to improve the model (Nassar, Thom, & Parry, 2016). The models generated for each response can be found significant through this analysis where the adequacy of the model was verified by the lack of fit test. To support the lack of fit test, the coefficient of determination, R^2 is required to validate the model generated for each response, where the R^2 indicates the total deviation of the response variable from the predicted model (Myers et al., 2016).

From the results displayed in the table below, the models obtained from the analysis show low p-values (<0.05) which implies the models are statistically significant for workability, compressive strength, splitting strength and flexural strength of concrete at all curing ages (7, 28, and 90 days). The quality of the predicted model evaluated is based on the coefficient of the determination, R^2 and standard deviation (SD) values. While the lack of fit test showed that the models were significant, reasonable agreement was found between the predicted R^2 and the adjusted R^2 for all the responses. In Table 5.4 to Table 5.13, R^2 obtained for each response were 0.92, 0.95, 0.99, 0.99, 0.97, 0.87, 0.90, 0.99, 0.97, and 0.95 for slump, compressive

strength, splitting tensile strength and flexural strength at 7, 28 and 90 days, respectively. The model is considered a good fit if the minimum value of R^2 is 0.80. The R^2 close to 1.00 indicates a good agreement between the predicted and experimental results (Noordin, Venkatesh, Sharif, Elting, & Abdullah, 2004). The models for all the cases are found to be well fitted with the experimental data due to the high degree of R^2 which implies good agreement with the adjusted R^2 (Ghafari, Abdul, Hasnain, & Akbar, 2009). Almost all the models were significant with the quadratic models except for the compressive and flexural strengths at 28 days. Both of the models were fitted well with the two factors interaction effect. An additional tool to measure the signal to noise ratio that compares the range of the predicted values at the design points to the average prediction error is called adequate precision. In this study, the adequate precision values of the models are 14.06, 16.08, 51.82, 33.72, 25.78, 9.22, 13.41, 67.67, 33.44 and 15.58 for slump, compressive strength, splitting tensile strength and flexural strength at 7, 28 and 90 days, respectively. The signal-to-noise ratio or adequate precision value for all the models are found to be greater than 4 which indicates adequate model discrimination (Aldahdooh et al., 2013). This full regression models confirm the adequacy of the model to navigate satisfactorily into the design space to determine the optimum mix design parameters and this also demonstrates reliable confidence in the estimation (Aldahdooh, Bunnori, & Johari, 2014; Ghafari, Costa, & Júlio, 2015).

Table 5.4: ANOVA and summary statistics for slump response surface quadratic model

Source	Sum of squares	DF	Mean	F	p-value
Model	17768.64	4	4442.16	22.20	0.0002
A	13066.67	1	13066.67	65.31	< 0.0001
B	4.17	1	4.17	0.021	0.0888
AB	900.00	1	900.00	4.50	0.0667
A^2	3797.80	1	3797.80	18.98	0.0024
Residual	1600.60	8	200.07		
Lack of Fit	1370.60	4	342.65	5.96	0.0560
Pure Error	230.00	4	57.50		
Total	19369.23	12			
R^2 = 0.92; Predicted R^2 = 0.51; Adjusted R^2 = 0.88					
Standard deviation = 14.14; Mean = 66.54; PRESS = 9433.16					
Adequate precision = 14.06					

Table 5.5: ANOVA and summary statistics for 7 days' compressive strength response surface quadratic model

Source	Sum of squares	DF	Mean	F	p-value
Model	222.86	5	44.57	24.68	0.0003
A	192.67	1	192.67	106.68	< 0.0001
B	6.20	1	6.20	3.43	0.1063
AB	11.22	1	11.22	6.21	0.0414
A^2	7.41	1	7.41	4.10	0.0825
B^2	10.10	1	10.10	5.59	0.0500
Residual	12.64	7	1.81		
Lack of Fit	12.35	3	4.12	56.39	0.0010
Pure Error	0.29	4	0.073		
Total	235.50	12			
R^2 = 0.95; Predicted R^2 = 0.62; Adjusted R^2 = 0.91					
Standard deviation = 1.34; Mean = 43.22; PRESS = 88.38					
Adequate precision = 16.08					

Table 5.6: ANOVA and summary statistics for 28 days' compressive strength response surface two-factor interaction (2FI) model

Source	Sum of squares	DF	Mean	F	p-value
Model	453.85	3	151.28	309.34	< 0.0001
A	430.11	1	430.11	879.47	< 0.0001
B	15.04	1	15.04	30.76	0.0004
AB	8.70	1	8.70	17.79	0.0022
Residual	4.40	9	0.49		
Lack of Fit	4.21	5	0.84	17.54	0.0080
Pure Error	0.19	4	0.048		
Total	458.25	12			
R^2 = 0.99; Predicted R^2 = 0.95; Adjusted R^2 = 0.99					
Standard deviation = 0.70; Mean = 54.55; PRESS = 20.97					
Adequate precision = 51.82					

Table 5.7: ANOVA and summary statistics for 90 days' compressive strength response surface quadratic model

Source	Sum of squares	DF	Mean	F	p-value
Model	293.59	5	58.72	115.97	< 0.0001
A	272.03	1	272.03	537.27	< 0.0001
B	12.04	1	12.04	23.78	0.0018
AB	3.06	1	3.06	6.05	0.0435
A^2	2.76	1	2.76	5.45	0.0522
B^2	5.81	1	5.81	11.47	0.0117
Residual	3.54	7	0.51		
Lack of Fit	3.35	3	1.12	23.28	0.0054
Pure Error	0.19	4	0.048		
Total	297.13	12			
R^2 = 0.99; Predicted R^2 = 0.89; Adjusted R^2 = 0.98					
Standard deviation = 0.71; Mean = 60.51; PRESS = 32.02					
Adequate precision = 33.72					

Table 5.8: ANOVA and summary statistics for 7 days splitting tensile strength response surface quadratic model

Source	Sum of squares	DF	Mean	F	p-value
Model	0.96	5	0.19	49.01	< 0.0001
A	0.74	1	0.74	190.37	< 0.0001
B	0.010	1	0.010	2.67	0.1461
AB	0.15	1	0.15	39.02	0.0004
A^2	0.038	1	0.038	9.77	0.0167
B^2	$8.375x10^{-4}$	1	$8.375x10^{-4}$	0.21	0.6570
Residual	0.027	7	$3.898x10^{-3}$		
Lack of Fit	0.027	3	8.988E-003	112.35	0.0003
Pure Error	$3.200x10^{-4}$	4	$8.000x10^{-5}$		
Total	0.98	12			
R^2 = 0.97; Predicted R^2 = 0.72; Adjusted R^2 = 0.95					
Standard deviation = 0.06; Mean = 2.81; PRESS = 0.27					
Adequate precision = 25.78					

Table 5.9: ANOVA and summary statistics for 28 days splitting tensile strength response surface quadratic model

Source	Sum of squares	DF	Mean	F	p-value
Model	0.42	5	0.084	9.75	0.0047
A	0.27	1	0.27	31.23	0.0008
B	0.029	1	0.029	3.42	0.1071
AB	0.000	1	0.000	0.000	1.0000
A^2	0.056	1	0.056	6.52	0.0379
B^2	0.021	1	0.021	2.46	0.1606
Residual	0.060	7	$8.607x10^{-3}$		
Lack of Fit	0.060	3	0.020	668.12	< 0.0001
Pure Error	1.20010^{-4}	4	$3.000x10^{-5}$		
Total	0.48	12			
R^2 = 0.87; Predicted R^2 = 0.07; Adjusted R^2 = 0.78					
Standard deviation = 0.09; Mean = 3.22; PRESS = 0.45					
Adequate precision = 9.22					

Table 5.10: ANOVA and summary statistics for 90 days splitting tensile strength response surface quadratic model

Source	Sum of squares	DF	Mean	F	p-value
Model	0.77	5	0.15	13.21	0.0019
A	0.47	1	0.47	40.18	0.0004
B	0.15	1	0.15	12.85	0.0089
AB	0.053	1	0.053	4.52	0.0711
A^2	0.073	1	0.073	6.22	0.0413
B^2	0.064	1	0.064	5.49	0.0516
Residual	0.082	7	0.012		
Lack of Fit	0.076	3	0.025	18.18	0.0086
Pure Error	$5.600x10^{-3}$	4	$1.400x10^{-3}$		
Total	0.86	12			
R^2 = 0.90; Predicted R^2 = 0.14; Adjusted R^2 = 0.84					
Standard deviation = 0.11; Mean = 4.47; PRESS = 0.73					
Adequate precision = 13.41					

Table 5.11: ANOVA and summary statistics for 7 days' flexural strength response surface quadratic model

Source	Sum of squares	DF	Mean	F	p-value
Model	1.81	5	0.36	488.34	< 0.0001
A	1.59	1	1.59	2152.55	< 0.0001
B	0.073	1	0.073	98.20	< 0.0001
AB	$2.500x10^{-5}$	1	$2.500x10^{-5}$	0.034	0.8593
A^2	0.12	1	0.12	157.00	< 0.0001
B^2	$2.762x10^{-4}$	1	$2.762x10^{-4}$	0.37	0.5604
Residual	$5.175x10^{-3}$	7	$7.393x10^{-4}$		
Lack of Fit	$3.855x10^{-3}$	3	$1.285x10^{-3}$	3.89	0.1111
Pure Error	$1.320x10^{-3}$	4	$3.300x10^{-4}$		
Total	1.81	12			
R^2 = 0.99; Predicted R^2 = 0.98; Adjusted R^2 = 0.99					
Standard deviation = 0.03; Mean = 9.05; PRESS = 0.04					
Adequate precision = 67.67					

Table 5.12: ANOVA and summary statistics for 28 days' flexural strength response surface 2FI model

Source	Sum of squares	DF	Mean	F	p-value
Model	4.08	3	1.36	111.12	< 0.0001
A	3.87	1	3.87	316.41	< 0.0001
B	$9.600x10^{-3}$	1	$9.600x10^{-3}$	0.78	0.3988
Residual	0.20	1	0.20	16.18	0.0030
Lack of Fit	0.11	9	0.012		
Pure Error	0.11	5	0.022	146.05	0.0001
Total	$6.000x10^{-4}$	4	$1.500x10^{-4}$		
R^2 = 0.997; Predicted R^2 = 0.90; Adjusted R^2 = 0.97					
Standard deviation = 0.11; Mean = 9.50; PRESS = 0.41					
Adequate precision = 33.44					

Table 5.13: ANOVA and summary statistics for 90 days' flexural strength response surface quadratic model

Source	Sum of squares	DF	Mean	F	p-value
Model	1.85	5	0.37	24.30	0.0003
A	1.14	1	1.14	74.68	< 0.0001
B	0.084	1	0.084	5.53	0.0510
AB	0.19	1	0.19	12.45	0.0096
A^2	0.31	1	0.31	20.68	0.0026
B^2	0.013	1	0.013	0.83	0.3938
Residual	0.11	7	0.015		
Lack of Fit	0.11	3	0.035	207.34	< 0.0001
Pure Error	$6.800x10^{-4}$	4	$1.700x10^{-4}$		
Total	1.95	12			
R^2 = 0.95; Predicted R^2 = 0.47; Adjusted R^2 = 0.91					
Standard deviation = 0.12; Mean = 10.69; PRESS = 1.04					
Adequate precision = 15.58					

R^2: coefficient of determination, A: micro POFA, B: nano POFA, DF: degree of freedom PRESS: predicted residual error sum of squares,

5.4.3 Contour and Response Surface Plot

The model graphs in the RSM analysis highlights the graphical interpretation of the interaction between the variables for the optimum responses. In this section, there are two plots that will be discussed to understand the significant models generated, such as contour plot and three-dimensional (3D) response surface plot. The plots show where the micro POFA values, which is denoted as A and nano POFA as B. The contour plot provides a two-dimensional (2D) representation while the 3D response surface plot adds shape to the contour plot. These plots explain the interaction of the micro and nano POFA in coded value to signal the enhancement of the slump, compressive, splitting tensile and flexural strengths at all ages. The prediction equations obtained from the regression analysis were used to plot the 3D response surface plot. The variables of each model were plotted on the X and Y-axis associated with the response on the Z-axis (Kockal & Ozturan, 2011; Muthukumar & Mohan, 2004).

The effects of the combination of micro and nano POFA on the concrete slump can be seen from the contour plot and 3D response surface plot in Figure 5.6. The figure illustrates the effects of the low replacement level for both micro and nano POFA on the slump height of concrete. As a replacement, a rise in the level of OPC by micro POFA increase, the slump of concrete decrease whereas for nano POFA, the slump is observed to have increase. The findings show that the combination of 10% of micro POFA with 1 to 3% of nano POFA, the slump results is within the 100 to 150 mm. The range of the slump height is within the targeted slump in the mix design. The 3D response surface shows the highest slump is observed at 10% of micro POFA and 1 to 3% of nano POFA. The slump continues decreasing as the micro POFA increases within the 1 to 3% of nano POFA. According to these plots, the combination of 10% of micro and 1 to 3% of nano POFA showed a higher slump as compared with other amounts of micro and nano POFA.

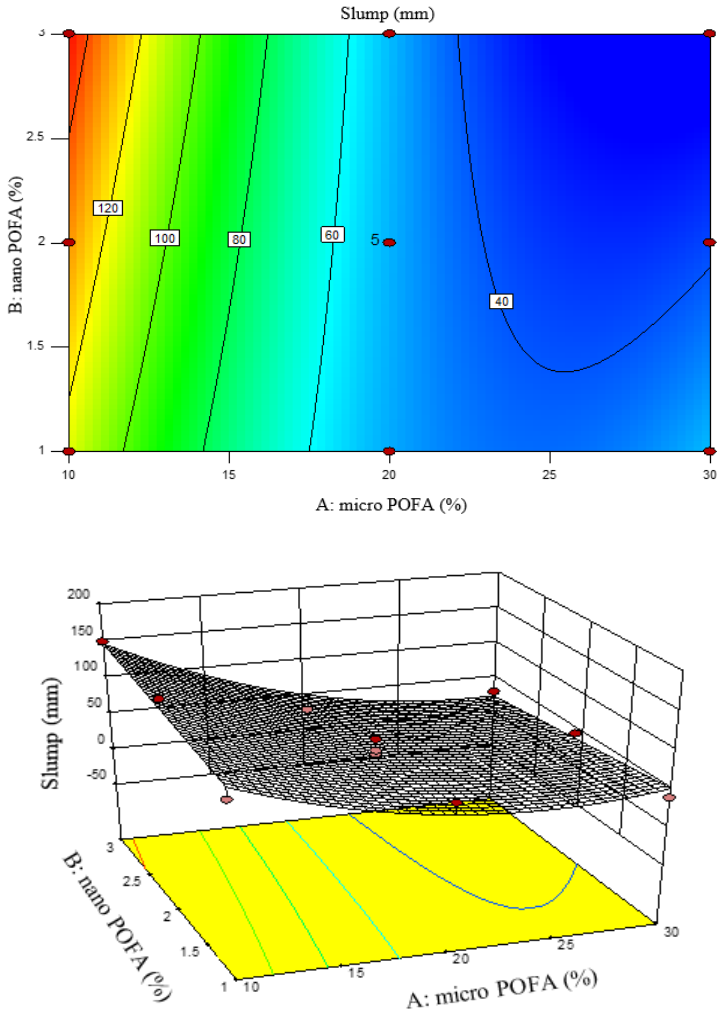

Figure 5.6: Contour plot and 3D response surface plot for slump

Figure 5.7 demonstrates the interaction effect of the combination of micro and nano POFA on compressive strength at the age of 7, 28 and 90 days. The pattern of compressive strength development can be seen from these plots and helps in understanding the parameters for optimum responses at certain age. From the findings, at all age, the compressive strength of concrete shows the same trend where at low replacement level of micro POFA with 1 to 3 % of nano POFA, the higher values were observed. At the early age, it shows that the maximum point of the compressive strength points at the contour area of low level of micro POFA and high level of nano POFA. The 3D shape shows that as the micro POFA increases, the compressive strength decreases whereas the nano POFA factor does not affect much of the compressive strength. However, at 10% replacement level of micro POFA with increasing amounts of nano POFA, the compressive strength is observed to be slightly increases. The same patterns are shown by the contour plot and 3D response surface plot for the compressive strength at 28 and 90 days. The replacement level of 10% micro POFA with 3% of nano POFA appears to be the highest peak as displayed in the 3D plot. The highest compressive strength was recorded at 7, 28 and 90 days are 49.2 MPa, 64.1 MPa and 67.2 MPa. These maximum responses refer to the micro POFA of 10% and 3% of nano POFA and could be attributed to the pozzolanic reaction due to higher silica content of the processed POFA and high surface area of the nano POFA as described in the previous chapter. The results of the compressive strength at all ages are in line with those that display high workability of concrete mix. The lowest point of compressive strength at all ages can be seen at 30% of micro POFA and 1% of nano POFA for all contour plot and 3D response surface plot. Due to lower workability exhibited by these mixes, the concrete mix becomes dry and stiff hence contributing to lower strength of concrete. The lower compressive strength at higher replacement levels of micro POFA with low replacement level of nano POFA could be partly attributed to the higher amount of the porous POFA in the concrete mix. It can also be related to higher demand of water content during the mixing (Chandara, Sakai, Azizi, et al., 2010). Some researchers also suggested in the RSM analysis to study the interaction effects of the compressive strength with other supplementary cementitious materials such as metakaolin, fly ash, crumb rubber, quartz flour and steel fiber. The most influential parameters that provide optimised responses are highlighted in the findings (Ghafari et al., 2015; Güneyisi, Gesog, Algın, & Mermerdas, 2014; Rezaifar, Hasanzadeh, & Gholhaki, 2016).

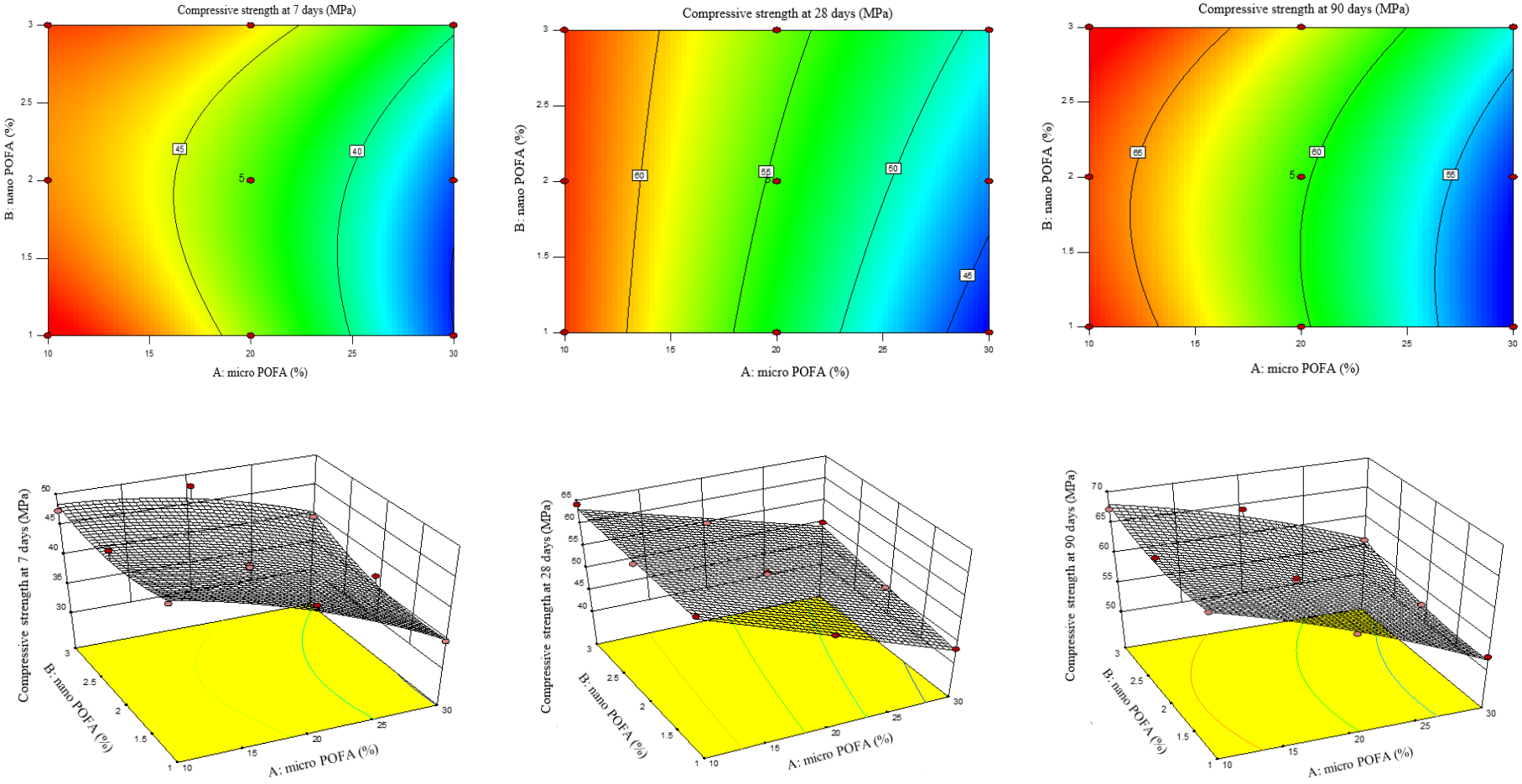

Figure 5.7: Contour plot and 3D response surface plot for compressive strength at 7, 28 and 90 days

The contour plot and 3D fitted response surface plot that was statistically developed for effect of micro and nano POFA on splitting tensile strength at all ages is shown in Figure 5.8. The plots are generated according to age of concrete based on the design parameters and responses to quantify the dominance of control parameter on measured response. The shape of the 3D response surface plots is displayed according to the mathematical model obtained in the previous section. As can be found in Figure 5.8, the splitting tensile strength at 7, 28 and 90 days are plotted as a function of micro and nano POFA. The labels at the axis of the graphs define the interaction effects between the variables and the responses for each generated model. The peak of the tensile strength at early age of 7 days occurred at 10% of micro POFA within the range of 1 to 3% of nano POFA. Similar trends occurred for splitting tensile strength at 28 and 90 days whereas the value is consistently found to lie at contour areas of 10% micro POFA and 1 to 3% of nano POA. The highest peak of splitting tensile strength values was recorded around 2.9, 3.2 and 3.2 MPa at 7, 28 and 90 days, respectively. From both the plots, the splitting tensile strength values tends to decrease markedly with the increasing of micro POFA content from 20% to 30%. Meanwhile, the increase of nano POFA from 1 to 3% affects the splitting tensile strength and shows that there is a slight increase. The combined effects of the micro and nano POFA can be seen at the region of optimum response at around 10 to 15% of micro POFA with 2-3% of nano POFA at 7 and 28 days and 10% of micro POFA with 1.5-3% of nano POFA at 90 days. The rest of the region shown in contour plots do not significantly affect the splitting tensile strength of concrete. However, the optimum region at 28 days' age is clearer than those regions at 7 and 90 days and show distorted parabolic contour. These cases normally occurred with the analysis that involves fewer interactions between the variables (Muralidhar, Chirumamila, Marchant, & Nigam, 2001; Wang, Chen, Wang, Yuan, & Yu, 2011). Therefore, it is reasonable to mark the optimum binders in the mix design that provides the optimum responses at different ages of concrete. Similar analysis is also reported by other researchers to understand the interaction effects of ultrafine POFA and densified silica fume on tensile strength of ultra-high performance concrete that founds 50% of ultrafine POFA yielded the highest tensile strength (Aldahdooh et al., 2014).

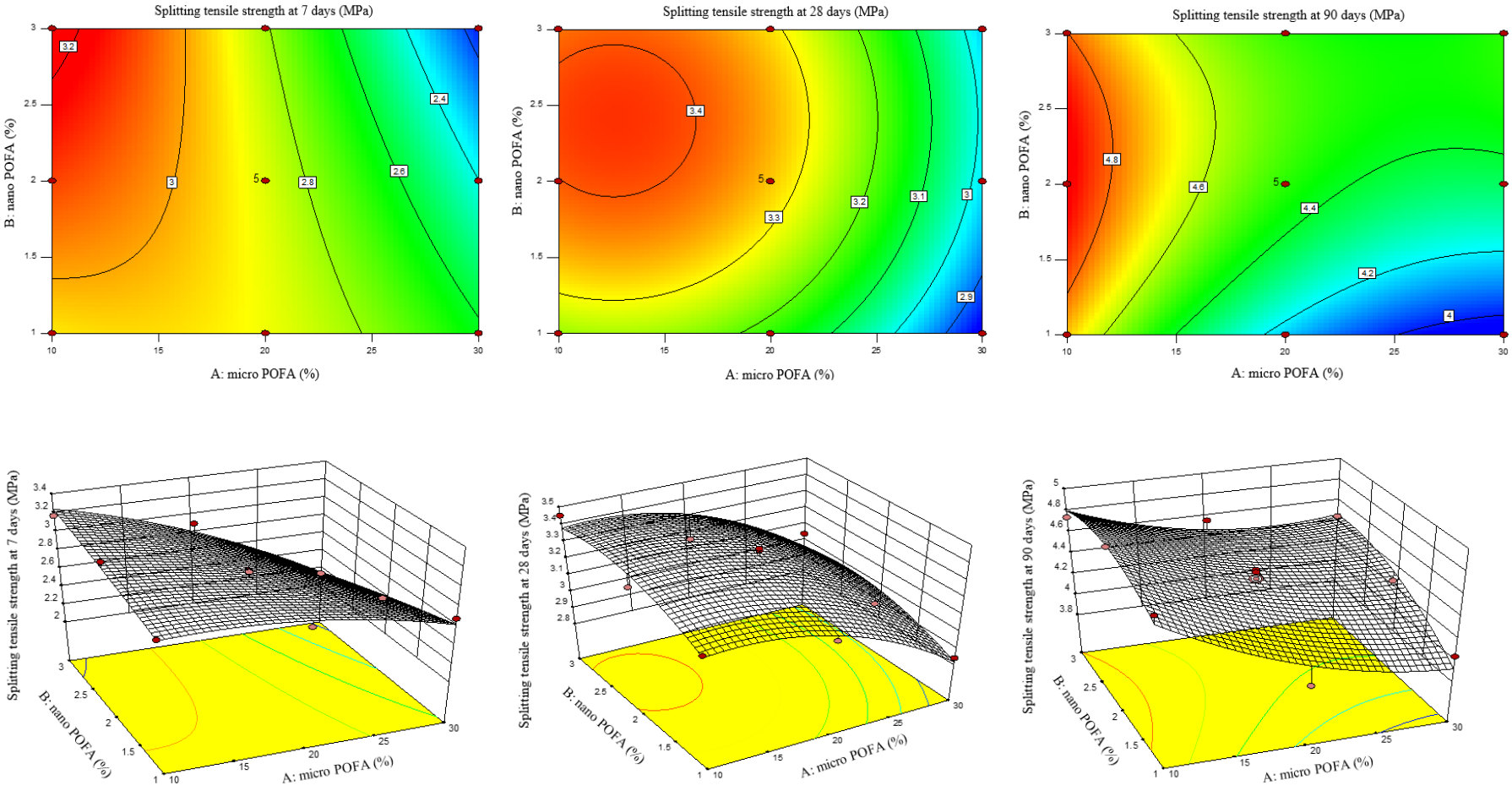

Figure 5.8: Contour plot and 3D response surface plot for splitting tensile strength at 7, 28 and 90 days

Lastly, in Figure 5.9, the same type of plots show the variation of flexural strength with the micro and nano POFA at 7, 28 and 90 days. It is noted that the surface plot for flexural strength at 90 days is clearer than those at 7 and 28 days which seem to be experiencing distorted parabolic contour. However, the optimum region can be seen from the contour plots that exhibit the higher flexural strength. The highest peak occurred with the combination of micro and nano POFA of between 10-15% with 1-3% at 7 days, 10% with 1-2% at 28 days and 10-15% with 1-2% at 90 days, respectively. The maximum value of flexural strength obtained from the optimum combined variables are 9.6 MPa, 10.7 MPa and 11.3 MPa at 7, 28 and 90 days, respectively. From the 3D response surface plots, the findings show that as the micro POFA increase, the flexural strength markedly decreases. The findings also showed similar patterns with the analysis for compressive and splitting tensile strength, but the only difference lies in the magnitude. The lowest point at the fitted plot of flexural strength occurs at the 30% of micro POFA with 1% of nano POFA. The reduction in workability due to high moisture absorption in fresh concrete mix affects the flexural strength of concrete. Similar observations were noticed in compressive and splitting tensile strength plots. Researcher that study the effects of ultrafine POFA on flexural strength also reported significant effects of ultrafine POFA compared to the densified silica fume. Hence, the finding concluded that the high volume of ultrafine POFA of approximately 50% was proposed as the optimum binder to achieve high flexural strength for ultra-high performance concrete (Aldahdooh et al., 2014). It is worth noting that in this study, the combination of micro and low volume of nano POFA significantly enhances the workability, compressive, splitting tensile and flexural strength. Overall, the optimum region that exhibits the highest responses are highlighted for each of process analysis. The optimisation analysis will be further discussed in the next section to determine the final optimum variables and measured response based on the optimisation criteria.

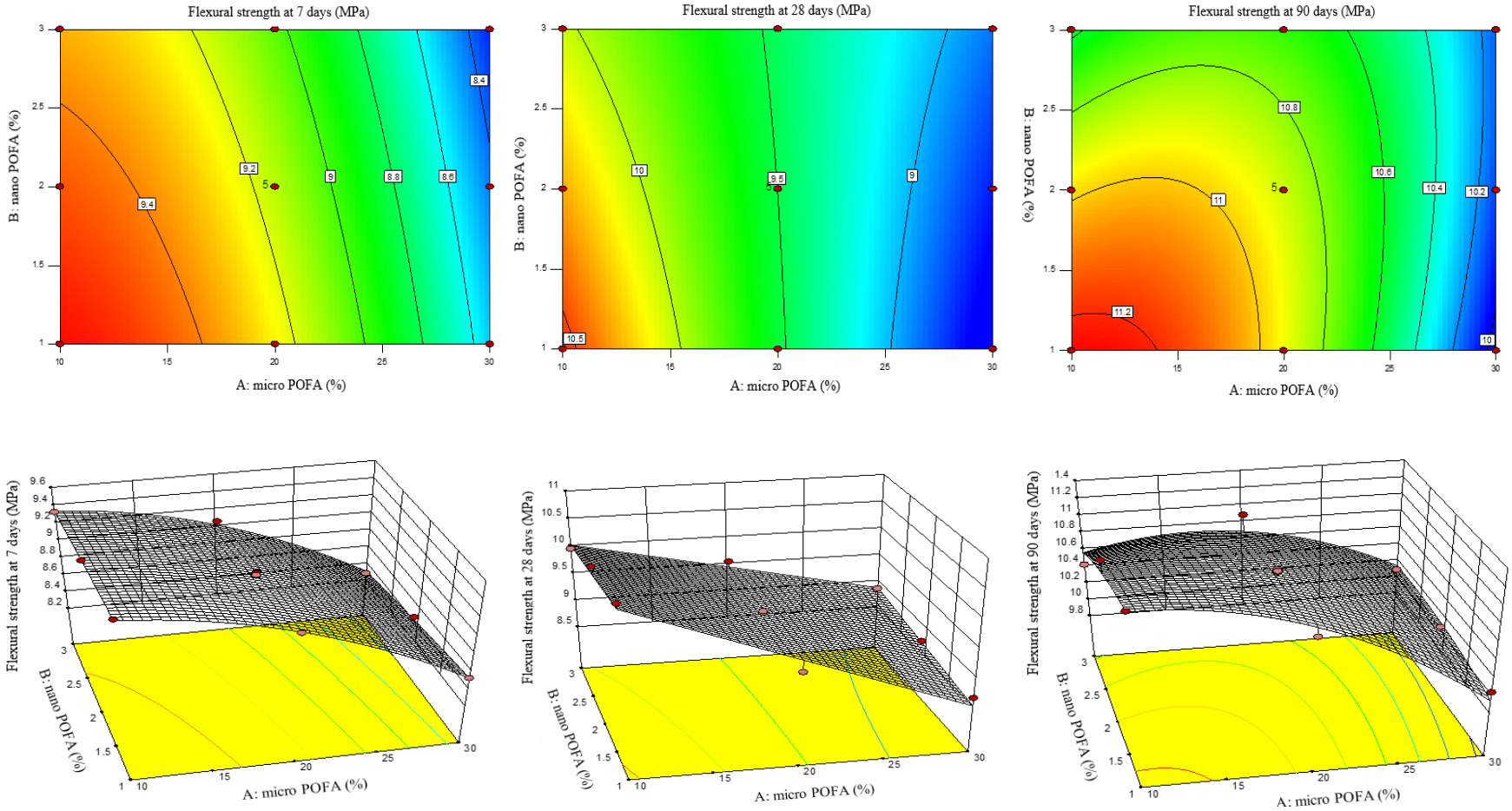

Figure 5.9: Contour plot and 3D response surface plot for flexural strength at 7, 28 and 90 day

5.5 Multiple-response Optimisation

After the mathematical model between the variables and responses were developed and checked for adequacy, the input variables were shown to vary simultaneously and independently in determining the optimum binders and measured responses. The optimization analysis was carried out using the developed mathematical model in order to obtain the optimal composition of micro and nano POFA. The criteria to optimise the responses can be set to implement the analysis. The optimum solution tends to satisfy the optimisation criteria for each response as much as possible without excessively compromising any of the requirements (Myers et al., 2016). In other words, this statistical approach of RSM is done to conduct the analysis of multiple-response optimisation that affected by multiple variables. The optimisation criteria for each response was introduced in Table 5.14. The lower and upper limits, the goal and the importance were specified in the table. The criteria was set to achieve the aim of getting the most accurate percentage replacement of micro and nano POFA with targeted slump height, maximize compressive strength, maximize splitting strength and maximize flexural strength at 7, 28 and 90 days. The design-expert software was used to implement the optimisation criteria as explained in Table 5.14. There are two types of optimisation methods, namely numerical and graphical optimisation. A numerical optimisation method highlights each of target response with highest desirability functions in order to optimise the responses (Anderson & Whitcomb, 2005). Meanwhile, the graphical optimisation method enables visual selection in the desirability plot that highlights the optimum region of certain criteria. Table 5.15 summarises the optimal solutions determined by the software according to the set of optimisation criteria. The best solution out of all the optimal solution refers to the highest desirability where all the criteria are almost achieved. The goal of each optimisation process can be altered depending on the importance or weight factor. In this particular study, all the responses were set with the same importance in terms of the goal due to the fresh and mechanical properties of concrete, which are both important properties in high performance concrete. The proposed optimal solutions presented in Table 5.15 are the end of multi- response optimisation analysis after all the responses were combined into a desirability function (Myers et al., 2016). In the table, the desirability of the optimal solutions ranges from 0.906 to 0.845.

Table 5.14: Optimisation criteria of individual responses

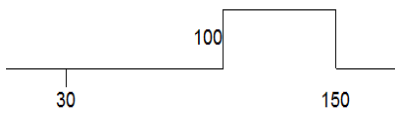 Slump height (mm): within the range	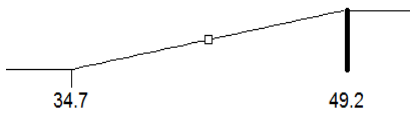 Compressive strength (MPa) at 7 days: maximize	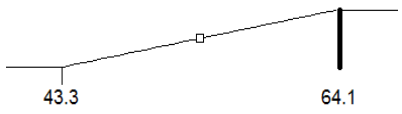 Compressive strength (MPa) at 28 days: maximize	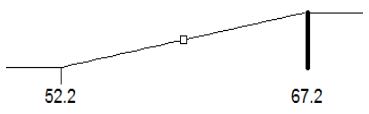 Compressive strength (MPa) at 90 days: maximize
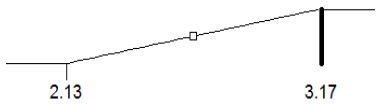 Splitting tensile strength (MPa) at 7 days: maximize	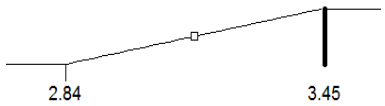 Splitting tensile strength (MPa) at 28 days: maximize	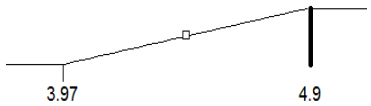 Splitting tensile strength (MPa) at 90 days: maximize	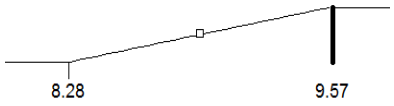 Flexural strength (MPa) at 7 days: maximize
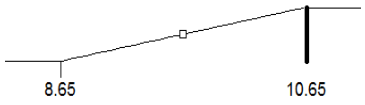 Flexural strength (MPa) at 7 days: maximize	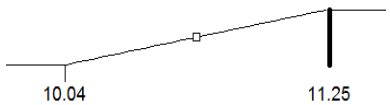 Flexural strength (MPa) at 7 days: maximize		

Table 5.15: Preferred solution suggested from the optimisation

Solutions														
No.	**A (%)**	**B (%)**	**Slump (mm)**	**Compressive strength (MPa)**			**Splitting tensile strength (MPa)**			**Flexural strength (MPa)**			**Desirability**	
				7 days	**28 days**	**90 days**	**7 days**	**28 days**	**90 days**	**7 days**	**28 days**	**90 days**		
1	10	1.50	123.754	47.932	62.959	66.125	3.024	3.342	4.852	9.511	10.432	11.129	0.906	
2	10	1.51	123.895	47.909	62.960	66.117	3.025	3.343	4.854	9.510	10.430	11.127	0.906	
3	10	1.49	123.541	47.967	62.957	66.137	3.022	3.339	4.849	9.513	10.436	11.133	0.906	
4	10	1.52	124.053	47.884	62.961	66.108	3.027	3.344	4.856	9.509	10.427	11.124	0.906	
5	10	1.48	123.398	47.990	62.956	66.146	3.020	3.338	4.847	9.513	10.438	11.135	0.906	
6	10	1.55	124.603	47.799	62.964	66.080	3.033	3.350	4.862	9.506	10.418	11.115	0.906	
7	10	1.38	121.842	48.270	62.946	66.255	3.003	3.321	4.826	9.523	10.464	11.161	0.905	
8	10	1.63	125.844	47.626	62.973	66.030	3.046	3.361	4.875	9.498	10.398	11.093	0.905	
9	10	1.29	120.441	48.553	62.936	66.378	2.987	3.305	4.804	9.531	10.487	11.182	0.904	
10	10	1.23	119.509	48.758	62.930	66.472	2.977	3.293	4.788	9.537	10.503	11.196	0.903	
11	10	1.85	129.291	47.267	62.997	65.985	3.082	3.386	4.902	9.476	10.340	11.027	0.902	
12	10	1.12	117.804	49.167	62.918	66.671	2.957	3.270	4.757	9.546	10.531	11.221	0.900	
13	10	1.91	130.225	47.201	63.003	65.996	3.091	3.391	4.907	9.470	10.325	11.008	0.900	
14	10	1.12	117.647	49.207	62.917	66.690	2.956	3.268	4.754	9.547	10.533	11.223	0.900	
15	10	2.10	133.226	47.079	63.023	66.101	3.120	3.404	4.915	9.449	10.275	10.945	0.894	
16	10	2.34	137.085	47.124	63.050	66.389	3.155	3.412	4.909	9.422	10.211	10.855	0.885	
17	10	2.65	141.958	47.505	63.083	66.998	3.197	3.407	4.875	9.386	10.130	10.732	0.865	
18	10	2.85	145.120	47.947	63.105	67.541	3.223	3.395	4.838	9.361	10.078	10.644	0.845	

The selected optimal solution with the highest durability function occurred at 10% of micro POFA and 1.5% of nano POFA with 0.906 of desirability function. These optimum binders were predicted to experience a slump of 123.75mm, 47.9, 62.96, 66.13 MPa of compressive strength at 7, 28 and 90 days, respectively. For the splitting tensile, the selected optimum level of binders was predicted to occur about 3.02, 3.34 and 4.85 MPa at 7, 28 and 90 days, respectively. Meanwhile, 9.51, 10.43 and 11.13 MPa were predicted for flexural strength at 7, 28, and 90 days, respectively. There are six optimal solutions with the highest desirability function as presented in Table 5.15 but the software will select the only one as the optimum response based on desired goals. However, the value of the responses within the same highest desirability function are not significantly affected. Therefore, the combination of 10% of micro POFA with nano POFA that range from 1.48 to 1.55 % are also significant variables to the optimum responses. The other optimal solutions shown in the table reveals that the combination of 10% micro with 1.12 to 2.85 % of nano POFA also significantly contribute to the enhancement of workability, compressive, splitting tensile and flexural strength properties of high performance concrete at 7, 28 and 90 days. It is worth noting that the optimal solution 16 predicted the highest slump height compared with other solutions where high workability is one of the important characteristics to identify high performance concrete.

The desirability function of all the optimal solution change according to the multi-response optimisation as illustrated in Figure 5.10. It can be seen from the plot that the flat surface indicates the lowest desirability function, which occurred at the area of >10% of micro POFA and 1-3% of nano POFA. The maximum point of the plot with highest desirability function is covered by the area of 10% of micro POFA and 1 to 3% of nano POFA. Beyond that optimum region, the plot is remarkably declined toward the area > 10% of micro POFA and 1 to 3% of nano POFA indicating low desirability function. The graphical optimisation of the selected optimal function can be obtained from the overlay plot. Figure 5.11 shows the selected overlay plot from the 18 optimal solutions, to visualise the optimum region that was obtained from the multi-response optimisation. The shaded area in yellow colour highlights the optimum range of binders that meet the specified goals with the highest desirability function.

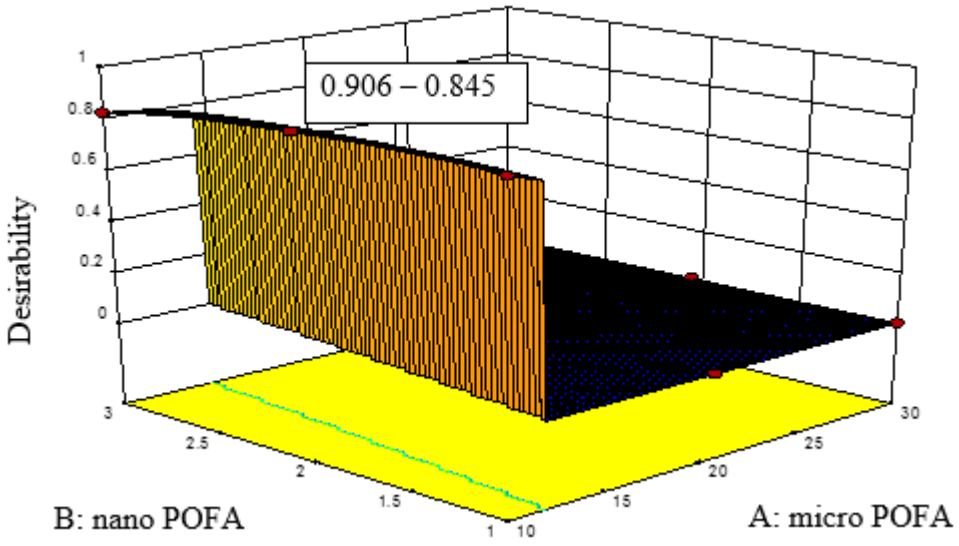

Figure 5.10: Desirability plot of the multi-response optimisation

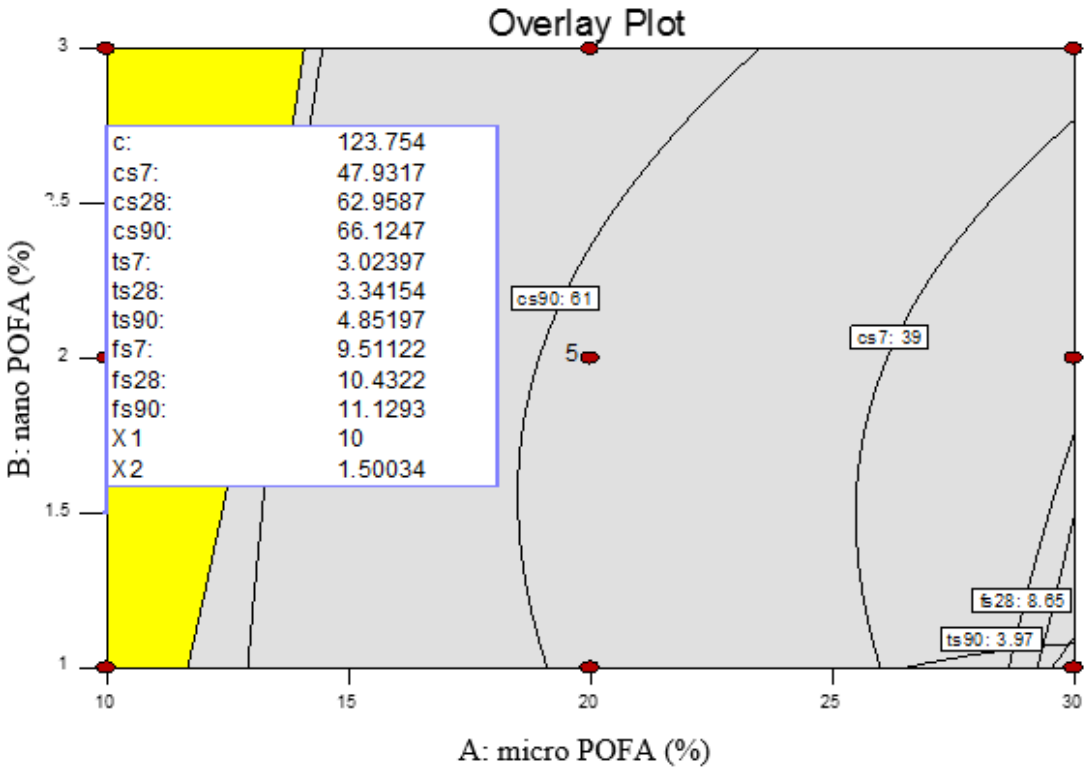

Figure 5.11: Overplay plot of the selected optimal solution

5.6 Concluding Remarks

In this chapter, the implementation of the statistical approaches using response surface methodology (RSM) was applied to determine the interaction effects of the micro and nano POFA as supplementary cementitious materials on workability, compressive, splitting tensile and flexural strength of high performance concrete. Mathematical models were developed to predict the properties of concrete using regression analysis. The models were compared to the experimental results to check for the adequacy of the models obtained. Based on each model, the p value that indicates the level of significance was less than 0.05. The ANOVA and model summary statistics showed that the predicted models were in good agreement based on the adjusted and predicted R^2. A quadratic model was obtained for slump, compressive strength at 7 and 90 days, splitting tensile strength at 7, 28 and 90 days, and flexural strength at 7 and 90 days. Meanwhile, the two-factor interactions model was fitted for compressive strength at 28 days and flexural strength at 28 days. The results of the experimental works also were supported with the SEM micrographs to study the main hydrated phases formed in the concrete structure. The CSH gel structures can be found in the concrete mix containing 10% of micro POFA and 1-3% of nano POFA that exhibited the highest compressive, splitting tensile and flexural strength as compared to the control concrete mix. Meanwhile, the hexagonal platelets of $Ca(OH)_2$ were observed clearly in the control mix due to the absence of pozzolanic materials, which would use weak products for secondary CSH gel formation. The optimisation analysis was implemented by identifying the criteria and the weight factors. The optimal solutions from the analysis were obtained using the Design Expert software. Numerical optimisation highlighted eight optimal solutions that ranged the nano POFA from 1.12-2.85% and 10% of micro POFA with highest workability and maximum compressive, splitting tensile and flexural strength. In addition, the graphical optimisation graph also supported the numerical by visualising the optimum region of the optimum variables and responses. The 3D graph pointed signaled to optimal solutions within the highest value of R^2 at the area of 10% of micro POFA and 1-3% of nano POFA. The optimum responses range obtained from the optimum regions were 117 to 145 mm for slump height. Whilst 47.1 to 49.2 MPa, 62.9 to 63.1MPa, 66 to 67.5 MPa for compressive strength, 3 to 3.2 MPa, 3.3 to 3.4 MPa, 4.8 to 4.9 MPa for splitting tensile strength, 9.4 to 9.5 MPa, 10.1 to 10.5 MPa, 10.6 to 11.2

MPa for flexural strength at the age of 7, 28 and 90 days, respectively. By referring to graphical optimisation, the optimal composition of 10% micro and 1-3% nano POFA were utilised as binder in concrete mix design to satisfy the durability properties of concrete in the next section.

Chapter 6

Durability Properties of High Performance Concrete Containing Micro and Nano POFA

6.1 Introduction

This chapter presents the durability properties of high performance concrete containing optimum dosage of micro and nano POFA. As discussed in the previous section, concrete containing 10% of micro POFA with 1 to 3% of nano POFA is proven to satisfy the workability and strength properties of concrete. However, strength is not the only significant property for concrete; durability is also a main concern especially for high performance concrete to avoid concrete deterioration and structural damages. Therefore, this chapter focuses on the durability study of high performance concrete containing micro and nano POFA with the optimum solutions proposed from the previous chapter denoted as OS1, OS2 and OS3 that contains 10% of micro POFA with 1%, 2% and 3% of nano POFA, respectively. Studies on the resistance of concrete to chloride ingress, acidic environment, water absorption, water sorptivity and reinforcement corrosion were conducted through rapid chloride penetration test (RCPT), acid resistance test, water absorption test, sorptivity test and corrosion test, respectively. The RCPT test is used to simulate the concrete in coastal areas, acid resistance to simulate the concrete in acidic environments such as septic tanks of concrete structures and sewer concrete pipes. The water absorption test is an additional test to study the durability of concrete in terms of moisture absorption. The sorptivity test is a test to determine the initial surface absorption of concrete and to determine the cycle period of wet and dry condition for preparation of corrosion test. The accelerated corrosion test, electrochemical impedance spectroscopy (EIS), and Tafel plot are the techniques that will be discussed for the durability properties of concrete in terms of corrosion effect on reinforcement bars embedded in concrete.

6.2 Water absorption and voids volume

Utilisation of supplementary cementitious materials in concrete plays a significant role in enhancing the strength properties of concrete as well as its durability. Several durability aspects of concrete including water absorption reflect how the pozzolanic materials alter the pores in concrete matrix. The water penetration into concrete is one of the transport properties of concrete that governs the physical process of deterioration. A concrete with high water absorption value is susceptible, and this affects the durability of the reinforcement embedded in the concrete (Ithuralde, 1992). Figure 6.1 shows the results of water absorption test for control mix, C and mix containing micro and nano POFA namely as OS1, OS2 and OS3. The experiment was conducted to study the effects of POFA in concrete throughout the curing age in terms of immersed water absorption. Based on the results, the pattern clearly shows that control concrete specimens absorbs more water compared to other specimens containing POFA in the design mix. At the curing age of 28 days, control specimens absorb 4.27% of water whilst OS1, OS2 and OS3 mix absorbs 4.21%, 3.81% and 2.71%, respectively. The decreasing trend in water absorption was consistent with increasing age of curing and increasing amount of nano POFA present in the specimen. For example, at the age of 56, 90 and 180 days, concrete containing 10% of micro POFA and 3% of nano POFA had water absorption by 1.79%, 1.18% and 0.72%, respectively. The lower water absorption exhibited by concrete containing finer particles can be correlated with pore modification in the concrete matrix that results in the reduction of water penetration as studied by previous researchers (Chindaprasirt et al., 2007). In addition, recent studies by Zeyad et al. (2016) also presented a similar pattern where the concrete containing ultrafine POFA exhibited lower water absorption hence, resulting in greater reduction in porosity. However, findings also points out that there was negative impact on the water absorption and porosity because the POFA used contained a high amount of unburned carbon. The result indicate that the use of ultrafine POFA contributed to the tortuosity of the microstructures due to the high fineness of particles and its low value of loss on ignition (LOI). In this study,

the micro and nano POFA used in concrete was according to the permissible limit as outlined in ASTM C618.

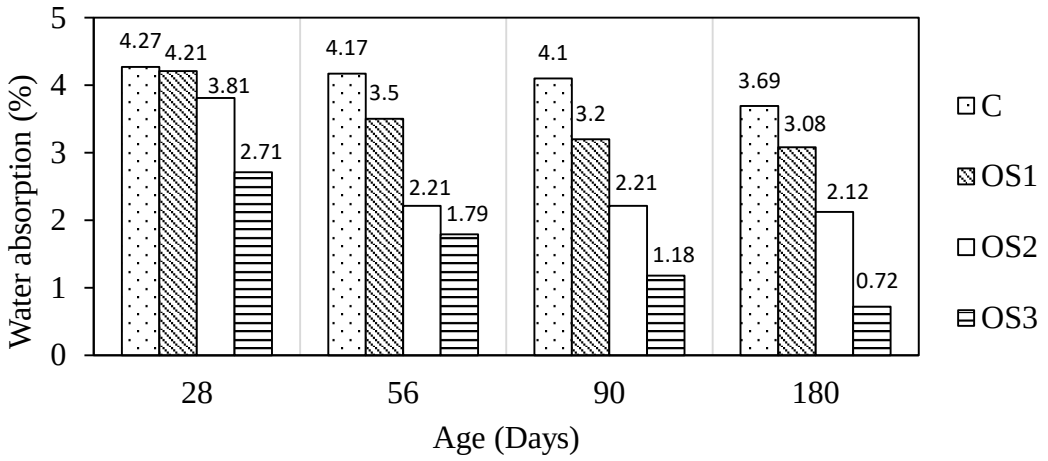

* C (0%M, 0%N); OS1 (10%M, 1%N); OS2 (10%M, 2%N); OS1 (10%M, 3%N)
M: micro POFA; N: nano POFA

Figure 6.1: Water absorption of all mixes at different curing age

The apparent void volume or boiled permeability was calculated based on the results of the water absorption. Similar patterns were observed in the results shown in Figure 6.2 that proves the concrete containing micro and nano POFA (OS1, OS2 and OS3) reduced the permeable void volume at all ages compared to those of the control specimens. However, the permeable void volume data was observed to be higher than water absorption due to the boiling process that reduces the ability of the concrete containing POFA to resist water penetration. It can be seen that the permeable void volume is decreased by nearly by 20-30% at the age of 28 days in concrete containing micro and nano POFA compared to those of the control mix. The lowest permeable void volume can be clearly observed at the age of 6 months (180 days) especially in OS3 mix that contains the highest amount of nano POFA. This obvious trend was attributed to satisfactory micro filling ability and pozzolanic activity of the micro and nano POFA that leads concrete to the concrete's ability to produce strengthening gel hence, reducing the void in concrete. Similar findings were found by Noorvand et al. (2013) who concluded that admixing nano silica with the unground POFA reduced the water absorption as well as the permeable void volume due to higher pozzolanic activity in the concrete system. The study mentioned the incompatibility of the

unground POFA could be improved by adding the nano silica in concrete to improve the strength and durability performance of mortar.

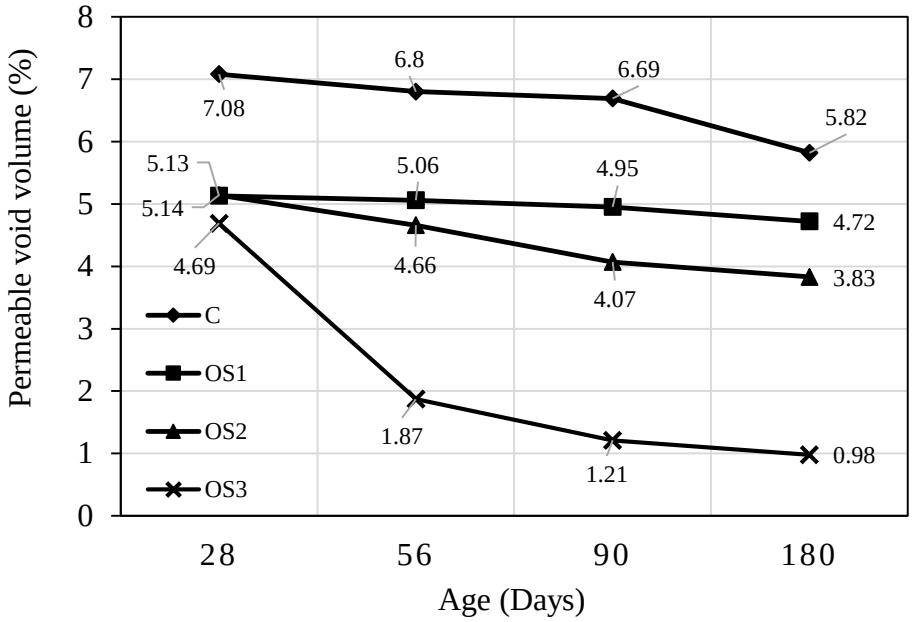

* C (0%M, 0%N); OS1 (10%M, 1%N); OS2 (10%M, 2%N); OS3 (10%M, 3%N)
M: micro POFA; N: nano POFA

Figure 6.2: Apparent permeable void volume of all mixes

6.3 Chloride penetration

The rapid chloride penetration test is a method to determine the performance of concrete to resist chloride ions penetration. The major issue related to chloride penetration is corrosion in reinforced concrete structures. The ingress of chloride ions into concrete increases due to seawater wetting and air drying exposure (Hong & Hooton, 1999; Taylor, 2017; Thomas, 1996). Figure 6.3 shows the rapid chloride penetration test (RCPT) results of the control mix, C and concrete containing 10 % of micro and 1-3% of nano POFA, OS1, OS2 and OS3. Based on the results, all the concrete mixes including the control mix are classified as moderate in terms of chloride penetrability at the age of 28, 56 and 90 days. At 6 months of curing, the concrete is classified as having low permeability as stated in ASTM C1202-18. The expected trend showed in the figure shows that as the nano POFA increases, the total charge passed is reduced. Referring to the results, concrete specimens that were cured longer

showed a pattern of reduced of charge passed and exhibited higher resistance to chloride attacks. Johari et al. (2012b) revealed that the dilution effect and delay of the pozzolanic reaction occurred at the early age of curing hence, the total charge passed of concrete containing ultrafine POFA increased. Therefore, the study found that the longer the curing period, the better the ability to reduce the total charge passed for concrete containing high volume of ultrafine POFA. The study also showed that at the age of one year, the POFA concrete was classified negligible in terms of chloride permeability compared with the control concrete.

It is worth noting that the total charge passed for concrete containing 10% of micro POFA and 3% of nano POFA, OS3 reduced about 12% in comparison with the control concrete at the age of 180 days. At the curing age of 28 days, concrete specimen OS1 shows a reduction of charge passed of 3.76% compared with the control specimen and OS2 and OS3 mix show a reduction of charge passed of 5.89% and 8.51% respectively. Similar pattern was observed at the age of 56 and 90 days; the reduction of total charge passed was recorded to be apprximately 2-4% and maximum reduction of 22%, respectively. The pattern of reduction in chloride permeability that occurred in concrete containing micro and nano POFA was attributed to the fineness of nano POFA reacting with the weak products during the hydration process, forming a secondary CSH gel. This secondary CSH-gel fills up the pores in the concrete and makes the concrete impermeable to chloride penetration hence, reducing the total charge passed (Islam, Mo, Alengaram, & Jumaat, 2016). Similar findins were reported by Thomas, Kumar, & Arel (2017) that stated as the amount of ultrafine POFA increases, the amount of alumina contents such as C_3A and C_4AF in a concrete specimen also increases. Alumina will react with chloride ions to produce calcium chloro-aluminates and calcium chloro-ferrites hence reducing the content of chlorides penetration into the mixture (Thomas, Kumar, & Arel, 2017). The amount of C_3A in POFA was found to be very important in this study as it leads to the chloride chemical binding effect. The study highlighted that the decrease of free chlorides is due to the formation of calcium chloro-aluminates and calcium chloro ferrites from the reaction between the C_3A and C_4AF (Mujah, 2016).Chlorides penetration into concrete can be correlated with the porosity of concrete. The transportations of chloride ion in a concrete will occur in the anodic and cathodic region. These will result in electrolytic

action, thus causing corrosion of steel reinforcement and subsequently, the rupture of concrete (Hossain et al., 2016).

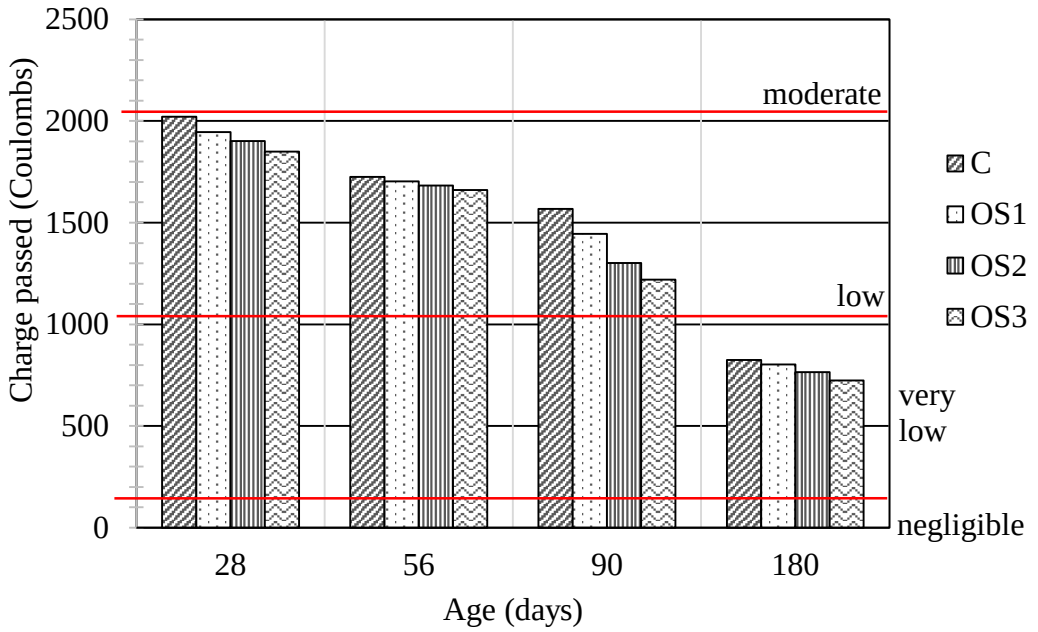

* C (0%M, 0%N); OS1 (10%M, 1%N); OS2 (10%M, 2%N); OS3 (10%M, 3%N)
M:micro POFA; N: nano POFA

Figure 6.3: Total charge passed of all mixes

6.4 Acid resistance

The presence of sulphuric acid can be found in waste from chemical based industries, ground water, or in acid rain. The concrete structures built that surround those environments are exposed to aggressive attack where degradation can take easily place. This type of durability issue affects the performance of the concrete structures. It increases maintenance costs and affects the life cycle performance of structures. In comparison with sulphate attack, the attack from sulphuric acid is riskier due to the dissolution effect by hydrogen ions when acid reacts with the calcium hydroxide that will weaken the concrete paste structure (Bassuoni & Nehdi, 2007). Gypsum formation is the product of sulphuric acid attacks in cement pastes that is produced from the reaction between calcium hydroxide and sulphuric acid. It may also originate from the acidic reaction with the CSH phase and producing amorphous hydrous silica. (Skalny,

Marchand, & Odler, 2002). Moreover, Skalny et al. (2002) explained that the resulting low pH from acid exposure reduces the stability of the mineral phases, thus converting them to gypsum and aluminum sulphate. The main effect of the attack is disintegration of the hydrated paste, leading to loss of strength. Small amounts of ettringite may form in the bulk material where the pH level is not as low. This can only be achieved if the recently formed calcium sulphate is capable of migrating to those regions of the cementitious matrix. Figure 6.4 shows the concrete specimens in 5% acid sulphuric solution. The cubes were removed from the solution after 28, 56, 90 and 180 days. At each of the immersion period, the mass and strength loss are calculated. The concentration of the acid solution was monitored throughout the immersion period. After certain periods of immersion, the surface of cube specimens were cleaned and the weight of concrete specimens were recorded. The original specimens of concrete are shown in Figure 6.5.

Figure 6.4: Concrete specimens in 5% acid sulphuric solution

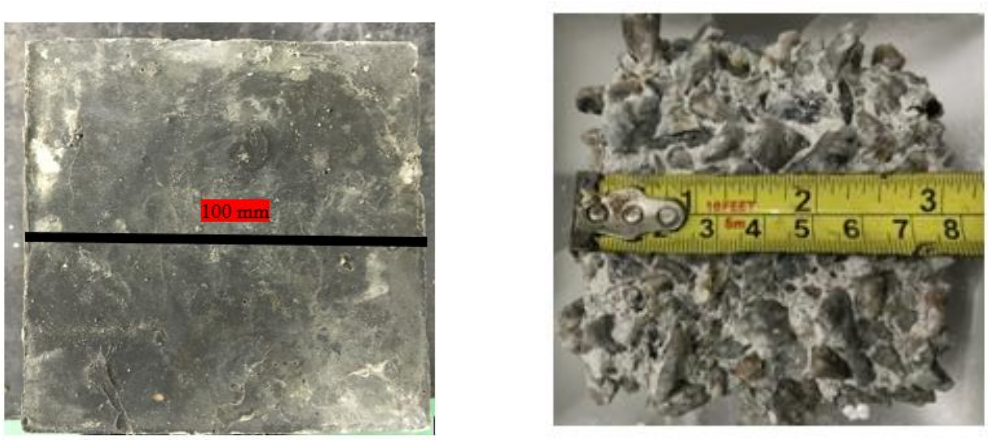

Figure 6.5: Control specimen, C before (left) and after (right) 180 days immersion in 5% acid sulphuric solution (C: 0%M, 0%N)

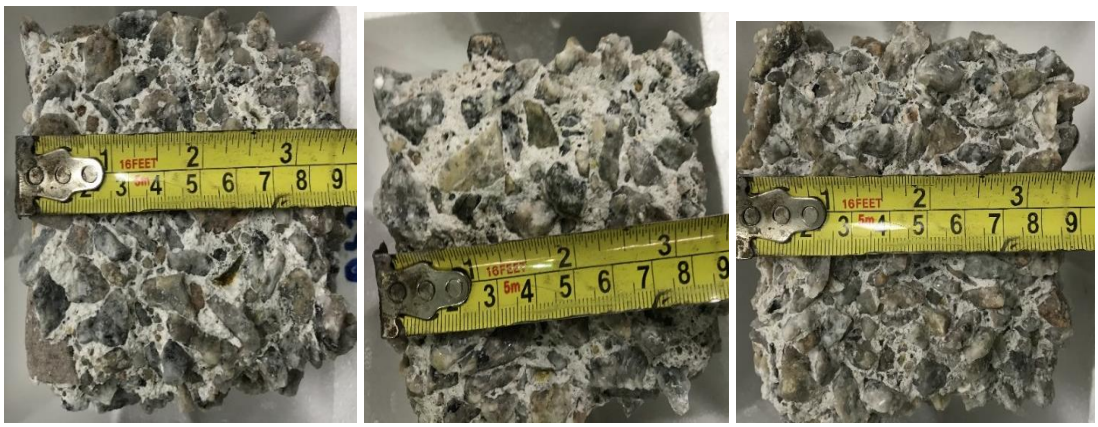

Figure 6.6: Surface condition and average length measurement of concrete mixes at 6 months expose to 5% of H_2SO_4 solution (left to right: *OS1, OS2, OS3)

*OS1 (10%M, 1%N); OS2 (10%M, 2%N); OS3 (10%M, 3%N)
M: micro POFA; N: nano POFA

Figure 6.5 and Figure 6.6 show the surface condition of control concrete and concrete mix containing micro and nano POFA after 6 months immersion in 5% acid sulphuric solution. Visually, the surface of the concretes have deteriorated after being immersed in 5% of acid sulphuric solution. Based on the figures, there are reductions in length after the aggressive exposure as compared with the original concrete specimen as shown in Figure 6.5. Control or plain concrete reduced the length of specimen by 20 mm and the concrete containing micro and nano POFA showed consistent reduction of length by 10 mm. Other than length of the specimen, other effects were also observed such as spalling, surface crack, colour change and deposit on the surface of concrete specimens. The acid attack will starts on the surface of the

concrete into the interior parts of the concrete specimens. Cement when reacting with acid will results in concrete disruption through the decomposition of chemical structure of hydrated concrete. Acid will react with $Ca(OH)_2$ and calcium silicate hydrate C-S-H, to produce a highly soluble compound, called calcium salt. The decomposition of concrete depends on several factors which are, concrete porosity, acid concentration, the solubility of the acid calcium salt, stability of the deteriorated layer and the fluid transport rate of the concrete (Hadigheh et al., 2017).

Sulphuric acid (H_2SO_4) is one of the strongest acids that reacts with concrete and causes severe damage to the concrete. This is due to the existence of two components (acid and sulphate) that induces chemical reactions in concrete. The sulphuric acid could cause serious damage to the concrete by dislodging the aggregates in the concrete (Kwak & Filippou, 1990). Gypsum and ettringite were produced, resulting in the increase in the volume of concrete subsequently causing the concrete to crack. Thus, concrete spalling, surface cracks, change of colour and deposits on the concrete surface were observed, as shown in the Figure 6.5 and Figure 6.6. Micro and nano POFA in concrete has increased the production of secondary CSH gel through reaction with the calcium hydroxide $Ca(OH)_2$. The utilization of $Ca(OH)_2$ in the production of secondary CSH gel has reduced the production of calcium salt hence reducing the effects of acid attack. Due to that, replacement of cement with the higher fineness of POFA has reduced the effects of acid attack by reducing the formation of gypsum and ettringite hence, reducing permeability and penetration of aggressive ion into the concrete (Jaturapitakkul et al., 2007).

The presence of gypsum was observed in control concrete as shown in Figure 6.7. The needle-like crystals can be seen in the figure to show how the gypsum and ettringite were formed from the acid attack reaction. For control concrete samples, the EDX analysis provides the ration of Ca/Si, percentage of carbon and sulphur. Low Ca/Si and higher sulphur percentage were observed in the control specimen due to the highly soluble compound generated from the reaction between the acid sulphuric and $Ca(OH)_2$ was dissolved. Due to that, it resulted in the reduction of Ca from the formation of CSH gel (Li, Xiong, lü, & Yin, 2009). These formations of gypsum and ettringite are induced to concrete spalling, cracking and left of the white deposits on the surface of concrete specimen. It was observed that these factors lead to lower

resistance of acid attacks. The findings taken from Lloyd, Provis, & Van Deventer (2012) also concluded that H_3O^+ and HSO_4^- ions found in acid sulphuric solutions could spread over the CSH gel phase and disintegrated and damaging the network. Furthermore, the x-ray diffraction (XRD) analysis also shows notable traces of gypsum, ettrigitte and $Ca(OH)_2$ in the control concrete sample as shown in Figure 6.8. The highest peak of gypsum can be observed at about 21 2-theta due to the reaction between the calcium and sulphuric ions from the sulphuric acid. Similarly, Deb, Sarker, & Barbhuiya (2016) also found the same finding in geopolymer mortar without nano silica. The authors concluded that the presence of gypsum was likely due to the chemical reaction between the weak product and the sulphuric ions.

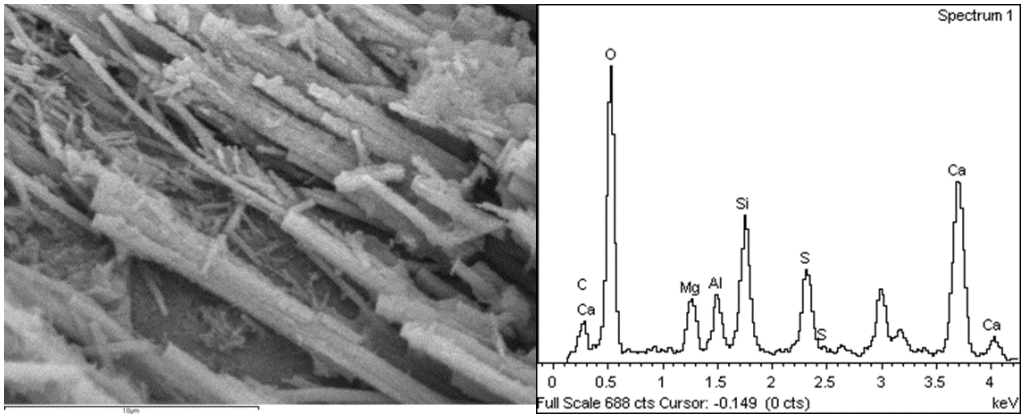

Figure 6.7: SEM image and EDX analysis of control concrete sample after 6 months of immersion in 5% acid sulphuric solution

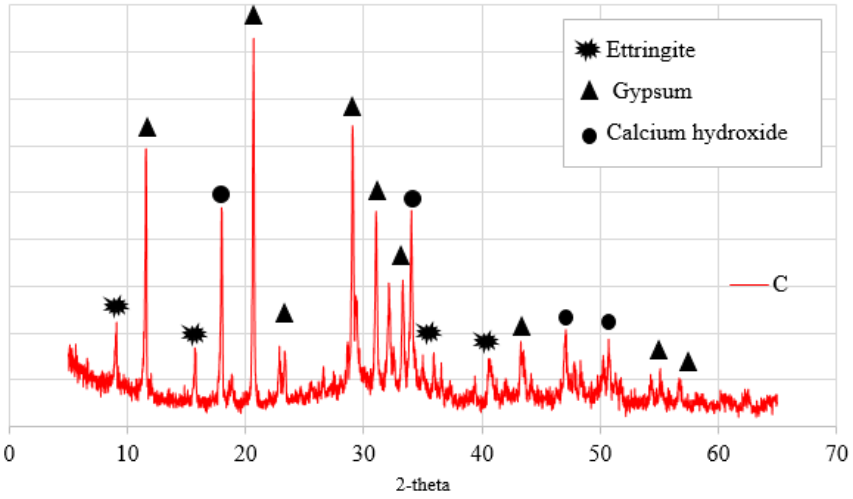

C: 0% of micro POFA, 0% of nano POFA

Figure 6.8: X-ray diffraction (XRD) of deteriorated control concrete sample after 6 months immersion

SEM images of concrete containing micro and nano POFA after 6 months of immersion in acid sulphuric solution are presented in Figure 6.9 (a-f). In comparison with the control concrete, images of the concrete containing micro and nano POFA can be seen to be more compact and less gypsum formation formed in the microstructure images. The dominance of gypsum can be seen in concrete without micro and nano POFA due to the exchange ions between the calcium and acid sulphuric solution, resulting in the deposition of the gypsum and leading to disintegration of the microstructure. In Figure 6.9(a,c,e), it can be observed that there is less of gypsum formation in the microstructure and the EDX analysis also shows a higher ratio of silica content that indicates the dominance of CSH gel in the samples. The EDX analysis confirmed that there are no sulphur content traces in these particular samples for concrete samples containing 2% and 3% of nano POFA as shown in Figure 6.9 (c, e). The SEM images confirmed the EDX by providing clear images without the appearances of gypsum. The three images taken from the samples concrete show similar features due to the small difference of nano POFA content in each sample. Therefore, based on the three SEM images, the EDX analysis indicates that the low calcium oxide content results in low amount of calcium hydroxide in the samples as well. This finding is similar to a study conducted by Alsubari et al. (2016). In his study,

the author found that the low amount of calcium oxide caused a low amount of weak product as well, which led to denser concrete. The weak product in hydration process is highly susceptible to chemical attacks and causes concrete deterioration. The study proved that POFA concrete had more resistance against acid attacks compared to that of control concrete. X-ray diffraction analysis was also conducted to study the mineralogy of the concrete containing micro and nano POFA. Similar features can be seen of pattern can be seen in the three patterns of XRD graph as presented in Figure 6.10. Due to the small differences in replacement of nano POFA in three of the concrete mixes, the XRD shows almost similar chemical reaction products except for the existence of quartz and disappearance of $Ca(OH)_2$. Although there was no detection of $Ca(OH)_2$, the visual appearance shown by the concrete containing micro and nano POFA was quite deteriorated. Therefore, notable traces of gypsum and ettringite can be seen in the OS1, OS2 and OS3 samples.

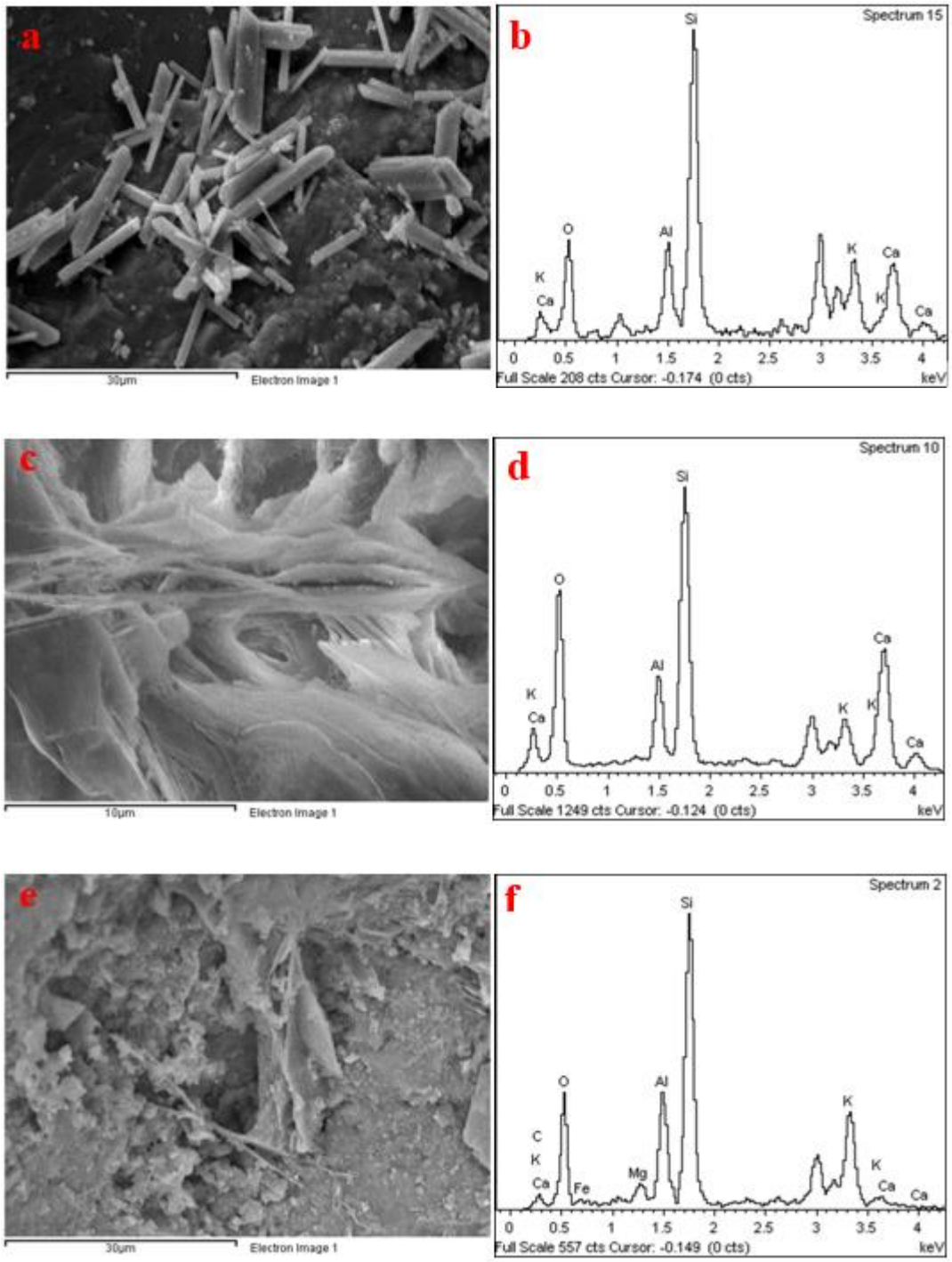

Figure 6.9: SEM image and EDX analysis of a, b) OS1, c, d) OS2, and e, f) OS3 concrete sample after 6 months of immersion in 5% acid sulphuric solution

OS1 (10%M, 1%N); OS2 (10%M, 2%N); OS3 (10%M, 3%N)
M: micro POFA; N: nano POFA

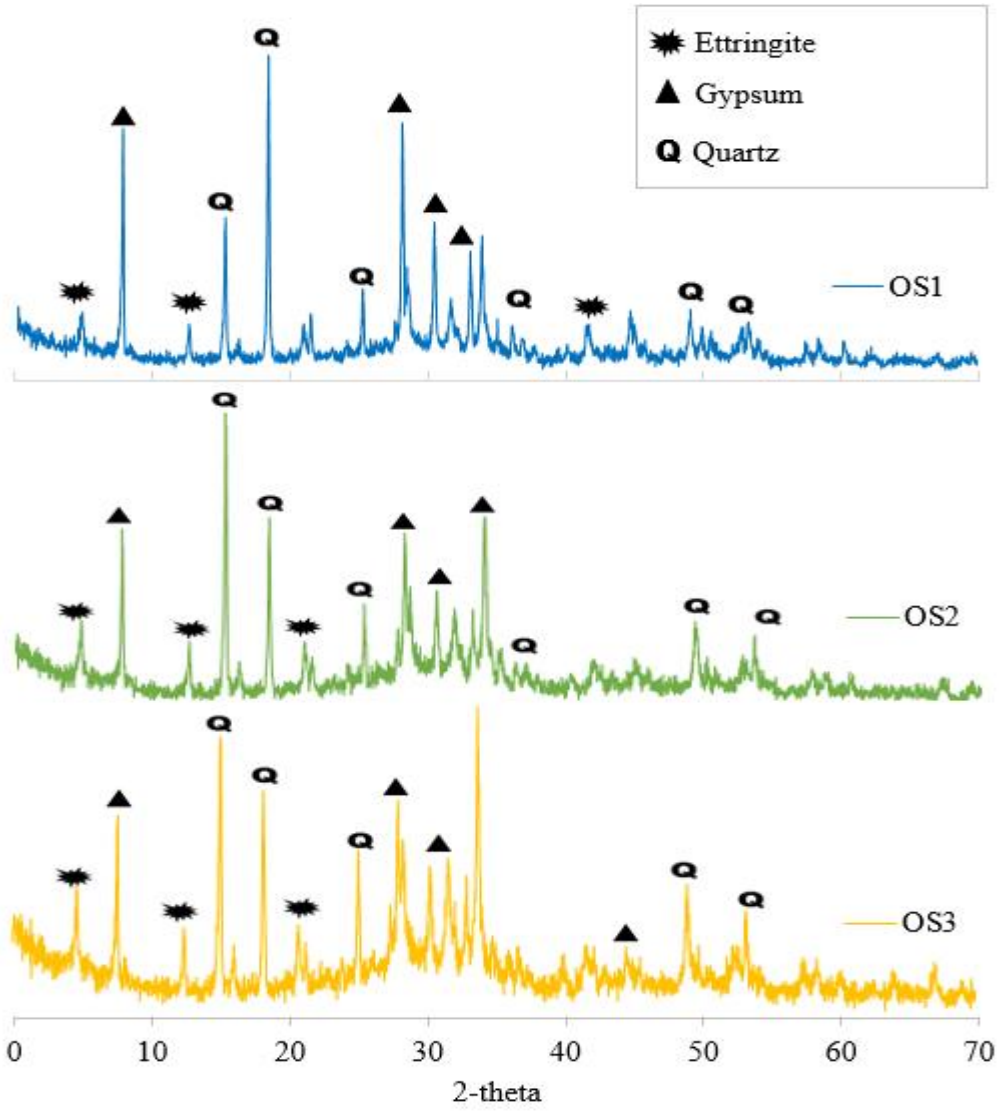

* OS1 (10%M, 1%N); OS2 (10%M, 2%N); OS3 (10%M, 3%N)
M: micro POFA; N: nano POFA

Figure 6.10: X-ray diffraction (XRD) of deteriorated concrete samples (OS1, OS2 and OS3) after 6 months immersion

Figure 6.11 shows the mass loss percentage of all the concrete specimens after immersion in 5% acid sulphuric solution. It can be seen that the slope of all curves are negative due to the weight loss of the concrete after the sulphuric ions reacted with the weak product in concrete. Under acid attack, portlandite or weak product will react very quickly with the sulphuric ions to form calcium sulphate and the reaction is quicker than that of CSH formation (Girardi, Vaona, & Di Maggio, 2010). Control

specimens without any replacement of micro and nano POFA shows the most deteriorated mass loss compared with OS1, OS2, and OS3. At the age of 28 days, the mass loss of control specimen recorded was 19%, 15%, 13% and 11% of mass loss exhibited by OS1, OS2 and OS3 were respectively. The pattern of the results is the same for the concrete age of 56, 90 and 180 days. At 6 months of age, about 30-35% loss in weight was exhibited by all the mixes and concrete without micro and nano POFA and this was recorded to have the highest mass loss. Concrete that contains micro and nano POFA shows better resistance to acid attacks due to the mass loss measurement. This finding was supported in a study done by Mohammadhosseini et al. (2018) which showed that concrete containing POFA exhibited reasonable level of resistance against acid attacks where the lowest mass loss can be observed in concrete that contain 20% POFA.

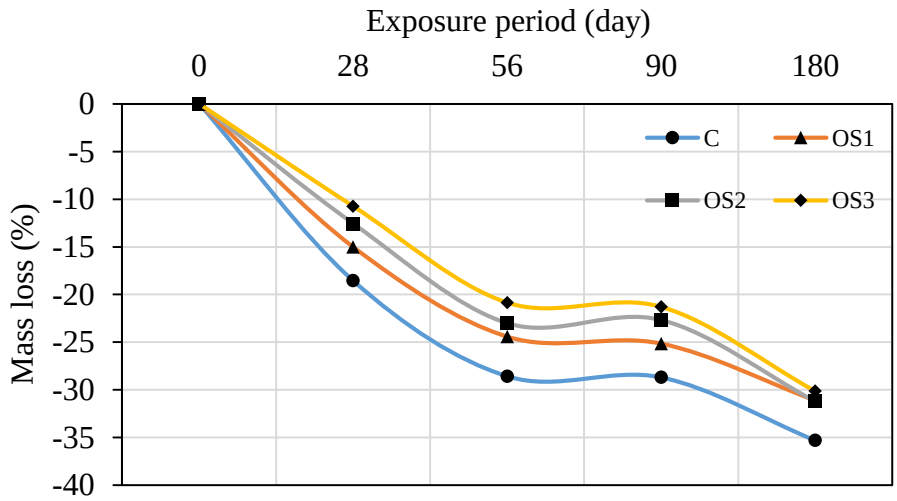

* C (0%M, 0%N); OS1 (10%M, 1%N); OS2 (10%M, 2%N); OS3 (10%M, 3%N)
M: micro POFA; N: nano POFA

Figure 6.11: Mass loss of concrete samples under acid attack

Figure 6.12 shows the results of reduction in compressive strength for all the concrete specimens that were immersed in 5% acid sulphuric solution. It shows that the strength of concrete at all ages are greatly reduced due to the exposure of acid attacks. For example, at the age of 28 days, significant strength loss of 68.48%, 67.34%, 61.35% and 60.84% was yielded by control specimen, OS1, OS2 and OS3,

respectively. The results also shows that the strength had reduced with the increase of exposure time. Similar patterns were observed for concrete specimens at the age of 56, 90 and 180 days. The strength of concrete specimens was greatly reduced because of the chemical reaction between the sulphuric ions and $Ca(OH)_2$, consequently inducing the concrete cracking and reducing the compressive strength of the concrete. Therefore, severe deterioration can be seen at the age of 28 days whereby all the concrete mixes have lost the strength by more than 60%. However, there is significant effect of concrete containing micro and nano POFA as compared with control mix. By increasing the nano POFA dosage, the resistance of concrete specimens under acid attack has also increased, reducing the effects of reduction in strength. The results of concrete specimens containing micro and nano POFA shows better resistance to acid attacks and is mainly due to the consumption of calcium hydroxide $Ca(OH)_2$ during the hydration process to produce secondary C-S-H gel, thus reducing the micro voids in the concrete specimens. This finding is similar to a study conducted by Mohammadhosseini et al. (2018). The author found that POFA could reduce the effects of acid penetration hence, reduction of concrete strength was minimal. In another study done by Alsubari, Shafigh, & Jumaat, (2016) they also mentioned that the treated POFA in concrete provides a good finish and reduced the voids on the concrete surface resulting in a reduction of acid penetration into concrete.

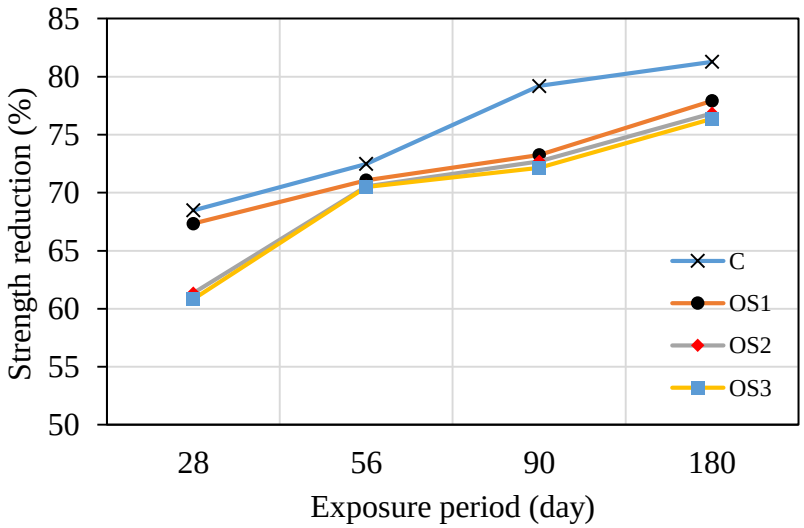

* C (0%M, 0%N); OS1 (10%M, 1%N); OS2 (10%M, 2%N); OS3 (10%M, 3%N)
M: micro POFA; N: nano POFA

Figure 6.12: Compressive strength reduction of concrete mixes

6.5 Resistance to corrosion

There are two types of techniques employed to determine the durability properties of concrete in terms of corrosion resistance. To simulate the corrosion process there are two types of measurements used. First, the rapid or short-term test was an accelerated corrosion test using impressed voltage. Second, an electrochemical technique of corrosion measurements using electrochemical impedance spectroscopy (EIS) and Tafel plot was employed. The accelerated corrosion test provides the actual weight loss of the steel reinforcement bar due to the significant corrosion occurring on the steel bar. The EIS provides information on the corrosion resistance and proposes the equivalent circuit that represents the concrete specimen, whilst the Tafel plot technique was employed to determine the corrosion rate.

6.5.1 Steel weight loss using accelerated corrosion test by impressed voltage

The accelerated corrosion technique has been used to study the effects of steel reinforcement corrosion on the cracking concrete within a short period of time. This technique induces a significant degree of corrosion by using constant direct current which is applied to steel reinforcement embedded in concrete. Although this approach measures the corrosion at high constant rate and does not fully simulate the natural conditions that induce the corrosion, this technique is considered valid due to its ability to control the rate of corrosion within a short period of time (Caré & Raharinaivo, 2007). In the setup test, the steel reinforcement that acts as anode was connected to a 12V DC power supply and the negative terminal was connected to the stainless steel that acts as the cathode (counter electrode). A fixed DC was impressed between the electrodes and the current fluctuation was monitored. The measurement of the current for each specimen was recorded every hour using the DTS-303 data logger. The test continued running until cracks appeared on the surface of the concrete. The parameter of corrosion is based on the weight loss of steel reinforcement bar caused by the voltage supplied. The anodic process was accelerated and a corrosion product formed, resulting in the expansion of the rebar until the concrete cracks. The ingress of the

electrolyte (NaCl) into the small opening of concrete depassivates the film layer on the surface of the steel bar and allow the corrosion process to occur.

A summary of current obtained due to the supplied constant voltage for each mix is shown in Figure 6.13. All the specimens were continuously immersed in 3.5% NaCl and the data logger records the current applied until the surface crack appears. Once the specimen cracks, and considered fail, the circuit was disconnected and the value of current dropped to zero as shown in Figure 6.13. In the Figure 6.13, the time taken by the control concrete specimen was about 37 days and a high current reading was observed. The current reading of 92.5 mA was recorded when the crack appeared. According to Shaikh & Supit (2015), the high current reading was attributed to the rapid penetration of oxygen and chloride into concrete. In OS1, OS2 and OS3 concrete mixes, it took about 43 days of OS1 to fail, and this was followed by OS2 and OS3 the next day, with the current reading of 61.4 mA, 69.1 mA and 52.4 mA, respectively. The longer duration time taken by the concrete containing micro and nano POFA showed that the pozzolanic materials have improved the permeability of concrete hence, reduce the chloride penetration and improve the corrosion resistance in comparison to that of the control concrete. There are limited studies on the effects of POFA concrete on corrosion resistance to steel reinforcement were found, however one corrosion study that utilised POFA in concrete was done by Rukzon & Chindaprasirt (2008). The authors used open circuit potential to measure the corrosion resistance of POFA concrete but the study only provided data on the guideline and threshold limit of the corrosion activity.

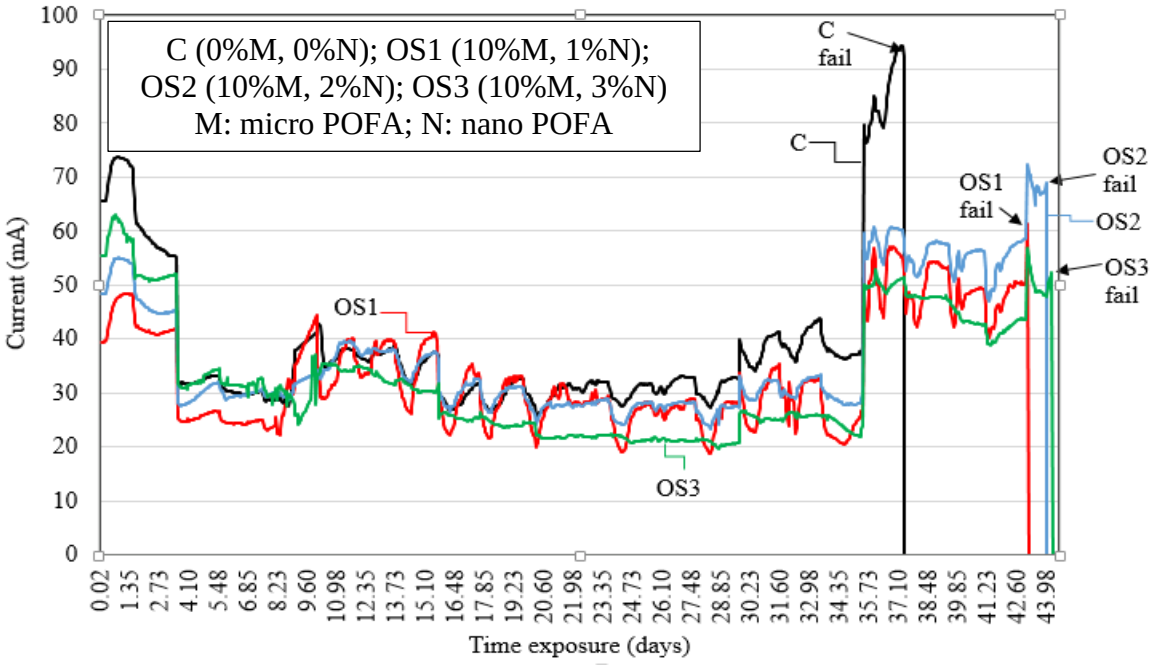

Figure 6.13: Current-time relationship

Figure 6.14 shows the surface condition of the concrete specimens after a certain period of impressed voltage applied. The orange colour of rust can be observed in almost all the specimen and wide surface cracks was observed at control, C and OS1 specimen while OS2 and OS3 specimens exhibited a thin layer of cracks. Due to the micro and nano POFA content in concrete, OS2 and OS3 showed less deterioration compared with the control concrete. The pozzolanic reaction occurred in OS2 and OS3 reflected better durability properties of concrete containing 10% of micro POFA and 2-3% of nano POFA, respectively. The secondary CSH gel produced resulted in the reduction of weak product in concrete hence, decreasing the concrete permeability and increasing the resistance to corrosion. Similar finding was observed by Shaikh & Supit (2015) that proved that high volume fly ash concrete containing nano materials such as nano silica and nano calcium carbonate improved the corrosion resistance by showing the minimum area of corroded surface on the steel reinforcement bar in comparison to that of ordinary concrete.

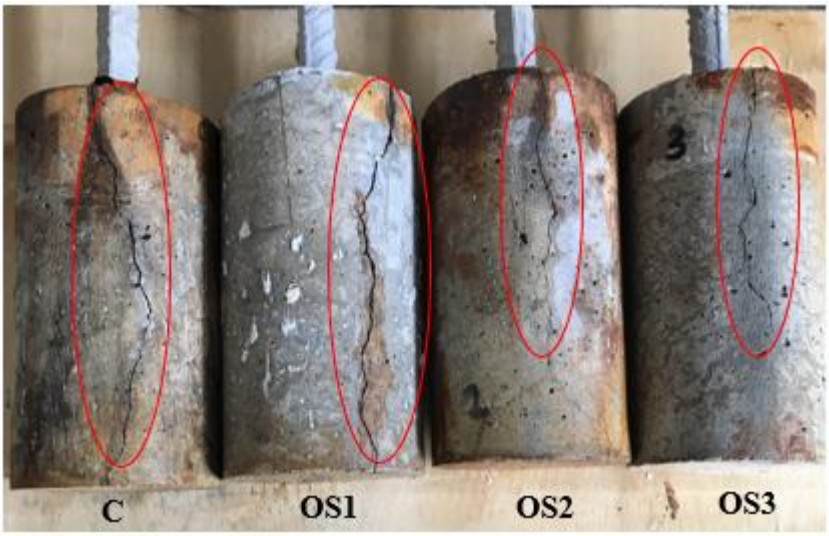

C (0%M, 0%N); OS1 (10%M, 1%N); OS2 (10%M, 2%N); OS3 (10%M, 3%N)
M: micro POFA; N: nano POFA

Figure 6.14: Surface crack of the concrete specimens under impressed voltage

After the crack initiated on any of the specimens, the circuit of the particular specimen was disconnected. The corroded steel embedded in concrete was removed and the weight of the corroded rebar recorded. Figure 6.15 shows the appearance of the exposed steel reinforcement bar embedded in C, OS1, OS2 and OS3 concrete. The left side of the steel bar was exposed to the atmosphere, while another part of it placed near to the surface of concrete. To avoid the corrosion from occurring in this part, the epoxy coating was used to cover this part of steel bar. Significant differences can be observed on the surface of the steel bar after the accelerated corrosion test using impressed voltage as shown in Figure 6.15. There is large area of corroded parts that can be seen on the surface of the steel bars embedded in control concrete C, as compared with the other steel bar embedded in concrete containing micro and nano POFA, OS1, OS2 and OS3. The less visible corrosion can be found on steel bar embedded in concrete containing 10% of micro POFA and 3% of nano POFA, OS3. To confirm the visual measurement of the corroded steel reinforcement bar, the weight loss of the steel bar was carried out and the result as presented in Table 6.1. For cleaning up the steel reinforcement after the test, the mechanical procedure was applied according to ASTM G1-03(17). The procedures include the scrubbing and brushing the steel reinforcement using non-metallic brush and mild abrasive-distilled water slurry to remove corrosion products.

* C (0%M, 0%N); OS1 (10%M, 1%N); OS2 (10%M, 2%N); OS3 (10%M, 3%N)
M: micro POFA; N: nano POFA

Figure 6.15: Corroded steel reinforcement bar embedded in concrete.

(Pitting corrosion showed in the circle)

The actual weight loss of steel reinforcement was calculated based on ASTM G1-17. To determine the weight of corroded bar, the steel bar was extracted after the crack initiated by breaking the concrete specimen.

$$Actual\ weight\ loss = \frac{W_f - W_i}{\pi DL} \qquad \text{Equation 6.1}$$

Where, W_f is final weight (g), W_i is initial weight (g), D is diameter of the steel reinforcement (cm) and L is length of steel reinforcement (cm).

According to Table 6.1, the actual weight loss of the steel reinforcement bars embedded in control concrete without micro and nano POFA, C was the highest among with a loss of about 13.95%. On the other hand, the weight of OS1, OS2 and OS3 concrete specimens containing 10% micro POFA and 1-3% nano POFA were lost at a lower value which was about 6.5%, 4.6% and 3.8%, respectively. The weight loss

result confirmed that the concrete without the micro and nano POFA has provide lower corrosion resistance. Studies by Shaikh & Supit (2015) also showed similar agreement in a study of corrosion resistance to concrete containing pozzolanic material such as nano silica and nano calcium carbonate. Better corrosion resistance was found in concrete containing 1-2% of nano materials due to the ability of the nanoparticles to lower the corrosion current and improve the resistance of chloride permeability to concrete.

Table 6.1: Weight loss of the steel reinforcement before and after corrosion process

Mix	Initial steel bar weight, W_i (g)	Final steel bar weight, W_f (g)	Actual steel bar weight loss (g/cm^2)	Percentage weight loss based on actual weight (%)
C	731	629	1.48	13.95
OS1	733	685	0.69	6.5
OS2	735	701	0.49	4.6
OS3	732	704	0.41	3.8

* C (0%M, 0%N); OS1 (10%M, 1%N); OS2 (10%M, 2%N); OS3 (10%M, 3%N)
M: micro POFA; N: nano POFA

6.5.2 Corrosion rate measurement using electrochemical impedance spectroscopy (EIS) and Tafel plot

6.5.2.1 Moisture absorption profile

For the electrochemical measurement, the corrosion of the steel bar embedded in concrete showed an accelerated in the corrosion process under the exposure of wetting and drying cycle. For wetting cycle, all the reinforced concrete specimens were immersed in 3% sodium chloride, (NaCl) solution and specimens were exposed to the outdoor lab environment for drying cycle. This section deals with the moisture absorption transport in all the reinforced concrete specimens. Drying process refers to the moisture transport in concrete subjected to atmosphere with relative humidity. Wetting process is referred to the moisture transport due to the moisture absorption under capillary suction. The discussion is valid for the case of one-dimensional diffusion and the diffusion is studied through the concrete cylinder specimen according to ASTM 1585-13. Equation 6.2 explains the one-dimensional absorption process.

$$I = St^{1/2}$$

Equation 6.2

Where, I is absorption, $t^{1/2}$ is square root of time, S is sorptivity coefficient

Therefore, the moisture absorption of concrete can be calculated by determining the accumulative water gains at specific intervals of time. The period of wetting and drying cycle can be obtained after a certain moisture content is exposed to the concrete in uniform distribution. Figure 6.16 shows the graph of accumulative water gain by concrete over square root of time. It can be seen in the graph that all concrete specimens reached almost constant weight at $t^{1/2}$ equals to 800 sec, that is equivalent to almost 7 days. This means that the 7 days period of wetting process is enough to allow the sodium chloride, NaCl to reach the reinforcing steel bar embed in concrete.

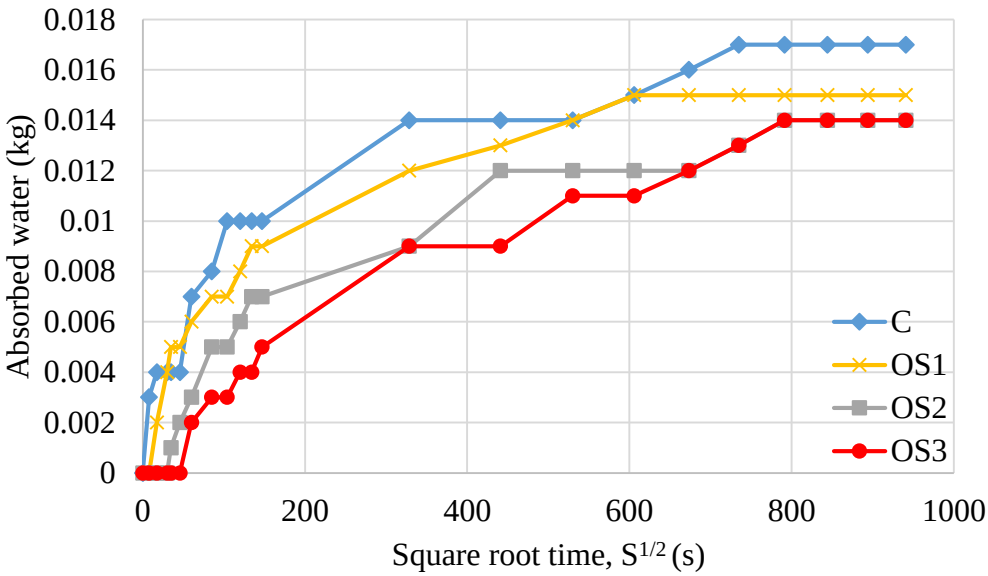

* C (0%M, 0%N); OS1 (10%M, 1%N); OS2 (10%M, 2%N); OS3 (10%M, 3%N)
M: micro POFA; N: nano POFA

Figure 6.16: Accumulative weight over square root of time

6.5.2.2 Polarization resistance using electrochemical impedance spectroscopy (EIS)

The EIS method was employed to study and analyse the corrosion measurement as an electrochemical phenomenon and detect small corrosion occurrences in metal (Ribeiro & Abrantes, 2016). This non-destructive technique is more reliable and is more commonly used especially in concrete due to the heterogeneity of concrete. It works based on the frequency domain and the concept of concrete interface represented is a combination of passive equivalent electrical circuit elements such as resistance, capacitance and inductance. The EIS results are interpreted using the EIS impedance data and equivalent electrical circuit obtained to represent the physical process under graphical representations (Ribeiro & Abrantes, 2016). This test was conducted using the VersaSTAT 3 Potentiostat/Galvanostat (Princeton Applied Research) with a built-in software called ZSimpWin. The cylindrical specimen with steel reinforcement bars embedded was prepared with all surface covered with epoxy coating except the radial surface to allow the one-dimensional diffusion of chloride ions. The specimens were subjected to 28 days of water immersion and then, to an alternate 7-days wetting and drying cycle. For 7-days of wetting cycle, the specimens were immersed in 3.5% of sodium chloride solution, and 7-days drying in an indoor environment (22 ºC $\pm$ 2, 80% RH). Three electrodes were needed for the test where a reinforcement bar was employed as a working electrode, stainless steel worked as a counter electrode and a saturated calomel electrode (SCE) as the reference electrode. A wide range of frequency was set, between 100 kHz and 10 mHz to get coverage of the Nyquist and Bode plot diagrams. Suitable equivalent circuit was used to analyze the impedance data and to fit the Nyquist plot. The EIS measurement was recorded at 91, 182 and 365 days.

The impedance spectra obtained from EIS technique are presented in Nyquist format for all steel reinforcement embedded in concrete mixes as shown Figure 6.18Figure 6.20 at 13^{th}, 26^{th} and 52^{nd} cycle, respectively. In the Nyquist plot, the data is plotted in the complex plane of real component *Z'* (resistive) and imaginary component *–Z"* (capacitive). There are two semi loops that represent capacitive characteristics shown in Figure 6.18 for concrete mix OS1, OS2 and OS3. In Figure 6.19 and Figure *6.20*, almost all the curves consist of two capacitive characteristics. A

small semi loop was shown in the region of high frequency which indicates the surface film that is related to dielectric of concrete. Under the same Nyquist plot, the second large loop shown in the region of low frequency corresponds to the charge transfer process that is related to the electrochemical reaction on the surface of the steel reinforcement (Jiang et al., 2018). The impedance spectra plotted in all EIS results are well fitted with equivalent electrical circuit proposed.

The model of equivalent circuit was selected as the best describes and fit with the measured impedance data. Model *R (QR (QR) (QR) (CR))* was used to model the EIS data as shown in Figure 6.17. The schematic diagram was utilised to relate the reinforced concrete and the equivalent electric circuit as shown in the same figure. The equivalent circuit in the figure below consist of the elements such as the resistance of electrolyte solution (R_s), polarization resistance (R_p), constant phase element (Q_p), resistance of oxide layers (R_1, R_2), modified phase element (Q_1, Q_2), empirical constant (n_p, n_1, n_2), capacitance double layer (C_{dl}) and resistance bilayer electrode (R_{dl}). The values of the fitting parameter are tabulated in Table 6.2 for each concrete mix at three different cycles.

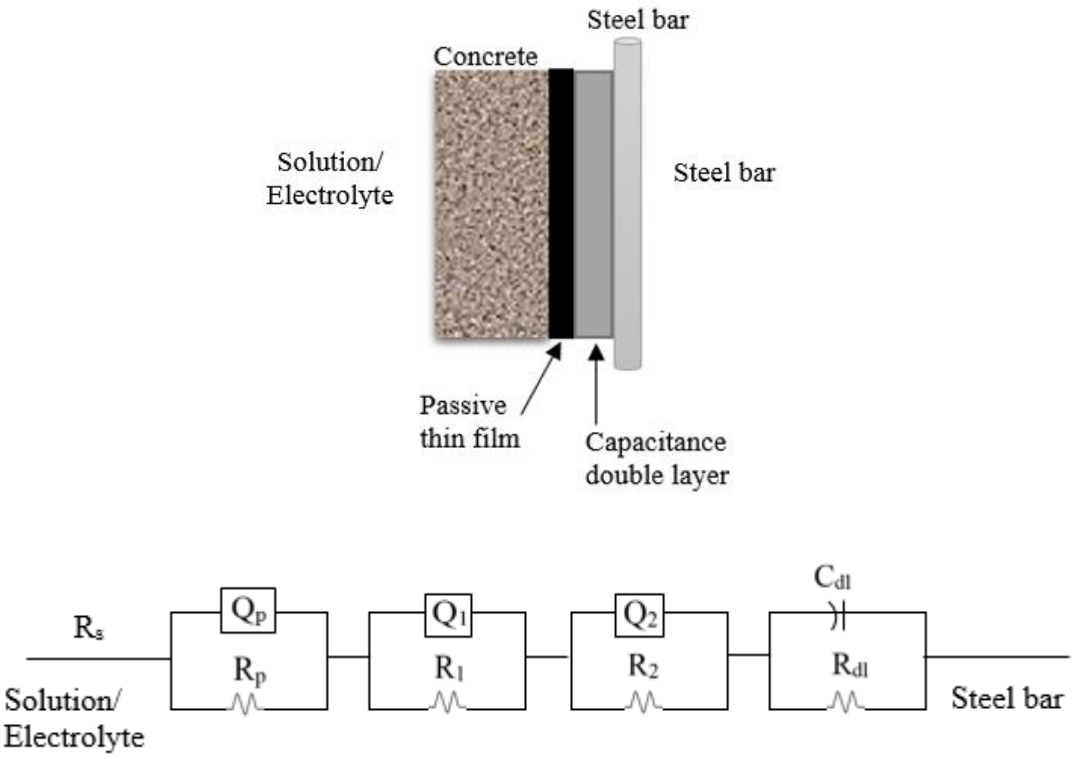

Figure 6.17: Schematic diagram for reinforced concrete interface and proposed equivalent circuit

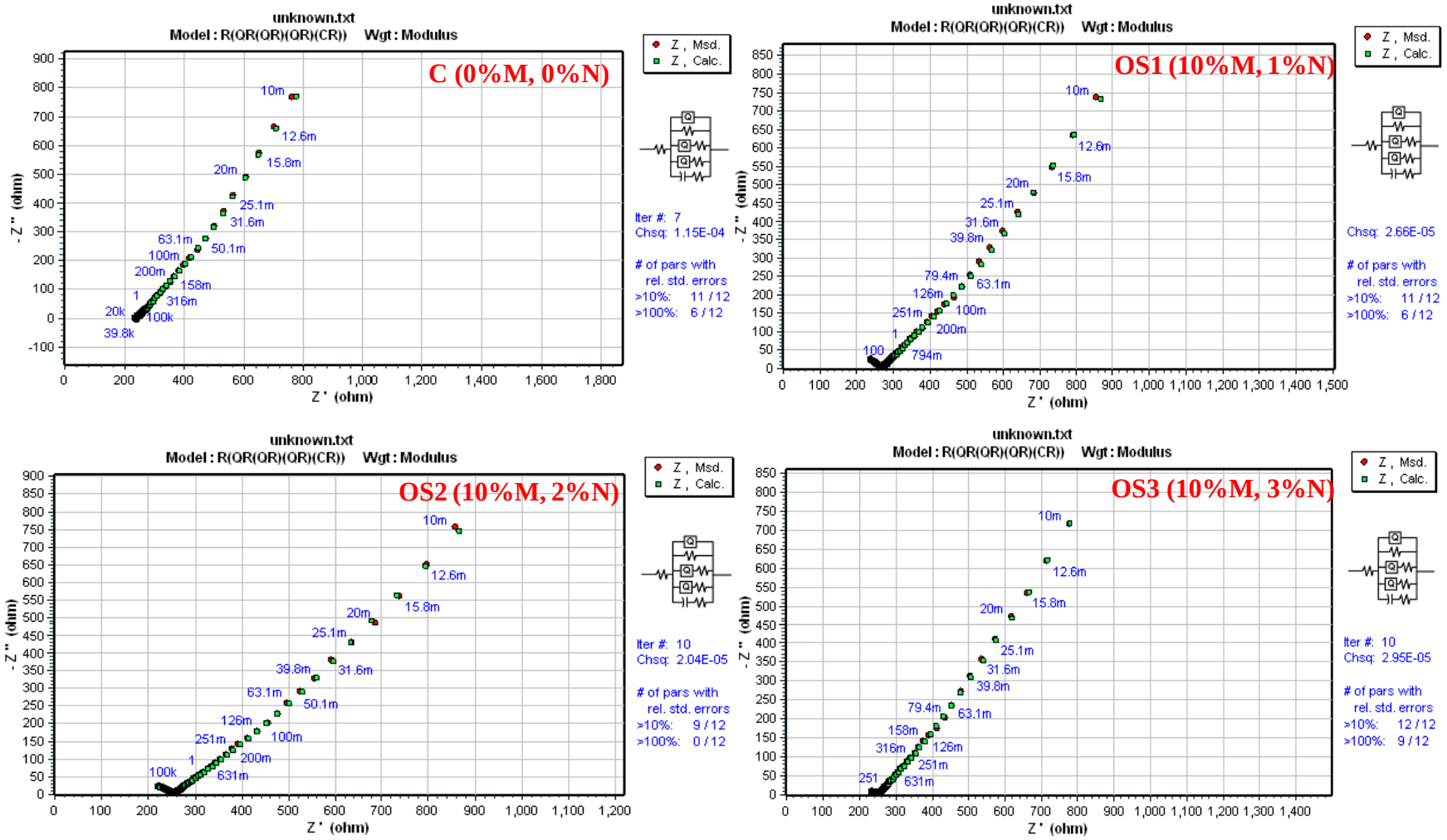

Figure 6.18: Impedance spectra in Nyquist plot and fitting data of all concrete mixes after 91days. (M: micro POFA, N: nano POFA)

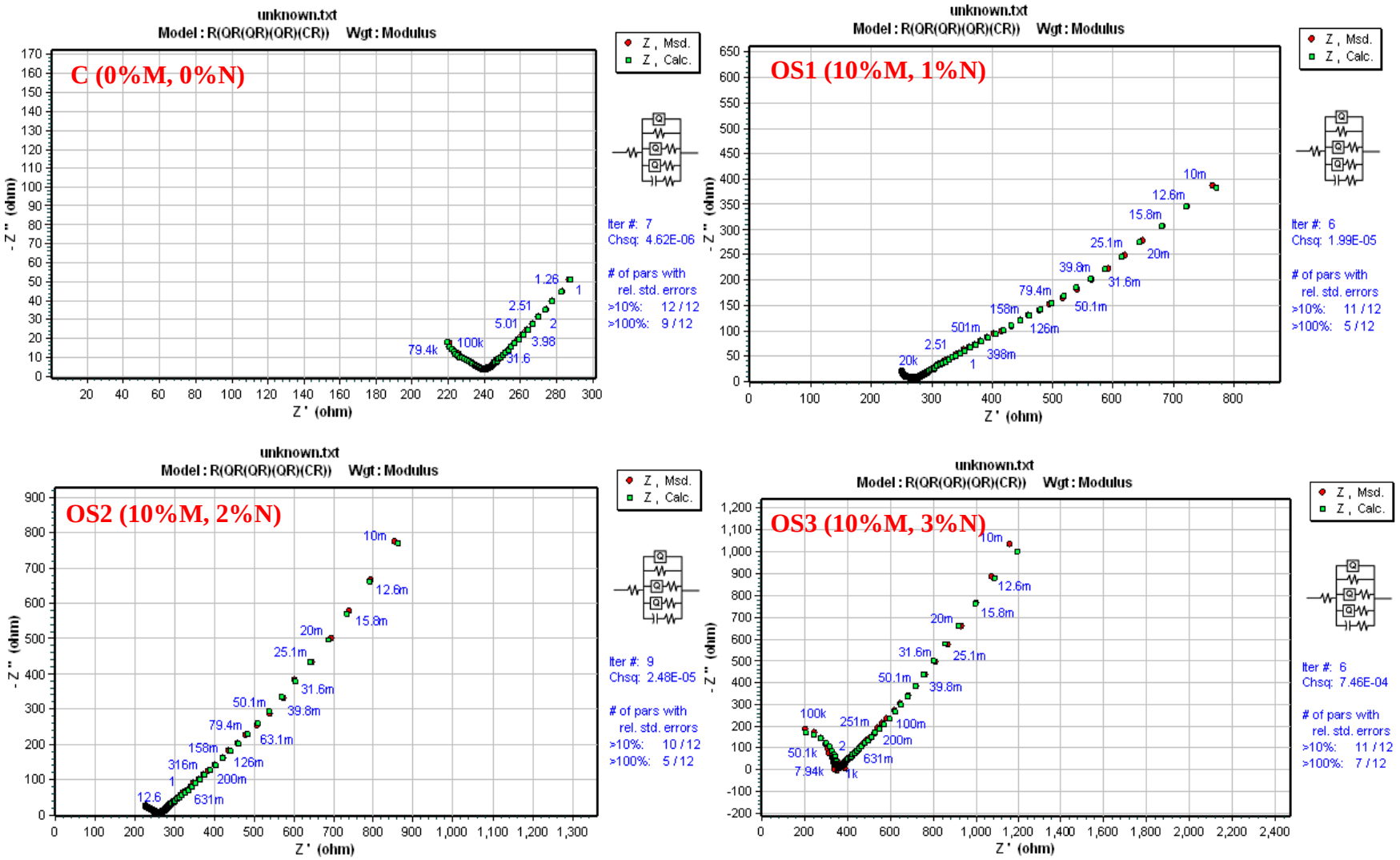

Figure 6.19: Impedance spectra in Nyquist plot and fitting data of all concrete mixes after 182days. (M: micro POFA, N: nano POFA)

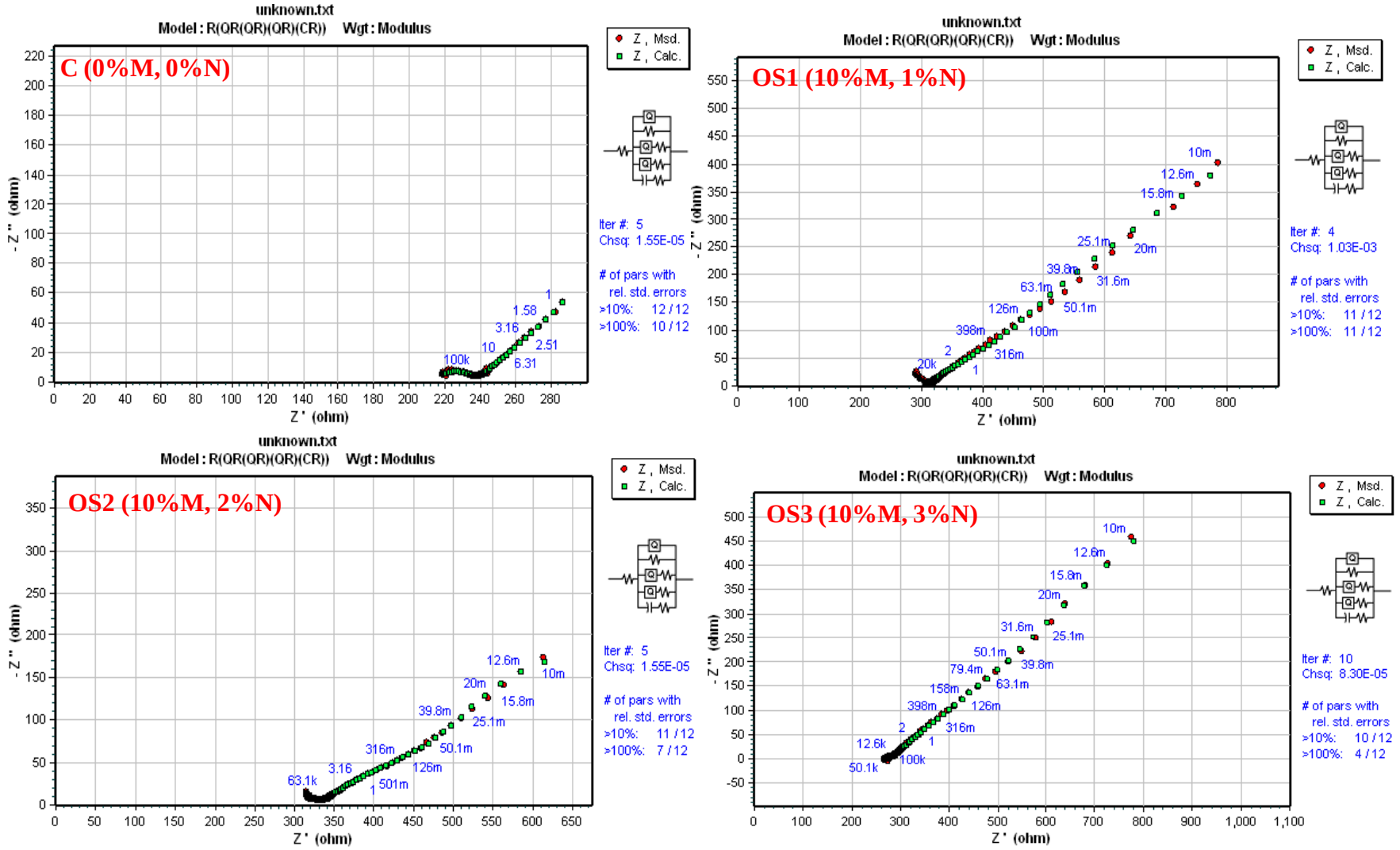

Figure 6.20: Impedance spectra in Nyquist plot and fitting data of all concrete mixes after 365days. (M: micro POFA, N: nano POFA)

Table 6.2: Fitting parameter obtained from each of equivalent circuit for all concrete mixes at different cycles

Mix	Cycle	R_s / $\Omega.cm^2$	Q_p-Y_0 / $S.s^n.cm^2$	n_p	R_p / $\Omega.cm^2$	Q_1-Y_{01} / $S.s^n.cm^2$	n_1	R_1 / $\Omega.cm^2$	Q_2-Y_{02} / $S.s^n.cm^2$	n_2	R_2 / $\Omega.cm^2$	C_{dl} / $F.cm^2$	R_{dl} / $\Omega.cm^2$
C	13 (91 days)	2395.7	$6.89x10^{-9}$	1.00	$2.08x10^{11}$	$2.45x10^{-1}$	0.50	$1.71x10^{4}$	$1.17x10^{-5}$	0.71	$1.23x10^{5}$	0.086	75410
OS1		1.10	$1.41x10^{-4}$	0.43	$1.19x10^{12}$	$2.64x10^{-1}$	0.52	$2.00x10^{4}$	$8.86x10^{-9}$	1.00	$3.22x10^{4}$	$1.58x10^{-2}$	283530
OS2		0.3	$2.63x10^{-7}$	1.00	$7.38x10^{15}$	$7.93x10^{-19}$	0.81	$1.22x10^{17}$	$1.82x10^{-1}$	0.49	$2.64x10^{4}$	$1.08x10^{-1}$	296387
OS3		21068	$3.50x10^{-1}$	0.41	$7.56x10^{18}$	$1.49x10^{-16}$	0.47	$1.12x10^{19}$	$6.77x10^{9}$	0.09	$4.72x10^{11}$	0.083	132572
C	26 (182 days)	4.40	$4.23x10^{-9}$	1.00	$5.49x10^{9}$	$3.00x10^{-4}$	0.65	$4.55x10^{5}$	$3.06x10^{-1}$	0.57	$1.84x10^{4}$	$1.74x10^{-1}$	243717
OS1		0.691	$1.06x10^{-15}$	0.86	$1.53x10^{10}$	$6.7x10^{-1}$	0.37	$2.47x10^{4}$	$2.23x10^{-7}$	1.00	$6.91x10^{3}$	$4.94x10^{-4}$	126000
OS2		4.7	$3.10x10^{-8}$	1.00	$1.01x10^{11}$	$8.83x10^{-6}$	0.68	$1.64x10^{5}$	$3.68x10^{-1}$	0.47	$1.79x10^{4}$	$1.38x10^{-2}$	206531
OS3		10609	$1.26x10^{-2}$	0.22	$4.35x10^{12}$	$1.84x10^{-1}$	0.60	$9.42x10^{3}$	$2.16x10^{-1}$	0.74	$3.82x10^{4}$	$2.03x10^{-2}$	408154
C	52 (365 days)	0.7	$1.29x10^{-8}$	1.00	$7.24x10^{4}$	$1.12x10^{-1}$	0.40	$4.29x10^{4}$	$9.22x10^{-6}$	0.66	$4.06x10^{5}$	0.428	151649
OS1		18801	$6.42x10^{-4}$	1.00	$2.48x10^{5}$	$7.13x10^{-2}$	0.79	$7.95x10^{4}$	$2.82x10^{-1}$	0.52	$6.11x10^{2}$	0.263	169966
OS2		3.1	$8.83x10^{-5}$	0.48	$8.31x10^{5}$	$1.69x10^{-1}$	0.68	$6.09x10^{4}$	$1.09x10^{-1}$	0.53	$2.94x10^{4}$	$2.44x10^{-1}$	267287
OS3		5110	$2.67x10^{-4}$	0.45	$1.71x10^{6}$	$3.49x10^{-1}$	0.66	$3.39x10^{4}$	$8.26x10^{-2}$	0.57	$2.20x10^{4}$	$1.05x10^{-2}$	312699

C (0%M, 0%N); OS1 (10%M, 1%N); OS2 (10%M, 2%N); OS3 (10%M, 3%N)

M:micro POFA; N: nano POFA

The highest polarization resistance or charge transfer resistance, R_p can be interpreted according to each cycle. For example, at 13th cycle, the highest R_p was exhibited by OS3 concrete mix containing 10% of micro POFA and 3% of nano POFA with value of R_p is 7.567.56x10^{18} Ω.cm^2. In the same cycle, other mix contatining 10% of micro POFA and 1-2 % of nano POFA showed the highest polarization resitance in comparison to that of the control mix. Throughout the cycles, all the concrete mix containing micro and nano POFA showed better resistance to corrosion by interpreting the results with the value of R_p. At the longest period of exposure, the R_p of each concrete mix showed a reduction compared to the R_p at 2 previous cycles due to 1 year of alternate (wetting and drying) cycles exposed to the concrete mixes. Therefore, the value of R_p for control concrete mix without micro and nano POFA yielded about 2.45x10^4 Ω.cm^2. Based on the value of R_p, all the concrete mixes are still in passive state even at 1 year age but R_p yielded by control mix showed the lowest at 13th, 26th and 52nd cycles. The value of R_p is inversely proportional to corroison rate. Therefore,it can be seen from the Table 6.2 that concrete mix of OS1, OS2 and OS3 containing 10% of micro POFA and 1-3% of nano POFA showed better resistance to corrosion than that of the control mix. The use of micro and enhanced with nano POFA as supplementary cementitious concrete improved permeability of concrete and increased the resistance of corrosion. Similar finding also were ound by Lee, Song, Ann, & Ismail (2009) that utilized 30% of POFA in producing concrete, the R_p value yielded by POFA concrete showed the highest than that of the control mix at 2 years exposure period. In other corrosion study of the POFA concrete, Yahaya, Muthusamy, & Sulaiman (2014) stated that POFA concrete showed a better resistance against corrosion due to the enhancement of C-S-H gel that makes the concrete denser. To calculate the corrosion rate of the steel reinforcement embedded in each concrete mix, the next section provides the information of the corrosion rate using the Tafel plot technique.

6.5.2.3 Corrosion rate evaluation using Tafel plot technique

The Tafel plot technique was employed to determine the corrosion current density in order to calculate the corrosion rate of steel reinforcement in concrete. As shown in Equation 6.3, the corrosion current density i_{corr} can be calculated from the Tafel constants. The value of Tafel constant can be evaluated from the running of the potentiostat using Tafel plot technique. The potential scan, E_{corr} of $\pm$ 250 mV was applied at scan rate of 0.2 mV/sec. The three electrodes were needed for these methods, similar to those used in the EIS corrosion measurement and employing the same setup was used as well. The details of the reinforcement bars were inserted in the software including the exposed area (69.12 cm^2), equivalent weight (27.92 gm) and density of the reinforcement bar (7.85 g/cm^3).

$$i_{corr} = \frac{\beta_a \beta_c}{2.3 R_p (\beta_a + \beta_c)} \qquad \text{Equation 6.3}$$

For each concrete specimen, a Tafel plot consisting of anodic and cathodic region was produced. As shown in Figure 6.21, the intersection of two straight lines indicates of value E_{corr} and from the point i_{corr} can be obtained. The slope of the both straight lines is called Tafel constant, β. Slope at the anodic region called anodic Tafel, β_a and slope at the cathodic region called cathodic Tafel, β_c. From those values, the corrosion rate can be calculated using the following equation:

$$Corrosion\ rate = \frac{i_{corr} E}{Ad} \qquad \text{Equation 6.4}$$

Where, E is the equivalent weight, A is area of steel reinforcement and d is density of steel reinforcement.

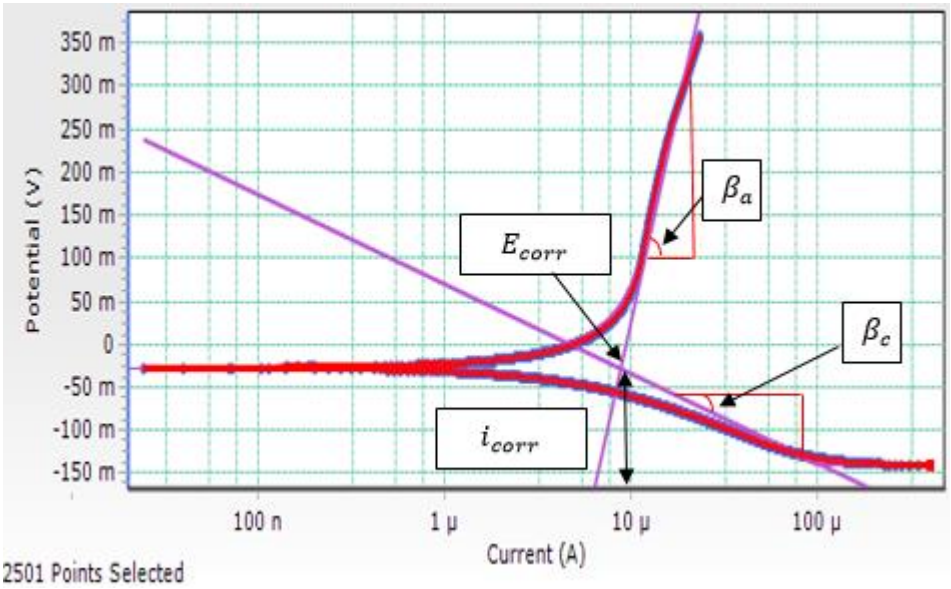

Figure 6.21: Tafel plots

Results of corrosion analysis using Tafel plot technique is summarised in Table 6.3. The data interpretation of the significant values are presented in graphs as shown in Figure 6.22 and Figure 6.23. Both Tafel constants were determined from each Tafel plot generated at certain period of cycle as shown in Table 6.3. From the Tafel constant, the i_{corr} can be obtained. Broomfield (1994) provided the guideline to interpret the data of i_{corr} value. If more than 1 µA/cm^2, the extent of corrosion can be categorized as the high corrosion. Based on i_{corr} given in Table 6.3, the potential of the high corrosion was yielded by the reinforced concrete that exposed to alternate cycle for about 1 year. At the exposure of about 91 days, the i_{corr} values indicated passive conditions of corrosion for all the mix whilst at the 183 days; the corrosion is categorized under moderate.

Table 6.3: Tafel plots results

Cycle (days)	Mix	β_c (mV)	β_a (mV)	i_{corr} (μA/cm^2)	E_{corr} (mV/SCE)	Corrosion rate (mm/y)
13th (91 days)	C	103.33	1763	0.155	-27.53	0.00180
	OS1	104.00	985	0.128	-27.31	0.00149
	OS2	95.00	1180	0.127	-14.38	0.00147
	OS3	97.00	1094	0.124	-19.04	0.00143
26th (182 days)	C	215.02	1219	0.59	-127.90	0.00725
	OS1	233.78	94.35	0.57	-92.31	0.00660
	OS2	212.10	1724	0.55	-111.51	0.00600
	OS3	208.50	1587	0.50	-140.75	0.00582
52nd (365 days)	C	218	828	0.62	-339.65	0.0721
	OS1	210	1400	0.39	-359.10	0.0452
	OS2	285	952	1.37	-384.75	0.0159
	OS3	195	967	1.28	-427	0.0148

C (0%M, 0%N); OS1 (10%M, 1%N); OS2 (10%M, 2%N); OS3 (10%M, 3%N)
M:micro POFA; N: nano POFA

Other than that, E_{corr} value also can be related to probability of corrosion. If the corrosion potential measurement is more positive that -126 mV over SCE reference electrode, the probability of no corrosion occurring is 90%. If the corrosion potential is more negative than -276 mV, the probability of corrosion to occur is 90% while in between those values; the corrosion activity is considered uncertain (ASTM C876-15). In this study, the E_{corr} values are observed to be more negative than -276 mV, and can be seen at all reinforced concrete mix after 1 year exposure to wetting and drying which is categorized under 90% probability of corrosion to occur. Other values of E_{corr} showed uncertain corrosion activity and 90% of no corrosion.

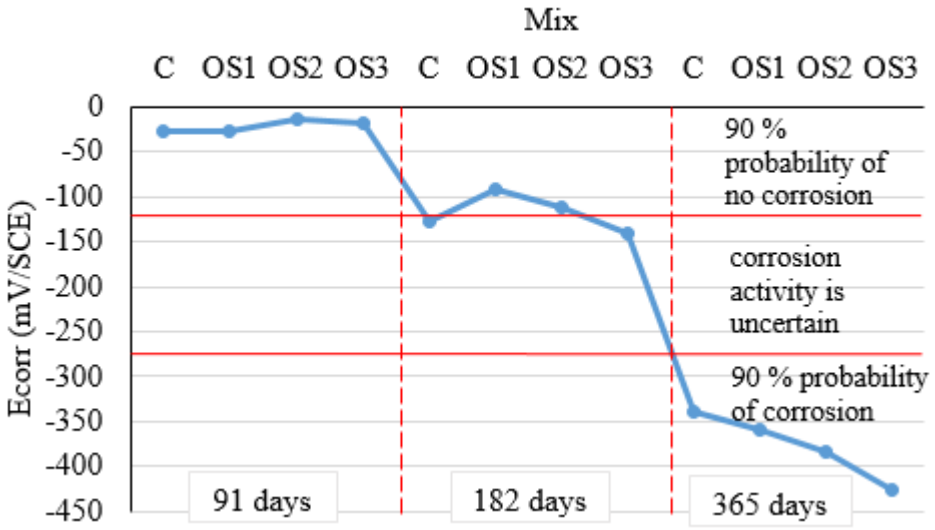

C (0%M, 0%N); OS1 (10%M, 1%N); OS2 (10%M, 2%N); OS3 (10%M, 3%N)
M: micro POFA; N: nano POFA

Figure 6.22: Corrosion potential measurements for each concrete mix at different exposure period

Figure 6.23 shows the corrosion rate values obtained from the Tafel plot technique for each concrete mix. At the early cycle, there is no significant difference between the mixes due to low corrosion activity. Value of E_{corr} and i_{corr} showed the potential of no probability of corrosion occuring at the 13th and 26th cycles. Therefore, the corrosion rate showed by the control, OS1, OS2 and OS3 were 0.00180, 0.00149, 0.00147, 0.00143 mm/year, respectively at the 13th of alternate cycle. A lower corrosion rate was observed from the steel reinforcement bar embedded in concrete mix containing 10% of micro POFA and 1-3% of nano POFA than that of control concrete. The higher of corrosion rate in control mix is mainly attributed to high permeability of the control mix that allows the chloride ions to penetrate through and reach the steel bar. However, the corrosion activity was minimal at the early period of exposure. At 6 months cycle, a small difference of corrosion rates can be observed among the mixes. The corrosion rate for control mix was 0.00725 mm/year, while for reinforced concrete containing 10% of micro POFA and 1,2,3% of nano POFA were 0.00660, 0.00600, 0.00582 mm/year, respectively. The lowest corrosion rate at 26th cycle was exhibited by OS3. The micro and nano POFA in the OS3 concrete specimens reduced the chloride ions penetration and increase the resistance to corrosion due to the consequence of the pozzolanic reaction with the $Ca(OH)_2$. The corrosion rate changes dramatically after a 1-year period of exposure. The highest corrosion rate was

exhibited by control mix with the corrosion rate value of 10 times than previous cycle (6 months). In comparison with the control mix, the corrosion rate for OS1, OS2 and OS3 mix were recorded to decrease by 37%, 80% and 79%, respectively. The corrosion rates obtained at 1-year exposure period were 0.0721, 0.0452, 0.0159 and 0.0148 mm/year for control, OS1, OS2 and OS3 mix, respectively. This pattern of corrosion rate throughout the whole cycle showed the positive effects of combining micro and nano POFA as supplementary cementitious materials. The improvement through permeability of the hardened structure increases the resistance of chloride ions penetration and corrosion as well. This was attributed to the pozzolanic reaction that form extra CSH gel in concrete hence, blocking the chloride ions to reach the steel reinforcement and reducing the corrosion activities. This finding is in agreement with the study conducted by Garcés, Andión, Zornoza, Bonilla, & Payá, (2010). Their study concluded that the mortar containing lowest pozzolanic materials showed the poorest corrosion resistance.

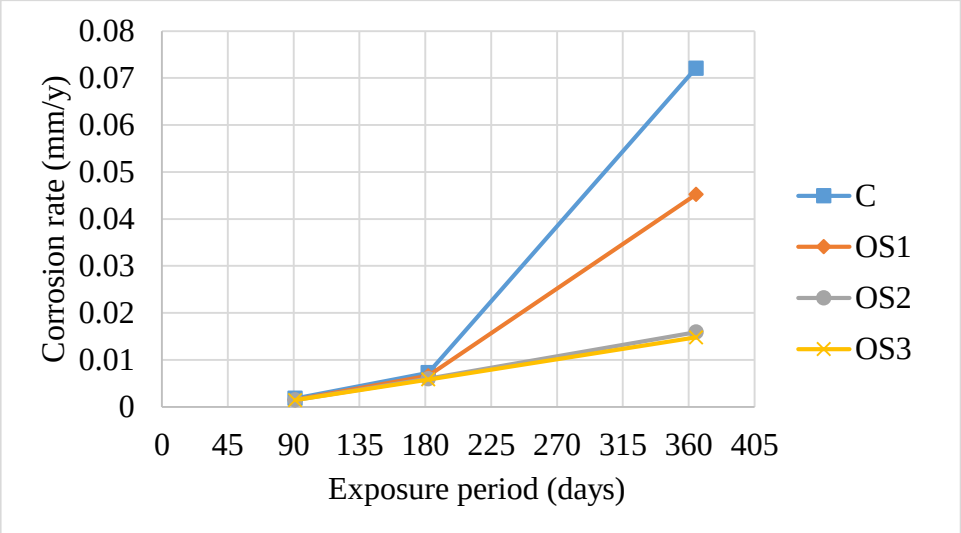

C (0%M, 0%N); OS1 (10%M, 1%N); OS2 (10%M, 2%N); OS3 (10%M, 3%N)
M: micro POFA; N: nano POFA

Figure 6.23: Corrosion rate of steel reinforcement embedded in each concrete mix

6.6 Concluding remarks

Based on the durability test conducted and the corrosion measurements of high performance concrete containing optimum dosage of micro and nano POFA, the results lead to the following conclusions:

a) The water absorption values of concrete mix containing 10% of micro POFA and 1 to 3% of nano POFA were lower than those of the control mix by an average reduction of 16%, 40%, 46% and 47% at 28, 56, 90 and 180 days, respectively. The apparent void volume or boiled permeability of concrete containing 10% of micro POFA and 3% of nano POFA was the lowest due to the micro fillingability and extra strengthening gel produced. An average reduction of permeable void volume of OS1, OS2 and OS3 were 30%, 43%, 49% and 45% at 28, 56, 90 and 180 days, respectively.

b) The performance of concrete containing micro and nano POFA improved the resistance to chloride ions penetration. The significant reduction of total charge passed can be seen in concrete containing 10% of micro POFA and 3% of nano POFA with a decrease of 8.5%, 3.7%, 22% and 12% at 28, 56, 90 and 180 days, respectively compared with control mix.

c) From acid resistance test, mass loss measurement results showed the significant reduction of 31%, 21%, 20% and 12% exhibited by concrete containing 10% of micro POFA and 1-3% of nano POFA at 28, 56, 90 and 180 days, respectively. The results of compressive strength reduction due to the acid attacks were greatly reduced especially at the longest period of exposure (6 months). The strength of concrete was reduced approximately by 76-77% and was yielded by concrete containing 10% of micro POFA and 1-3% of nano POFA while a 80% reduction in compressive strength was exhibited by the control concrete. The microstructural analyses have confirmed the results of acid resistance test by highlighting the presence of gypsum in SEM images of the control mix that induced concrete spalling and cracking. XRD analysis of the control mix without micro and nano POFA also

showed notable traces of gypsum, ettringite and $Ca(OH)_2$. In contrast, compact microstructure can be seen in concrete containing micro and nano POFA with less gypsum content, and the EDX analysis showed low calcium hydroxide content due to pozzolanic reaction. EDX analysis also confirmed the high ratio of silica indicating the dominance of secondary CSH gel in concrete mix containing micro and nano POFA.

d) By accelerated corrosion test using impressed voltage, the corrosion of steel reinforcement bar embedded in concrete can be measured through steel weight loss. The mass loss of steel bar embedded in control concrete was observed to be about 13.95% whilst in concrete containing 10% of micro POFA and 1-3% of nano POFA, the steel bar weight was reduced to about 6.5%, 4.6% and 3.8%, respectively. The time taken by the control mix specimen to crack due to impressed voltage was 37 days while it was observed that concrete specimens containing micro and nano POFA showed cracks after a period of 42-45 days.

e) The graph of current-time relationship is provided to highlight the current fluctuation throughout the testing period until the specimens failed. The low current reading and longer time to initiate the crack was found in concrete containing 10% of micro POFA and 1-3% of nano POFA due to reduction in concrete permeability that blocks the chloride ion from reaching the steel reinforcement embedded in concrete.

f) Using EIS technique, one electrical equivalent circuit model was proposed to represent the physical process of concrete. A model of R (QR (QR) (QR) (CR)) was selected as the best to fit all the impedance data from all the concrete mixes. The highest polarization resistance was exhibited by steel reinforcement bar embedded in concrete containing 10% of micro POFA and 3% of nano POFA compared with control mix at all cycles.

g) Corrosion rate measurements showed significant effects after a 1-year period of exposure by all the concrete mix. In comparison with the control mix, the corrosion rate for concrete containing 10% of micro

POFA and 1-3% of nano POFA mix showed a decreased of 37%, 80% and 79%, respectively at 1-year age. The corrosion rate obtained after a 1-year exposure period were 0.0721, 0.0452, 0.0159 and 0.0148 mm/year for control and OS1, OS2 and OS3 mix, respectively.

Chapter 7

Conclusions and Recommendations

7.1 Introduction

This study was carried out to investigate the potential of using micro and nano POFA as a supplementary cementitious material to improve mechanical and durability properties of high performance concrete. The main objectives of this study were to develop mathematical models to predict the fresh and hardened properties of concrete utilising micro and nano POFA and to determine the optimal amount of micro and nano POFA as binder in concrete mix design. Then, the study proceeded to determine the durability properties of high performance concrete containing optimum content of micro and nano POFA. Based on the results and discussion in previous sections, this chapter presents the conclusions drawn and provides few recommendations for future works.

7.2 Conclusions

Based on the aim and objectives of this study, the following conclusions can be drawn:

7.2.1 Characteristics of micro and nano POFA as potential supplementary cementitious material

a) The physical properties of raw POFA showed that the unburned residue left and the LOI value was not according to ASTM C618-15 permissible limit. Therefore, the heat treatment is necessary for raw POFA to fulfil the requirement as a pozzolanic material. Due to heat treatment, the LOI of micro and nano POFA were reduced to 4.67% and 1.80%, respectively and the colour of the POFA changed from darkish to greyish due to the removal of unburned carbon during the heat treatment. The higher the LOI value, the higher of unburned carbon and volatile substances that can reduce the mechanical properties of concrete.

b) Fineness of micro POFA was observed at 90%, passing the 45 µm sieve size while 100% passing for nano POFA. The strength activity index for the combination of micro and nano POFA exhibited 97% that is above the permissible limit as stated in ASTM C618-15. The result indicates a good reactivity or pozzolanic reaction of the supplementary cementitious material.

c) The chemical composition of micro and nano POFA showed that the total three main oxide components (SiO_2, Fe_2O_3, Al_2O_3) are all equal and above 70% which chemically fulfill the requirement of Class F-fly ash. Higher silica content was observed in micro and nano POFA with 66.62% and 65.08%, respectively. The high content of silica in micro and nano POFA is necessary in formation of secondary CSH gel to enhance the strength and durability properties of concrete.

d) SEM analysis confirmed the surface morphology of micro and nano POFA with round shape and less porous in comparison with raw POFA. Both elemental analysis of micro and nano POFA showed that the major element is silica, which can contribute to the formation of addition CSH gel. Micro POFA showed more porous than nano POFA which can potentially affect higher water absorption in concrete fresh mix if higher percentage replacement used.

e) Nano POFA was successfully obtained by mechanical milling method using high energy ball mill. Two stages of grinding with one heat treatment were required to produce nano POFA with average particles size of 20 to 90 nm. TEM analysis has confirmed the single size of nano POFA and the particle size distribution graph was developed. From the measured particles data, approximately 90% of nano POFA particles are smaller than 60 nm. The high surface area of nano POFA is significant in accelerating the hydration process especially at strength properties of concrete at early age and form denser concrete.

f) In the XRD analysis, the crystalline phase in the micro and nano POFA showed that quartz is the major phase in both of the materials at a peak of 26.5º (2-theta). The higher intensity of 3900 counts was recorded in nano POFA. The FTIR spectrum confirmed the mineralogy properties found from XRD

analysis. The FTIR spectrum data for micro and nano POFA showed the Si-O stretching band was found in micro and nano POFA at 1000 cm^{-1} and 1041 cm^{-1}, respectively. The wider stretching was observed from the nano POFA spectrum. The crystalline mineralogical phase such as quarts showed the pozzolanicity of micro and nano POFA as supplementary cementitious material.

7.2.2 Development of mathematical models to predict the fresh and hardened properties of concrete containing micro and nano POFA and optimal solutions of concrete mix design

a) The interaction effect of the combination of micro and nano POFA on workability, compressive, splitting tensile and flexural strengths of high performance concrete was determined by development of the mathematical models. The adequacy of the models obtained were compared with the experimental results with the the level of significance was less than 0.05. The ANOVA and model summary statistics showed that the predicted models were in good agreement based on the adjusted and predicted R^2.
b) A quadratic model was obtained for slump, compressive strength at 7 and 90 days, splitting tensile strength at 7, 28 and 90 days, and flexural strength at 7 and 90 days. Meanwhile, the two-factor interactions model was fitted for both compressive strength and flexural strength at 28 days.
c) Results of workability and strengths (compressive, splitting tensile and flexural) showed lower strength at the 20-30% of micro POFA with 1-3% of nano POFA. The finding showed that higher than 10% of micro POFA replacement showed negative finding due to the porous particles of micro POFA that absorb the water in fresh mix hence, reduce the workability and strength properties as well. The water content in design mix is supposedly use for hydration process was absorbed by the micro POFA.
d) Combination of 10% of micro POFA and 2, 3% of nano POFA improved the workability by increment 3.6% and 7.1%, respectively in comparison with control concrete without micro and nano POFA. Compressive strength of concrete also showed greater enhancement especially at the early age by increment 3-4%. Splitting tensile and flexural strengths were similarly

improved as compressive strength but in different magnitude. The significant improvement in workability and early strength due to nanoparticle act as lubricant by closing the gap in concrete matrix and higher surface area of nano POFA that accelerates the hydration process to form secondary strengthening gel. The combination of micro POFA and low volume of nano POFA was proposed due to dilution effect in concrete matrix (if high volume of nano POFA used) that affects the maturity of concrete hence, reduces the workability and delays the hydration process.

e) The results of the experimental works also were supported with the SEM micrographs to study the main hydrated phases formed in the concrete structure. The CSH gel structures can be found in the concrete mix containing 10% of micro POFA and 1-3% of nano POFA that exhibited the highest compressive, splitting tensile and flexural strengths as compared to the control concrete mix. Meanwhile, the hexagonal platelets of $Ca(OH)_2$ were observed clearly in the control mix due to the absence of pozzolanic materials, which would use weak products for secondary CSH gel formation.

f) Based on optimisation analysis, optimal compositions was within the highest value of R^2 at the area of 10% of micro POFA and 1-3% of nano POFA. The optimum responses range obtained from the optimum regions were 117 to 145 mm for slump height. Whilst 47.1 to 49.2 MPa, 62.9 to 63.1 MPa, 66 to 67.5 MPa for compressive strength, 3 to 3.2 MPa, 3.3 to 3.4 MPa, 4.8 to 4.9 MPa for splitting tensile strength, 9.4 to 9.5 MPa, 10.1 to 10.5 MPa, 10.6 to 11.2 MPa for flexural strength at the age of 7, 28 and 90 days, respectively.

7.2.3 Durability properties of concrete utilising optimal content of micro and nano POFA

Based on the durability test conducted including corrosion measurements of high performance concrete containing optimum dosage of micro and nano POFA, the results lead to the following conclusions:

a) Water absorption value of concrete mix containing 10% of micro POFA and 1 to 3% of nano POFA were lower than control mix by average reduction of 16%, 40%, 46% and 47% at 28, 56, 90 and 180 days, respectively. The lower water absorption of concrete containing micro and nano POFA modified the pore in

the concrete thus reducing the water penetration as well as the porosity of concrete. The apparent void volume or boiled permeability of concrete containing 10% of micro POFA and 3% of nano POFA was the lowest due to the micro filling ability and extra strengthening gel produced. An average reduction of permeable void volume of OS1, OS2 and OS3 were 30%, 43%, 49% and 45% at 28, 56, 90 and 180 days, respectively in comparison than that of control mix without micro and nano POFA.

b) On the other hand, the performance of concrete containing micro and nano POFA also improved to resist the chloride ions penetration. The significant reduction of total charge passed can be seen in concrete containing 10% of micro POFA and 3% of nano POFA with the decrease by 8.5%, 3.7%, 22% and 12% at 28, 56, 90 and 180 days, respectively compared with control mix. The reduction of total charge passed was due to secondary CSH gel filling up the pores in concrete and makes the concrete impermeable to chloride penetration.

c) Durability in terms of acid resistance, by visual inspection, all of the concrete mix showed almost same surface condition with white deposit on the surface of concrete specimen. By dimension measurement, the control mix specimen reduced the width about 20 mm while the concrete containing 10% of micro POFA and 1-3% of nano POFA reduced a bit lower by about 10 mm. Mass loss measurement results showed the average reduction of 31%, 21%, 20% and 12% exhibited by concrete containing 10% of micro POFA and 1-3% of nano POFA at 28, 56, 90 and 180 days, respectively as in comparison with that of control mix. The results of compressive strength reduction due to the acid attack were greatly reduced especially at the longest period of exposure (6 months). The strength reduced about 76-77% yielded by concrete containing 10% of micro POFA and 1-3% of nano POFA while 80% reduction in compressive strength exhibited by control concrete. The microstructural analyses have confirmed the results of acid resistance test by highlighting the present of gypsum in SEM images of control mix that induce to concrete spalling and cracking. XRD analysis of control mix without micro and nano POFA also showed the notable traces of gypsum, ettringite and $Ca(OH)_2$. Whilst, compact microstructure can be seen in concrete containing micro and nano POFA with less gypsum content and EDX analysis showed low calcium

hydroxide content due to pozzolanic reaction. EDX analysis also confirmed the high ratio of silica that indicates the dominance of secondary CSH gel in concrete mix containing micro and nano POFA.

d) By accelerated corrosion test using impressed voltage, the corrosion of steel reinforcement bar embedded in concrete can be measured through steel weight loss. The mass loss of steel bar embedded in control concrete lost about 13.95% whilst in concrete containing 10% of micro POFA and 1-3% of nano POFA, the steel bar reduced about 6.5%, 4.6% and 3.8%, respectively. The time taken by control mix to crack due to impressed voltage was 37 days and 43-45 days needed by concrete containing micro and nano POFA. The graph of current-time relationship is provided to highlight the current fluctuation throughout the testing until the specimens fail. The low current reading and longer time to initiate the crack were found in concrete containing 10% of micro POFA and 1-3% of nano POFA due to reduction in concrete permeability that block the chloride ion to reach the steel reinforcement embedded in concrete.

e) Using EIS technique, one electrical equivalent circuit model was proposed to represent the physical process of concrete. A model of R (QR (QR) (QR) (CR)) was selected as the best to fit all the impedance data for all the concrete mixes. The highest polarization resistance exhibited by steel reinforcement bar embedded in concrete containing 10% of micro POFA and 3% of nano POFA compared with control mix at all cycles.

f) Corrosion rate measurement showed the significant effect by reduced the corrosion rate after 1-year period of exposure by all the concrete mix. In comparison with the control mix, the corrosion rate for steel reinforcement bar embedded in concrete specimen containing 10% of micro POFA and 1-3% of nano POFA mix were decreased by 37%, 80% and 79%, respectively at 1-years age of exposure. The corrosion rate obtained at 1-year exposure period were 0.0721, 0.0452, 0.0159 and 0.0148 mm/year for control, OS1, OS2 and OS3 mix, respectively. The improvement through permeability of the hardened structure increases the resistance of chloride ions penetration and corrosion as well. This was attributed to the pozzolanic reaction that form the extra CSH gel in concrete hence, block the chloride ions to reach the steel reinforcement and reduce the corrosion activities.

7.3 Recommendations for Future Work

Based on the findings obtained from this study, few recommendations have been proposed to improve the utilisation of micro and nano POFA as the supplementary cementitious materials.

a) Since POFA has been utilised in producing normal, high strength and high performance concrete, utilisation of POFA should also been studied in producing ultra-high performance concrete. To date, none of the works done on utilisation of nano POFA in producing ultra-high performance concrete and its significant effect in terms of mechanical and durability properties.
b) Study the cost analysis of utilisation waste as supplementary cementitious material and educate the cement industry in Malaysia to promote the palm oil waste as one of the potential binders.
c) Extend the study of corrosion until 3 to 5 years to determine the effect of supplementary cementitious materials to improve the corrosion of steel bar embedded in concrete by reducing the concrete permeability and blocking the pore in concrete matrix.
d) Develop mathematical models by considering other variables (coarse, fine aggregates, admixtures, w/c ratio) and responses (durability properties of concrete).

References

Awal, A. S. M. A., & Hussin, M. W. (1997). The effectiveness of palm oil fuel ash in preventing expansion due to alkali-silica reaction. Cement and Concrete Composites, 19(4), 367–372. https://doi.org/10.1016/S0958-9465(97)00034-6.

Abdoli, H., Farnoush, H. R., Asgharzadeh, H., & Sadrnezhaad, S. K. (2011). Effect of high energy ball milling on compressibility of nanostructured composite powder. Powder Metallurgy, 54(1), 24–29. https://doi.org/10.1179/003258909X12573447241662

Abdullah, A. Z., Salamatinia, B., Mootabadi, H., & Bhatia, S. (2009). Current status and policies on biodiesel industry in Malaysia as the world ' s leading producer of palm oil. Energy Policy, 37, 5440–5448. https://doi.org/10.1016/j.enpol.2009.08.012

Abdullah, K, Hussin, M.W., Zakaria, F. & Muhamad, Z.A.H.R. (2006). Pofa : a Potential Partial Cement Replacement Material in Aerated Concrete. 6th Asia Pacific Structural Engineering and Construction (APSEC 2006), (September), 5–6. https://doi.org/10.4028/www.scientific.net/AMM.567.446

Abutaha, F., Abdul Razak, H., & Kanadasan, J. (2016). Effect of palm oil clinker (POC) aggregates on fresh and hardened properties of concrete. Construction and Building Materials, 112, 416–423. https://doi.org/10.1016/j.conbuildmat.2016.02.172

ACI Committee 201. (2008). 201.2R-08: Guide to Durable Concrete. American Concrete Institute.

ACI Committee 363. (2005). High-Strength Concrete (ACI 363R). American Concrete Institute, 228, 79-80.

Adak, D., Sarkar, M., & Mandal, S. (2014). Effect of nano-silica on strength and durability of fly ash based geopolymer mortar. Construction and Building Materials, 70, 453–459. https://doi.org/10.1016/j.conbuildmat.2014.07.093

Aggarwal, P., Singh, R. P., & Aggarwal, Y. (2015). Use of nano-silica in cement based

materials — A review. Cogent Engineering, 33(1). https://doi.org/10.1080/23311916.2015.1078018

Aitcin, P.C. (1998). High-performance concrete. London: E and FN Spon.

Aïtcin, P.C. (2000). Cements of yesterday and today. Cement and Concrete Research, 30(9), 1349–1359. https://doi.org/10.1016/S0008-8846(00)00365-3

Aldahdooh, M. A. A., Bunnori, N. M., & Johari, M. A. M. (2014). Influence of palm oil fuel ash on ultimate flexural and uniaxial tensile strength of green ultra-high performance fiber reinforced cementitious composites. Materials and Design, 54, 694–701. https://doi.org/10.1016/j.matdes.2013.08.094

Aldahdooh, M. A. A., Muhamad Bunnori, N., & Megat Johari, M. A. (2013). Development of green ultra-high performance fiber reinforced concrete containing ultrafine palm oil fuel ash. Construction and Building Materials, 48, 379–389. https://doi.org/10.1016/j.conbuildmat.2013.07.007

Aldahdooh, M. A. A., Muhamad Bunnori, N., & Megat Johari, M. A. (2013b). Evaluation of ultra-high-performance-fiber reinforced concrete binder content using the response surface method. Materials and Design, 52, 957–965. https://doi.org/10.1016/j.matdes.2013.06.034

Al-Mulali, M. Z., Awang, H., Abdul Khalil, H. P. S., & Aljoumaily, Z. S. (2015). The incorporation of oil palm ash in concrete as a means of recycling: A review. Cement and Concrete Composites, 55, 129–138. https://doi.org/10.1016/j.cemconcomp.2014.09.007

Alqadi, A. N. S., Mustapha, K. N., Naganathan, S., & Al-Kadi, Q. N. S. (2012). Uses of Central Composite Design and Surface Response to Evaluate the Influence of Constituent Materials on Fresh and Hardened Properties of Self-Compacting Concrete. KSCE Journal of Civil Engineering, 16(3), 407–416. https://doi.org/10.1007/s12205-012-1308-z

Alsubari, B., Shafigh, P., & Jumaat, M. Z. (2016). Utilization of high-volume treated palm oil fuel ash to produce sustainable self-compacting concrete. Journal of Cleaner Production, 137, 982–996. https://doi.org/10.1016/j.jclepro.2016.07.133

Alsubari, B., Shafigh, P., Ibrahim, Z., & Jumaat, M. Z. (2018). Heat-treated palm oil fuel ash as an effective supplementary cementitious material originating from agriculture waste. Construction and Building Materials, 167, 44–54. https://doi.org/10.1016/j.conbuildmat.2018.01.134

Altwair, M.N., Johari, M. A. M., & Hashim, S. F. S. (2014). Influence of treated palm oil fuel ash on compressive properties and chloride resistance of engineered cementitious composites. Materials and Structures, 47, 667–682. https://doi.org/10.1617/s11527-013-0087-4

Altwair, N. M., Johari, M. A. M., & Hashim, S. F. S. (2012). Fracture and tensile characteristics of engineered cementitious composites containing high volume of palm oil fuel ash. Construction and Building Materials, 37, 518–525. https://doi.org/10.1680/adcr.11.00056

Amin, N. U., Alam, S., & Gul, S. (2015). Assessment of pozzolanic activity of thermally activated clay and its impact on strength development in cement mortar. RSC Advances, 5(8), 6079–6084. https://doi.org/10.1039/c4ra12237b

Anand, S., Vrat, P., & Dahiya, R. P. (2006). Application of a system dynamics approach for assessment and mitigation of CO2emissions from the cement industry. Journal of Environmental Management, 79, 383–398. https://doi.org/10.1016/j.jenvman.2005.08.007

Anderson, M. J., & Whitcomb, P. J. (2005). RSM simplified : optimizing processes using response surface methods for design of experiments. New York, New York : Productivity Press.

Ariffin, M. A. M., Bhutta, M. A. R., Hussin, M. W., Tahir, M. M., & Aziah, N. (2013). Sulfuric acid resistance of blended ash geopolymer concrete. Construction and Building Materials, 43, 80–86.

ASTM C 29-17 (2017). Standard test method for bulk density (“unit weight”) and voids in aggregate. Annual Book of ASTM Standard American Society for Testing and Materials.

ASTM C33-13 (2013). Standard specification for concrete aggregates. Annual Book

of ASTM Standards, American Society for Testing and Materials.

ASTM C618-15 (2015). Standard specification for coal fly ash and raw or calcined natural pozzolan for use in concrete. Annual Book of ASTM Standards, American Society for Testing and Materials.

ASTM C876, 1994. Standard Test Method for Corrosion Potentials of Uncoated Reinforcing Steel in Concrete. Annual Book of ASTM Standards, American Society for Testing and Materials.

ASTM D7348-13 (2013). Standard test methods for loss on ignition (LOI) of solid combustion residues, Annual Book of ASTM Standard, American Society for Testing and Materials.

ASTM G1-03 (2017), Standard practice for preparing, cleaning, and evaluation corrosion test specimens. Annual Book of ASTM Standards, American Society for Testing and Materials.

Awal, A. S. A., & Hussin, M. W. (1999). Durability of High Performance Concrete Containing Palm Oil Fuel Ash. Durability of Building Materials and Components, 465–474.

Awal, A. S. A., & Nguong, S. K. (2010). A Short-Term Investigation On High Volume Palm Oil Fuel Ash (POFA) Concrete. In 35th Conference on OUR WORLD IN CONCRETE & STRUCTURES: 25 - 27 August 2010, Singapore.

Awal, A. S. M. A., & Abubakar, S. I. (2011). Properties of Concrete Containing High Volume Palm Oil Fuel Ash: a Short-Term Investigation. Malaysian Jpurnal of Civil Engineering, 23(2), 54–66.

Awal, A. S. M. A., & Hussin, M. W. (1997). The effectiveness of palm oil fuel ash in preventing expansion due to alkali-silica reaction. Cement and Concrete Composites, 19(4), 367–372. https://doi.org/10.1016/S0958-9465(97)00034-6

Awal, A. S. M. A., & Hussin, M. W. (2011). Effect of palm oil fuel ash in controlling heat of hydration of concrete. Procedia Engineering, 14, 2650–2657. https://doi.org/10.1016/j.proeng.2011.07.333

Awal, A. S. M. A., & Mohammadhosseini, H. (2016). Green concrete production incorporating waste carpet fiber and palm oil fuel ash. Journal of Cleaner Production, 137, 157–166. https://doi.org/10.1016/j.jclepro.2016.06.162

Awal, A. S. M. A., & Shehu, I. A. (2013). Evaluation of heat of hydration of concrete containing high volume palm oil fuel ash. Fuel, 105, 728–731. https://doi.org/10.1016/j.fuel.2012.10.020

Awal, A. S.A., & Hussin, M. W. (1999). Durability of High Performance Concrete Containing Palm Oil Fuel Ash. Durability of Building Materials and Components, 465–474.

Awalludin, M. F., Sulaiman, O., Hashim, R., & Nadhari, W. N. A. W. (2015). An overview of the oil palm industry in Malaysia and its waste utilization through thermochemical conversion, specifically via liquefaction. Renewable and Sustainable Energy Reviews, 50, 1469–1484. https://doi.org/10.1016/j.rser.2015.05.085

Bamaga, S. O., Ismail, M., Majid, Z. A., Ismail, M., & Hussin, M. W. (2013). Evaluation of Sulfate Resistance of Mortar Containing Palm Oil Fuel Ash from Different Sources. Arabian Journal for Science And Engineering, 38(9), 2293–2301. https://doi.org/10.1007/s13369-012-0503-z

Bamaga, S., Ismail, M.A., Lee, H.S & Budiea, A. M. A. (2010). Effect of Incorporation of Waste Ash on the Behavior of Concrete and Mortar,International Journal of Sustainable Building Technology and Urban Development, 1:1, 74-79, DOI: 10.5390/SUSB.2010.1.1.074

Bashar, I. I., Alengaram, U. J., Jumaat, M. Z., Islam, A., Santhi, H., & Sharmin, A. (2016). Engineering properties and fracture behaviour of high volume palm oil fuel ash based fibre reinforced geopolymer concrete. Construction and Building Materials, 111, pp.286-297. Construction and Building Materials, 111, 286–297. https://doi.org/10.1016/j.conbuildmat.2016.02.022

Bassuoni, M. T., & Nehdi, M. L. (2007). Resistance of self-consolidating concrete to sulfuric acid attack with consecutive pH reduction. Cement and Concrete Research, 37, 1070–1084. https://doi.org/10.1016/j.cemconres.2007.04.014

Bayramov, F., Tasdemir, C., & Tasdemir, M. A. (2004). Optimisation of steel fibre reinforced concretes by means of statistical response surface method, 26, 665–675. https://doi.org/10.1016/S0958-9465(03)00161-6

Berry, M., Kappes, B., & Kappes, L. (2015). Optimization of concrete mixtures containing reclaimed asphalt pavement. ACI Materials Journal, 112(6), 723–733. https://doi.org/10.14359/51687854

Birgisson, B., K.Mukhopadhyay, A., Geary, G., Khan, M., & Sobolev, Ko. (2012). Nanotechnology in Concrete Materials. Tranportation Research Board. https://doi.org/10.1016/0165-3806(91)90006-5

Bjornstrom, J., Martinelli, A., Matic, A., Borjesson, L., & Panas, I. (2004). Accelerating effects of colloidal nano-silica for beneficial calcium – silicate – hydrate formation in cement, 392, 242–248. https://doi.org/10.1016/j.cplett.2004.05.071

Bouzoubaâ, N., & Lachemi, M. (2001). Self-compacting concrete incorporating high volumes of class F fly ash: Preliminary results. Cement and Concrete Research, 31(3), 413–420. https://doi.org/10.1016/S0008-8846(00)00504-4

Caré, S., & Raharinaivo, A. (2007). Influence of impressed current on the initiation of damage in reinforced mortar due to corrosion of embedded steel. Cement and Concrete Research, 37(12), 1598–1612. https://doi.org/10.1016/j.cemconres.2007.08.022

Chandara, C., Mohd Azizli, K. A., Ahmad, Z. A., Saiyid Hashim, S. F., & Sakai, E. (2012). Heat of hydration of blended cement containing treated ground palm oil fuel ash. Construction and Building Materials, 27(1), 78–81. https://doi.org/10.1016/j.conbuildmat.2011.08.011

Chandara, C., Sakai, E., Azizi, K., Azizli, M., Arifin, Z., Fuad, S., & Hashim, S. (2010). The effect of unburned carbon in palm oil fuel ash on fluidity of cement pastes containing superplasticizer. Construction and Building Materials, 24(9), 1590–1593. https://doi.org/10.1016/j.conbuildmat.2010.02.036

Chen, J. J., Thomas, J. J., Taylor, H. F. W., & Jennings, H. M. (2004). Solubility and

structure of calcium silicate hydrate. Cement and Concrete Research, 34(9), 1499–1519. https://doi.org/10.1016/j.cemconres.2004.04.034

Chindaprasirt, P., Chotetanorm, C., & Rukzon, S. (2011). Use of Palm Oil Fuel Ash to Improve Chloride and Corrosion Resistance of High-Strength and High-Workability Concrete. Journal of Materials in Civil Engineering, 23(4), 499–503. https://doi.org/10.1061/(ASCE)MT.1943-5533.0000187.

Chindaprasirt, P., Homwuttiwong, S., & Jaturapitakkul, C. (2007). Strength and water permeability of concrete containing palm oil fuel ash and rice husk-bark ash. Construction and Building Materials, 21(7), 1492–1499. https://doi.org/10.1016/j.conbuildmat.2006.06.015

Cihan, M. T., Güner, A., & Yüzer, N. (2013). Response surfaces for compressive strength of concrete. Construction and Building Materials, 40, 763–774. https://doi.org/10.1016/j.conbuildmat.2012.11.048

Cordeiro, G. C., Filho, R. D. T., & Fairbairn, E. M. R. (2009). Effect of calcination temperature on the pozzolanic activity of sugar cane bagasse ash. Construction and Building Materials, 23, 3301–3303. https://doi.org/10.1016/j.conbuildmat.2009.02.013

Dalimin, M. N. (1995). Renewable energy update: Malaysia. Renewable Energy, 6(4), 435–439. https://doi.org/10.1016/0960-1481(94)00070-M

Damtoft, J. S., Lukasik, J., Herfort, D., Sorrentino, D., & Gartner, E. M. (2008). Sustainable development and climate change initiatives. Cement and Concrete Research, 38(2), 115–127. https://doi.org/10.1016/j.cemconres.2007.09.008

Dash, M. K., Patro, S. K., & Rath, A. K. (2016). Sustainable use of industrial-waste as partial replacement of fine aggregate for preparation of concrete- A review. International Journal of Sustainable Built Environement, 5, 484–516. https://doi.org/10.1016/j.ijsbe.2016.04.006

de Larrard, F. & Sedran, T. (1994). Optimization of Ultra High Performance Concrete by the Use of a Packing Model. Cement and Concrete Research, 24(6), 997–1009. https://doi.org/10.1016/0165-1889(94)90039-6

de Larrard, F. & Sedran, T. (2002). Mixture-proportioning of high-performance concrete. Cement and Concrete Research, 32, 1699–1704.

de Larrard, F. (1990). A method for proportioning high strength concrete mixtures. Cement, Concrete and Aggregates, 12(2), 47–52. https://doi.org/10.1520/CCA10388J

Deb, P. S., Sarker, P. K., & Barbhuiya, S. (2016). Sorptivity and acid resistance of ambient-cured geopolymer mortars containing nano-silica. Cement and Concrete Composites, 72, 235–245. https://doi.org/10.1016/j.cemconcomp.2016.06.017

Derringer, G.C., & Suich, R. (1980). Simultaneous optimization of several response variables. J Qual Technol, 12(4):214–9.

Dias, W. P. S. (2000). Reduction of concrete sorptivity with age through carbonation. Cement and Concrete Research, 30(8), 1255–1261. https://doi.org/10.1016/S0008-8846(00)00311-2

Du, H., Du, S., & Liu, X. (2014). Durability performances of concrete with nano-silica. Construction and Building Materials, 73, 705–712. https://doi.org/10.1016/j.conbuildmat.2014.10.014

Eldagal, O. E. A. (2008). Study on the Behaviour of High Strength Palm Oil Fuel Ash Concrete. Universiti Teknologi Malaysia.

El-Dieb, A. S. (2009). Mechanical, durability and microstructural characteristics of ultra-high-strength self-compacting concrete incorporating steel fibers. Materials and Design, 30(10), 4286–4292. https://doi.org/10.1016/j.matdes.2009.04.024

Elsener, B., Buchler, M., Stalder, F., & Bohni, H. (1999). Migrating corrosion inhibitor blend for reinforced concrete : Part 1--prevention of corrosion. Corrosion Science, 55(12), 1155–1163.

European Comission. (2013). Guidance on the protection of the health and safety of workers from the potential risks related to nanomaterials at work: Guidance for employers and health and safety practitioners.

Fisher, R. A., & Mackenzie, W. A. (1923). Studies in crop variation: II. The manurial

response of different potato varieties. The Journal of Agricultural Science, 13(3), 311–320. https://doi.org/10.1017/S0021859600003592

Garcés, P., Andión, L. G., Zornoza, E., Bonilla, M., & Payá, J. (2010). The effect of processed fly ashes on the durability and the corrosion of steel rebars embedded in cement-modified fly ash mortars. Cement and Concrete Composites, 32(3), 204–210. https://doi.org/10.1016/j.cemconcomp.2009.11.006

Ghafari, E., Costa, H., & Júlio, E. (2015). Critical review on eco-efficient ultra high performance concrete enhanced with nano-materials. Construction and Building Materials, 101, 201–208. https://doi.org/10.1016/j.conbuildmat.2015.10.066

Ghafari, S., Abdul, H., Hasnain, M., & Akbar, A. (2009). Application of response surface methodology (RSM) to optimize coagulation – flocculation treatment of leachate using poly-aluminum chloride (PAC) and alum. Journal of Hazardous Materials, 163, 650–656. https://doi.org/10.1016/j.jhazmat.2008.07.090

Girardi, F., Vaona, W., & Di Maggio, R. (2010). Resistance of different types of concretes to cyclic sulfuric acid and sodium sulfate attack. Cement and Concrete Composites, 32(8), 595–602. https://doi.org/10.1016/j.cemconcomp.2010.07.002

Güneyisi, E., Gesog, M., Algın, Z., & Mermerdas, K. (2014). Optimization of concrete mixture with hybrid blends of metakaolin and fly ash using response surface method. Composites: Part B, 60, 707–715. https://doi.org/10.1016/j.compositesb.2014.01.017

Ha, T. H., Muralidharan, S., Bae, J. H., Ha, Y. C., Lee, H. G., Park, K. W., & Kim, D. K. (2007). Accelerated short-term techniques to evaluate the corrosion performance of steel in fly ash blended concrete. Building and Environment, 42(1), 78–85. https://doi.org/10.1016/j.buildenv.2005.08.019

Hadi, F.A., Hanizam Awang, M. Z. A. (2015). The Effect of Oil Palm Ash Incorporation in Foamed Concrete. Jurnal Teknologi (Sciences & Engineering), 63–68.

Hadigheh, S. A., Gravina, R. J., & Smith, S. T. (2017). Effect of acid attack on FRP-to-concrete bonded interfaces. Construction and Building Materials, 152, 285–

303. https://doi.org/10.1016/j.conbuildmat.2017.06.140

Hamada, H. M., Jokhio, G. A., Yahaya, F. M., Humada, A. M., & Gul, Y. (2018). The present state of the use of palm oil fuel ash (POFA) in concrete. Construction and Building Materials, 175, 26–40. https://doi.org/10.1016/j.conbuildmat.2018.03.227

Hesas, R.H., Arami-Niya, A., Daud, W.M.A.W. & Sahu, J. (2013). Comparison of oil palm shell-based activated carbons produced by microwave and conventional heating methods using zinc chloride activation. J. Anal. Appl. Pyrol., 104, 176–184.

Hill, R. & Folliard, K. (2006). The impact of fly ash on air-entrained concrete, Concr. In Focus, 5 (3) ,71–72.

Hong, K., & Hooton, R. D. (1999). Effects of cyclic chloride exposure on penetration of concrete cover. Cement and Concrete Research, 29(March), 1379–1386.

Hossain, M. M., Karim, M. R., Hasan, M., Hossain, M. K., & Zain, M. F. M. (2016). Durability of mortar and concrete made up of pozzolans as a partial replacement of cement : A review. Construction and Building Materials, 116, 128–140.

Hussin, M. W. & Awal, A. S. M. A. (1996). Influence of palm oil fuel ash on strength and durability of concrete. Proc. of the 7th International Conference on the Durability of Building Materials and Components. Vol. 1. Ed. By C. Sjostrom. May 19–23, 1996, Stockholm, Sweden.

Hussin, M. W., & Abdullah, K. (2009). Properties of palm oil fuel ash cement based aerated concrete panel subjected to different curing regimes. Malaysian Journal of Civil Engineering, 21(1), 17–31.

Hussin, M. W., Ismail, M. A., Budiea, A., & Muthusamy, K. (2009). Durability of high strength concrete containing palm oil fuel ash of different fineness. Malaysian Journal of Civil Engineering, 21(2), 180–194.

Hussin, M. W.; Awal, A. S. M. A. (1997). Palm oil fuel ash: a potential pozzolanic material in concrete construction,Journal of Ferrocement 27(4): 321–327.

Imbabi, M. S., Carrigan, C., & McKenna, S. (2012). Trends and developments in green cement and concrete technology. International Journal of Sustainable Built Environement, 1, 194–216. https://doi.org/10.10106/j.ijsbe.2013.05.001

International Energy Agency (IEA). (2009). Cement Technology Roadmap 2009 - Carbon emissions reductions up to 2050. Retrieved from http://www.iipnetwork.org/cement-technology-roadmap-2009-carbon-emissions-reductions-2050

Isaia, G. C., Gastaldini, A. L. G., & Moraes, R. (2003). Physical and pozzolanic action of mineral additions on the mechanical strength of high-performance concrete. Cement and Concrete Composites, 25(1), 69–76. https://doi.org/10.1016/S0958-9465(01)00057-9

Islam, M. M. U., Mo, K. H., Alengaram, U. J., & Jumaat, M. Z. (2016). Durability properties of sustainable concrete containing high volume palm oil waste materials. Journal of Cleaner Production, 137, 167–177. https://doi.org/10.1016/j.jclepro.2016.07.061

Islam, M.N., Al-Mattarneh, H.M.A., Zain, M.F.M., Basri, H.B. (2002). Towards an expert system for HPC mix design. Proceedings of the world conference on concrete materials and structures, Shah Alam, Malaysia, May.

Ithuralde G. (1992). Permeability: The Owner's Viewpoint. In: Mailer Y. ed. High Performance Concrete from Material to Structure. London: 276-294.

Jankowska, E., & Zatorski, W. (2009). Emission of nanosize particles in the process of nanoclay blending. Proceedings of the 3rd International Conference on Quantum, Nano and Micro Technologies, ICQNM 2009, 147–151. https://doi.org/10.1109/ICQNM.2009.33

Jaturapitakkul, C., Kiattikomol, K., Tangchirapat, W., & Saeting, T. (2007). Evaluation of the sulfate resistance of concrete containing palm oil fuel ash. Construction and Building Materials, 21(7), 1399–1405. https://doi.org/10.1016/j.conbuildmat.2006.07.005

Jaturapitakkul, C., Tangpagasit, J., Songmue, S., & Kiattikomol, K. (2011). Filler

effect and pozzolanic reaction of ground palm oil fuel ash. Construction and Building Materials, 25(11), 4287–4293. https://doi.org/10.1016/j.conbuildmat.2011.04.073

Jiang, S., Gao, S., Jiang, L., Guo, M. Z., Jiang, Y., Chen, C., … Bai, S. (2018). Effects of Deoxyribonucleic acid on cement paste properties and chloride-induced corrosion of reinforcing steel in cement mortars. Cement and Concrete Composites, 91(May), 87–96. https://doi.org/10.1016/j.cemconcomp.2018.05.002

Jimma, B. E., & Rangaraju, P. R. (2015). Chemical admixtures dose optimization in pervious concrete paste selection - A statistical approach. Construction and Building Materials, 101, 1047–1058. https://doi.org/10.1016/j.conbuildmat.2015.10.003

Jin, R., & Chen, Q. (2013). An Investigation of Current Status of "Green" Concrete in the Construction Industry. In 49th ASC Annual International Conference Proceedings.

Kabir, S., Al-Shayeb, A., & Khan, I. M. (2016). Recycled Construction Debris as Concrete Aggregate for Sustainable Construction Materials. Procedia Engineering, 145, 1518–1525. https://doi.org/10.1016/j.proeng.2016.04.191

Kafi, M. A., Sadeghi-nik, A., Bahari, A., Sadeghi-nik, A., & Mirshafiei, E. (2016). Microstructural Characterization and Mechanical Properties of Cementitious Mortar Containing Montmorillonite Nanoparticles, 28(12), 1–10. https://doi.org/10.1061/(ASCE)MT.1943-5533.0001671.

Karim, M. R., Hashim, H., & Abdul Razak, H. (2016). Thermal activation effect on palm oil clinker properties and their influence on strength development in cement mortar. Construction and Building Materials, 125, 670–678. https://doi.org/10.1016/j.conbuildmat.2016.08.092

Khodaii, A., Haghshenas, H. F., & Tehrani, H. K. (2012). Effect of grading and lime content on HMA stripping using statistical methodology, 34, 131–135. https://doi.org/10.1016/j.conbuildmat.2012.02.025

Knickerbocker, D. J. (2005). Behavior of High Performance Concrete Integral Abutment Bridges. Vanderbilt University.

Kockal, N. U., & Ozturan, T. (2011). Optimization of properties of fly ash aggregates for high-strength lightweight concrete production. Materials and Design, 32(6), 3586–3593. https://doi.org/10.1016/j.matdes.2011.02.028

Kosmatka, S. H., Kerkhoff, B., & Panarese, W. C. (2008). Design and Control Design of concrete mixtures. Portland Cement Association.

Kroehong, W., Damrongwiriyanupap, N., Sinsiri, T., & Jaturapitakkul, C. (2016). The Effect of Palm Oil Fuel Ash as a Supplementary Cementitious Material on Chloride Penetration and Microstructure of Blended Cement Paste. Arab J Sci Eng, 41, 4799–4808. https://doi.org/10.1007/s13369-016-2143-1

Kroehong, W., Sinsiri, T., & Jaturapitakkul, C. (2011). Effect of palm oil fuel ash fineness on packing effect and pozzolanic reaction of blended cement paste. Procedia Engineering, 14, 361–369. https://doi.org/10.1016/j.proeng.2011.07.045

Kutner, M. H. (2005). Applied Linear Statitical Models (Vol. 5). McGraw-Hill.

Kwak, H.-G., & Filippou, F. C. (1990). Finite Element Analysis of Reinforced Concrete Structures Under Monotonic Loads. California Department of Transportation Report. https://doi.org/10.1007/978-81-322-2725-0_3

Lau, P. C., Teo, D. C. L., & Mannan, M. A. (2017). Characteristics of lightweight aggregate produced from lime-treated sewage sludge and palm oil fuel ash. Construction and Building Materials, 152, 558–567.

Lau, P. C., Teo, D. C. L., & Mannan, M. A. (2018). Mechanical , durability and microstructure properties of lightweight concrete using aggregate made from lime-treated sewage sludge and palm oil fuel ash. Construction and Building Materials, 176, 24–34. https://doi.org/10.1016/j.conbuildmat.2018.04.179

Le Roy, R., Le Maou, F., & Torrenti, J. M. (2017). Long term basic creep behavior of high performance concrete: data and modelling. Materials and

Structures/Materiaux et Constructions, 50(1). https://doi.org/10.1617/s11527-016-0948-8

Lee, C., Song, H., Ann, K., & Ismail, M. A. (2009). Material Characteristic of POFA Concrete and Its Application to Corrosion Resistance Evaluation. Journal of the Korea Concrete Institute, 21(5), 565–572. https://doi.org/10.4334/JKCI.2009.21.5.565

Li, G., Xiong, G., lü, Y., & Yin, Y. (2009). The physical and chemical effects of long-term sulphuric acid exposure on hybrid modified cement mortar. Cement and Concrete Composites, 31(5), 325–330. https://doi.org/10.1016/j.cemconcomp.2009.02.014

Liew, K. M., Sojobi, A. O., & Zhang, L. W. (2017). Green concrete: Prospects and challenges. Construction and Building Materials, 156, 1063–1095. https://doi.org/10.1016/j.conbuildmat.2017.09.008

Lim, J. L. G., Raman, S. N., Lai, F. C., Zain, M. F. M., & Hamid, R. (2018). Synthesis of nano cementitious additives from agricultural wastes for the production of sustainable concrete. Journal of Cleaner Production, 171, 1150–1160. https://doi.org/10.1016/j.jclepro.2017.09.143

Lim, N. H. A. S., Ismail, M. A., Lee, H. S., Hussin, M. W., Sam, A. R. M., & Samadi, M. (2015). The effects of high volume nano palm oil fuel ash on microstructure properties and hydration temperature of mortar. Construction and Building Materials, 93, 29–34. https://doi.org/10.1016/j.conbuildmat.2015.05.107

Lim, S. K., Tan, C. S., Lim, O. Y., & Lee, Y. L. (2013). Fresh and hardened properties of lightweight foamed concrete with palm oil fuel ash as filler. Construction and Building Materials, 46, 39–47. https://doi.org/10.1016/j.conbuildmat.2013.04.015

Liu, M. Y. J., Alengaram, U. J., Santhanam, M., Zamin, M., & Mo, K. H. (2016). Microstructural investigations of palm oil fuel ash and fly ash based binders in lightweight aggregate foamed geopolymer concrete. Construction and Building Materials, 120, 112–122.

Lloyd, R. R., Provis, J. L., & Van Deventer, J. S. J. (2012). Acid resistance of inorganic polymer binders. 1. Corrosion rate. Materials and Structures, 45(1–2), 1–14. https://doi.org/10.1617/s11527-011-9744-7

Lovato, P. S., Possan, E., Molin, D. C. C. D., Masuero, Â. B., & Ribeiro, J. L. D. (2012). Modeling of mechanical properties and durability of recycled aggregate concretes. Construction and Building Materials, 26(1), 437–447. https://doi.org/10.1016/j.conbuildmat.2011.06.043

Ludwig, H. M., & Zhang, W. (2015). Research review of cement clinker chemistry. Cement and Concrete Research, 78, 24–37. https://doi.org/10.1016/j.cemconres.2015.05.018

Madurwar, M. V., Ralegaonkar, R. V., & Mandavgane, S. A. (2013). Application of agro-waste for sustainable construction materials: A review. Construction and Building Materials, 38, 872–878. https://doi.org/10.1016/j.conbuildmat.2012.09.011

Malaysia Innovation Agency. (2013). National Biomass Strategy 2020: New wealth creation for Malaysia's biomass industry. International Journal of Greenhouse Gas Control, 2(June), 1–37. https://doi.org/10.1016/j.ijggc.2012.07.010

Malaysia Innovation Agency. (2013). National Biomass Strategy 2020: New wealth creation for Malaysia's biomass industry. International Journal of Greenhouse Gas Control, 2(June), 1–37. https://doi.org/10.1016/j.ijggc.2012.07.010

Mangat, P. S., & Molloy, B. T. (1992). Factors influencing chloride-induced corrosion of reinforcement in concrete. Materials and Structures, 25, 404–411.

Martys, N. S., & Ferraris, C. F. (1997). Capillary transport in mortars and concrete. Cement and Concrete Research, 27(5), 747–760. https://doi.org/https://doi.org/10.1016/S0008-8846(97)00052-5

Massa, M. A., Covarrubias, C., Bittner, M., Fuentevilla, I. A., Capetillo, P., Von Marttens, A., & Carvajal, J. C. (2014). Synthesis of new antibacterial composite coating for titanium based on highly ordered nanoporous silica and silver nanoparticles. Materials Science and Engineering C, 45, 146–153.

https://doi.org/10.1016/j.msec.2014.08.057

Matos, A. M., Maia, L., Nunes, S., & Milheiro-Oliveira, P. (2018). Design of self-compacting high-performance concrete: Study of mortar phase. Construction and Building Materials, 167, 617–630. https://doi.org/10.1016/j.conbuildmat.2018.02.053

Megat Johari, M. A., Brooks, J. J., Kabir, S., & Rivard, P. (2011). Influence of supplementary cementitious materials on engineering properties of high strength concrete. Construction and Building Materials, 25(5), 2639–2648. https://doi.org/10.1016/j.conbuildmat.2010.12.013

Megat Johari, M. A., Zeyad, A. M., Muhamad Bunnori, N., & Ariffin, K. S. (2012). Engineering and transport properties of high-strength green concrete containing high volume of ultrafine palm oil fuel ash. Construction and Building Materials, 30, 281–288. https://doi.org/10.1016/j.conbuildmat.2011.12.007

Mehta, A., & Siddique, R. (2016). An overview of geopolymers derived from industrial by-products. Construction and Building Materials, 127, 183–198. https://doi.org/10.1016/j.conbuildmat.2016.09.136

Mehta, P. K. (2009). Global Concrete Industry Sustainability. Concrete International, (February), 45–49.

Mehta, P. K., & Aitcin, P.-C. C. (1990). Principles Underlying Production of High-Performance Concrete. Cement, Concrete and Aggregates, 12(2), 70–78. https://doi.org/10.1520/CCA10274J

Memon, A. H., Radin, S. S., Zain, M. F. M., & Trottier, J. F. (2002). Effects of mineral and chemical admixtures on high-strength concrete in seawater. Cement and Concrete Research, 32, 373–377. https://doi.org/10.1016/S0008-8846(01)00687-1

Mihashi, H., De Barros Leite, J.P., Yamakoshi, S., Kawamata, A. (2007). Controlling fracture toughness of matrix with mica flake inclusions to design pseudo- ductile fibre reinforced cementitious composites. Eng Fract Mech;74(1–2):210–22.

Miller, R. A. (2001). High performance concrete showcase bridge. PCI J., 46(6), 42–55.

Mo, K. H., Alengaram, U. J., Zamin, M., Yong, M., Liu, J., & Lim, J. (2016). Assessing some durability properties of sustainable lightweight oil palm shell concrete incorporating slag and manufactured sand. Journal of Cleaner Production, 112, 763–770. https://doi.org/10.1016/j.jclepro.2015.06.122

Mo, K. H., Ling, T. C., Alengaram, U. J., Yap, S. P., & Yuen, C. W. (2017). Overview of supplementary cementitious materials usage in lightweight aggregate concrete. Construction and Building Materials, 139, 403–418. https://doi.org/10.1016/j.conbuildmat.2017.02.081

Mo, L., Liu, M., Al-Tabbaa, A., Deng, M. & Lau, W.Y. (2015) Deformation and mechanical properties of quaternary blended cements containing ground granulated blast furnace slag, fly ash and magnesia. Cem. Concr. Res., 71, 7–13.

Mohammadhosseini, H., Tahir, M. M., Mohd Sam, A. R., Abdul Shukor Lim, N. H., & Samadi, M. (2018). Enhanced performance for aggressive environments of green concrete composites reinforced with waste carpet fibers and palm oil fuel ash. Journal of Cleaner Production, 185, 252–265. https://doi.org/10.1016/j.jclepro.2018.03.051

Mohammadhosseini, H., Yatim, J. M., Sam, A. R. M., & Awal, A. S. M. A. (2017). Durability performance of green concrete composites containing waste carpet fi bers and palm oil fuel ash. Journal of Cleaner Production, 144, 448–458.

Mohammed, B. S., Fang, O. C., Anwar Hossain, K. M., & Lachemi, M. (2012). Mix proportioning of concrete containing paper mill residuals using response surface methodology. Construction and Building Materials, 35, 63–68. https://doi.org/10.1016/j.conbuildmat.2012.02.050

Mondal, P., Shah, S., Marks, L., & Gaitero, J. (2010). Comparative Study of the Effects of Microsilica and Nanosilica in Concrete. Transportation Research Record: Journal of the Transportation Research Board, 2141(2141), 6–9. https://doi.org/10.3141/2141-02

Montemor, M. F., Simoes, A. M. P., & Ferreira, M. G. S. (2003). Chloride-induced corrosion on reinforcing steel : from the fundamentals to the monitoring techniques. Cement and Concrete Composites, 25, 491–502. https://doi.org/10.1016/S0958-9465(02)00089-6

Montgomery, D.C. (2017). Design and Analysis of Experiments, 8th ed., John Wiley & Sons, Inc., Hoboken. doi:10.1198/tech.2006.s372.

Morsy, M. S., Alsayed, S. H., & Aqel, M. (2011). Hybrid effect of carbon nanotube and nano-clay on physico-mechanical properties of cement mortar. Construction and Building Materials, 25(1), 145–149. https://doi.org/10.1016/j.conbuildmat.2010.06.046

Mujah, D. (2016). Compressive strength and chloride resistance of grout containing ground palm oil fuel ash. Journal of Cleaner Production, 112, 712–722. https://doi.org/10.1016/j.jclepro.2015.07.066

Muralidhar, R. V, Chirumamila, R. R., Marchant, R., & Nigam, P. (2001). A response surface approach for the comparison of lipase production by Candida cylindracea using two different carbon sources, 9, 17–23.

Muthukumar, M., & Mohan, D. (2004). Optimization of mechanical properties of polymer concrete and mix design recommendation based on design of experiments. Journal of Applied Polymer Science, 94(3), 1107–1116. https://doi.org/10.1002/app.21008

Muthukumar, M., Mohan, D., & Rajendran, M. (2003). Optimization of mix proportions of mineral aggregates using Box Behnken design of experiments. Cement and Concrete Composites, 25(7), 751–758. https://doi.org/10.1016/S0958-9465(02)00116-6

Muthusamy, K., Zamri, N., Zubir, M. A., Kusbiantoro, A., & Ahmad, S. W. (2015). Effect of mixing ingredient on compressive strength of oil palm shell lightweight aggregate concrete containing palm oil fuel ash. Procedia Engineering, 125, 804–810. https://doi.org/10.1016/j.proeng.2015.11.142

Myers, R. H., Montgomery, D. C., & Anderson-Cook, C. M. (2016). Response Surface

Methodology Process and Product Optimization Using Designed Experiments. John Wiley & Sons. Retrieved from http://link.springer.com/10.1007/978-3-642-04898-2_492

Nagi, M. (2007) Evaluating air-Entraining Admixtures for Highway Concrete, Transportation Research Board.

Nambiar, E. K. K., & Ramamurthy, K. (2006). Models relating mixture composition to the density and strength of foam concrete using response surface methodology. Cement and Concrete Composites, 28(9), 752–760. https://doi.org/10.1016/j.cemconcomp.2006.06.001

Nassar, A. I., Thom, N., & Parry, T. (2016). Optimizing the mix design of cold bitumen emulsion mixtures using response surface methodology. Construction and Building Materials, 104, 216–229. https://doi.org/10.1016/j.conbuildmat.2015.12.073

Nasterlack, M., Zober, A., & Oberlinner, C. (2008). Considerations on occupational medical surveillance in employees handling nanoparticles. International Archives of Occupational and Environmental Health, 81(6), 721–726. https://doi.org/10.1007/s00420-007-0245-5

Navarro-Blasco, I., Pérez-Nicolás, M., Fernández, J. M., Duran, A., Sirera, R., & Alvarez, J. I. (2014). Assessment of the interaction of polycarboxylate superplasticizers in hydrated lime pastes modified with nanosilica or metakaolin as pozzolanic reactives. Construction and Building Materials, 73, 1–12. https://doi.org/10.1016/j.conbuildmat.2014.09.052

Neville A., & Aitcin P. C. (1998). High performance concrete - an overview. Materials and Structures, 31(1), 111–117.

Neville A., & Aitcin P. C. (1998). High performance concrete - an overview. Materials and Structures, 31(1), 111–117.

Neville, A.M. (2011) Properties of Concrete 5th Edition. London, UK: Longman

Nik, A. S. & Bahari, A. (2012). Nano-Particles in Concrete and Cement Mixtures.

Applied Mechanics and Materials, 110-116, 3853-3855.

Noordin, M. Y., Venkatesh, V. C., Sharif, S., Elting, S., & Abdullah, A. (2004). Application of response surface methodology in describing the performance of coated carbide tools when turning AISI 1045 steel. Journal of Materials Processing Technology, 145, 46–58. https://doi.org/10.1016/S0924-0136(03)00861-6

Noorvand, H., Ali, A. A. A., Demirboga, R., Noorvand, H., & Farzadnia, N. (2013). Physical and chemical characteristics of unground palm oil fuel ash cement mortars with nanosilica. Construction and Building Materials, 48, 1104–1113. https://doi.org/10.1016/j.conbuildmat.2013.07.070

Ollivier, J. P., Maso, J. C., & Bourdetted, B. (1995). Interfacial Transition Zone in Concrete. Advance Cement Based Material, 21, 30–38.

OSHA. (2013). Working Safely with Nanomaterials. OSHA - Fact sheet.

Ozbay, E., Gesoglu, M., & Guneyisi, E. (2011). Transport properties based multi-objective mix proportioning optimization of high performance concretes. Materials and Structures/Materiaux et Constructions, 44(1), 139–154. https://doi.org/10.1617/s11527-010-9615-7

Papadakis, V. G., Antiohos, S., & Tsimas, S. (2002). Supplementary cementing materials in concrete Part II : A fundamental estimation of the efficiency factor. Cement and Concrete Research, 32, 1533–1538. https://doi.org/http://dx.doi.org/10.1016/S0008-8846(02)00829-3

Rajak, M. A. A., Majid, Z. A., & Ismail, M. (2015). Morphological Characteristics of Hardened Cement Pastes Incorporating Nano-palm Oil Fuel Ash. Procedia Manufacturing, 2(February), 512–518. https://doi.org/10.1016/j.promfg.2015.07.088

Ramezanianpour, A. A. (2014). Cement Replacement Materials : Properties, Durability, Sustainability (Vol. 1). Springer-Verlag Berlin Heidelberg. https://doi.org/10.1007/978-3-642-36721-2

Ranjbar, N., Behnia, A., Alsubari, B., Birgani, P. M., & Jumaat, M. Z. (2016). Durability and mechanical properties of self-compacting concrete incorporating palm oil fuel ash. Journal of Cleaner Production, 112, 723–730. https://doi.org/10.1007/s12046-016-0549-9

Ranjbar, N., Mehrali, M., Alengaram, U. J., Simon, H., & Metselaar, C. (2014). Compressive strength and microstructural analysis of fly ash / palm oil fuel ash based geopolymer mortar under elevated temperatures. Construction and Building Materials, 65, 114–121. https://doi.org/10.1016/j.conbuildmat.2014.04.064

Rashad, A. M., Bai, Y., Basheer, P. A. M., Milestone, N. B., & Collier, N. C. (2013). Hydration and properties of sodium sulfate activated slag. Cement and Concrete Composites, 37(1), 20–29. https://doi.org/10.1016/j.cemconcomp.2012.12.010

Reches, Y. (2018). Nanoparticles as concrete additives : Review and perspectives. Construction and Building Materials, 175, 483–495.

Rezaifar, O., Hasanzadeh, M., & Gholhaki, M. (2016). Concrete made with hybrid blends of crumb rubber and metakaolin : Optimization using Response Surface Method. Construction and Building Materials, 123, 59–68. https://doi.org/10.1016/j.conbuildmat.2016.06.047

Ribeiro, D. V., & Abrantes, J. C. C. (2016). Application of electrochemical impedance spectroscopy (EIS) to monitor the corrosion of reinforced concrete: A new approach. Construction and Building Materials, 111, 98–104. https://doi.org/10.1016/j.conbuildmat.2016.02.047

Rukzon, S., & Chindaprasirt, P. (2008). Use of waste ash from various by-product materials in increasing the durability of mortar, 30(3), 485–489.

Safiuddin, M. (2008). Development of Self-consolidating High Performance Concrete Incorporating Rice Husk Ash. Uneversity of Waterloo.

Safiuddin, M., Abdus Salam, M., & Jumaat, M. Z. (2011). Utilization of palm oil fuel ash in concrete: a review. Journal of Civil Engineering and Management, 17(2), 234–247. https://doi.org/10.3846/13923730.2011.574450

Safiuddin, M., Gonzalez, M., Cao, J., & Tighe, S. L. (2014). State-of-the-art report on use of nano-materials in concrete. International Journal of Pavement Engineering, 15(10), 940–949. https://doi.org/10.1080/10298436.2014.893327

Sajedi, F., & Razak, H. A. (2011). Effects of thermal and mechanical activation methods on compressive strength of ordinary Portland cement-slag mortar. Materials and Design, 32(2), 984–995. https://doi.org/10.1016/j.matdes.2010.08.038

Sakulich, A. R., Miller, S., & Barsoum, M. W. (2010). Chemical and microstructural characterization of 20-month-old alkali-activated slag cements. Journal of the American Ceramic Society, 93(6), 1741–1748. https://doi.org/10.1111/j.1551-2916.2010.03611.x

Salami, B. A., Johari, M. A. M., Ahmad, Z. A., & Maslehuddin, M. (2016). Impact of added water and superplasticizer on early compressive strength of selected mixtures of palm oil fuel ash-based engineered geopolymer composites. Construction and Building Materials, 109, 198–206. https://doi.org/10.1016/j.conbuildmat.2016.01.033

Saleh, N. J., Ibrahim, R. I., & Salman, A. D. (2015). Characterization of nano-silica prepared from local silica sand and its application in cement mortar using optimization technique. Advanced Powder Technology, 26(4), 1123–1133. https://doi.org/10.1016/j.apt.2015.05.008

Samad, S., & Shah, A. (2017). Role of binary cement including Supplementary Cementitious Material (SCM), in production of environmentally sustainable concrete: A critical review. International Journal of Sustainable Built Environment, 6(2), 663–674. https://doi.org/10.1016/j.ijsbe.2017.07.003

Sanchez, F., & Sobolev, K. (2010). Nanotechnology in concrete - A review. Construction and Building Materials, 24(11), 2060–2071. https://doi.org/10.1016/j.conbuildmat.2010.03.014

Sanchez, F., & Sobolev, K. (2010). Nanotechnology in concrete - A review. Construction and Building Materials, 24(11), 2060–2071. https://doi.org/10.1016/j.conbuildmat.2010.03.014

Saremi, M., & Mahallati, E. (2002). A study on chloride-induced depassivation of mild steel in simulated concrete pore solution. Cement and Concrete Research, 32, 1915–1921.

Sata, V., Jaturapitakkul, C., & Kiattikomol, K. (2004). Utilization of palm oil fuel ash in high-strength concrete. Journal of Materials in Civil Engineering, 16(6), 623–628. https://doi.org/10.1061/(ASCE)0899-1561(2004)16:6(623)

Sata, V., Jaturapitakkul, C., & Kiattikomol, K. (2007). Influence of pozzolan from various by-product materials on mechanical properties of high-strength concrete. Construction and Building Materials, 21(7), 1589–1598. https://doi.org/10.1016/j.conbuildmat.2005.09.011

Sata, V., Jaturapitakkul, C., & Rattanashotinunt, C. (2010). Compressive Strength and Heat Evolution of Concretes Containing Palm Oil Fuel Ash. Journal of Materials in Civil Engineering, 22(10), 1033–1038. https://doi.org/10.1061/(ASCE)MT.1943-5533.0000104

Schneider, C. A., Rasband, W. S., & Eliceiri, K. W. (2012). NIH Image to ImageJ: 25 years of Image Analysis. Nature Methods, 9(7), 671–675. https://doi.org/10.1038/nmeth.2089

Shah, S. P., Konsta-Gdoutos, M. S., Metaxa, Z. S., & Mondal, P. (2009). Nanoscale Modification of Cementitious Materials. Nanotechnology in Construction 3, 125–130. https://doi.org/10.2514/1.T4176

Shaikh, F. U. A., & Supit, S. W. M. (2015). Chloride induced corrosion durability of high volume fly ash concretes containing nano particles. Construction and Building Materials, 99, 208–225. https://doi.org/10.1016/j.conbuildmat.2015.09.030

Shi, C., & Day, R. L. (2000). Pozzolanic reaction in the presence of chemical activators: Part II — Reaction products and mechanism. Cement and Concrete Research, 30(4), 607–613. https://doi.org/10.1016/S0008-8846(00)00214-3

Shi, C., Wu, Z., Xiao, J., Wang, D., Huang, Z., & Fang, Z. (2015). A review on ultra high performance concrete: Part II. Hydration, microstructure and properties.

Construction and Building Materials, 101, 741–751. https://doi.org/10.1016/j.conbuildmat.2015.10.088

Simon, M. J. (2003). Concrete Mixture Optimization Using Statistical Methods: Final Report. Retrieved from https://www.fhwa.dot.gov/publications/research/infrastructure/pavements/03060/03060.pdf

Simon, M.J., Lagergren, E.S., & Wathne, L.G. (1999). Optimizing HPC Mixtures Using Statistical Response Surface Methods. In: Proceedings of the 5th International Symposium on Utilization of High Strength/High-Performance Concrete. Oslo, Norway: Norwegian Concrete Association, 1311–21.

Singh, G., & Siddique, R. (2012). Abrasion resistance and strength properties of concrete containing waste foundry sand (WFS). Construction and Building Materials, 28, 421–426. https://doi.org/10.1016/j.conbuildmat.2011.08.087

Singh, L. P., Karade, S. R., Bhattacharyya, S. K., Yousuf, M. M., & Ahalawat, S. (2013). Beneficial role of nanosilica in cement based materials - A review. Construction and Building Materials, 47, 1069–1077. https://doi.org/10.1016/j.conbuildmat.2013.05.052

Skalny, J.P., Marchand, J., & Odler, I. (2002). Sulfate Attack on Concrete. https://doi.org/https://doi-org.dbgw.lis.curtin.edu.au/10.4324/9780203301623

Soares, R. C., Mohamed, A., Venturini, W. S., & Lemaire, M. (2002). Reliability analysis of non-linear reinforced concrete frames using the response surface method. Reliability Engineering and System Safety, 75, 1–16. https://doi.org/10.1016/S0951-8320(01)00043-6

Sohail, M. G., Wang, B., Jain, A., Kahraman, R., Ozerkan, N. G., Gencturk, B., … Belarbi, A. (2018). Advancements in Concrete Mix Designs: High-Performance and Ultrahigh-Performance Concretes from 1970 to 2016. Journal of Materials in Civil Engineering, 30(3), 040173101-20. https://doi.org/10.1061/(ASCE)MT.1943-5533.0002144

Sonebi, M., & Bassuoni, M. T. (2013). Investigating the effect of mixture design parameters on pervious concrete by statistical modelling. Construction and Building Materials, 38, 147–154. https://doi.org/10.1016/j.conbuildmat.2012.07.044

Song, H., & Saraswathy, V. (2007). Corrosion Monitoring of Reinforced Concrete Structures - A Review. International Journal of Electrochemical Sceince, 2, 1–28.

Soudki, K. A., El-Salakawy, E. F., & Elkum, N. B. (2001). FULL FACTORIAL OPTIMIZATION OF CONCRETE MIX DESIGN FOR HOT CLIMATES. Journal of Materials in Civil Engineering, 13(6), 427–433. https://doi.org/10.1016/j.apenergy.2016.07.008

Srikanth, M., & Asmatulu, R. (2013). Nanotechnology Safety in the Construction and Infrastructure Industries. In R. Asmatulu (Eds.), Nanotechnology Safety (pp. 99-113. http://dx.doi.org/10.1016/B978-0-444-59438-9.00008-4

Stroeven, P., & Stroeven, M. (1999). Assessment of packing characteristics by computer simulation. Cement and Concrete Research, 29, 1201–1206.

Stroeven, P., & Stroeven, M. (2001). Reconstructions by SPACE of the Interfacial Transition Zone. Cement and Concrete Composites, 23, 189–200.

Sumadi, R.S & Hussin, M. (1995). Palm oil fuel ash (POFA) as a future partial cement replacement material in housing construction. Journal of Ferrocement. 25. 25-34.

Sumathi, S., Chai, S. ., & Mohamed, A. (2008). Utilization of oil palm as a source of renewable energy in Malaysia. Renewable and Sustainable Energy Reviews, 12, 2404–2421. https://doi.org/10.1016/j.rser.2007.06.006

Suryanarayana, C., Ivanov, E., & Boldyrev, V. V. (2008). The science and technology of mechanical alloying. Materials Science and Engineering A, 306, 151–158. https://doi.org/10.1016/S0921-5093(00)01465-9

Tangchirapat, W., & Jaturapitakkul, C. (2010). Strength, drying shrinkage, and water permeability of concrete incorporating ground palm oil fuel ash. Cement and Concrete Composites, 32(10), 767–774.

https://doi.org/10.1016/j.cemconcomp.2010.08.008

Tangchirapat, W., Jaturapitakkul, C., & Chindaprasirt, P. (2009). Use of palm oil fuel ash as a supplementary cementitious material for producing high-strength concrete. Construction and Building Materials, 23, 2641–2646. https://doi.org/10.1016/j.conbuildmat.2009.01.008

Tangchirapat, W., Khamklai, S., & Jaturapitakkul, C. (2012). Use of ground palm oil fuel ash to improve strength , sulfate resistance , and water permeability of concrete containing high amount of recycled concrete aggregates. Materials and Design, 41, 150–157. https://doi.org/10.1016/j.matdes.2012.04.054

Tangchirapat, W., Saeting, T., Jaturapitakkul, C., Kiattikomol, K., & Siripanichgorn, A. (2007). Use of waste ash from palm oil industry in concrete. Waste Management, 27(1), 81–88. https://doi.org/10.1016/j.wasman.2005.12.014

Tangpagasit, J.,Cheerarot, R., Jaturapitakkul, C. & Kiattikomol, K, (2005) Packing effect and pozzolanic reaction of fly ash in mortar. Cem. Concr. Res.,35 (6) , 1145–1151.

Tay, J. (1990). Ash from oil palm waste as concrete material. Journal of Materials in Civil Engineering, 2(2), 94–105.

Tay, J. H., & Show, K. Y. (1995). Use of ash derived from oil-palm waste incineration as a cement replacement material. Resources, Conservation and Recycling, 13, 27–36. https://doi.org/10.1080/0969725012008793

Taylor, H. F. W. (2017). Cement chemistry. Thomas Telford.

Taylor, M., Tam, C., & Gielen, D. (2006). Energy Efficiency and CO2 Emissions from the Global Cement Industry. Energy Technology Policy Division, (September), 61-67. https://doi.org/10.1016/j.ijms.2011.08.030

Thomas, B. S., Kumar, S., & Arel, H. S. (2017). Sustainable concrete containing palm oil fuel ash as a supplementary cementitious material – A review. Renewable and Sustainable Energy Reviews, 80(July 2016), 550–561. https://doi.org/10.1016/j.rser.2017.05.128

Thomas, M. (1996). Chloride Thresholds in Marine Concrete. Cement and Concrete Research, 26(4), 513–519. https://doi.org/0008-8846/96

Tonnayopas, D., Nilrat, F., Putto, K. & Tantiwitayawanich, J. (2006). Effect of oil palm fiber fuel ash on compressive strength of hardening concrete, in Proceedings of the 4th Thailand Materials Science and Technology Conference, Pathumthani, Thailand, March 31-April 1, 2006, 1–3.

U.S. Geological Survey. (2018). MINERAL COMMODITY SUMMARIES 2018.

Upasani, R. S., & Banga, A. K. (2004). Response surface methodology to investigate the iontophoretic delivery of tacrine hydrochloride. Pharmaceutical Research, 21(12), 2293–2299. https://doi.org/10.1007/s11095-004-7682-6

Wang, J., Chen, Y., Wang, Y., Yuan, S., & Yu, H. (2011). Optimization of the coagulation-flocculation process for pulp mill wastewater treatment using a combination of uniform design and response surface methodology. Water Research, 45(17), 5633–5640. https://doi.org/10.1016/j.watres.2011.08.023

Wang, Y. et al., Recycling of switchgrass combustion ash in cement:characteristics and pozzolanic activity with chemical accelerators, Constr. Build. Mater. 73 (2014) 472–478.

Wesseling, J. H., & Van der Vooren, A. (2017). Lock-in of mature innovation systems: the transformation toward clean concrete in the Netherlands. Journal of Cleaner Production, 155, 114–124. https://doi.org/10.1016/j.jclepro.2016.08.115

Xiaoyong, L., & Wendi, M. (2011). Optimization for Mix Design of High-Performance. Communications in Computer and Information Science, 232(2), 364–372.

Yadav,P, Manohar, T., Yadav, R., & Pratap Singh, D. (2012). Mechanical Milling: a Top Down Approach for the Synthesis of Nanomaterials and Nanocomposites. Nanoscience and Nanotechnology, 2(3), 22–48. https://doi.org/10.5923/j.nn.20120203.01

Yahaya, F. M., Muthusamy, K., & Sulaiman, N. (2014). Corrosion Resistance of High

Strength Concrete Containing Palm Oil Fuel Ash as Partial Cement Replacement. Journal of Applied Sciences, Engineering and Technology, 7(22), 4720–4722.

Yu, R., Spiesz, P., & Brouwers, H. J. H. (2014). Effect of nano-silica on the hydration and microstructure development of Ultra-High Performance Concrete (UHPC) with a low binder amount. Construction and Building Materials, 65, 140–150. https://doi.org/10.1016/j.conbuildmat.2014.04.063

Yusoff, S. (2006). Renewable energy from palm oil - Innovation on effective utilization of waste. Journal of Cleaner Production, 14(1), 87–93. https://doi.org/10.1016/j.jclepro.2004.07.005

Yusuf, M. O. (2015). Performance of slag blended AAGU in sulfate environments. Construction and Building Materials, 98, 417–424. https://doi.org/10.1016/j.conbuildmat.2015.07.012

Yusuf, M. O., Megat Johari, M. A., Ahmad, Z. A., & Maslehuddin, M. (2015). Effects of H2O/Na2O molar ratio on the strength of alkaline activated ground blast furnace slag-ultrafine palm oil fuel ash based concrete. Materials and Structures/Materiaux et Constructions, 48(3), 733–741. https://doi.org/10.1617/s11527-014-0318-3

Zaitri, R., Bederina, M., Bouziani, T., Makhloufi, Z., & Hadjoudja, M. (2014). Development of high performances concrete based on the addition of grinded dune sand and limestone rock using the mixture design modelling approach. Construction and Building Materials, 60, 8–16. https://doi.org/10.1016/j.conbuildmat.2014.02.062

Zeyad, A. M., Johari, M. A. M., Bunnori, N. M., Ariffin, K. S., & Altwair, N. M. (2012). Characteristics of Treated Palm Oil Fuel Ash and its Effects on Properties of High Strength Concrete. Advanced Materials Research, 626(March), 152–156. https://doi.org/10.4028/www.scientific.net/AMR.626.152

Zeyad, A. M., Megat Johari, M. A., Tayeh, B. A., & Yusuf, M. O. (2016). Efficiency of treated and untreated palm oil fuel ash as a supplementary binder on engineering and fluid transport properties of high-strength concrete. Construction and Building Materials, 125, 1066–1079.

https://doi.org/10.1016/j.conbuildmat.2016.08.065

Zeyad, A. M., Megat Johari, M. A., Tayeh, B. A., & Yusuf, M. O. (2017). Pozzolanic reactivity of ultrafine palm oil fuel ash waste on strength and durability performances of high strength concrete. Journal of Cleaner Production, 144, 511–522. https://doi.org/10.1016/j.jclepro.2016.12.121

Živica, V. (1999). Acidic resistance of materials based on the novel use of silica fume in concrete. Construction and Building Materials, 13(5), 263–269. https://doi.org/10.1016/S0950-0618(99)00029-X